1. Parameter of Principal Interest

Leaching rates from activated spent fuel hardware.

2. Test Conditions and Other Qualifying Data

The basis of the estimate of the number and type of fuel assemblies is the 1989 EIA's no new orders case (ref.1 is the annual estimate based on data through 1988: the report incorporating the 1989 data has not yet been published). The no new orders case uses data provided by the utilities on the RW-859 annual report. The projected number of fuel assemblies assumes that the reactors run to their anticipated end of life and are then shutdown. Fuel assemblies are assumed to be discharged on a routine basis, and the type of assemblies are assumed to be the type currently in use, unless information has been provided by the utilities to the contrary. The projection does not account for future design changes that are inevitable. For example, the predominant fuel type for boiling water reactors (BWRs) is currently an 8X8 configuration. Fuel assemblies with 9X9 and 10X10 configurations are being marketed and are expected to constitute a significant portion of the BWR fuel in the future. This, and other similar situations, are not accounted for in these estimates. Additionally, higher burnup of fuels is expected in the future. This would decrease the number of assemblies requiring disposal. This unknown is one of the greatest sources of uncertainty.

The mass and composition of the fuel assemblies was taken from ref.2. The distribution of materials in the core was also obtained from that report. This distribution was necessary in order to account for differing activation levels in the core (e.g. top end fittings vs. material in the active core). A small number of assemblies are not included in these estimates. They include some of the very odd fuel, such as West 15X16, that constitutes less than 1% of the manufacturers projected production.

Estimates of the numbers of non-fuel bearing components were taken from ref.3. Table 4-1 of that report provided estimates of the number of NFBC requiring disposal. Currently, efforts are underway to better define these estimates, but the results of that work will not be available until FY91. The estimates used in this report will likely prove to be

conservative. Estimates of the masses and compositions of the non-fuel bearing components was compiled using data in ref.2, 4, & 5.

The activation of the hardware was estimated using the ORIGEN2 computer code, and incorporating the appropriate scaling factors from ref.2. PWR hardware was activated to a burnup of 33,000 MWD/MTU and BWR to 27,500 MWD/MTU. These values reflect the average burnup expected from these fuel types. Non-fuel bearing components used fluxes commensurate with those burnups, but for component specific residence times. ORIGEN2 was then used to decay the radionuclides out to one million years. The results of these calculations were folded with the material quantities estimated above, and total inventories, as a function of time were developed. These are provided in the attached tables.

Surface area estimates were developed based on detailed measurements of a number of available hardware components. These included both top and bottom end fittings of a GE 8X8 BWR, West 14X14 PWR (top only), West 17X17 PWR, and CE 14X14 PWR. Measurements of grid spacers for these assembly types were also made. These represent a large fraction of the fuel assembly types that were considered. The results of these measurements were used to infer surface areas of fuel assembly types that were not available for measurements. An example of this is the surface area of a West 15X15 assembly. From drawings in ref.2, it can be seen that a 15X15 assembly is similar to a 14X14 assembly with an extra row of fuel pins added to two sides. To estimate the surface area of the end fittings and grid spacers, the measured values from the 14X14 are scaled up by a factor of (15*15)/(14*14). For the guide tubes, the surface area of a single guide tube multiplied by the actual number in each fuel type is used (i.e. 20 in the 15X15 vs. 16 in the 14X14).

In evaluating the leaching of radionuclides from the hardware, the thickness of the materials is important. Though this data was not part of the scope of work, some generalizations can be made that should prove helpful. The end fittings are the most massive pieces. They are generally cast stainless steel, and their thickness varies between 1/8" to 5/8" in individual pieces. Grid spacers, made either of Inconel or Zircaloy, are thin pieces of sheet metal. The thickness of the individual strips are approximately 0.025" in the samples we have measured. The guide tubes, mostly Zircaloy but some stainless steel, are only slightly thicker, at about 0.035" - 0.045". Overall, the bulk of the Zircaloy and Inconel are relatively

thin. Leaching and/or corrosion would occur from both sides of the material. Given the high surface to volume ratio for the bulk of the Zircaloy and Inconel, a higher percentage of their inventory would be expected to be released earlier than the stainless steel end fittings. Leaching from the guide tubes and grid spacers would occur twice as fast as from the fuel cladding, because the grid spacers and guide tubes will corrode and leach from both sides.

Table IV provides the total inventory of actinides and transuranics for the no new orders case that can be used as a comparison to the results in Tables II-A through II-J for the spent fuel hardware and Tables III-A through III-J7 for the non-fuel bearing components. Overall, the number of curies associated with the actinides and transuranics is several orders of magnitude more than the activation products.

List of Tables

TABLE I

Repository Hardware Inventory Characteristics

MATERIAL	Stainless Steel	Inconel	Zircaloy
Surface Area (M^2)	652,000	1,480,000	400,000
Weight (MT)	3,260	750	6,800
Total Activity At Discharge (Ci)	3,130,000	17,600,000	14,000,000
Total Activity 100 Years (Ci)	1,490,000	8,410,000	7,740
Total Activity 200 Years (Ci)	720,000	4,050,000	6,140
Total Activity 500 Years (Ci)	105,000	587,000	5,210
Total Activity 1,000 Years (Ci)	34,300	190,000	4,980
Total Activity 2,000 Years (Ci)	31,300	177,000	4,680
Total Activity 5,000 Years (Ci)	27,800	167,000	3,960
Total Activity 10,000 Years (Ci)	23,900	152,000	3,190
Total Activity 100,000 Years (Ci)	9,270	54,800	1,980
Total Activity 1 Million Years (Ci)	5	25	1,290

A.T. Luksic, Battelle PNL Letter Report LLYMP 9104248

Table II-A

Radioactivity at Discharge in Spent Fuel Hardware
Ci

Isotope	SS	Inc	Zr-4	Total
BE 10	1.43E-03	0.00E+00	0.00E+00	1.43E-03
C 14	1.22E+04	1.18E+04	2.85E+03	2.68E+04
CL 36	1.09E+01	1.05E+01	4.14E+01	6.28E+01
NI 59	2.20E+04	1.27E+05	1.91E+01	1.49E+05
CO 60	0.00E+00	0.00E+00	1.93E+06	1.93E+06
NI 63	3.10E+06	1.75E+07	2.73E+03	2.06E+07
SR 90	0.00E+00	0.00E+00	1.04E+01	1.04E+01
Y 90	0.00E+00	0.00E+00	1.20E+07	1.20E+07
ZR 93	0.00E+00	2.75E-01	1.03E+03	1.03E+03
NB 93M	0.00E+00	1.82E-02	6.84E+01	6.84E+01
NB 94	8.62E+01	4.56E+04	3.91E+02	4.61E+04
MO 93	0.00E+00	8.98E+02	0.00E+00	8.98E+02
TC 99	0.00E+00	4.80E+01	0.00E+00	4.80E+01
SN121M	0.00E+00	0.00E+00	4.67E+03	4.67E+03
Total	3.13E+06	1.76E+07	1.40E+07	3.48E+07

Table II-B

100 Year Radioactivity in Spent Fuel Hardware
Ci

Isotope	SS	Inc	Zr-4	Total
BE 10	1.43E-03	0.00E+00	0.00E+00	1.43E-03
C 14	1.20E+04	1.16E+04	2.82E+03	2.64E+04
CL 36	1.09E+01	1.05E+01	4.14E+01	6.28E+01
NI 59	2.20E+04	1.27E+05	1.91E+01	1.49E+05
CO 60	0.00E+00	0.00E+00	3.73E+00	3.73E+00
NI 63	1.46E+06	8.22E+06	1.29E+03	9.68E+06
SR 90	0.00E+00	0.00E+00	9.66E-01	9.66E-01
Y 90	0.00E+00	0.00E+00	9.66E-01	9.66E-01
ZR 93	0.00E+00	2.75E-01	1.03E+03	1.03E+03
NB 93M	0.00E+00	2.59E-01	9.77E+02	9.77E+02
NB 94	8.59E+01	4.55E+04	3.90E+02	4.59E+04
MO 93	0.00E+00	8.80E+02	0.00E+00	8.80E+02
TC 99	0.00E+00	4.82E+01	0.00E+00	4.82E+01
SN121M	0.00E+00	0.00E+00	1.17E+03	1.17E+03
Total	1.49E+06	8.41E+06	7.74E+03	9.91E+06

A.T. Luksic, Battelle PNL Letter Report LLYMP 9104248

Table II-C

200 Year Radioactivity in Spent Fuel Hardware
Ci

Isotope	SS	Inc	Zr-4	Total
BE 10	1.43E-03	0.00E+00	0.00E+00	1.43E-03
C 14	1.19E+04	1.15E+04	2.78E+03	2.61E+04
CL 36	1.09E+01	1.05E+01	4.14E+01	6.28E+01
NI 59	2.20E+04	1.27E+05	1.91E+01	1.49E+05
CO 60	0.00E+00	0.00E+00	7.24E-06	7.24E-06
NI 63	6.86E+05	3.87E+06	6.06E+02	4.56E+06
SR 90	0.00E+00	0.00E+00	8.94E-02	8.94E-02
Y 90	0.00E+00	0.00E+00	8.94E-02	8.94E-02
ZR 93	0.00E+00	2.75E-01	1.03E+03	1.03E+03
NB 93M	0.00E+00	2.61E-01	9.82E+02	9.82E+02
NB 94	8.57E+01	4.53E+04	3.89E+02	4.58E+04
MO 93	0.00E+00	8.63E+02	0.00E+00	8.63E+02
TC 99	0.00E+00	4.82E+01	0.00E+00	4.82E+01
SN121M	0.00E+00	0.00E+00	2.91E+02	2.91E+02
Total	7.20E+05	4.05E+06	6.14E+03	4.78E+06

Table II-D

500 Year Radioactivity in Spent Fuel Hardware
Ci

Isotope	SS	Inc	Zr-4	Total
BE 10	1.43E-03	0.00E+00	0.00E+00	1.43E-03
C 14	1.15E+04	1.11E+04	2.68E+03	2.52E+04
CL 36	1.09E+01	1.05E+01	4.14E+01	6.28E+01
NI 59	2.19E+04	1.26E+05	1.90E+01	1.48E+05
CO 60	0.00E+00	0.00E+00	0.00E+00	0.00E+00
NI 63	7.16E+04	4.04E+05	6.32E+01	4.75E+05
SR 90	0.00E+00	0.00E+00	7.08E-05	7.08E-05
Y 90	0.00E+00	0.00E+00	7.08E-05	7.08E-05
ZR 93	0.00E+00	2.75E-01	1.03E+03	1.03E+03
NB 93M	0.00E+00	2.61E-01	9.82E+02	9.82E+02
NB 94	8.48E+01	4.49E+04	3.85E+02	4.53E+04
MO 93	0.00E+00	8.13E+02	0.00E+00	8.13E+02
TC 99	0.00E+00	4.81E+01	0.00E+00	4.81E+01
SN121M	0.00E+00	0.00E+00	4.54E+00	4.54E+00
Total	1.05E+05	5.87E+05	5.21E+03	6.97E+05

A.T. Luksic, Battelle PNL Letter Report LLYMP 9104248

Table II-E

1000 Year Radioactivity in Spent Fuel Hardware
Ci

Isotope	SS	Inc	Zr-4	Total
BE 10	1.43E-03	0.00E+00	0.00E+00	1.43E-03
C 14	1.08E+04	1.04E+04	2.53E+03	2.37E+04
CL 36	1.09E+01	1.05E+01	4.13E+01	6.27E+01
NI 59	2.18E+04	1.26E+05	1.89E+01	1.47E+05
CO 60	0.00E+00	0.00E+00	0.00E+00	0.00E+00
NI 63	1.66E+03	9.33E+03	1.46E+00	1.10E+04
SR 90	0.00E+00	0.00E+00	4.80E-10	4.80E-10
Y 90	0.00E+00	0.00E+00	4.80E-10	4.80E-10
ZR 93	0.00E+00	2.75E-01	1.03E+03	1.03E+03
NB 93M	0.00E+00	2.61E-01	.82E+02	9.82E+02
NB 94	8.33E+01	4.41E+04	3.78E+02	4.46E+04
MO 93	0.00E+00	7.37E+02	0.00E+00	7.37E+02
TC 99	0.00E+00	4.81E+01	0.00E+00	4.81E+01
SN121M	0.00E+00	0.00E+00	4.42E-03	4.42E-03
Total	3.43E+04	1.90E+05	4.98E+03	2.30E+05

Table II-F

2000 Year Radioactivity in Spent Fuel Hardware
Ci

Isotope	SS	Inc	Zr-4	Total
BE 10	1.43E-03	0.00E+00	0.00E+00	1.43E-03
C 14	9.55E+03	9.23E+03	2.24E+03	2.10E+04
CL 36	1.09E+01	1.05E+01	4.12E+01	6.25E+01
NI 59	2.16E+04	1.25E+05	1.88E+01	1.46E+05
CO 60	0.00E+00	0.00E+00	0.00E+00	0.00E+00
NI 63	8.85E-01	4.99E+00	7.81E-04	5.87E+00
SR 90	0.00E+00	0.00E+00	0.00E+00	0.00E+00
Y 90	0.00E+00	0.00E+00	0.00E+00	0.00E+00
ZR 93	0.00E+00	2.74E-01	1.03E+03	1.03E+03
NB 93M	0.00E+00	2.61E-01	9.81E+02	9.82E+02
NB 94	8.05E+01	4.26E+04	3.66E+02	4.31E+04
MO 93	0.00E+00	6.04E+02	0.00E+00	6.04E+02
TC 99	0.00E+00	4.79E+01	0.00E+00	4.79E+01
SN121M	0.00E+00	0.00E+00	4.18E-09	4.18E-09
Total	3.13E+04	1.77E+05	4.68E+03	2.13E+05

A.T. Luksic, Battelle PNL Letter Report LLYMP 9104248

Table II-G

5000 Year Radioactivity in Spent Fuel Hardware
Ci

Isotope	SS	Inc	Zr-4	Total
BE 10	1.43E-03	0.00E+00	0.00E+00	1.43E-03
C 14	6.64E+03	6.42E+03	1.56E+03	1.46E+04
CL 36	1.08E+01	1.04E+01	4.09E+01	6.21E+01
NI 59	2.11E+04	1.21E+05	1.83E+01	1.42E+05
CO 60	0.00E+00	0.00E+00	0.00E+00	0.00E+00
NI 63	1.35E-10	7.62E-10	1.19E-13	8.97E-10
SR 90	0.00E+00	0.00E+00	0.00E+00	0.00E+00
Y 90	0.00E+00	0.00E+00	0.00E+00	0.00E+00
ZR 93	0.00E+00	2.74E-01	1.03E+03	1.03E+03
NB 93M	0.00E+00	2.60E-01	9.80E+02	9.80E+02
NB 94	7.27E+01	3.85E+04	3.30E+02	3.89E+04
MO 93	0.00E+00	3.33E+02	0.00E+00	3.33E+02
TC 99	0.00E+00	4.74E+01	0.00E+00	4.74E+01
SN121M	0.00E+00	0.00E+00	0.00E+00	0.00E+00
Total	2.78E+04	1.67E+05	3.96E+03	1.98E+05

Table II-H

10,000 Year Radioactivity in Spent Fuel Hardware
Ci

Isotope	SS	Inc	Zr-4	Total
BE 10	1.42E-03	0.00E+00	0.00E+00	1.42E-03
C 14	3.63E+03	3.51E+03	8.50E+02	7.98E+03
CL 36	1.07E+01	1.03E+01	4.05E+01	6.14E+01
NI 59	2.02E+04	1.16E+05	1.75E+01	1.36E+05
CO 60	0.00E+00	0.00E+00	0.00E+00	0.00E+00
NI 63	0.00E+00	0.00E+00	0.00E+00	0.00E+00
SR 90	0.00E+00	0.00E+00	0.00E+00	0.00E+00
Y 90	0.00E+00	0.00E+00	0.00E+00	0.00E+00
ZR 93	0.00E+00	2.73E-01	1.03E+03	1.03E+03
NB 93M	0.00E+00	2.60E-01	9.78E+02	9.78E+02
NB 94	6.13E+01	3.24E+04	2.78E+02	3.28E+04
MO 93	0.00E+00	1.24E+02	0.00E+00	1.24E+02
TC 99	0.00E+00	4.67E+01	0.00E+00	4.67E+01
SN121M	0.00E+00	0.00E+00	0.00E+00	0.00E+00
Total	2.39E+04	1.52E+05	3.19E+03	1.79E+05

A.T. Luksic, Battelle PNL Letter Report LLYMP 9104248

Table II-I

100,000 Year Radioactivity in Spent Fuel Hardware
Ci

Isotope	SS	Inc	Zr-4	Total
BE 10	1.37E-03	0.00E+00	0.00E+00	1.37E-03
C 14	6.77E-02	6.55E-02	1.59E-02	1.49E-01
CL 36	8.67E+00	8.35E+00	3.29E+01	4.99E+01
NI 59	9.25E+03	5.33E+04	8.03E+00	6.26E+04
CO 60	0.00E+00	0.00E+00	0.00E+00	0.00E+00
NI 63	0.00E+00	0.00E+00	0.00E+00	0.00E+00
SR 90	0.00E+00	0.00E+00	0.00E+00	0.00E+00
Y 90	0.00E+00	0.00E+00	0.00E+00	0.00E+00
ZR 93	0.00E+00	2.62E-01	9.88E+02	9.88E+02
NB 93M	0.00E+00	2.49E-01	9.39E+02	9.39E+02
NB 94	2.84E+00	1.50E+03	1.29E+01	1.52E+03
MO 93	0.00E+00	2.23E-06	0.00E+00	2.23E-06
TC 99	0.00E+00	3.48E+01	0.00E+00	3.48E+01
SN121M	0.00E+00	0.00E+00	0.00E+00	0.00E+00
Total	9.27E+03	5.48E+04	1.98E+03	6.61E+04

Table II-J

1 Million Year Radioactivity in Spent Fuel Hardware
Ci

Isotope	SS	Inc	Zr-4	Total
BE 10	9.26E-04	0.00E+00	0.00E+00	9.26E-04
C 14	0.00E+00	0.00E+00	0.00E+00	0.00E+00
CL 36	1.09E+00	1.05E+00	4.14E+00	6.28E+00
NI 59	3.80E+00	2.19E+01	3.30E-03	2.57E+01
CO 60	0.00E+00	0.00E+00	0.00E+00	0.00E+00
NI 63	0.00E+00	0.00E+00	0.00E+00	0.00E+00
SR 90	0.00E+00	0.00E+00	0.00E+00	0.00E+00
Y 90	0.00E+00	0.00E+00	0.00E+00	0.00E+00
ZR 93	0.00E+00	1.75E-01	6.57E+02	6.57E+02
NB 93M	0.00E+00	1.66E-01	6.24E+02	6.24E+02
NB 94	1.28E-13	6.76E-11	5.80E-13	6.83E-11
MO 93	0.00E+00	0.00E+00	0.00E+00	0.00E+00
TC 99	0.00E+00	1.86E+00	0.00E+00	1.86E+00
SN121M	0.00E+00	0.00E+00	0.00E+00	0.00E+00
Total	4.89E+00	2.51E+01	1.29E+03	1.32E+03

A.T. Luksic, Battelle PNL Letter Report LLYMP 9104248

TABLE III-A

Radioactivity at Discharge in Non-Fuel Bearing Components
Ci

Isotope	SS	Inc	Zr-4	Total
BE 10	1.31E-06	0.00E+00	0.00E+00	1.31E-06
C 14	1.21E+01	3.89E+02	7.03E+03	7.43E+03
CL 36	1.09E-02	3.47E-01	1.03E+02	1.04E+02
NI 59	2.12E+01	4.21E+03	4.30E+01	4.28E+03
CO 60	0.00E+00	0.00E+00	4.83E+06	4.83E+06
NI 63	3.08E+03	5.75E+05	6.75E+03	5.85E+05
SR 90	0.00E+00	0.00E+00	0.00E+00	0.00E+00
Y 90	0.00E+00	0.00E+00	0.00E+00	0.00E+00
ZR 93	0.00E+00	9.36E-03	2.77E+03	2.77E+03
NB 93M	0.00E+00	6.19E-04	1.85E+02	1.85E+02
NB 94	8.64E-02	1.51E+03	9.96E+02	2.51E+03
MO 93	0.00E+00	2.99E+01	0.00E+00	2.99E+01
TC 99	0.00E+00	1.24E+00	0.00E+00	1.24E+00
SN121M	0.00E+00	0.00E+00	1.16E+04	1.16E+04
Total	3.11E+03	5.81E+05	4.86E+06	5.44E+06

TABLE III-B

100 Year Radioactivity in Non-Fuel Bearing Components
Ci

Isotope	SS	Inc	Zr-4	Total
BE 10	1.31E-06	0.00E+00	0.00E+00	1.31E-06
C 14	1.19E+01	3.84E+02	6.94E+03	7.34E+03
CL 36	1.09E-02	3.47E-01	1.03E+02	1.04E+02
NI 59	2.12E+01	4.21E+03	4.29E+01	4.27E+03
CO 60	0.00E+00	0.00E+00	9.35E+00	9.35E+00
NI 63	1.45E+03	2.71E+05	3.18E+03	2.75E+05
SR 90	0.00E+00	0.00E+00	0.00E+00	0.00E+00
Y 90	0.00E+00	0.00E+00	0.00E+00	0.00E+00
ZR 93	0.00E+00	9.36E-03	2.77E+03	2.77E+03
NB 93M	0.00E+00	8.84E-03	2.62E+03	2.62E+03
NB 94	8.61E-02	1.51E+03	9.92E+02	2.50E+03
MO 93	0.00E+00	2.93E+01	0.00E+00	2.93E+01
TC 99	0.00E+00	1.25E+00	0.00E+00	1.25E+00
SN121M	0.00E+00	0.00E+00	2.91E+03	2.91E+03
Total	1.48E+03	2.77E+05	1.96E+04	2.98E+05

A.T. Luksic, Battelle PNL Letter Report LLYMP 9104248

TABLE III-C

200 Year Radioactivity in Non-Fuel Bearing Components
Ci

Isotope	SS	Inc	Zr-4	Total
BE 10	1.31E-06	0.00E+00	0.00E+00	1.31E-06
C 14	1.18E+01	3.79E+02	6.86E+03	7.25E+03
CL 36	1.09E-02	3.47E-01	1.03E+02	1.04E+02
NI 59	2.12E+01	4.21E+03	4.29E+01	4.27E+03
CO 60	0.00E+00	0.00E+00	1.81E-05	1.81E-05
NI 63	6.83E+02	1.27E+05	1.50E+03	1.30E+05
SR 90	0.00E+00	0.00E+00	0.00E+00	0.00E+00
Y 90	0.00E+00	0.00E+00	0.00E+00	0.00E+00
ZR 93	0.00E+00	9.35E-03	2.77E+03	2.77E+03
NB 93M	0.00E+00	8.89E-03	2.63E+03	2.63E+03
NB 94	8.58E-02	1.50E+03	9.89E+02	2.49E+03
MO 93	0.00E+00	2.87E+01	0.00E+00	2.87E+01
TC 99	0.00E+00	1.25E+00	0.00E+00	1.25E+00
SN121M	0.00E+00	0.00E+00	7.27E+02	7.27E+02
Tota l	7.16E+02	1.34E+05	1.56E+04	1.50E+05

TABLE III-D

500 Year Radioactivity in Non-Fuel Bearing Components
Ci

Isotope	SS	Inc	Zr-4	Total
BE 10	1.31E-06	0.00E+00	0.00E+00	1.31E-06
C 14	1.14E+01	3.66E+02	6.62E+03	7.00E+03
CL 36	1.08E-02	3.47E-01	1.03E+02	1.04E+02
NI 59	2.11E+01	4.20E+03	4.28E+01	4.26E+03
CO 60	0.00E+00	0.00E+00	0.00E+00	0.00E+00
NI 63	7.12E+01	1.33E+04	1.56E+02	1.35E+04
SR 90	0.00E+00	0.00E+00	0.00E+00	0.00E+00
Y 90	0.00E+00	0.00E+00	0.00E+00	0.00E+00
ZR 93	0.00E+00	9.35E-03	2.77E+03	2.77E+03
NB 93M	0.00E+00	8.89E-03	2.63E+03	2.63E+03
NB 94	8.49E-02	1.49E+03	9.79E+02	2.47E+03
MO 93	0.00E+00	2.71E+01	0.00E+00	2.71E+01
TC 99	0.00E+00	1.24E+00	0.00E+00	1.24E+00
SN121M	0.00E+00	0.00E+00	1.13E+01	1.13E+01
Total	1.04E+02	1.94E+04	1.33E+04	3.28E+04

A.T. Luksic, Battelle PNL Letter Report LLYMP 9104248

TABLE III-E

1,000 Year Radioactivity in Non-Fuel Bearing Components
Ci

Isotope	SS	Inc	Zr-4	Total
BE 10	1.31E-06	0.00E+00	0.00E+00	1.31E-06
C 14	1.07E+01	3.44E+02	6.23E+03	6.58E+03
CL 36	1.08E-02	3.46E-01	1.03E+02	1.03E+02
NI 59	2.10E+01	4.18E+03	4.26E+01	4.24E+03
CO 60	0.00E+00	0.00E+00	0.00E+00	0.00E+00
NI 63	1.65E+00	3.07E+02	3.61E+00	3.12E+02
SR 90	0.00E+00	0.00E+00	0.00E+00	0.00E+00
Y 90	0.00E+00	0.00E+00	0.00E+00	0.00E+00
ZR 93	0.00E+00	9.35E-03	2.77E+03	2.77E+03
NB 93M	0.00E+00	8.88E-03	2.63E+03	2.63E+03
NB 94	8.35E-02	1.46E+03	9.63E+02	2.43E+03
MO 93	0.00E+00	2.45E+01	0.00E+00	2.45E+01
TC 99	0.00E+00	1.24E+00	0.00E+00	1.24E+00
SN121M	0.00E+00	0.00E+00	1.10E-02	1.10E-02
Total	3.35E+01	6.32E+03	1.27E+04	1.91E+04

TABLE III-F

2,000 Year Radioactivity in Non-Fuel Bearing Components
Ci

Isotope	SS	Inc	Zr-4	Total
BE 10	1.31E-06	0.00E+00	0.00E+00	1.31E-06
C 14	9.47E+00	3.05E+02	5.52E+03	5.83E+03
CL 36	1.08E-02	3.46E-01	1.03E+02	1.03E+02
NI 59	2.09E+01	4.14E+03	4.22E+01	4.20E+03
CO 60	0.00E+00	0.00E+00	0.00E+00	0.00E+00
NI 63	8.80E-04	1.64E-01	1.93E-03	1.67E-01
SR 90	0.00E+00	0.00E+00	0.00E+00	0.00E+00
Y 90	0.00E+00	0.00E+00	0.00E+00	0.00E+00
ZR 93	0.00E+00	9.35E-03	2.77E+03	2.77E+03
NB 93M	0.00E+00	8.88E-03	2.63E+03	2.63E+03
NB 94	8.07E-02	1.41E+03	9.30E+02	2.34E+03
MO 93	0.00E+00	2.01E+01	0.00E+00	2.01E+01
TC 99	0.00E+00	1.24E+00	0.00E+00	1.24E+00
SN121M	0.00E+00	0.00E+00	1.04E-08	1.04E-08
Total	3.04E+01	5.88E+03	1.20E+04	1.79E+04

A.T. Luksic, Battelle PNL Letter Report LLYMP 9104248

TABLE III-G

5,000 Year Radioactivity in Non-Fuel Bearing Components
Ci

Isotope	SS	Inc	Zr-4	Total
BE 10	1.31E-06	0.00E+00	0.00E+00	1.31E-06
C 14	6.59E+00	2.12E+02	3.84E+03	4.06E+03
CL 36	1.07E-02	3.43E-01	1.02E+02	1.03E+02
NI 59	2.03E+01	4.03E+03	4.11E+01	4.10E+03
CO 60	0.00E+00	0.00E+00	0.00E+00	0.00E+00
NI 63	1.34E-13	2.51E-11	2.95E-13	2.55E-11
SR 90	0.00E+00	0.00E+00	0.00E+00	0.00E+00
Y 90	0.00E+00	0.00E+00	0.00E+00	0.00E+00
ZR 93	0.00E+00	9.33E-03	2.76E+03	2.76E+03
NB 93M	0.00E+00	8.87E-03	2.62E+03	2.62E+03
NB 94	7.28E-02	1.28E+03	8.40E+02	2.12E+03
MO 93	0.00E+00	1.11E+01	0.00E+00	1.11E+01
TC 99	0.00E+00	1.23E+00	0.00E+00	1.23E+00
SN121M	0.00E+00	0.00E+00	0.00E+00	0.00E+00
Total	2.70E+01	5.54E+03	1.02E+04	1.58E+04

TABLE III-H

10,000 Year Radioactivity in Non-Fuel Bearing Components
Ci

Isotope	SS	Inc	Zr-4	Total
BE 10	1.30E-06	0.00E+00	0.00E+00	1.30E-06
C 14	3.60E+00	1.16E+02	2.10E+03	2.22E+03
CL 36	1.06E-02	3.39E-01	1.01E+02	1.01E+02
NI 59	1.95E+01	3.86E+03	3.94E+01	3.92E+03
CO 60	0.00E+00	0.00E+00	0.00E+00	0.00E+00
NI 63	0.00E+00	0.00E+00	0.00E+00	0.00E+00
SR 90	0.00E+00	0.00E+00	0.00E+00	0.00E+00
Y 90	0.00E+00	0.00E+00	0.00E+00	0.00E+00
ZR 93	0.00E+00	9.31E-03	2.76E+03	2.76E+03
NB 93M	0.00E+00	8.85E-03	2.62E+03	2.62E+03
NB 94	6.14E-02	1.08E+03	7.08E+02	1.78E+03
MO 93	0.00E+00	4.12E+00	0.00E+00	4.12E+00
TC 99	0.00E+00	1.21E+00	0.00E+00	1.21E+00
SN121M	0.00E+00	0.00E+00	0.00E+00	0.00E+00
Total	2.31E+01	5.06E+03	8.32E+03	1.34E+04

A.T. Luksic, Battelle PNL Letter Report LLYMP 9104248

TABLE III-I

100,000 Year Radioactivity in Non-Fuel Bearing Components
Ci

Isotope	SS	Inc	Zr-4	Total
BE 10	1.25E-06	0.00E+00	0.00E+00	1.25E-06
C 14	6.72E-05	2.16E-03	3.91E-02	4.14E-02
CL 36	8.63E-03	2.76E-01	8.21E+01	8.24E+01
NI 59	8.93E+00	1.77E+03	1.81E+01	1.80E+03
CO 60	0.00E+00	0.00E+00	0.00E+00	0.00E+00
NI 63	0.00E+00	0.00E+00	0.00E+00	0.00E+00
SR 90	0.00E+00	0.00E+00	0.00E+00	0.00E+00
Y 90	0.00E+00	0.00E+00	0.00E+00	0.00E+00
ZR 93	0.00E+00	8.94E-03	2.65E+03	2.65E+03
NB 93M	0.00E+00	8.50E-03	2.51E+03	2.51E+03
NB 94	2.84E-03	4.98E+01	3.28E+01	8.25E+01
MO 93	0.00E+00	7.42E-08	0.00E+00	7.42E-08
TC 99	0.00E+00	9.00E-01	0.00E+00	9.00E-01
SN121M	0.00E+00	0.00E+00	0.00E+00	0.00E+00
Total	8.94E+00	1.82E+03	5.29E+03	7.13E+03

TABLE III-J

1 Million Year Radioactivity in Non-Fuel Bearing Components
Ci

Isotope	SS	Inc	Zr-4	Total
BE 10	8.50E-07	0.00E+00	0.00E+00	8.50E-07
C 14	0.00E+00	0.00E+00	0.00E+00	0.00E+00
CL 36	1.09E-03	3.47E-02	1.03E+01	1.04E+01
NI 59	3.66E-03	7.27E-01	7.42E-03	7.39E-01
CO 60	0.00E+00	0.00E+00	0.00E+00	0.00E+00
NI 63	0.00E+00	0.00E+00	0.00E+00	0.00E+00
SR 90	0.00E+00	0.00E+00	0.00E+00	0.00E+00
Y 90	0.00E+00	0.00E+00	0.00E+00	0.00E+00
ZR 93	0.00E+00	5.95E-03	1.76E+03	1.76E+03
NB 93M	0.00E+00	5.65E-03	1.67E+03	1.67E+03
NB 94	1.28E-16	2.24E-12	1.48E-12	3.72E-12
MO 93	0.00E+00	0.00E+00	0.00E+00	0.00E+00
TC 99	0.00E+00	4.81E-02	0.00E+00	4.81E-02
SN121M	0.00E+00	0.00E+00	0.00E+00	0.00E+00
Total	4.75E-03	8.22E-01	3.44E+03	3.44E+03

A.T. Luksic, Battelle PNL Letter Report LLYMP 9104248

Table IV

Spent Fuel Activity Inventory
CI

Time	PWR	BWR	Total
Discharge	9.94E+12	4.06E+12	1.40E+13
100 Years	2.27E+09	9.31E+08	3.20E+09
200 Years	4.47E+08	1.88E+08	6.35E+08
500 Years	1.64E+08	7.25E+07	2.37E+08
1,000 Years	9.75E+07	4.33E+07	1.41E+08
2,000 Years	5.40E+07	2.41E+07	7.81E+07
5,000 Years	3.57E+07	1.60E+07	5.17E+07
10,000 Years	2.59E+07	1.17E+07	3.76E+07
100,000 Years	2.64E+06	1.14E+06	3.78E+06
1 Million Yrs	1.08E+06	4.67E+05	1.54E+06

A.T. Luksic, Battelle PNL Letter Report LLYMP 9104248

References

1 SR/CNEAF/90-01, Spent Nuclear Fuel Discharges from U.S. Reactors 1988, prepared by the Energy Information Administration, U.S. Department of Energy, March 1990.

2 DOE/RW-0184, Characteristics of Spent Fuel, High-Level Waste, and Other Radioactive Wastes Which May Require Long-Term Isolation, prepared by Oak Ridge National Laboratory, December 1987.

3 ORNL/Sub/86-SA094/8, Acceptance of Non-Fuel Assembly Hardware by the Federal Waste Management System, prepared by E.R. Johnson Associates,Inc., March 1990.

4 PNL-6046, Spent Fuel Disassembly Hardware and Other Non-Fuel Bearing Components: Characterization, Disposal Cost Estimates, and Proposed Repository Acceptance Criteria, A.T. Luksic, et al, October 1986

5 PNL-6906, Spent Fuel Assembly Hardware: Characterization and 10CFR61 Classification for Waste Disposal, A.T. Luksic, et al, June 1989.

2.2 Glass Waste Form

2.2.1 Radionuclide Content

2.2.1.1 Present Inventory

2.2.1.2 Projected Inventory

2.2.1.3 Radioactivity and Decay Heat vs. Time

2.2.1.4 Glass Species Composition Statistics

2.2.1.5 Fracture/Fragmentation Statistics

2.2.2 Repository Response

2.2.2.1 Gaseous Release from Glass

2.2.2.2 Dissolution Radionuclide Release from Glass

2.2.2.3 Soluble-Precipitated/Colloidal Species

2.2 Glass Waste Form

The glass form is the most probable disposal form for the various High-Level Wastes (HLW) other than Spent Fuel. HLW originates from domestic fuel reprocessing plants that are both commercial and defense related.

2.2 Glass Waste Form

2.2.1 Radionuclide Content

2.2.1.1 Present Inventory

2.2.1.2 Projected Inventory

2.2.1.3 Radioactivity and Decay Heat vs. Time

2.2.1.4 Glass Species Composition Statistics

2.2.1.5 Fracture/Fragmentation Statistics

2.2.2 Repository Response

2.2.2.1 Gaseous Release from Glass

2.2.2.2 Dissolution Radionuclide Release from Glass

2.2.2.3 Soluble-Precipitated/Colloidal Species

2.2 Glass Waste Form

2.2.1 Radionuclide Content

2.2.1.1 Present Inventory

2.2.1.2 Projected Inventory

2.2.1.3 Radioactivity and Decay Heat vs. Time

2.2.1.4 Glass Species Composition Statistics

2.2.1.5 Fracture/Fragmentation Statistics

2.2.2 Repository Response

2.2.2.1 Gaseous Release from Glass

2.2.2.2 Dissolution Radionuclide Release from Glass

2.2.2.3 Soluble-Precipitated/Colloidal Species

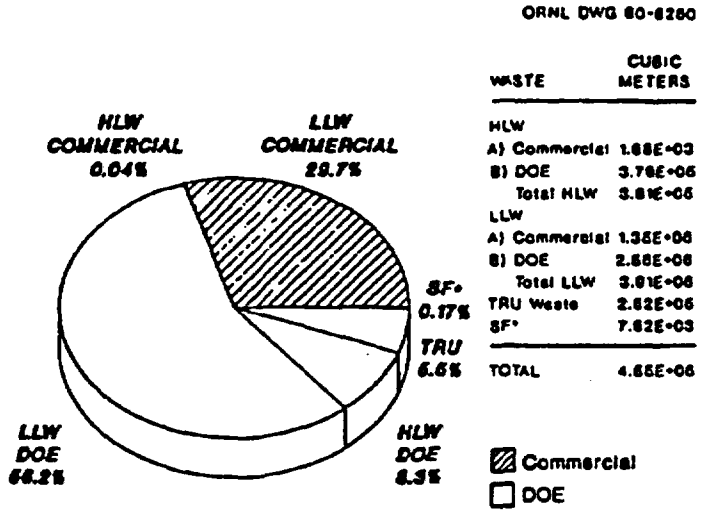

WASTE	CUBIC METERS
HLW	
A) Commercial	1.68E+03
B) DOE	3.76E+06
Total HLW	3.81E+06
LLW	
A) Commercial	1.35E+06
B) DOE	2.68E+06
Total LLW	3.91E+06
TRU Waste	2.62E+06
SF*	7.62E+03
TOTAL	4.65E+06

*Includes spacing between fuel assembly rods.
Does not include DOE spent fuel to be reprocessed.

Fig. 0.1. Volumes of commercial and DOE wastes and spent fuel accumulated through 1989.

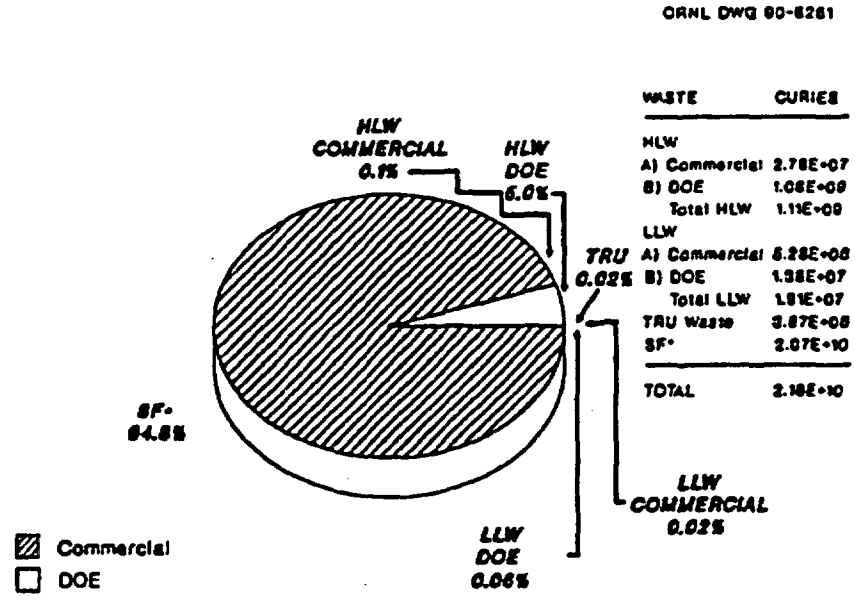

WASTE	CURIES
HLW	
A) Commercial	2.78E+07
B) DOE	1.06E+09
Total HLW	1.11E+09
LLW	
A) Commercial	5.28E+06
B) DOE	1.38E+07
Total LLW	1.91E+07
TRU Waste	3.87E+08
SF*	2.07E+10
TOTAL	2.16E+10

*Does not include DOE spent fuel to be reprocessed.

Fig. 0.2. Radioactivities of commercial and DOE wastes and spent fuel accumulated through 1989.

Integrated Data Base for 1990: U.S. Spent Fuel and Radioactive Waste Inventories, Projections, and Characteristics. USDOE/RW-0006 Rev. 6, October 1990.

Table 6.2. Dimensions, weights, and radioactivity of canisters

	West Valley Demonstration Project	Savannah River Site	Hanford Site	Idaho Nat'l Engineering Laboratory
Outside diameter, cm	61	61	61	61
Overall height, cm	300	300	300	300
Material	SS	SS	SS	SS
Wall thickness, mm	3.4	9.5	9.5	9.5
Weights (kg)				
Canister	252	500	500	500
Glass or ceramic	1900	1682	1650	1825
Total	2152	2182	2150	2325
Curies per canister[a]	114,700	234,400	298,000[b]	109,000
Watts per canister[a]	342	709	869[c]	339

[a]aThese are estimated maximum values from ORIGEN2 calculations based on radionuclide compositions supplied by the sites. Curies and watts shown are at time of filling the canister, except for West Valley Demonstration Project where the values shown are for the start of year 1992. For West Valley Demonstration Project, maximum values are assumed to be 110% of average values, and average values are based on the Revision 7 mass balance (Crocker 1989a). Maximum values for the defense sites do not necessarily represent initial operations.

[b]Based on Mitchell and Nelson 1988, maximum case.

[c]Based on ORIGEN2 calculations using Mitchell and Nelson maximum case.

K.J. Notz, T.D. Welch, R.S. Moore, and W.J. Reich, *Preliminary Waste Form Characteristics*, ORNL-TM-11681 (draft) September, 1990.

Table 6.3. West Valley Demonstration Project.
High-level waste form and canister characteristics[a]

Waste form	Borosilicate glass in sealed canister
Canister material	Stainless steel type 304L
Borosilicate glass density, g/cm^3 at 25°C	2.7
Weights per canister:	
Empty canister, kg	234
Cover, kg	18
Borosilicate glass, kg	1,900
Total loaded weight, kg	2,152
Canister dimensions:	
Outside diameter, cm	61
Height overall, cm	300
Wall thickness, cm	0.34
Radionuclide content, curies per canister (1992)[b]	
Average	104,300
Maximum[c]	114,700
Thermal power, watts per canister (1992)[b]	
Average	311
Maximum[c]	342

[a]Source: Crocker 1989a and ORNL calculations based on Rev. 7 mass balance.

[b]Quantities shown are at 85% fill. Curies and watts per canister are for the start of year 1992.

[c]Maximum activity is assumed to be 110% of average.

K.J. Notz, T.D. Welch, R.S. Moore, and W.J. Reich, *Preliminary Waste Form Characteristics*, ORNL-TM-11681 (draft) September, 1990.

Table 6.4. Savannah River Site. High-level waste form and canister characteristics[a]

	Canister 85% fill
Canister inside volume, m^3	0.736
Glass volume at average fill temperature (see note b), m^3	0.626
Glass density at average fill temperature (see note b), g/cm^3	2.69
Glass weight, kg	1,682
Canister weight, kg	500
Gross weight, kg	2,182
Total activity, curies	234,000[c]
Decay heat, watts	690[c]

[a]Sources: DWPF Basic Data Report, DPSP 80-1033, Rev. 91, April 1985

[b]The average fill temperature (i.e. the average temperature of the glass upon completion of filling to 85% of canister volume) is 825°C. The glass volume per canister when cooled to 25°C is about 0.59 m^3 . The density of the glass is about 2.69 g/cm3 at 825°C and 2.85 g/cm^3 at 25°C (SRP 1987).

[c]These figures are the ones given in DPSP 80-1033, Rev. 91. The corresponding figures calculated by ORIGEN2 are 234,400 Ci and 709W, as shown in Table 3.3.4. Activity and decay heat (thermal power) are at the time of filling the canister and are based on the maximum case, i.e. 5-yr old sludge and 15-yr old supernate.

K.J. Notz, T.D. Welch, R.S. Moore, and W.J. Reich, *Preliminary Waste Form Characteristics*, ORNL-TM-11681 (draft) September, 1990.

Table 6.5. Hanford Site. High-level waste form and canister characteristics[a]

Waste form	Borosilicate glass in sealed steel canister
Canister material	Type 304L stainless steel
Weights per canister	
Empty canister, kg	500
Borosilicate glass, kg	1650
Total loaded weight, kg	2150
Canister dimensions	
Outside diameter, cm	61
Height overall, cm	300
Wall thickness, cm	0.95
Inside volume, m^3	0.736
Glass volume at average fill temperature, m^3	0.626[b]
Radionuclide content, curies per canister[c]	
Nominal	137,000
Maximum	298,000
Thermal power, watts per canister[c]	
Nominal	389
Maximum	869

[a]Sources: Wolfe 1985, White 1986, Mitchell and Nelson 1988.

[b]Canister is filled to 85% of volume at average fill temperature of 825°C.

[c]All values shown are based on NCAW reference feed (neutralized current acid waste) with 25% wt waste oxide in glass. Activities and thermal power are at time of filling canister. Range of values shown is from Mitchell and Nelson 1988 in which estimated activities and radionuclide compositions were given for two NCAW feeds referred to as nominal and maximum. Radionuclide compositions are shown in Table 3.4.4.

K.J. Notz, T.D. Welch, R.S. Moore, and W.J. Reich, *Preliminary Waste Form Characteristics*, ORNL-TM-11681 (draft) September, 1990.

Table 6.6. Idaho National Engineering Laboratory. High level waste form and canister characteristics[a]

Waste form	Glass-ceramic blocks in sealed canister
Canister material	Stainless steel type 304L
Glass-ceramic density, g/cm³	3.2
Weights per canister:	
Empty canister, kg	500
Glass-ceramic, kg	1825
Total loaded weight, kg	2325
Waste loading in glass-ceramic, wt%	70[b]
Glass-ceramic volume per canister, m³	0.57[b]
Canister dimensions:	
Outside diameter, cm.	61
Height overall, cm.	300
Wall thickness, cm.	0.95
Radionuclide content, curies/canister	108,900[c]
Heat generation rate, watts/canister	339[c]

[a]Based on the following assumptions:

1. Glass-ceramic form is chosen for HLW immobilization. The term "glass-ceramic" denotes an immobilized waste form consisting of a glass phase dispersed in a ceramic phase.
2. Canister load is equivalent to 1277 kg calcine.
3. Calcine is 3 years old at time of immobilization.
4. Canister is similar in dimensions to DWPF canister.
5. Radionuclide content of calcine is as shown in IDO-10105 (see Table 3.5.3).

[b]Reference: Berreth 1987.

[c]At time of immobilization. Quantities shown are estimated maximum values; average values are expected to be considerably less.

K.J. Notz, T.D. Welch, R.S. Moore, and W.J. Reich, *Preliminary Waste Form Characteristics*, ORNL-TM-11681 (draft) September, 1990.

2.2 Glass Waste Form

2.2.1 Radionuclide Content

2.2.1.1 Present Inventory

2.2.1.2 Projected Inventory

2.2.1.3 Radioactivity and Decay Heat vs. Time

2.2.1.4 Glass Species Composition Statistics

2.2.1.5 Fracture/Fragmentation Statistics

2.2.2 Repository Response

2.2.2.1 Gaseous Release from Glass

2.2.2.2 Dissolution Radionuclide Release from Glass

2.2.2.3 Soluble-Precipitated/Colloidal Species

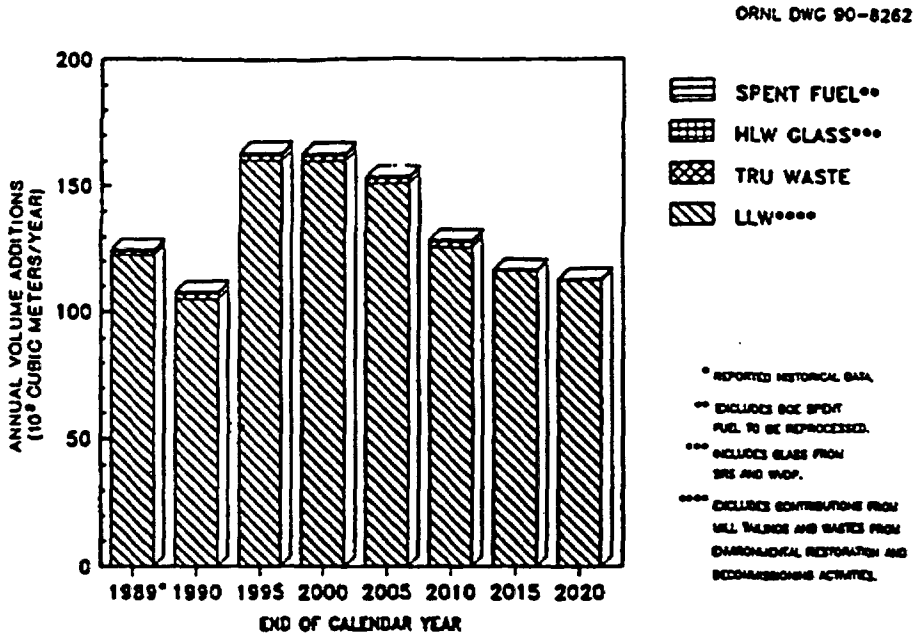

Fig. 0.3. Projections of annual volume additions for various wastes and spent fuel – DOE and commercial fuel cycle.

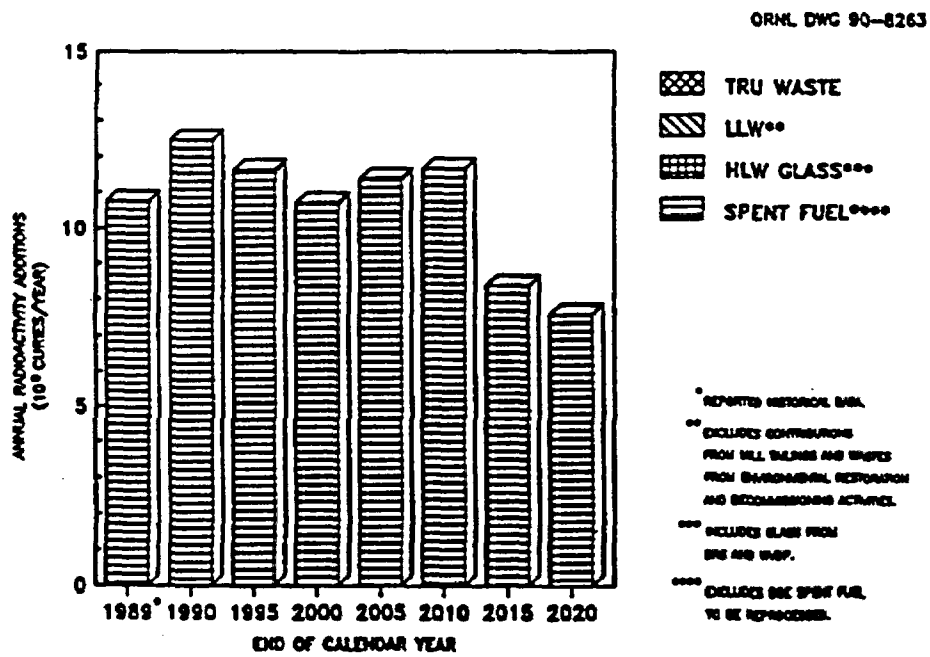

Fig. 0.4. Projections of annual radioactivity additions for various wastes and spent fuel – DOE and commercial fuel cycle.

Integrated Data Base for 1990: U.S. Spent Fuel and Radioactive Waste Inventories, Projections, and Characteristics. USDOE/RW-0006 Rev. 6, October 1990.

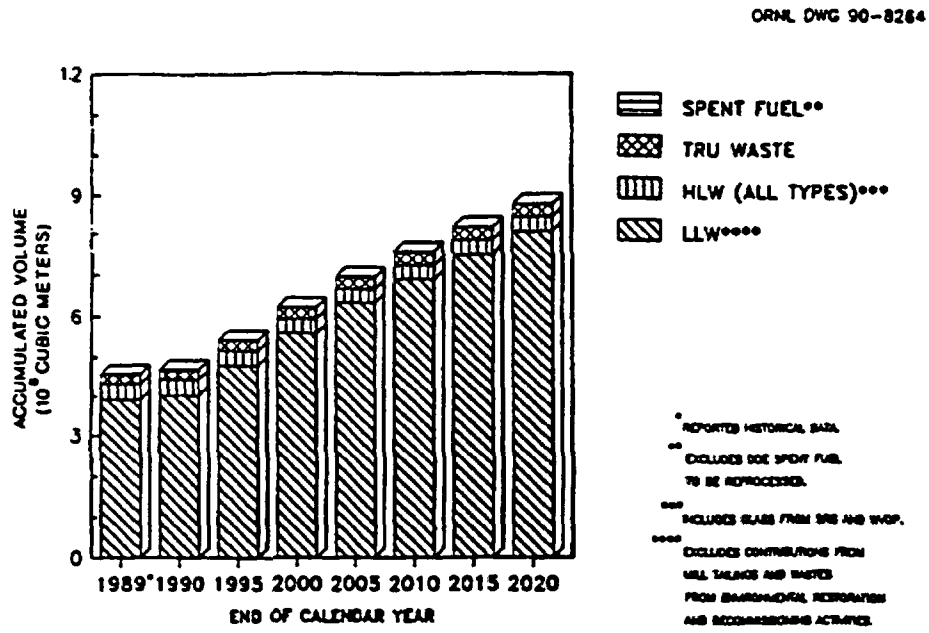

Fig. 0.5. Projections of accumulated volumes for various wastes and spent fuel – DOE and commercial fuel cycle.

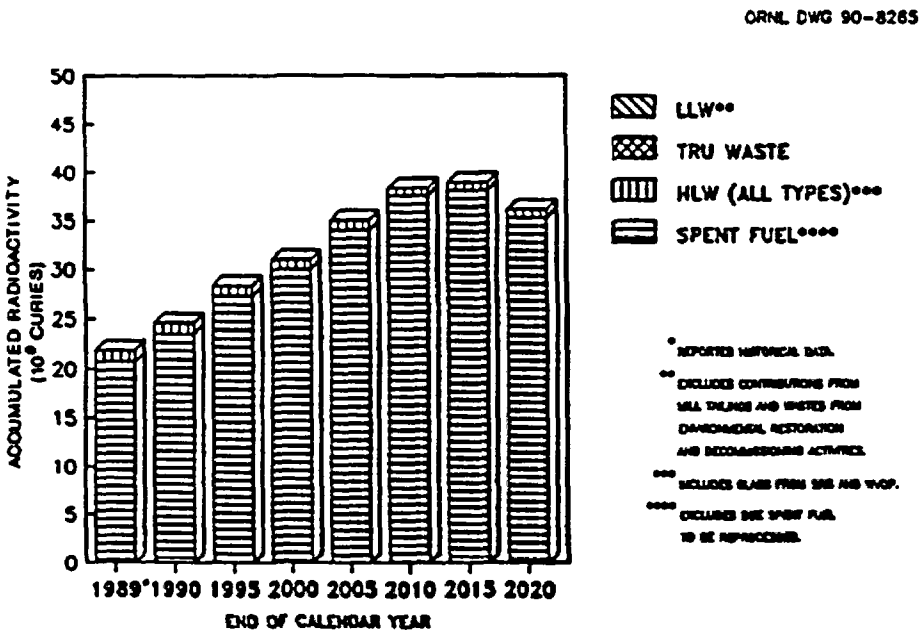

Fig. 0.6. Projections of accumulated radioactivity for various wastes and spent fuel – DOE and commercial fuel cycle.

Integrated Data Base for 1990: U.S. Spent Fuel and Radioactive Waste Inventories, Projections, and Characteristics. USDOE/RW-0006 Rev. 6, October 1990.

Table 6.7. Projected annual number of canisters of immobilized HLW produced at each site[a,b]

Calendar year	WVDP	SRS	Hanford	INEL	Total
1989	0	0	0	0	0
1990	0	0	0	0	0
1991	0	0	0	0	0
1992	0	136	0	0	136
1993	25	308	0	0	333
1994	200	376	0	0	576
1995	50	410	0	0	460
1996	0	410	0	0	410
1997	0	383	0	0	383
1998	0	369	0	0	369
1999	0	369	0	0	369
2000	0	342	240	0	582
2001	0	342	370	0	712
2002	0	342	345	0	687
2003	0	342	185	0	527
2004	0	302	370	0	672
2005	0	273	370	0	643
2006	0	273	80	0	353
2007	0	273	0	0	273
2008	0	32	0	0	32
2009	0	0	0	0	0
2010	0	0	0	0	0
2011	0	0	0	0	0
2012	0	0	0	500	500
2013	0	0	0	600	600
2014	0	0	0	700	700
2015	0	0	0	1000	1000
2016	0	0	0	1000	1000
2017	0	0	0	1000	1000
2018	0	0	0	1000	1000
2019	0	0	0	1000	1000
2020	0	0	0	1000	1000
Total	275	5282	1960	7800	15,317

[a]Sources: WVDP - Crocker 1989, 1989a, 1990
SRS - Garvin 1990
HANF - Turner 1990
INEL - Berreth 1990

[b]For assumptions used in compiling this table see Table 3.1.4. This table represents the 1990 Base Case for this report. Canisters produced after 2020 are not included here. Canister production figures represent most likely estimates rather than maximum potential.

K.J. Notz, T.D. Welch, R.S. Moore, and W.J. Reich, *Preliminary Waste Form Characteristics*, ORNL-TM-11681 (draft) September, 1990.

Figure 6.1 Annual Canister Production for each Site

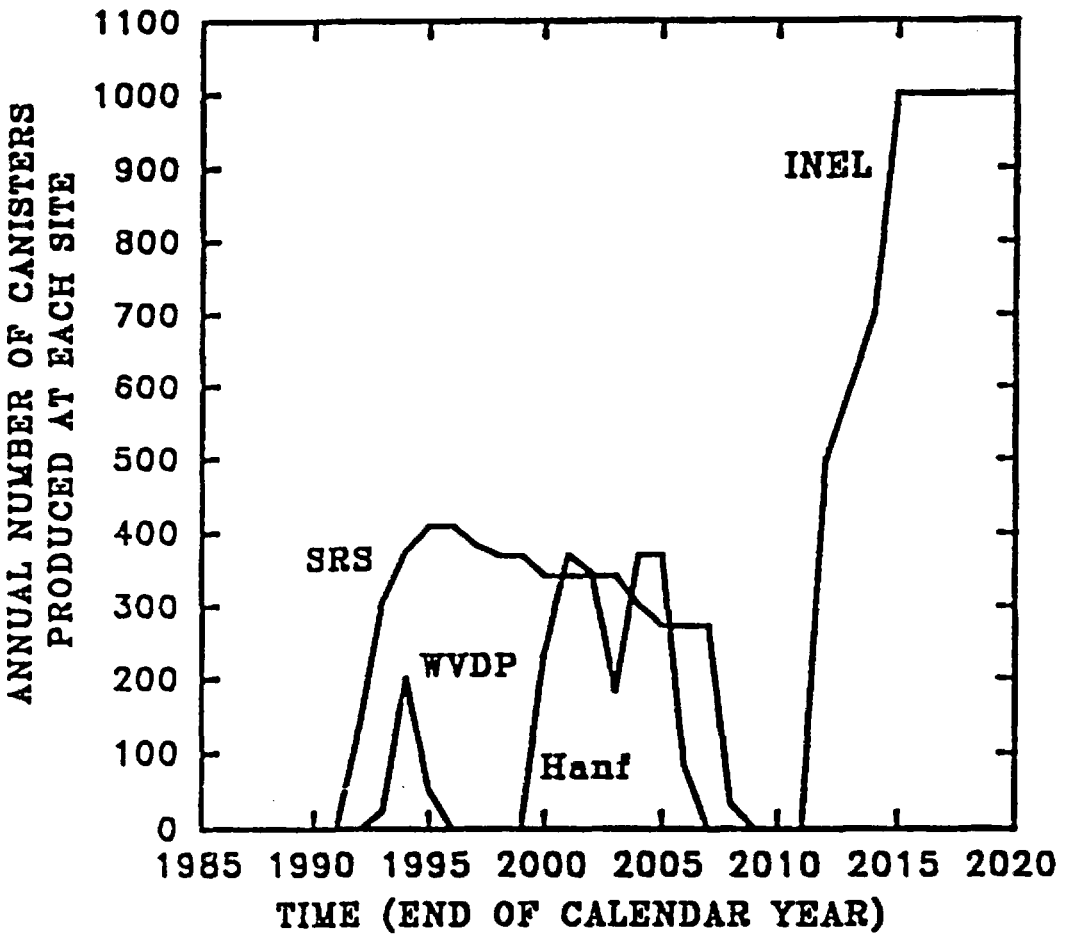

K.J. Notz, T.D. Welch, R.S. Moore, and W.J. Reich, *Preliminary Waste Form Characteristics*, ORNL-TM-11681 (draft) September, 1990.

Figure 6.2 Total Annual Canister Production

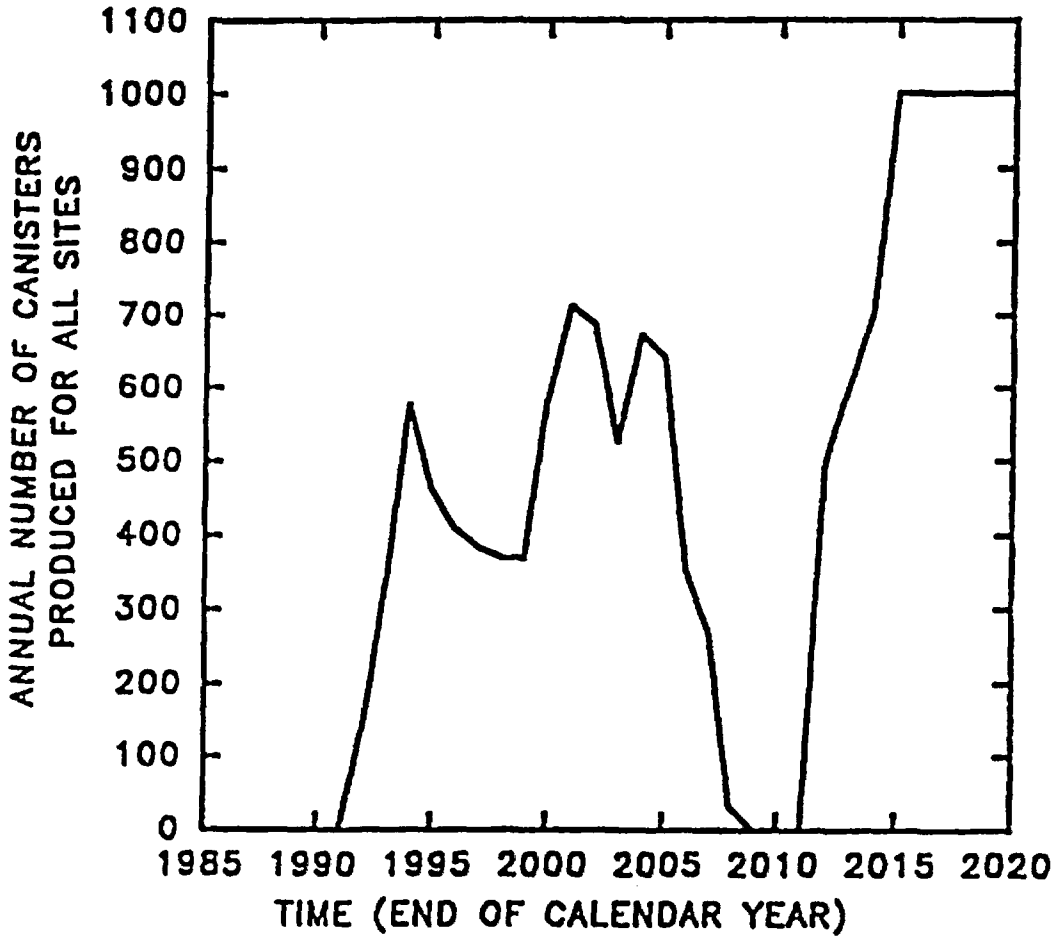

K.J. Notz, T.D. Welch, R.S. Moore, and W.J. Reich, *Preliminary Waste Form Characteristics*, ORNL-TM-11681 (draft) September, 1990.

Table 6.8. Projected cumulative production of canisters of immobilized HLW at each site[a,b]

Calendar year	WVDP	SRP	Hanford	INEL	Total
1989	0	0	0	0	0
1990	0	0	0	0	0
1991	0	0	0	0	0
1992	0	136	0	0	136
1993	25	444	0	0	469
1994	225	820	0	0	1045
1995	275	1230	0	0	1505
1996	275	1640	0	0	1915
1997	275	2023	0	0	2298
1998	275	2392	0	0	2667
1999	275	2761	0	0	3036
2000	275	3103	240	0	3618
2001	275	3445	610	0	4330
2002	275	3787	955	0	5017
2003	275	4129	1140	0	5544
2004	275	4431	1510	0	6216
2005	275	4704	1880	0	6859
2006	275	4977	1960	0	7212
2007	275	5250	1960	0	7485
2008	275	5282	1960	0	7517
2009	275	5282	1960	0	7517
2010	275	5282	1960	0	7517
2011	275	5282	1960	0	7517
2012	275	5282	1960	500	8017
2013	275	5282	1960	1100	8617
2014	275	5282	1960	1800	9317
2015	275	5282	1960	2800	10317
2016	275	5282	1960	3800	11317
2017	275	5282	1960	4800	12317
2018	275	5282	1960	5800	13317
2019	275	5282	1960	6800	14317
2020	275	5282	1960	7800	15317

[a]Sources: WVDP - Crocker 1989, 1989a, 1990.
SRS - Garvin 1990.
HANF - Turner 1990.
INEL - Berreth 1990.

[b]For assumptions used in compiling this table see Table 3.1.4. This table represents the 1990 Base Case for this report. Canisters produced after 2020 are not included here. Canister production figures represent most likely estimates rather than maximum potential.

K.J. Notz, T.D. Welch, R.S. Moore, and W.J. Reich, *Preliminary Waste Form Characteristics*, ORNL-TM-11681 (draft) September, 1990.

Figure 6.3 Cumulative Canister Production for each Site

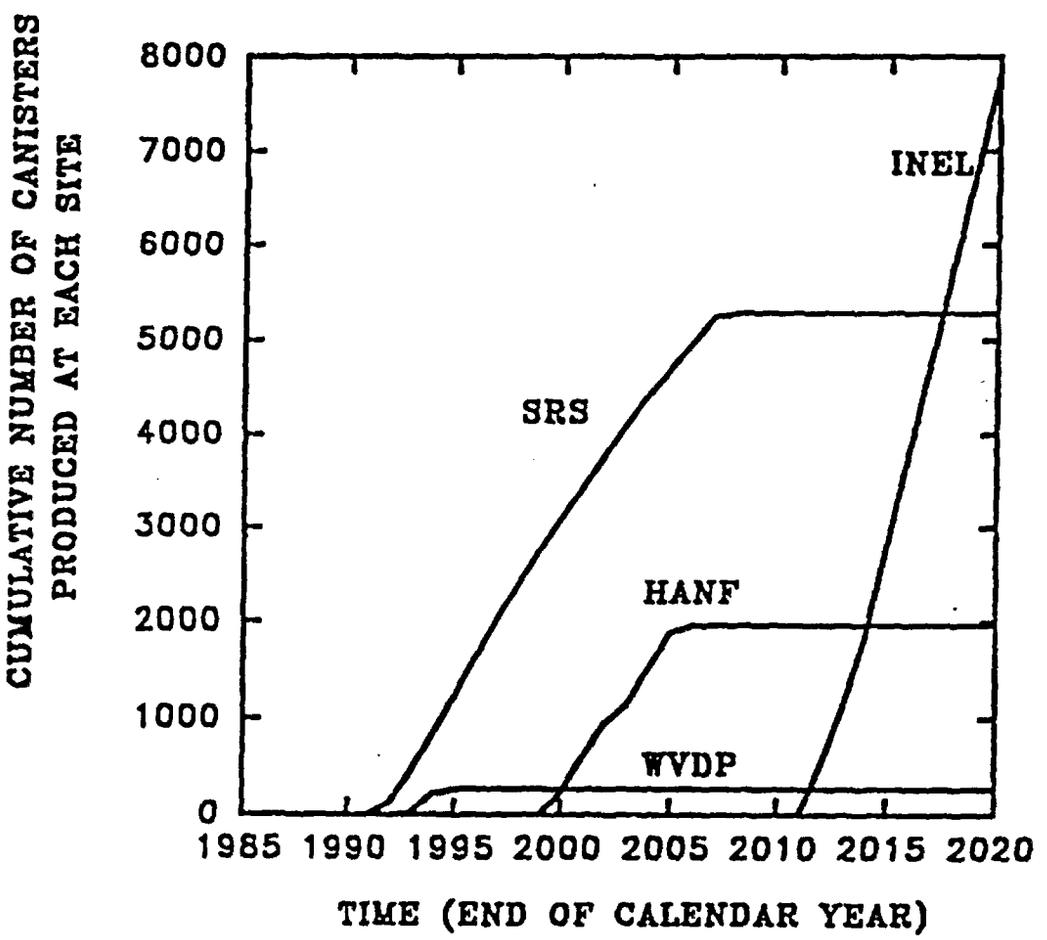

K.J. Notz, T.D. Welch, R.S. Moore, and W.J. Reich, *Preliminary Waste Form Characteristics*, ORNL-TM-11681 (draft) September, 1990.

Figure 6.4 Cumulative Canister Production for all Sites

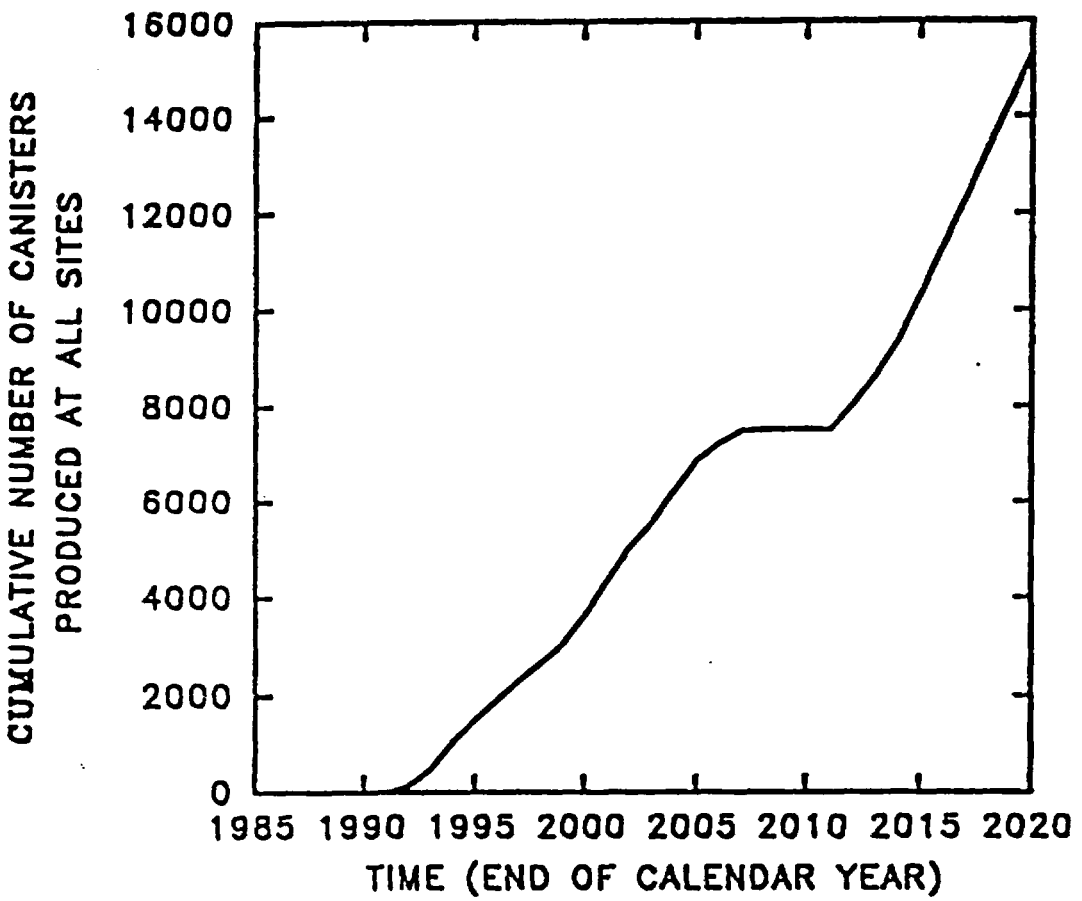

K.J. Notz, T.D. Welch, R.S. Moore, and W.J. Reich, *Preliminary Waste Form Characteristics*, ORNL-TM-11681 (draft) September, 1990.

2.2 Glass Waste Form

2.2.1 Radionuclide Content

2.2.1.1 Present Inventory

2.2.1.2 Projected Inventory

2.2.1.3 Radioactivity and Decay Heat vs. Time

2.2.1.4 Glass Species Composition Statistics

2.2.1.5 Fracture/Fragmentation Statistics

2.2.2 Repository Response

2.2.2.1 Gaseous Release from Glass

2.2.2.2 Dissolution Radionuclide Release from Glass

2.2.2.3 Soluble-Precipitated/Colloidal Species

Figure 6.5 Radioactivity and Thermal Power Per Canister

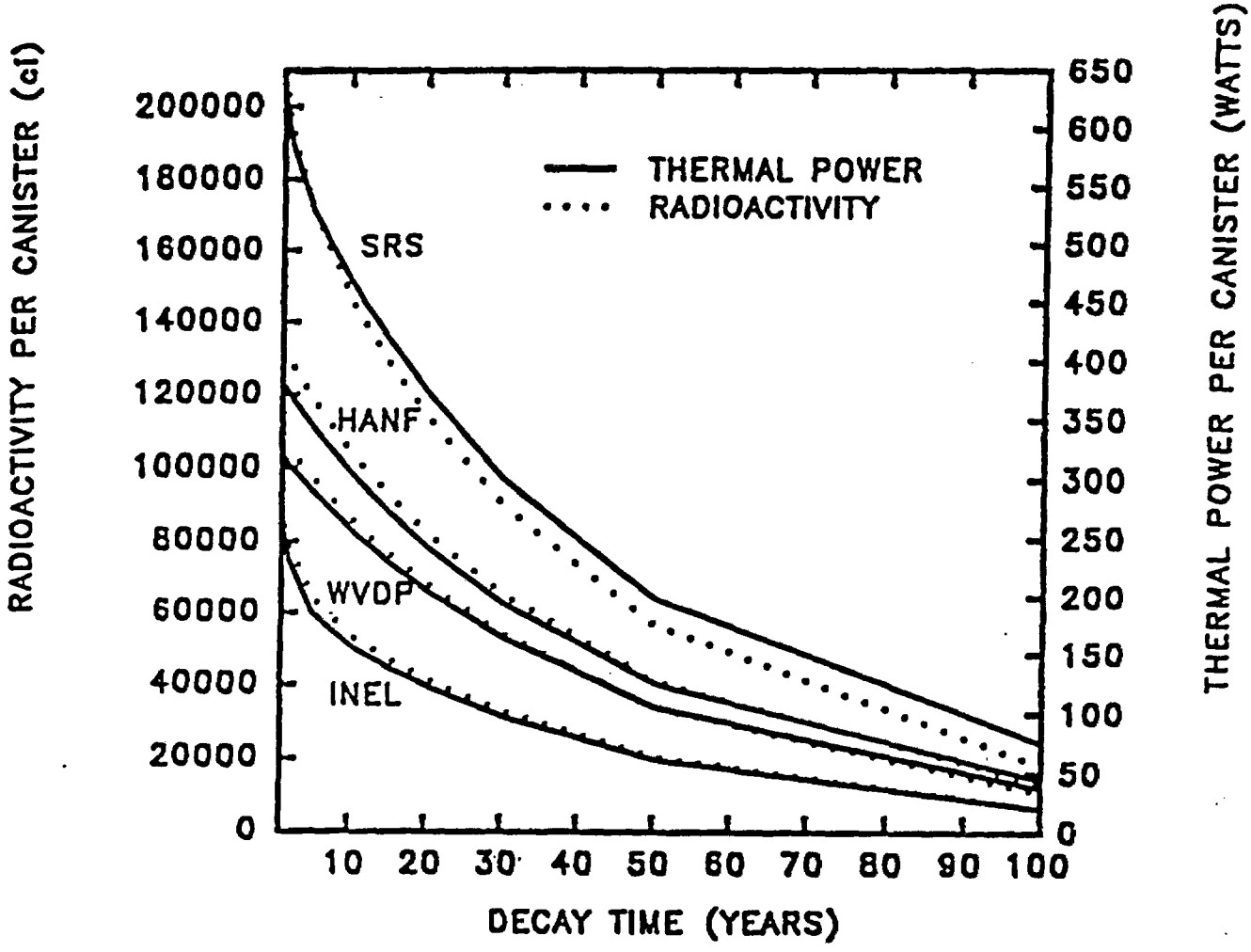

. K.J. Notz, T.D. Welch, R.S. Moore, and W.J. Reich, *Preliminary Waste Form Characteristics*, ORNL-TM-11681 (draft) September, 1990.

Table 6.9. West Valley Demonstration Project. Calculated radioactivity and thermal power per HLW canister[a]

Decay time after 1990, years	Average radioactivity per canister (Ci)	Average thermal power per canister (W)
0	109,600	326
1	106,900	319
2	104,300	311
5	97,080	290
10	86,230	258
15	76,660	230
20	68,180	205
30	53,970	164
50	33,890	105
100	10,730	37
200	1,260	8.9
300	291	5.4
350	202	4.8
500	128	3.7
1,000	63	1.9
1,050	60	1.8
2,000	26.7	0.70
5,000	15.8	0.33
10,000	13.2	0.26
20,000	10.3	0.18
50,000	6.8	0.08
100,000	5.2	0.04
500,000	3.8	0.04
1,000,000	3.1	0.03

[a]Calculations made with ORIGEN2 code based on data supplied by WVDP (Crocker 1989). Canister contains 1900 kg of HLW glass. Initial time point (0 years) is at the start of year 1990. The material balance used by WVDP for this case (Revision 7, October 1989) shows 484,000 kg of total glass and a total radioactivity of 27.9×10^6 Ci at the start of year 1990 in the HLW to be vitrified. Data are for the average canister and do not take into account possible variations in melter feed and fill level.

K.J. Notz, T.D. Welch, R.S. Moore, and W.J. Reich, *Preliminary Waste Form Characteristics*, ORNL-TM-11681 (draft) September, 1990.

Figure 6.6 Radioactivity and Thermal Power Per Canister.

WEST VALLEY DEMONSTRATION PROJECT

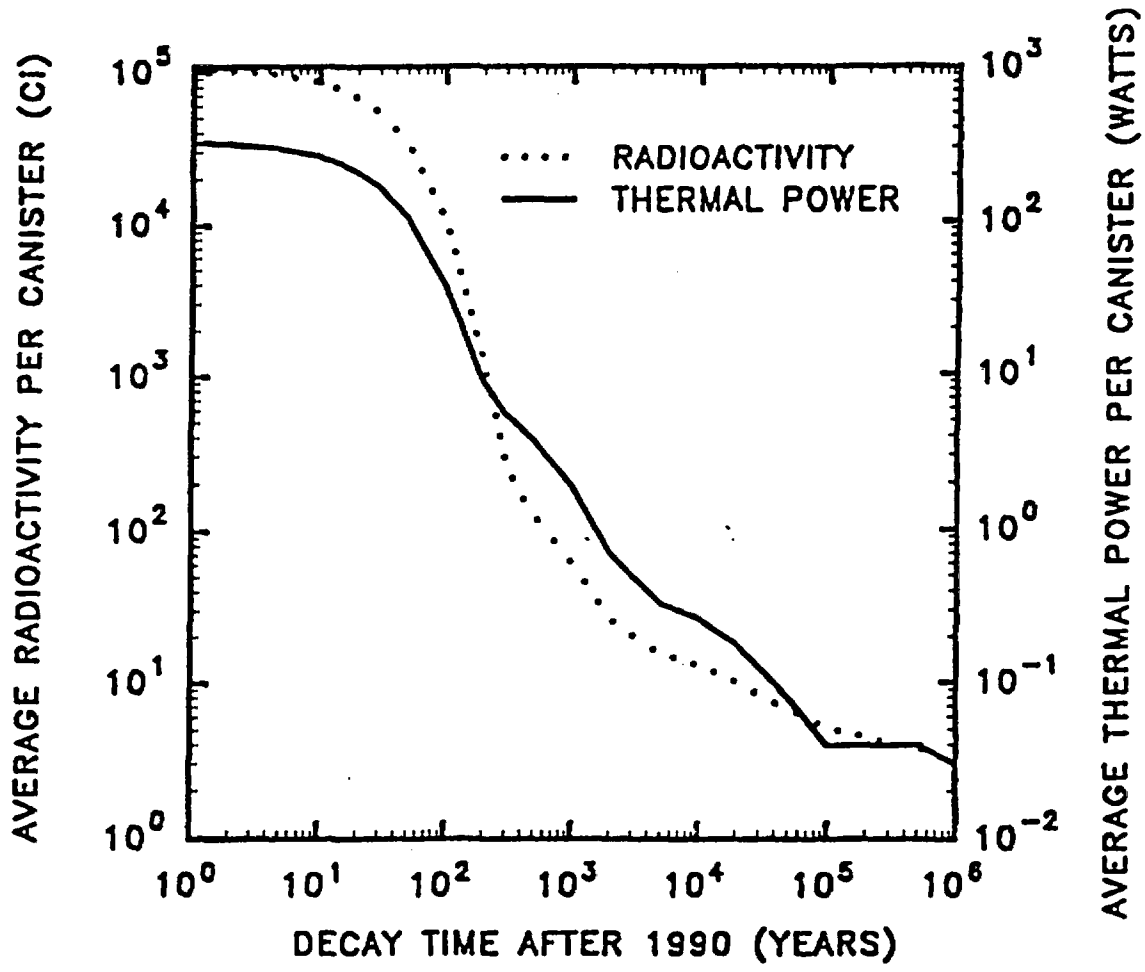

K.J. Notz, T.D. Welch, R.S. Moore, and W.J. Reich, *Preliminary Waste Form Characteristics*, ORNL-TM-11681 (draft) September, 1990.

Table 6.10. Savannah River Site. Calculated radioactivity and thermal power per HLW canister.[a]

Decay time, years[b]	Radioactivity per canister (Ci)[c]	Thermal power per canister (W)[c]
0	234,400	709
1	208,500	627
2	193,800	586
5	169,300	527
10	145,800	467
15	128,400	418
20	113,900	374
30	90,000	301
50	56,500	198
100	17,900	75
200	2,100	17
300	390	7.2
350	227	5.2
500	95	2.7
1,000	42	1.1
1,050	41	1.1
2,000	29	0.72
5,000	24	0.54
10,000	20	0.43
20,000	16	0.30
50,000	11	0.16
100,000	9.2	0.11
500,000	4.8	0.05
1,000,000	2.4	0.02

[a]Based on 5-yr cooled sludge and 15-yr cooled supernate. Calculations made by ORIGEN2 code based on data supplied by SRS (Basic Data Report, DPSP-80-1033, Rev. 91, April 1985). Canister is filled to 85% of capacity and contains 1682 kg of glass.

[b]Years after vitrification.

[c]Radioactivity and thermal power include contributions of actinides and activation products as well as fission products.

K.J. Notz, T.D. Welch, R.S. Moore, and W.J. Reich, *Preliminary Waste Form Characteristics*, ORNL-TM-11681 (draft) September, 1990.

Figure 6.7 Radioactivity and Thermal Power Per Canister.

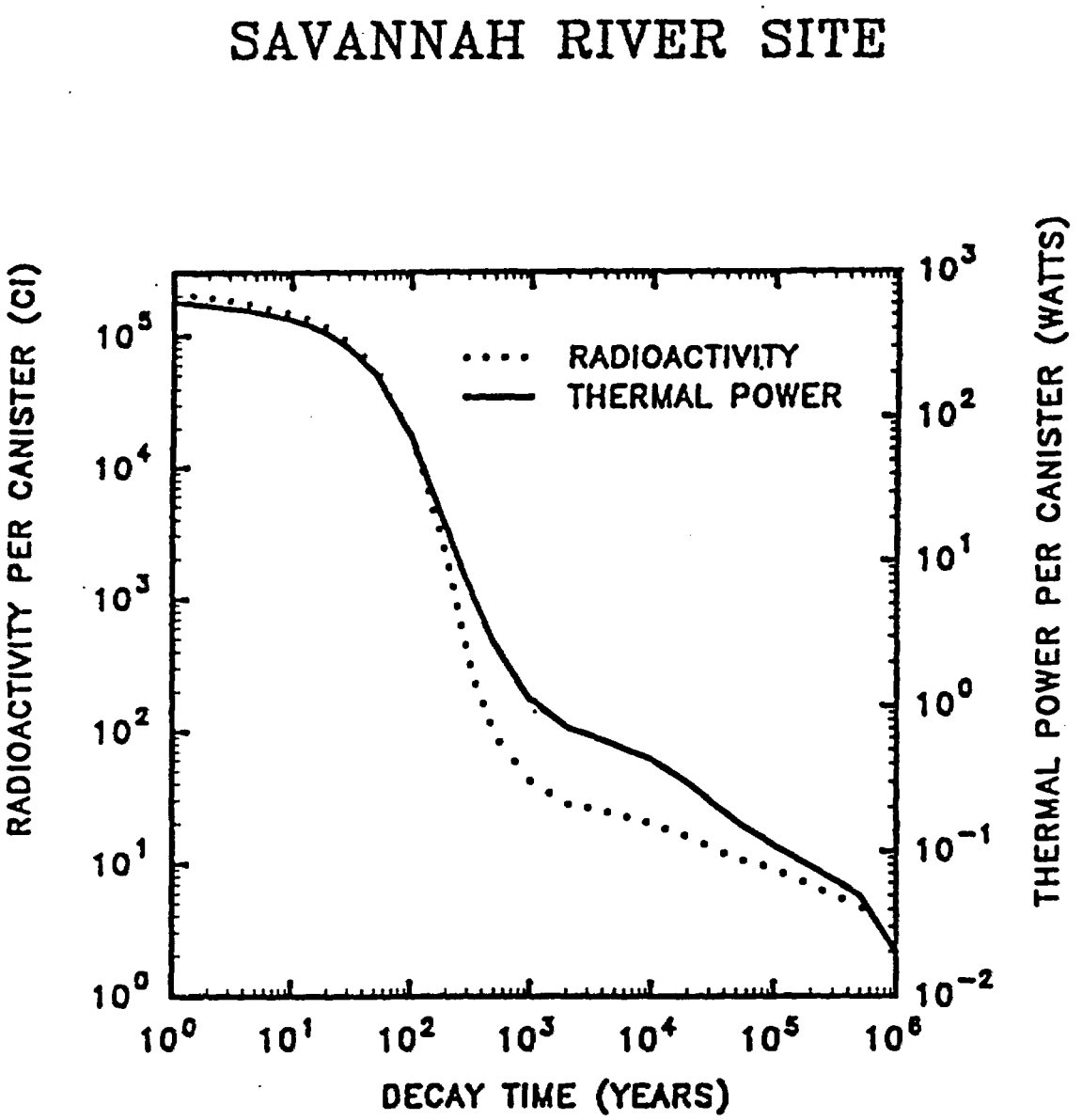

K.J. Notz, T.D. Welch, R.S. Moore, and W.J. Reich, *Preliminary Waste Form Characteristics*, ORNL-TM-11681 (draft) September, 1990.

Table 6.11. Hanford Site. Calculated radioactivity and thermal power per HLW canister[a]

Decay time, years[b]	Radioactivity per canister (Ci)		Thermal power per canister (W)	
	Nominal	Maximum	Nominal	Maximum
0	136,900	298,300	389	869
1	132,600	243,600	380	683
2	128,500	214,600	370	595
5	118,200	177,100	344	502
10	104,200	149,400	306	439
15	92,500	131,000	273	391
20	82,300	116,100	243	349
30	65,200	91,900	194	279
50	41,000	57,800	125	181
100	13,100	18,500	44	67
200	1,570	2,310	10	19
300	375	621	6.2	12
350	260	454	5.6	11
500	157	295	4.3	8.7
1,000	70	133	2.0	3.9
1,050	66	123	1.8	3.6
2,000	24	39	0.44	0.86
5,000	12	16	0.06	0.08
10,000	12	15	0.05	0.06
20,000	11	14	0.04	0.05
50,000	10	13	0.03	0.04
100,000	9.2	12	0.03	0.04
500,000	5.3	7.0	0.05	0.07
1,000,000	3.6	4.9	0.04	0.07

[a]Calculations made by ORIGEN2 code based on data supplied by HANF (Mitchell and Nelson 1988). Canister is filled to 85% of capacity and contains 1650 kg of HLW glass made from neutralized current acid waste (NCAW). Data are shown for two cases, the nominal case and the maximum case. The maximum case is based on a 21-month cooling time from fuel reprocessing to HWVP.

[b]Years after vitrification.

K.J. Notz, T.D. Welch, R.S. Moore, and W.J. Reich, *Preliminary Waste Form Characteristics*, ORNL-TM-11681 (draft) September, 1990.

Figure 6.8 Radioactivity and Thermal Power Per Canister.

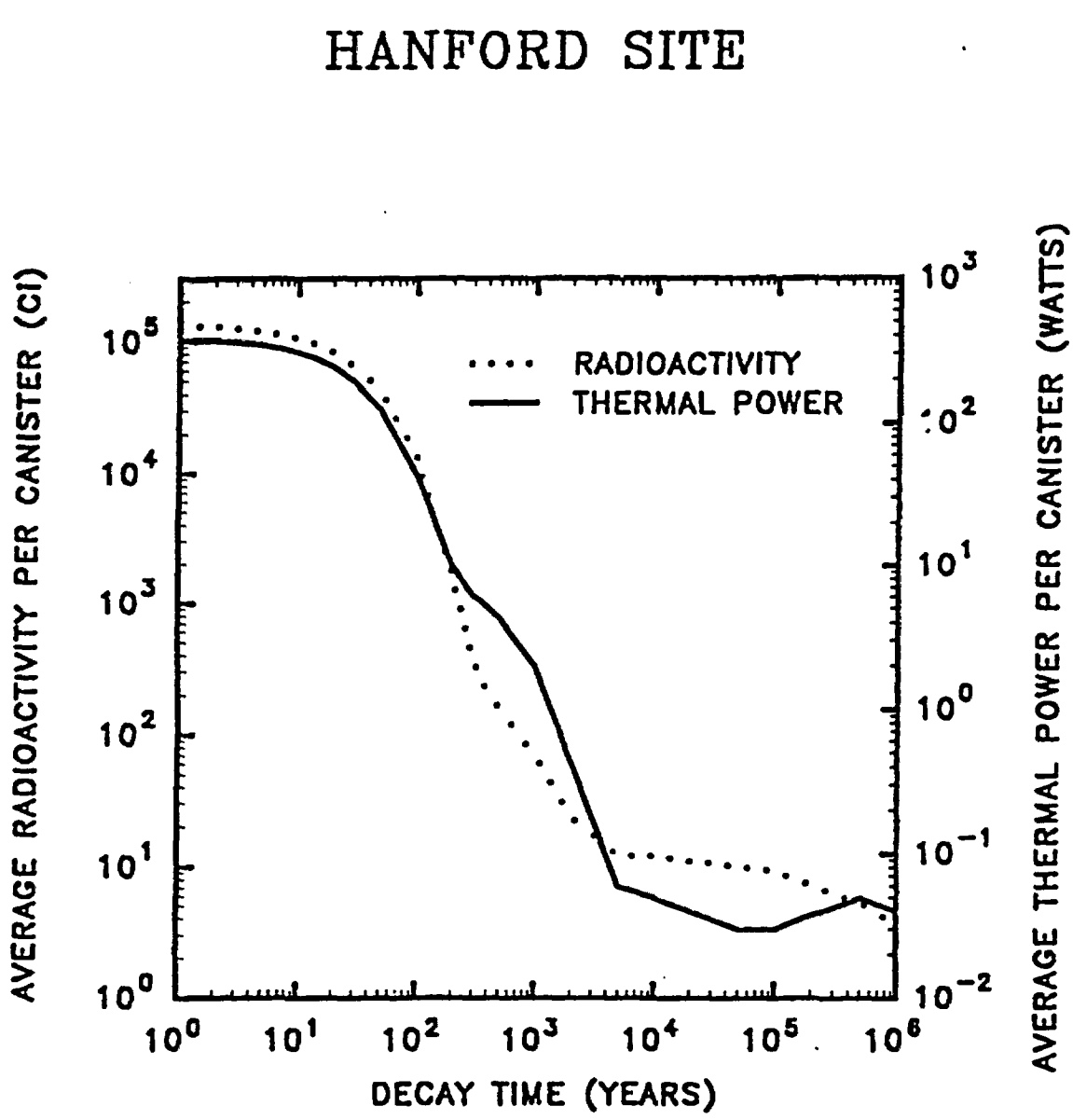

K.J. Notz, T.D. Welch, R.S. Moore, and W.J. Reich, *Preliminary Waste Form Characteristics*, ORNL-TM-11681 (draft) September, 1990.

Table 6.12. Idaho National Engineering Laboratory. Calculated radioactivity and thermal power per HLW canister[a]

Decay time after immobilization, years	Total radioactivity per canister (Ci)	Total thermal power per canister (W)
0	108,900	339
1	89,400	267
2	78,600	230
5	64,100	185
10	53,600	157
15	46,900	138
20	41,500	123
30	32,800	97
50	20,500	61
100	6,430	20
200	680	2.6
300	98	0.67
350	48	0.45
500	16	0.24
1,000	7.2	0.11
1,050	7.0	0.10
2,000	5.6	0.06
5,000	5.0	0.04
10,000	4.6	0.033
20,000	4.2	0.023
50,000	3.6	0.012
100,000	3.1	0.008
500,000	1.4	0.003
1,000,000	0.71	0.001

[a]Results of ORIGEN2 calculations based on glass-ceramic form, assuming 1277 kg of calcine per canister (1825 kg of glass-ceramic per canister), with the initial radionuclide composition shown in Table 3.5.3.

K.J. Notz, T.D. Welch, R.S. Moore, and W.J. Reich, *Preliminary Waste Form Characteristics*, ORNL-TM-11681 (draft) September, 1990.

Figure 6.9 Radioactivity and Thermal Power Per Canister.

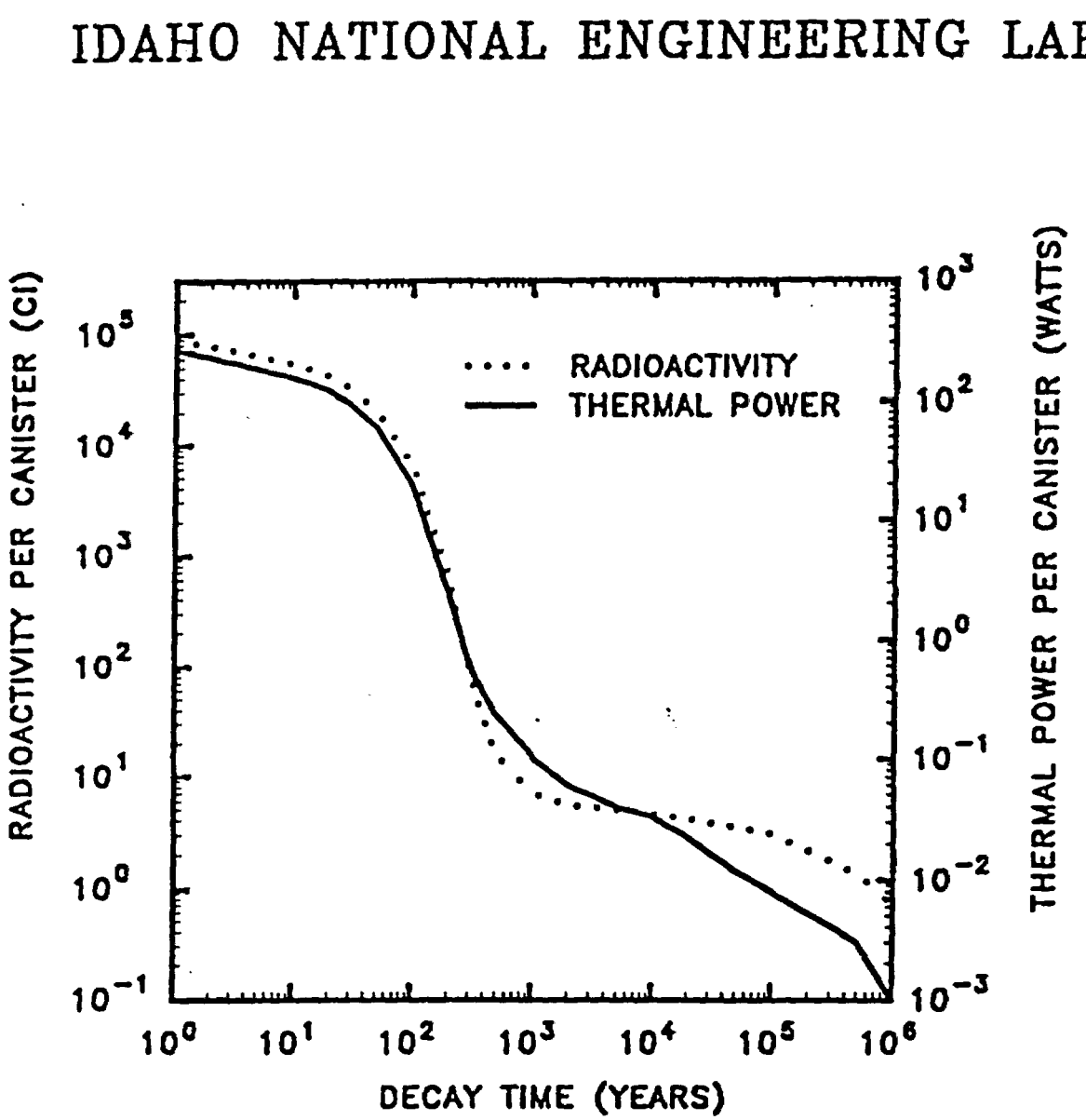

K.J. Notz, T.D. Welch, R.S. Moore, and W.J. Reich, *Preliminary Waste Form Characteristics*, ORNL-TM-11681 (draft) September, 1990.

2.2 Glass Waste Form

2.2.1 Radionuclide Content

2.2.1.1 Present Inventory

2.2.1.2 Projected Inventory

2.2.1.3 Radioactivity and Decay Heat vs. Time

2.2.1.4 Glass Species Composition Statistics

2.2.1.5 Fracture/Fragmentation Statistics

2.2.2 Repository Response

2.2.2.1 Gaseous Release from Glass

2.2.2.2 Dissolution Radionuclide Release from Glass

2.2.2.3 Soluble-Precipitated/Colloidal Species

Table 6.13. Radioisotope composition of West Valley Demonstration Project Vitrified High-Level Waste[a]

Radioisotope	Grams/canister	Curies/canister	Watts/canister
Fe-55	0.1104E-02	0.2760E+01	0.9313E-04
Co-60	0.2679E-02	0.3030E+01	0.4666E-01
Ni-59	0.5491E+01	0.4160E+00	0.1650E-04
Ni-63	0.4895E+00	0.3020E+02	0.3039E-02
Se-79	0.1980E+00	0.1380E-01	0.3431E-05
Sr-90	0.1928E+03	0.2630E+05	0.3048E+02
Y-90	0.4833E-01	0.2630E+05	0.1456E+03
Zr-93	0.4257E+03	0.1070E+01	0.1242E-03
Nb-93m	0.2529E-02	0.7150E+00	0.1265E-03
Tc-99	0.2524E+02	0.4280E+00	0.2144E-03
Ru-106	0.1655E-04	0.5540E-01	0.3290E-05
Rh-106	0.1556E-10	0.5540E-01	0.5307E-03
Pd-107	0.8416E+02	0.4330E-01	0.2563E-05
Cd-113m	0.3845E-01	0.8340E+01	0.1402E-01
Sn-121m	0.1160E-02	0.6860E-01	0.1373E-03
Sn-126	0.1441E+02	0.4090E+00	0.5095E-03
Sb-125	0.2769E-01	0.2860E+02	0.8929E-01
Sb-126	0.6852E-06	0.5730E-01	0.1057E-02
Sb-126m	0.5206E-08	0.4090E+00	0.5201E-02
Te-125m	0.3885E-03	0.7000E+01	0.5876E-02
Cs-134	0.1569E-01	0.2030E+02	0.2063E+00
Cs-135	0.5505E+03	0.6340E+00	0.2113E-03
Cs-137	0.3252E+03	0.2830E+05	0.3126E+02
Ba-137m	0.4981E-04	0.2680E+05	0.1051E+03
Ce-144	0.8023E-06	0.2560E-02	0.1696E-05
Pr-144	0.3387E-10	0.2560E-02	0.1879E-04
Pm-146	0.9566E-04	0.4260E-01	0.2146E-03
Pm-147	0.3721E+00	0.3450E+03	0.1236E+00
Sm-151	0.1258E+02	0.3310E+03	0.3876E-01
Eu-152	0.8267E-02	0.1430E+01	0.1080E-01
Eu-154	0.1389E+01	0.3750E+03	0.3350E+01
Eu-155	0.2014E+00	0.9370E+02	0.6806E-01
Tl-207	0.1690E-09	0.3220E-01	0.9444E-04
Tl-208	0.4312E-10	0.1270E-01	0.2985E-03
Pb-209	0.1815E-09	0.8250E-03	0.9475E-06
Pb-211	0.1308E-08	0.3230E-01	0.9666E-04
Pb-212	0.2540E-07	0.3530E-01	0.6712E-04
Bi-211	0.7718E-10	0.3230E-01	0.1287E-02
Bi-212	0.2409E-08	0.3530E-01	0.5995E-03
Bi-213	0.4265E-10	0.8250E-03	0.3464E-05
Po-212	0.1274E-18	0.2260E-01	0.1196E-02
Po-213	0.6231E-19	0.7860E-03	0.3972E-04
Po-215	0.1095E-14	0.3230E-01	0.1440E-02
Po-216	0.1013E-12	0.3530E-01	0.1443E-02
At-217	0.5124E-15	0.8250E-03	0.3516E-04
Rn-219	0.2482E-11	0.3230E-01	0.1339E-02
Rn-220	0.3826E-10	0.3530E-01	0.1339E-02
Fr-221	0.4653E-11	0.8250E-03	0.3180E-04
Fr-223	0.1117E-10	0.4320E-03	0.1120E-05
Ra-223	0.6306E-06	0.3230E-01	0.1149E-02

K.J. Notz, T.D. Welch, R.S. Moore, and W.J. Reich, *Preliminary Waste Form Characteristics*, ORNL-TM-11681 (draft) September, 1990.

Table 6.13. (continued)

Radioisotope	Grams/canister	Curies/canister	Watts/canister
Ra-224	0.2216E-06	0.3530E-01	0.1210E-02
Ra-225	0.2104E-07	0.8250E-03	0.5778E-06
Ra-228	0.2550E-04	0.5970E-02	0.4595E-06
Ac-225	0.1421E-07	0.8250E-03	0.2878E-04
Ac-227	0.4464E-05	0.3230E-03	0.1562E-06
Ac-228	0.2662E-08	0.5970E-02	0.5153E-04
Th-227	0.1034E-05	0.3180E-01	0.1159E-02
Th-228	0.4306E-04	0.3530E-01	0.1153E-02
Th-229	0.3877E-02	0.8250E-03	0.2521E-04
Th-230	0.1169E-01	0.2360E-03	0.6670E-05
Th-231	0.6657E-09	0.3540E-03	0.1984E-06
Th-232	0.5880E+05	0.6450E-02	0.1559E-03
Th-234	0.1356E-06	0.3140E-02	0.1271E-05
Pa-231	0.1264E+01	0.5970E-01	0.1796E-02
Pa-233	0.4422E-05	0.9180E-01	0.2081E-03
Pa-234m	0.4571E-11	0.3140E-02	0.1550E-04
U-232	0.1270E-02	0.2720E-01	0.8721E-03
U-233	0.3666E+01	0.3550E-01	0.1031E-02
U-234	0.2640E+01	0.1650E-01	0.4746E-03
U-235	0.1637E+03	0.3540E-03	0.9259E-05
U-236	0.1700E+02	0.1100E-02	0.2976E-04
U-238	0.9337E+04	0.3140E-02	0.7954E-04
Np-236	0.2823E+01	0.3720E-01	0.7494E-04
Np-237	0.1302E+03	0.9180E-01	0.2802E-02
Np-239	0.5861E-05	0.1360E+01	0.3283E-02
Pu-236	0.6209E-05	0.3300E-02	0.1147E-03
Pu-238	0.1904E+01	0.3260E+02	0.1079E+01
Pu-239	0.1028E+03	0.6390E+01	0.1967E+00
Pu-240	0.2053E+02	0.4680E+01	0.1455E+00
Pu-241	0.3076E+01	0.3170E+03	0.9815E-02
Pu-242	0.1668E+01	0.6370E-02	0.1879E-03
Am-241	0.6117E+02	0.2100E+03	0.6967E+01
Am-242	0.1435E-05	0.1160E+01	0.1315E-02
Am-242m	0.1204E+00	0.1170E+01	0.4616E-03
Am-243	0.6820E+01	0.1360E+01	0.4366E-01
Cm-242	0.2912E-03	0.9630E+00	0.3544E-01
Cm-243	0.1021E-01	0.5270E+00	0.1931E-01
Cm-244	0.3707E+00	0.3000E+02	0.1048E+01
Cm-245	0.2015E-01	0.3460E-02	0.1147E-03
Cm-246	0.1279E-02	0.3930E-03	0.1285E-04
Total	0.7029E+05	0.1096E+06	0.3260E+03

[a]Calculated from data in WVDP Mass Balance, Revision 7 (Crocker 1989). This is based on 484,000 kg of total glass and 1900 kg of glass per canister, and represents the average canister composition. Radioactivity shown is as of the start of year 1990.

K.J. Notz, T.D. Welch, R.S. Moore, and W.J. Reich, *Preliminary Waste Form Characteristics*, ORNL-TM-11681 (draft) September, 1990.

Table 6.14. Savannah River Site. Radioisotope content per HLW canister[a]

	Isotope	Curies/canister	Grams/canister
1	Cr-51	0.9312E-16	0.1008E-20
2	Co-60	0.1699E+03	0.1502E+00
3	Ni-59	0.2397E-01	0.3163E+00
4	Ni-63	0.2975E+01	0.4824E-01
5	Tl-208	0.1128E-02	0.3829E-11
6	U-232	0.1339E-01	0.6256E-03
7	U-233	0.1584E-05	0.1636E-03
8	U-234	0.3428E-01	0.5485E+01
9	U-235	0.1573E-03	0.7278E+02
10	U-236	0.1128E-02	0.1742E+02
11	U-238	0.1050E-01	0.3122E+05
12	Np-236	0.1744E-07	0.1323E-05
13	Np-237	0.8904E-02	0.1263E+02
14	Pu-236	0.1221E+00	0.2297E-03
15	Pu-237	0.8941E-11	0.7401E-15
16	Pu-238	0.1484E+04	0.8667E+02
17	Pu-239	0.1291E+02	0.2076E+03
18	Pu-240	0.8681E+01	0.3809E+02
19	Pu-241	0.1670E+04	0.1620E+02
20	Pu-242	0.1224E-01	0.3206E+01
21	Am-241	0.1102E+02	0.3210E+01
22	Am-242	0.1436E-01	0.1776E-07
23	Am-242m	0.1447E-01	0.1488E-02
24	Am-243	0.5788E-02	0.2902E-01
25	Cm-242	0.3495E-01	0.1057E-04
26	Cm-243	0.5565E-02	0.1078E-03
27	Cm-244	0.1076E+03	0.1329E+01
28	Cm-245	0.6715E-05	0.3910E-04
29	Cm-246	0.5342E-06	0.1739E-05
30	Cm-247	0.6604E-12	0.7116E-08
31	Cm-248	0.6864E-12	0.1614E-09
32	Se-79	0.1699E+00	0.2439E+01
33	Rb-87	0.8719E-06	0.9961E+01
34	Sr-89	0.4267E-04	0.1470E-08
35	Sr-90	0.4675E+05	0.3426E+03
36	Y-90	0.4786E+05	0.8795E-01
37	Y-91	0.7568E-03	0.3085E-07
38	Zr-93	0.1117E+01	0.4443E+03

K.J. Notz, T.D. Welch, R.S. Moore, and W.J. Reich, *Preliminary Waste Form Characteristics*, ORNL-TM-11681 (draft) September, 1990.

Table 6.14. (continued)

	Isotope	Curies/canister	Grams/canister
39	Zr-95	0.1005E-01	0.4680E-06
40	Nb-94	0.9646E-04	0.5147E-03
41	Nb-95	0.2115E-01	0.5407E-06
42	Nb-95m	0.1247E-03	0.3272E-09
43	Tc-99	0.3079E+01	0.1816E+03
44	Ru-103	0.1684E-07	0.5217E-12
45	Ru-106	0.2252E+04	0.6729E+00
46	Rh-103m	0.1636E-07	0.5028E-15
47	Rh-106	0.2259E+04	0.6346E-06
48	Pd-107	0.1473E-01	0.2863E+02
49	Ag-110m	0.1258E+00	0.2647E-04
50	Cd-113	0.5009E-13	0.1472E+00
51	Cd-115m	0.1213E-08	0.4763E-13
52	Sn-121m	0.7902E-01	0.1336E-02
53	Sn-123	0.2549E+00	0.3101E-04
54	Sn-126	0.4415E+00	0.1556E+02
55	Sb-124	0.7123E-07	0.4071E-11
56	Sb-125	0.8496E+03	0.8226E+00
57	Sb-126	0.6159E-01	0.7365E-06
58	Sb-126m	0.4415E+00	0.5619E-08
59	Te-125m	0.2760E+03	0.1532E-01
60	Te-127	0.1202E+00	0.4555E-07
61	Te-127m	0.1228E+00	0.1302E-04
62	Te-129	0.3053E-11	0.1457E-18
63	Te-129m	0.4749E-11	0.1576E-15
64	Cs-134	0.3372E+03	0.2606E+00
65	Cs-135	0.9943E-01	0.8633E+02
66	Cs-136	0.7828E-39	0.1068E-43
67	Cs-137	0.4341E+05	0.4989E+03
68	Ba-136m	0.8607E-38	0.3195E-49
69	Ba-137m	0.4155E+05	0.7724E-04
70	Ba-140	0.1024E-35	0.1404E-40
71	La-140	0.4304E-36	0.7734E-42
72	Ce-141	0.3591E-10	0.1260E-14
73	Ce-142	0.9609E-05	0.4005E+03
74	Ce-144	0.9869E+04	0.3093E+01
75	Pr-143	0.1198E-33	0.1780E-38
76	Pr-144	0.9869E+04	0.1306E-03
77	Pr-144m	0.1187E+03	0.6545E-06

K.J. Notz, T.D. Welch, R.S. Moore, and W.J. Reich, *Preliminary Waste Form Characteristics*, ORNL-TM-11681 (draft) September, 1990.

Table 6.14. (continued)

	Isotope	Curies/canister	Grams/canister
78	Nd-144	0.4860E-09	0.4110E+03
79	Nd-147	0.1261E-43	0.1570E-48
80	Pm-147	0.2419E+05	0.2609E+02
81	Pm-148	0.6975E-10	0.4243E-15
82	Pm-148m	0.1009E-08	0.4722E-13
83	Sm-147	0.2000E-05	0.8796E+02
84	Sm-148	0.5788E-11	0.1916E+02
85	Sm-149	0.1781E-11	0.7420E+01
86	Sm-151	0.2478E+03	0.9418E+01
87	Eu-152	0.3688E+01	0.2132E-01
88	Eu-154	0.6196E+03	0.2295E+01
89	Eu-155	0.4749E+03	0.1021E+01
90	Eu-156	0.5231E-31	0.9489E-36
91	Tb-160	0.1120E-05	0.9923E-10
Total		0.2344E+06	0.3427E+05

[a]Quantities shown are for sludge + supernate glass and are based on the DWPF Basic Data Report, DPSP 80-1033, Rev. 91, April 1985, assuming sludge aged an average of 5 years and supernate aged an average of 15 years, with a canister load of 3710 lb of glass (1682 kg). Radionuclide contents are at time of filling canister.

K.J. Notz, T.D. Welch, R.S. Moore, and W.J. Reich, *Preliminary Waste Form Characteristics*, ORNL-TM-11681 (draft) September, 1990.

Table 6.15. Hanford Site. Radioisotope content per HLW canister (NCAW glass)[a]

Isotope	Curies/canister		Grams/canister	
	Nominal	Maximum	Nominal	Maximum
Fe-55	1.80E+01	1.41E+02	7.20E-03	5.64E-02
Ni-59	1.09E-01	1.36E-01	1.44E+00	1.80E+00
Co-60	1.50E+00	4.29E+00	1.33E-03	3.79E-03
Ni-63	1.21E+01	1.57E+01	1.96E-01	2.54E-01
Se-79	3.15E-03	3.90E-03	4.52E-02	5.60E-02
Sr-89	5.35E-13	6.52E-02	1.84E-17	2.24E-06
Sr-90	2.98E+04	4.18E+04	2.18E+02	3.06E+02
Y-90	2.98E+04	4.18E+04	5.48E-02	7.68E-02
Y-91	1.38E-10	7.26E-01	5.63E-15	2.96E-05
Nb-93m	6.16E-01	5.77E-01	2.18E-03	2.04E-03
Zr-93	1.05E+00	1.29E+00	4.18E+02	5.13E+02
Zr-95	2.92E-09	2.76E+00	1.36E-13	1.28E-04
Nb-95	6.73E-09	5.67E+00	1.72E-13	1.45E-04
Tc-99	7.51E+00	9.35E+00	4.43E+02	5.51E+02
Ru-103	3.37E-18	2.98E-04	1.04E-22	9.23E-09
Rh-103m	3.04E-18	2.69E-04	9.34E-26	8.27E-12
Ru-106	4.18E+01	4.99E+03	1.25E-02	1.49E+00
Rh-106	4.18E+01	4.99E+03	1.17E-08	1.40E-06
Pd-107	3.02E-02	4.07E-02	5.87E+01	7.91E+01
Ag-110m	2.22E-03	1.59E+00	4.67E-07	3.35E-04
Cd-113m	8.53E+00	1.46E+01	3.93E-02	6.73E-02
In-113m	1.01E-07	2.52E-02	6.04E-15	1.51E-09
Sn-113	1.01E-07	2.52E-02	1.01E-11	2.51E-06
Cd-115m	3.20E-18	8.78E-06	1.26E-22	3.45E-10
Sn-119m	6.80E-03	5.42E+00	1.52E-06	1.21E-03
Sn-121m	7.76E-02	1.06E-01	1.31E-03	1.79E-03
Sn-123	3.65E-05	2.89E+00	4.44E-09	3.52E-04
Sn-126	3.65E-01	4.60E-01	1.29E+01	1.62E+01
Sb-124	1.15E-14	3.50E-05	6.57E-19	2.00E-09
Sb-126	5.10E-02	6.48E-02	6.10E-07	7.75E-07
Sb-126m	3.65E-01	4.60E-01	4.65E-09	5.86E-09
Sb-125	2.54E+02	1.76E+03	2.46E-01	1.70E+00
Te-125m	6.20E+01	4.29E+02	3.44E-03	2.38E-02
Te-127	6.55E-06	2.95E+00	2.48E-12	1.12E-06
Te-127m	6.66E-06	3.00E+00	7.06E-10	3.18E-04
Te-129	3.14E-23	3.75E-07	1.49E-30	1.79E-14
Te-129m	4.82E-23	5.77E-07	1.60E-27	1.91E-11
I-129	1.29E-05	1.63E-05	7.31E-02	9.23E-02

K.J. Notz, T.D. Welch, R.S. Moore, and W.J. Reich, *Preliminary Waste Form Characteristics*, ORNL-TM-11681 (draft) September, 1990.

Table 6.15. (continued)

Isotope	Curies/canister		Grams/canister	
	Nominal	Maximum	Nominal	Maximum
Cs-134	9.31E+01	1.20E+03	7.19E-02	9.27E-01
Cs-135	2.02E-01	2.51E-01	1.75E+02	2.18E+02
Cs-137	3.61E+04	5.10E+04	4.15E+02	5.86E+02
Ba-137m	3.40E+04	4.82E+04	6.32E-05	8.96E-05
Ce-141	2.93E-22	1.13E-05	1.03E-26	3.97E-10
Ce-144	8.00E+01	2.98E+04	2.51E-02	9.34E+00
Pr-144	8.00E+01	2.98E+04	1.06E-06	3.94E-04
Pr-144m	9.60E-01	3.58E+02	5.29E-09	1.97E-06
Pm-147	5.21E+03	3.97E+04	5.62E+00	4.28E+01
Pm-148m	6.23E-19	1.32E-05	2.92E-23	6.18E-10
Sm-151	6.98E+02	8.36E+02	2.65E+01	3.18E+01
Eu-152	1.40E-00	2.74E+00	8.09E-03	1.58E-02
Gd-153	1.35E-05	1.15E-02	3.83E-09	3.26E-06
Eu-154	1.45E+02	3.36E+02	5.37E-01	1.24E+00
Eu-155	1.37E+02	4.11E+02	2.94E-01	8.83E-01
Tb-160	9.49E-13	1.10E-04	8.41E-17	9.74E-09
U-234	4.57E-03	4.82E-03	7.31E-01	7.71E-01
U-235	1.91E-04	1.97E-04	8.83E+01	9.11E+01
U-236	4.21E-04	4.75E-04	6.51E+00	7.34E+00
U-238	3.51E-03	3.72E-03	1.04E+04	1.11E+04
Np-237	1.56E-01	1.99E-01	2.21E+02	2.82E+02
Pu-238	4.43E-01	7.68E-01	2.59E-02	4.48E-02
Pu-239	1.17E+00	1.41E+00	1.88E+01	2.27E+01
Pu-240	3.93E-01	5.42E-01	1.72E+00	2.38E+00
Pu-241	1.26E+01	2.58E+01	1.22E-01	2.50E-01
Pu-242	7.61E-05	1.31E-04	1.99E-02	3.43E-02
Am-241	2.84E+02	5.77E+02	8.27E+01	1.68E+02
Am-242	2.21E-01	4.14E-01	2.73E-07	5.12E-07
Am-243	3.79E-02	6.76E-02	1.90E-01	3.39E-01
Cm-242	1.82E-01	4.99E-01	5.50E-05	1.51E-04
Cm-244	5.03E+00	1.25E+01	6.22E-02	1.54E-01
Total	1.37E+05	2.98E+05	1.26E+04	1.40E+04

[a]This table identifies the nominal and maximum activity of HWVP canisters at the time of vitrification. The maximum is principally based on close-coupling the final accumulated tank of NCAW (21 mo. from fuel discharge to HWVP). The overall waste loading is 0.031 kg non-volatile oxides/l (0.26 lb non-volatile oxides/gal) of feed. Canister contains 1650 kg of HLW glass (85% fill). Source: Mitchell and Nelson 1988.

K.J. Notz, T.D. Welch, R.S. Moore, and W.J. Reich, *Preliminary Waste Form Characteristics*, ORNL-TM-11681 (draft) September, 1990.

Table . 6.16. Idaho National Engineering Laboratory. Radioisotope content per HLW canister[a]

	Isotope	Curies/canister	Grams/canister
1	Se-79	0.8173E-01	0.1173E+01
2	Rb-87	0.4597E-05	0.5252E+02
3	Sr-90	0.1660E+05	0.1217E+03
4	Y-90	0.1660E+05	0.3051E-01
5	Zr-93	0.3959E+00	0.1575E+03
6	Nb-93M	0.9577E-01	0.3387E-03
7	Tc-99	0.2682E+01	0.1582E+03
8	Ru-106	0.1239E+04	0.3701E+00
9	Rh-106	0.1239E+04	0.3479E-06
10	Pd-107	0.2554E-02	0.4965E+01
11	Sn-126	0.4086E-01	0.1440E+01
12	Sb-126M	0.4086E-01	0.5201E-09
13	Sb-126	0.4086E-01	0.4887E-06
14	Cs-134	0.4214E+04	0.3256E+01
15	Cs-135	0.9577E-01	0.8316E+02
16	Cs-137	0.1660E+05	0.1908E+03
17	Ba-137M	0.1532E+05	0.2848E-04
18	Ce-144	0.1047E+05	0.3282E+01
19	Pr-144	0.1047E+05	0.1386E-03
20	Pm-147	0.1532E+05	0.1653E+02
21	Sm-151	0.2171E+03	0.8250E+01
22	Eu-154	0.2299E+03	0.8513E+00
23	U-233	0.1532E-08	0.1583E-06
24	U-234	0.5491E-06	0.8785E-04
25	U-235	0.2299E-05	0.1063E+01
26	U-236	0.1277E-04	0.1973E+00
27	U-237	0.6130E-08	0.7507E-13
28	U-238	0.1277E-10	0.3797E-04
29	Np-237	0.6130E-04	0.8693E-01
30	Pu-238	0.8939E+02	0.5221E+01
31	Pu-239	0.8939E+00	0.1437E+02
32	Pu-240	0.8300E+00	0.3642E+01
33	Pu-241	0.2043E+03	0.1983E+01
34	Pu-242	0.2299E-02	0.6018E+00
35	Am-241	0.1162E+01	0.3385E+00
36	Am-243	0.1060E-01	0.5315E-01
37	Cm-242	0.8300E+00	0.2510E-03
38	Cm-244	0.6640E+00	0.8201E-02
Total		0.1088E+06	0.8315E+03

[a]Quantities are at time of filling canister and are based on 3-yr old calcine immobilized in glass-ceramic with a load of 1277 kg of calcine per canister (1825 kg of glass-ceramic per canister). Based on IDO-10105 (1982) and Berreth 1986.

K.J. Notz, T.D. Welch, R.S. Moore, and W.J. Reich, *Preliminary Waste Form Characteristics*, ORNL-TM-11681 (draft) September, 1990.

Table 6.17. West Valley Demonstration Project.
Chemical composition of reference HLW glass[a]

Component	Nominal composition (wt%)	Range (wt%)	
AgO	0.0001	-	-
Al_2O_3	2.8295	1.19	7.15
AmO_2	0.0073	-	-
BaO	0.0540	0.04	0.08
B_2O_3	9.9516	9.33	10.66
CaO	0.5993	0.39	0.93
CdO	0.0003	-	-
CeO_2	0.0670	0.04	0.10
CmO_2	0.0001	-	-
CoO	0.0002	-	-
Cr_2O_3	0.3112	0.21	0.48
Cs_2O	0.0826	0.05	0.13
CuO	0.0001	-	-
Eu_2O_3	0.0014	-	-
Fe_2O_3	12.1570	8.32	18.50
Gd_2O_3	0.0003	-	-
In_2O_3	0.0001	-	-
K_2O	3.5733	3.36	3.84
La_2O_3	0.0337	0.02	0.05
Li_2O	3.0315	2.84	3.25
MgO	1.3032	1.22	1.39
MnO_2	1.3107	0.84	1.96
MoO_3	0.0088	-	0.01
NaCl	0.0183	0.01	0.03
NaF	0.0013	-	-
Na_2O	10.9340	10.25	11.71
Nd_2O_3	0.1209	0.08	0.19
NiO	0.3358	0.22	0.52
NpO_2	0.0224	0.01	0.03
P_2O_5	2.5084	0.21	3.16
PdO	0.0062	-	-
Pm_2O_3	0.0003	-	-
Pr_6O_{11}	0.0321	0.02	0.05
PuO_2	0.0076	-	-
Rb_2O	0.0005	-	-

K.J. Notz, T.D. Welch, R.S. Moore, and W.J. Reich, *Preliminary Waste Form Characteristics*, ORNL-TM-11681 (draft) September, 1990.

Table 6.17. (continued)

Component	Nominal composition (wt%)	Range (wt%)	
RhO_2	0.0136	0.01	0.02
RuO_2	0.0759	0.05	0.12
SO_3	0.2164	0.14	0.33
Sb_2O_3	0.0001	-	-
SeO_2	0.0005	-	-
SiO_2	44.8770	42.08	48.10
Sm_2O_3	0.0267	0.02	0.04
SnO_2	0.0006	-	-
SrO	0.0269	0.02	0.04
Tc_2O_7	0.0021	-	-
ThO_2	3.5844	1.83	6.56
TeO_2	0.0028	-	-
TiO_2	0.9800	0.92	1.05
UO_2	0.5605	0.37	0.87
Y_2O_3	0.0177	0.01	0.03
ZnO	0.0010	-	-
ZrO_2	0.2943	0.19	0.45
Other	0.0084	-	-
Total	100.0000		

[a]Source: Eisenstatt 1986. Reference glass composition is WV-205.

K.J. Notz, T.D. Welch, R.S. Moore, and W.J. Reich, *Preliminary Waste Form Characteristics*, ORNL-TM-11681 (draft) September, 1990.

Table 6.18. Savannah River Site.
Chemical composition of HLW glass[a]

Component	Water free wt %
Ag	0.05
Al_2O_3	3.96
B_2O_3	10.28
$BaSO_4$	0.14
$Ca_3(PO_4)_2$	0.07
CaO	0.85
$CaSO_4$	0.08
Cr_2O_3	0.12
Cs_2O	0.08
CuO	0.19
Fe_2O_3	7.04
FeO	3.12
K_2O	3.58
Li_2O	3.16
MgO	1.36
MnO	2.00
Na_2O	11.00
Na_2SO_4	0.36
NaCl	0.19
NaF	0.07
NiO	0.93
PbS	0.07
SiO_2	45.57
ThO_2	0.21
TiO_2	0.99
U_3O_8	2.20
Zeolite	1.67
ZnO	0.08
Others	0.58
Total	100.00

[a]Source: Baxter 1988.

Chemical Composition of Sludge-Precipitate Glass, Baxter, R. G., DP-1606, Rev. 2, Savannah River Plan, SC, December 1988, p. 49.

K.J. Notz, T.D. Welch, R.S. Moore, and W.J. Reich, *Preliminary Waste Form Characteristics*, ORNL-TM-11681 (draft) September, 1990.

Table 6.19. Hanford Site.
Chemical compositions of HWVP reference HLW (NCAW), substituted NCAW, frit, and borosilicate glass[a]

Component	Reference NCAW waste composition wt %	Substituted NCAW waste composition[b] wt %	Frit composition wt %	Glass composition wt %
SiO_2	2.9	3.0	67.25	51.3
B_2O_3	0.0	0.0	12.75	9.6
Na_2O	10.5	10.7	10.25	10.4
Li_2O	0.0	0.0	5.0	3.8
CaO	0.3	0.3	3.75	2.9
MgO	0.2	0.3	1.0	0.8
Fe_2O_3	44.0	44.4	--	11.1
Al_2O_3	17.0	17.2	--	4.3
Cr_2O_3	5.3	5.3	--	1.3
ZrO_2	2.3	2.4	--	0.6
NiO	2.3	2.4	--	0.6
La_2O_3	2.2	2.2	--	0.6
SO_4	1.8	1.8	--	0.4
Nd_2O_3	1.7	2.1	--	0.5
MoO_3	1.2	1.2	--	0.3
F	1.2	1.2	--	0.3
CuO	0.6	0.6	--	0.1
TOCc	0.6	0.6	--	--
MnO_2	0.6	0.7	--	0.2
CeO_2	0.6	0.7	--	0.2
RuO_2	0.6	0.6	--	0.1
U_3O_8	0.6	Sub Nd	--	--
Cs_2O	0.4	1.0	--	0.2
BaO	0.4	0.4	--	0.1
SrO	0.4	0.4	--	0.1
Pr_6O_{11}	0.4	0.4	--	0.2
Tc_2O_7	0.4	Sub Mn	--	--
Rb_2O	0.2	Sub Cs	--	--
Y_2O_3	0.2	0.2	--	0.04
Sm_2O_3	0.2	0.2	--	0.04
PdO	0.2	Del	--	--
Rh_2O_3	0.2	Del	--	--
NpO_2	0.1	Sub Ce	--	--
TeO_2	0.1	Del	--	--
Pm_2O_3	0.1	Sub Nd	--	--
BeO	0.1	Sub Mg	--	--
SeO_2	0.03	Del	--	--
SnO_2	0.02	Del	--	--
CdO	0.02	Del	--	--

K.J. Notz, T.D. Welch, R.S. Moore, and W.J. Reich, *Preliminary Waste Form Characteristics*, ORNL-TM-11681 (draft) September, 1990.

Table 6.19. (continued)

Component	Reference NCAW waste composition wt %	Substituted NCAW waste composition[b] wt %	Frit composition wt %	Glass composition wt %
Eu_2O_3	0.02	Sub Nd	--	--
PuO_2	0.02	Sub Ce	--	--
Am_2O_3	0.02	Sub Nd	--	--
P_2O_5	0.02	Del	--	--
Ag_2O	0.01	Del	--	--
Nb_2O_5	0.01	Sub Mo	--	--
Gd_2O_3	0.01	0.01	--	0.003
Ta_2O	0.01	Del	--	--
TiO_2	0.01	Del	--	--
Total	100	100	100	100

[a]Source: Mitchell 1986. Reference glass is HW-39. Data given are for a waste oxide loading of 25 wt% and are based on approximately 4-year old waste.

[b]Components marked sub were substituted as indicated. Components marked Del were deleted. TOC = total organic carbon

K.J. Notz, T.D. Welch, R.S. Moore, and W.J. Reich, *Preliminary Waste Form Characteristics*, ORNL-TM-11681 (draft) September, 1990.

Table 6.20. Compositions of typical ceramic-based waste forms developed for immobilization of INEL calcined HLW[a]

Formulation number	SiO_2 (wt %)	Na_2O (wt %)	Li_2O (wt %)	B_2O_3 (wt %)	Waste (wt %)
12	8.6	1.1	0.5	2.6	87.2
11	16.0	0.0	0.0	1.4	82.6
17	30.3	0.0	0.0	2.3	67.5
6	28.6	2.1	0.9	3.5	64.9
1	14.2	2.6	1.2	1.7	80.3

[a]Source: Baker 1986.

K.J. Notz, T.D. Welch, R.S. Moore, and W.J. Reich, *Preliminary Waste Form Characteristics*, ORNL-TM-11681 (draft) September, 1990.

PROJECTED DWPF WASTE GLASS COMPOSITIONS

MAJOR GLASS COMPONENTS weight %	CONSTITUENT SLUDGE TYPE						
	Blend[d]	Batch 1	Batch 2	Batch 3	Batch 4	HM	Purex[w]
Al_2O_3	3.98	4.87	4.46	3.25	3.32	7.08	2.89
B_2O_3	8.01	7.69	7.70	7.69	8.11	6.94	10.21
$BaSO_4$	0.27	0.22	0.24	0.26	0.38	0.18	0.29
CaO	0.97	1.17	1.00	0.93	0.83	1.00	1.02
$CaSO_4$	0.077	0.12	0.11	0.10	0.0034	trace	0.12
Cr_2O_3	0.12	0.10	0.12	0.13	0.14	0.086	0.14
CuO	0.44	0.40	0.41	0.40	0.46	0.25	0.42
Fe_2O_3	10.41	12.52	10.61	11.16	11.32	7.38	12.74
Group A[a]	0.14	0.099	0.14	0.10	0.20	0.20	0.078
Group B[b]	0.36	0.22	0.44	0.25	0.60	0.89	0.084
K_2O	3.86	3.49	3.50	3.47	3.99	2.14	3.58
Li_2O	4.40	4.42	4.42	4.42	4.32	4.62	3.12
MgO	1.35	1.36	1.35	1.35	1.38	1.45	1.33
MnO	2.03	2.06	1.62	1.81	3.08	2.07	1.99
Na_2O	8.73	8.62	8.61	8.51	8.88	8.17	12.14
Na_2SO_4	0.10	0.10	0.12	0.096	0.13	0.14	0.12
NaCl	0.19	0.31	0.23	0.22	0.090	0.093	0.26
NiO	0.89	0.75	0.90	1.07	1.09	0.40	1.21
SiO_2	50.20	49.81	50.17	49.98	49.29	54.39	44.56
ThO_2	0.19	0.36	0.63	0.77	0.24	0.55	0.011
TiO_2	0.90	0.66	0.67	0.66	1.02	0.55	0.65
U_3O_8	2.14	0.53	2.30	3.16	0.79	1.01	2.89
Total	99.76	99.88	99.75	99.79	99.66	99.59	99.85

[a] Group A: semi-volatile radionuclides (Se, Te, Rb, Mo, Tc)

[b] Group B: nonvolatile radionuclides (e.g., Sm, Sn, Co, Np, Am, Cm)

[d] The "Blend" is the current DWPF design-basis glass

[w] The "Purex" glass is a possible "worst-case" composition

ACCEPTABLE GLASSES

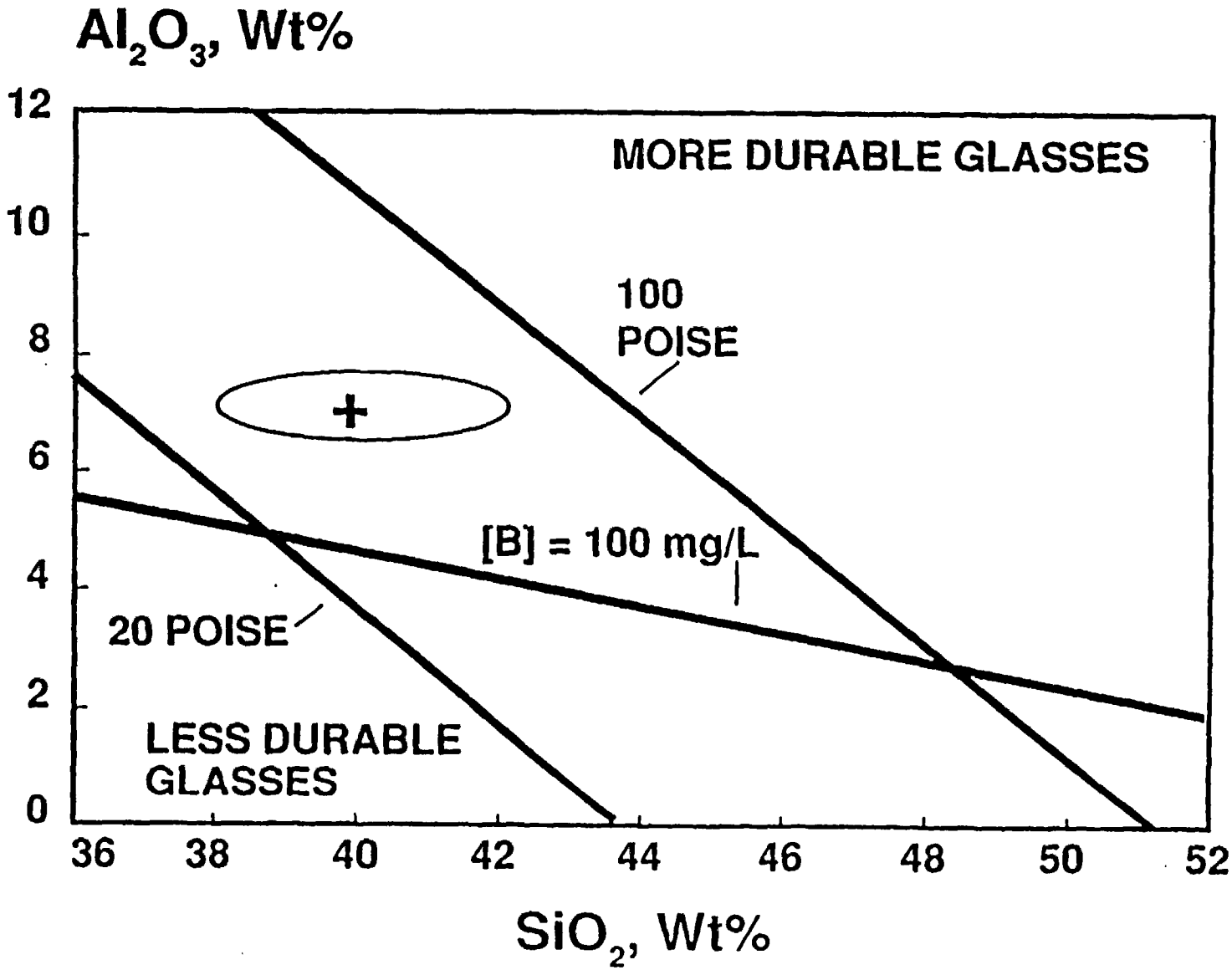

R.A. Palmer, *West Valley Demonstration Project High Level Waste Qualification Activities*, presented to the Nuclear Waste Technical Review Board, August, 1990.

DURABLE GLASS REGION

GLASS OXIDES	COMPOSITION (WT. %)	LOWER BOUND	UPPER BOUND
Si	43.1	38.0	45.0
Al	6.2	5.0	10.0
Fe	12.2	10.0	16.0
B	10.9	6.9	13.0
Na+K+Li	17.8	12.0	20.0
P	2.4	0.5	4.0
Mn	1.0	0.1	2.0

2.2 Glass Waste Form

2.2.1 Radionuclide Content

2.2.1.1 Present Inventory

2.2.1.2 Projected Inventory

2.2.1.3 Radioactivity and Decay Heat vs. Time

2.2.1.4 Glass Species Composition Statistics

2.2.1.5 Fracture/Fragmentation Statistics

2.2.2 Repository Response

2.2.2.1 Gaseous Release from Glass

2.2.2.2 Dissolution Radionuclide Release from Glass

2.2.2.3 Soluble-Precipitated/Colloidal Species

Table 1. Summary of studies examining surface area increases due to thermal fracturing

Glass Composition	Glass block size (relative)	Surface Area Increase (relative to unfractured glass)	Reference
SRL211	large-scale	2 - 40	Smith and Baxter 1981
SRL211, SRL131	large-scale	7 - 18	Peters and Slate 1981
SRL211, SRL131	small-scale	0 - 18	Peters and Slate 1981
borosilicate	large-scale	9.0 - 16.3	Laude et al. 1982
SRL165	large-scale	25 - 35	Bickford and Pellarin 1987
borosilicate	small- to large scale	1.1 - 86	Faletti and Ethridge 1988
borosilicate	medium-scale	2.0 - 10	Lutze et al. 1986
R7T7	small-scale, 1:10	10 -12	Vernaz and Godon 1991
PNL76-375	large-scale	8 - 45	Martin 1985
PNL76-375	small-scale	1.1 - 12	Martin 1985
borosilicate	medium-scale	not measured	Keinzler 1989
BRET HLW borosilicate glass	medium-scale	not measured	Farnsworth et al. 1985

BICKFORD D. F. and PELLARIN D. J. (1987) Large scale leach testing of DWPF canister sections. in Sci. Bas. for Nucl. Was. Mgmt. vol X, eds. J. K. Bates and W. B. Seefeldt, Mat. Res. Soc. Symp. Proc. vol. 84, 509-518.

FALETTI D. W. and ETHRIDGE L. J. (1988) A method for predicting cracking in waste glass canisters. *Nucl. and Chem. Waste Mgmt.* 8, 123-133.

FARNSWORTH R. K., CHAN M. K. W. and SLATE S. C. (1985) The effect of radial temperature gradients on glass fracture in simulated high-level waste canisters. in Sci. Bas. for Nucl. Was. Mgmt. vol VIII, eds. Jantzen, Stone and Ewing, Mat. Res. Soc. Symp. Proc. vol. 44, 191-198.

KIENZLER B. (1989) Cooling and cracking of technical HLW glass products: experimental and numerical studies. in Sci. Bas. for Nucl. Was. Mgmt.

LAUDE F., VERNAZ E., and SAINT-GAUDENS M. (1982) Fracture appraisal of large scale glass blocks under realistic thermal conditions. in Sci. Bas. for Nucl. Was. Mgmt. vol V, ed. W. Lutze, Mat. Res. Soc. Symp. Proc. vol. 11, 239-247.

LUTZE W., MANARA A., MARPLES J. A. C., OFFERMANN P. and van ISEGHEM P. (1986) Radioactive waste Management and Disposal, Luxembourg, ed. R. Simon (Cambridge Univ. Press, Cambridge).

MARTIN D. M. (1985) Fracture in Glass/High Level Waste Canisters. NUREG/CR-4198. Engineering Research Inst., Iowa State Univ., Ames.

PETERS, R. D., and SLATE S. C. (1981) Fracturing of simulated high-level waste glass in canisters. *Nucl. Eng. and Design* 67, 425-445.

SMITH P. K. and BAXTER C. A. (1981) Fracture during cooling of cast borosilicate glass containing nuclear wastes. USDOE report DP-1602. E. I. du Pont de Nemours & Co., Savannah River Laboratory, Aiken, SC.

VERNAZ E. Y. and GODON N. (1991) Key parameters of glass dissolution in integrated systems. in Scientific Basis for Nuclear Waste Mgmt. XIII eds. T. A. Abrajano and Lawrence, in press.

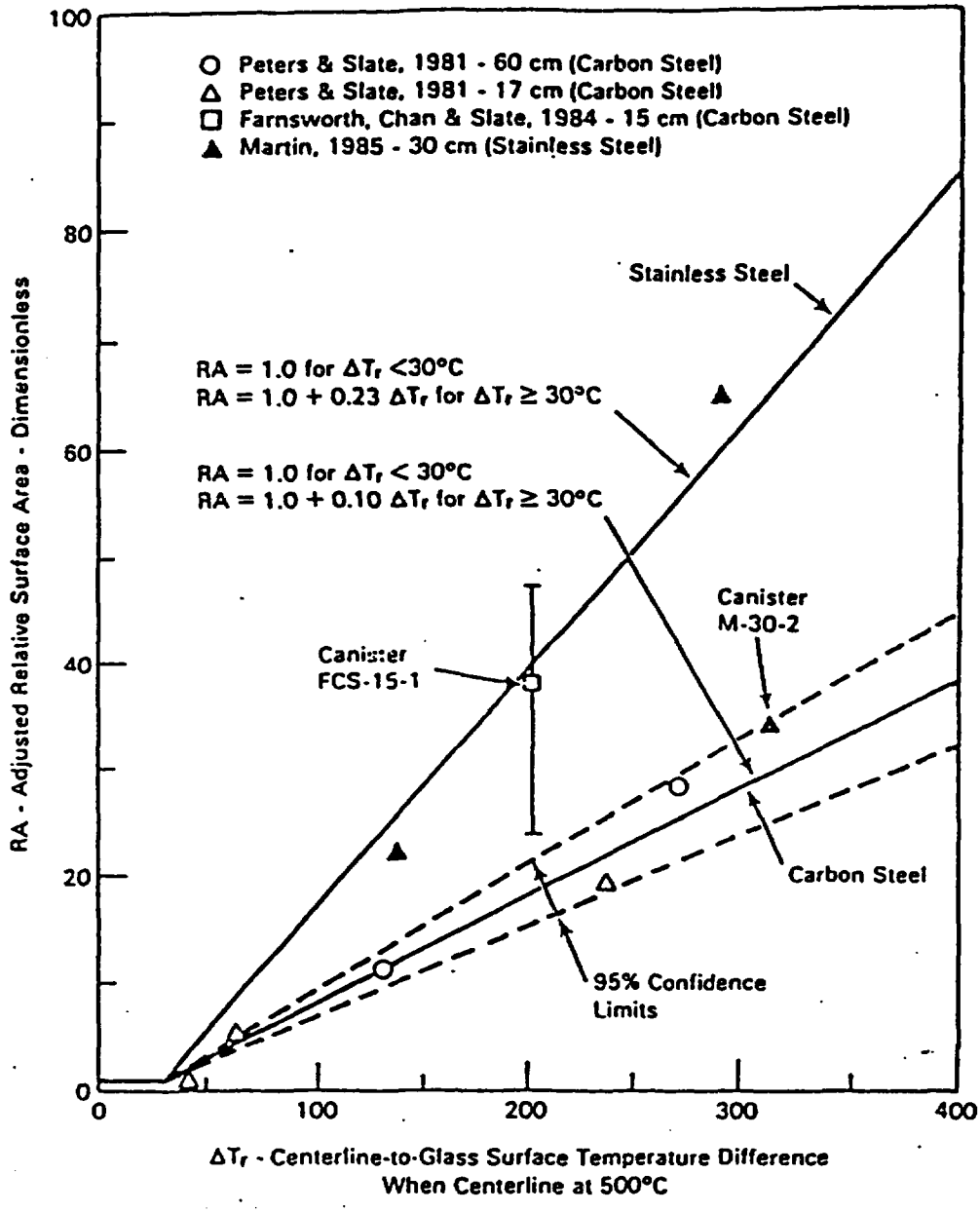

Figure 1. Correlation between Relative Surface Area and Radial Temperature Difference at 500°C Centerline Temperature. From Faletti and Ethridge (1988).

FALETTI D. W. and ETHRIDGE L. J. (1988) A method for predicting cracking in waste glass canisters. *Nucl. and Chem. Waste Mgmt.* 8, 123-133.

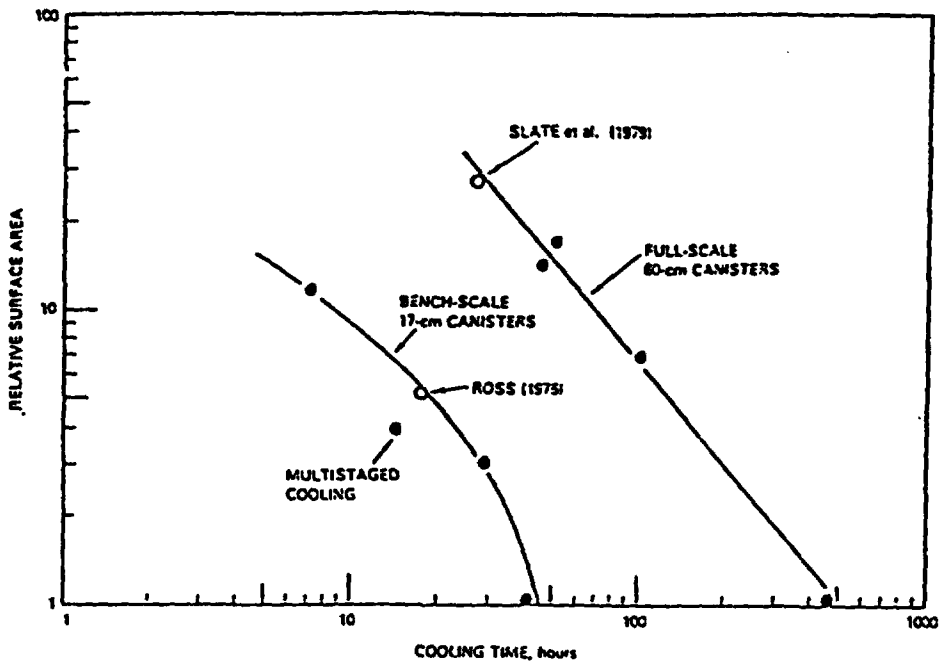

Figure 2. Effect of Cooling Time on Relative Surface Area of Thermal Cracks in 17 cm and 60 cm Dia Canisters. From Peters and Slate (1981).

PETERS, R. D., and SLATE S. C. (1981) Fracturing of simulated high-level waste glass in canisters. *Nucl. Eng. and Design* 67, 425-445.

2.2 Glass Waste Form

2.2.1 Radionuclide Content

2.2.1.1 Present Inventory

2.2.1.2 Projected Inventory

2.2.1.3 Radioactivity and Decay Heat vs. Time

2.2.1.4 Glass Species Composition Statistics

2.2.1.5 Fracture/Fragmentation Statistics

2.2.2 Repository Response

2.2.2.1 Gaseous Release from Glass

2.2.2.2 Dissolution Radionuclide Release from Glass

2.2.2.3 Soluble-Precipitated/Colloidal Species

2.2 Glass Waste Form

2.2.1 Radionuclide Content

2.2.1.1 Present Inventory

2.2.1.2 Projected Inventory

2.2.1.3 Radioactivity and Decay Heat vs. Time

2.2.1.4 Glass Species Composition Statistics

2.2.1.5 Fracture/Fragmentation Statistics

2.2.2 Repository Response

2.2.2.1 Gaseous Release from Glass

2.2.2.2 Dissolution Radionuclide Release from Glass

2.2.2.3 Soluble-Precipitated/Colloidal Species

2.2.2.1 Gaseous Release from Glass

Internal pressure within the canister is due to the accumulation of helium from alpha emission of transuranic nuclides. A DWPF canister filled with waste glass produces about 0.32 cm^3 of helium per year at 40 C. The helium produced is assumed to diffuse through the glass into the void space above the solid glass surface. At the end of 1,000 years the 103-liter void space pressure has increased by only 0.05 psi. This negligible pressure buildup is of no concern in waste package design. For the case of a canister filled to 25.3 ft^3 (733 L), the 23-liter void space pressure would increase by 0.2 psi.

Baxter, R.G., Defense Waste Form Processing Facility Waste Form and Canister Description, DuPont SRL Report DP-1606, p. 17 (December, 1988).

2.2 Glass Waste Form

2.2.1 Radionuclide Content

2.2.1.1 Present Inventory

2.2.1.2 Projected Inventory

2.2.1.3 Radioactivity and Decay Heat vs. Time

2.2.1.4 Glass Species Composition Statistics

2.2.1.5 Fracture/Fragmentation Statistics

2.2.2 Repository Response

2.2.2.1 Gaseous Release from Glass

2.2.2.2 Dissolution Radionuclide Release from Glass

2.2.2.3 Soluble-Precipitated/Colloidal Species

RATE LAW USED TO MODEL DISSOLUTION KINETICS

- RATE LAW FOR RELEASE OF ELEMENT η_i IN GLASS

$$\frac{dn_i}{dt} = \nu_i A k_r \left(1 - \frac{Q}{K}\right)$$

S/A	SURFACE AREA OF GLASS VOLUME
Q	ACTIVITY PRODUCT FOR DISSOLUTION REACTION
ν_i	STOICHIOMETRIC FACTOR
k_r	RATE CONSTANT
K	EQUILIBRIUM CONSTANT FOR DISSOLUTION REACTION

- EXPERIMENTS MUST PROVIDE k_r AND K

W.L. Bourcier, *Modeling of Glass Dissolution*, presented to the Nuclear Waste Technical Review Board, August, 1990.

REGRESSION OF THE Si-NORMALIZED GLASS DISSOLUTION RATES ($g/m^2 \cdot d$) VS. *IN SITU* pH AT 25°C, 50°C AND 70°C

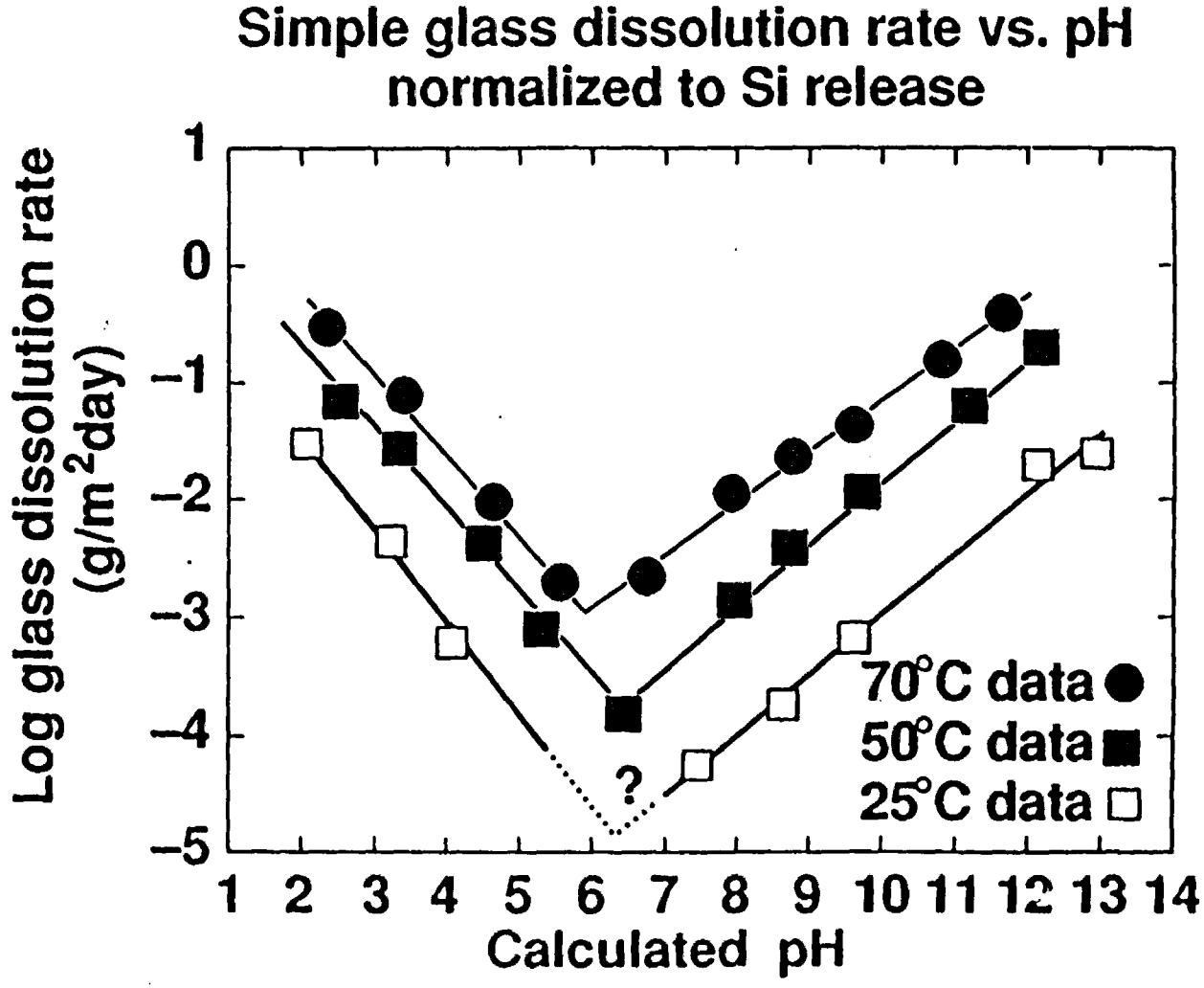

K.G. Knauss, *Experimental Basis for Glass Dissolution*, presented to the Nuclear Waste Technical Review Board, August, 1990.

EXAMPLE 2: STATIC LEACHING/SURFACE ANALYTICAL STUDIES

SOLUTION ANALYSES INDICATE THE REACTION OF BOTH GLASSES SLOWS WITH TIME, BUT DOES THAT TELL THE WHOLE STORY?

131 GLASS

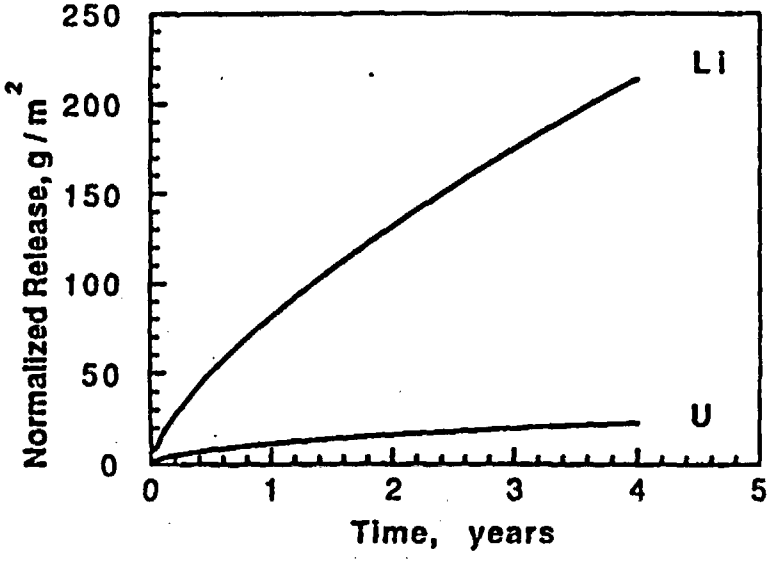

165 GLASS

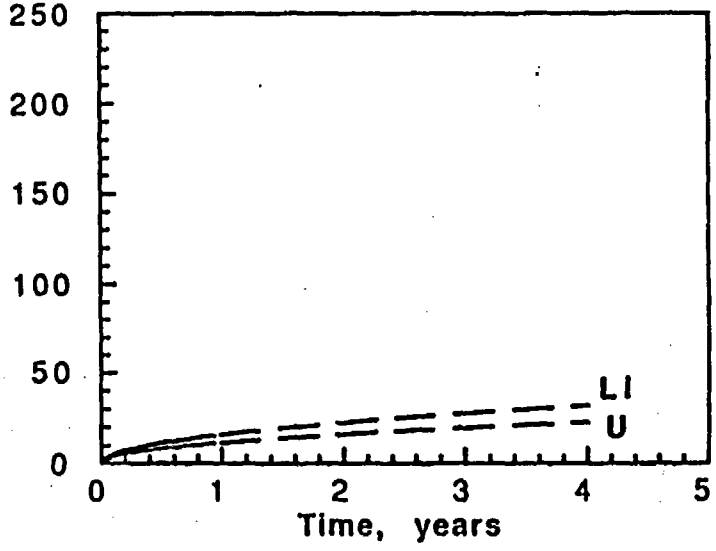

NOTE: WHILE 131 GLASS REACTION IS FASTER THAN 165 GLASS, U RELEASE IS SIMILAR FOR BOTH GLASSES

J.K. Bates, *Integrated Glass Alteration Tests*, presented to the Nuclear Waste Technical Review Board, August, 1990.

Input for simple glass model

Based on years of glass dissolution testing, the rate of release of radionuclides from the glass wasteform can be simplified to expressions involving three environmental parameters, temperature, solution pH, and solution silica concentration. Although many other environmental parameters (such as redox state) affect glass dissolution rates, a relatively simple model that incorporates just these three effects can provide fairly accurate estimates of radionuclide release rates from glass.

This treatment does not provide for the sequestering of radionuclides by precipitation in secondary phases or sorption onto solid surfaces. These phenomena have not yet been investigated to the extent that they can be treated in a rigorous quantitative model. Because sorption and precipitation act to reduce the rates of release of radionuclides, the treatment presented here therefore represents a conservative calculation.

Although glass composition also affects the release rate, we are assuming here that a glass of approximately the same durability as an SRL-165 or SRL-202 glass will be produced (about 53 wt. % silica). Significant deviations from this target composition would necessitate a re-evaluation of the rate equations given below, but probably not the basic assumptions and methodology.

The rate of release of a radionuclide from a borosilicate waste glass can be calculated from the equation:

$$dn_i/dt = \nu_i A k_r (1 - Q/K) \qquad (1)$$

where n_i is the number of moles of radionuclide i released from the glass per unit time t, ν_i is the concentration of i in the glass, A is the surface area of the glass, k_r is the rate constant for glass dissolution, Q is the concentration of silica in solution, and K is the silica solubility product for the glass. Values for each of the parameters in equation can be estimated using the following methods:

1. The concentrations of radionuclides in the glasses (n_i) must be obtained from the glass producers for actual glasses at the time of production. Estimates for these concentrations are available in Oversby (1984) but better estimates periodically become available from the glass producers at Savannah River Laboratories.
2. The surface area of glass (A) in the DWPF cannister of dimensions 61 centimeters diameter and 300 centimeters height is about 5 m^2. After the glass is cooled, however,

thermal contraction causes the glass to crack, effectively increases the available surface area for reaction with water. Baxter (1983) estimates that the cracking process increases the surface area by a factor of about 25 times. An appropriate surface area per cannister is therefore 125 m^2.

3. The rate constant for glass dissolution (r_k) is a function of temperature and pH. Laboratory measurements of the dissolution rate of an analog glass of SRL-165 have been made from pH 1-12 and temperatures of 25-70 °C (Knauss et al., 1990). The data are given in Table 1. A function that provides the rate constant as a function of temperature and pH has been regressed from these data and has the form:

$$r_k = -0.00172029 - 0.0231246 * T + 0.00148569 * T^2 - 0.0000113605 * T^3$$

$$-1.1558 * pH + 0.0812918 * pH^2 + 0.000137686 * pH^3$$

where T is temperature in degrees Celsius. The equation is valid up to 100°C over a pH range of 2 to 12.

4. The model assumes the effect of solution composition is limited to the effect of dissolved silica only. Other species are known to affect dissolution, but silica has the biggest effect (Grambow, 1987; Bourcier, 1991). A simple way to estimate the silica concentration in a groundwater at a potential repository site is to make the justifiable assumption that it is controlled by reactions of the groundwater with the local minerals present at the repository. At sites such a Yucca Mountain where significant amounts of water are not expected, the rock-water system will be rock dominated. The chemistry of evolved groundwater that has been heated and reacted at the waste repository site will be dominated by the local rock type, and less affected by its previous history and reactions with repository materials. However, a better evaluation of repository performance should take into account these other interactions as well.

   The potential repository at Yucca Mountain will be hosted by the Topopah Spring tuff. Experimental rock water interactions at elevated temperatures of samples of Topopah Springs tuff and J-13 well water from nearby have shown that the silica concentration appears to be controlled at saturation with respect to the silica polymorph cristobalite (Knauss et al., 1987). Therefore, for the value of Q in equation 1, we can use the value of the saturation concentration of silica with respect to the phase cristobalite. That value is given as a function of temperature in Table 2 (Walther and Helgeson, 1977).

5. The value of K, the thermodynamic solubility product for the glass, is a complex function of glass composition (Grambow, 1987). However, we can make a simple conservative estimate of its value by equating it to the solubility product of amorphous silica. Grambow (1987) has shown that empirically estimated values for K for a variety

Table 1. Dissolution Rate Constant for Glass

Temperature	pH	log rate ($gm/m^2/day$)
25	1	-1.25
25	2	-1.73
25	3	-2.21
25	4	-2.69
25	5	-3.17
25	7	-4.53
25	8	-4.02
25	9	-3.51
25	10	-3.0
25	12	-1.98
50	1	0.02
50	2	-0.68
50	3	-1.38
50	4	-2.08
50	5	-2.78
50	7	-3.43
50	8	-2.92
50	9	-2.41
50	10	-1.90
50	12	-0.88
70	1	0.51
70	2	-0.18
70	3	-0.87
70	4	-1.56
70	5	-2.25
70	6	-2.94
70	7	-2.3
70	8	-1.9
70	9	-1.5
70	10	-1.1
70	12	-0.3

of glass compositions are always less than but close to the value for amorphous silica. Because K corresponds physically to the silica-rich surface gel that forms on reacted glass surfaces, and it is extremely unlikely that this layer would ever be less stable than amorphous silica (because amorphous silica would then precipitate in the layer), we can use this assumption to provide values of K. These values are listed in column three of Table 2.

Table 2. Saturation Concentrations for Cristobalite and Amorphous Silica.

Temperature	Cristobalite	Amorphous Silica
	(log molal)	
0	-3.89	-2.99
25	-3.45	-2.71
60	-3.02	-2.43
90	-2.75	-2.26
100	-2.68	-2.20
150	-2.36	-1.98
200	-2.12	-1.80

Model Limitations

There are important limitations to the simple method for predicting borosilicate waste glass elemental releases presented here. The most important is that the method ignores all other solution chemistry other than solution pH and solution silica concentration. Some experiments have shown that glass dissolution rates can be orders of magnitude slower in the presence of certain cations such as magnesium (Barkatt et al., 1989). The effect may be due either to the poisoning of the glass surface by adsorbed magnesium or the precipitation of a magnesium-rich phase that armors the glass from further reaction. Other surface chemical reactions could increase the rate of reaction.

Another limitation of this model is that it does not account for the incorporation of radionuclides in secondary phases. Although experimental work has shown that radionuclides are incorporated into such phases (J. K. Bates, pers. com.), we cannot yet quantify the process and and incorporate it into chemical models of dissolution.

The model also ignores any glass reaction in humid environments that may take place during shipping and storage of the glass before reaction with liquid water. Vapor phase hydration of glass in humid environments is known to occur (Diebold and Bates, 1986). The subsequent effects on glass reaction with liquid water present are currently under investigation.

Finally, the effects of other repository materials must be included in the model. Cannister corrosion, the effects of backfill and other synthetic materials in the repository, and the radiation field must all be coupled to the glass dissolution model.

References

Barkatt, A., E. Saad, R. Adiga, W. Sousanpour, Al. Barkatt, M. Adel-Hadadi, J. O'Keefe, and S. Alterescu (1989) Leaching of natural and nuclear waste glasses in sea water. Applied Geochem. 4:593-603.

Baxter, R. G. (1983) Description of defense waste processing facility reference waste form and cannister. Savannah River Plant Report, DP-1606 rev. 1.

Bourcier, W. L. (1991) Overview of chemical modeling of nuclear waste glass dissolution. Mat. Res. Soc. Symp. Proc. v. 212, p. 3-18

Diebold, F. E. and J. K. Bates (1986) Glass-water vapor interaction. Advances in Ceramics, Vol. 20, Nuclear Waste Management II, p. 515-522.

Grambow, B. (1987) Nuclear waste glass dissolution: mechanism, model and application. JSS Project Technical Report 87-02.

Knauss, K. G., W. L. Bourcier, K. D. McKeegan, C. I. Merzbacher, S. N. Nguyen, F. J. Ryerson, D. K. Smith, H. C. Weed, and L. Newton (1990) Dissolution kinetics of a simple analogue nuclear waste glass as a function of pH, time and temperature. Mat. Res. Soc. Symp. Proc. v. 176, p. 371-381.

Knauss, K. G., W. J. Beiriger, and D. W. Peiffer (1987) Hydrothermal interaction of solid wafers of Topopah Spring Tuff with J-13 water at 90 and 150°C using Dickson-type gold bag rocking autoclaves: long-term experiments. Lawrence Livermore National Laboratory UCRL-53722.

Oversby, V. M. (1984) Reference waste forms and packing material for the Nevada Nuclear Waste Storage Investigations Project. Lawrence Livermore National Laboratory UCRL-53531, 26 p.

Walther, J. V., and H. C. Helgeson (1977) Calculation of the thermodynamic properties of aqueous silica and the solubility of quartz and its polymorphs at high temperatures and pressures. Amer. J. Sci. 277:1315-135.

2.2 Glass Waste Form

2.2.1 Radionuclide Content

2.2.1.1 Present Inventory

2.2.1.2 Projected Inventory

2.2.1.3 Radioactivity and Decay Heat vs. Time

2.2.1.4 Glass Species Composition Statistics

2.2.1.5 Fracture/Fragmentation Statistics

2.2.2 Repository Response

2.2.2.1 Gaseous Release from Glass

2.2.2.2 Dissolution Radionuclide Release from Glass

2.2.2.3 Soluble-Precipitated/Colloidal Species

Table 1. Description, Purpose, and Status of Parametric Experiments and N2 and N3 Unsaturated Tests

Experiment #	Description	Purpose	Status (Tests in Progress)	Reaction Rate ($g/m^2/d$)
P-II	Regular-sized glass waste form, no ss holder, 0.075 mL J-13/ 3.5 days, continuous and batch experiments	To study the release from glass only	7 years	0.010
P-III	Half-sized glass waste form, ss holder, 0.075 mL and EJ-13/ 3.5 days, continuous and batch experiments	To study the effect of changing the waste form surface area by reducing the as-cast surface are by half	6.5 years	0.005
P-IV	Half-sized glass waste form, ss holder, 0.0375 mL and EJ-13/ 3.5 days, continuous and batch experiments	To study the effect of drop volume by reducing the amount of water added and the as-cast surface area by half	6 years	0.014
P-V	Regular-sized glass waste form, ss holder, 0.075 mL and EJ-13/ 14 days, continuous and batch experiments	To study the effect of lengthening the time interval between water additions	5.5 years	0.002
P-VII	Regular-sized glass waste forms in presensitized ss holders (heat #699960), 0.075 mL EJ-13/ 3.5 days, continuous and batch experiments	To study the effect of presensitized ss waste form holder	3.5 years	0.017
P-VIII	Regular-sized glass waste forms in presensitized ss holders (heat #22841), 0.075 mL EJ-13/ 3.5 days, continuous and batch experiments	To study the effect of presensitized ss waste form holder	5 years	0.003
Test #				
N2	Regular-sized glass waste forms in presensitized ss holders (heat #699960), 0.075 mL EJ-13/ 3.5 days, continuous and batch experiments	QA I execution of Unsaturated Test on SRL 165 glass doped with Np, Pu, and Am	5 years	0.006
N3	Regular-sized glass waste forms in presensitized ss holders (heat #699960), 0.075 mL EJ-13/ 3.5 days, continuous and batch experiments	QA I execution of Unsaturated Test on ATM-10 glass doped with Np, Pu, and Am	3.5 years	0.011

Table 2. Estimated Forward and Final Rates Based on Static Leach Testing

Glass Type	Reference	Initial Rate $g/(m^2 \cdot d)$	Final Rate $(g/m^2 \cdot d)$
SRL 131	4, 5, 6	4.2	0.03
SRL 131 (Purex)	7	1.0	
SRL 131/11	8	0.05	
SRL 165	9	0.8	0.02
SRL 165/42	8	0.05	
SRL 202	7	0.2	
PNL 76-68	4,9	1.7	0.008, 0.08
JSS-A	4	1.5	0.003
EMS-11	9	0.08	0.002
SAN 60	10		0.2
SM 58	10		0.015

4. C. Grambow and D. M. Strachan, "A Comparison of Nuclear Waste Glasses by Modeling," Pacific Northwest Laboratory report PNL-6698 (1988).

5. J. Bates, D. Lam, and M. Steindler, Mater. Res. Soc. Symp. Proc. Vol. 15, 183 (1983).

6. G. G. Wicks, J. A. Stone, G. T. Chandler, and S. Williams, "Long-Term Leaching Behavior of Simulated Savannah River Plant Waste Glass. Part 1: MCC-1 Leachability Results, Four-Year Leaching Data," Savannah River Laboratory report DP-1728 (1986).

7. W. L. Ebert, Argonne National Laboratory, personal communication (1991).

8. J. K. Bates et al., "Unsaturated Glass Testing for DOE Program in Environmental Restoration and Waste Management, Annual Report, October 1989-September 1990," Argonne National Laboratory report ANL-90/40 (1991).

9. B. P. McGrail, D. M. Strachan, M. J. Apted, D. W. Engel, and P. W. Eslinger, "Preliminary Assessment of the Controlled Release of Radionuclides from Waste Packages Containing Borosilicate Waste Glass," PNL Draft Report (1990).

10. J. J. Mazer, Argonne National Laboratory, personal communication (1991).

Table 3. The Rate of Reaction of Glass in Vapor

Glass	Temp (°C)	Initial Rate (t^1)	Initial Rate ($t^{1/2}$)	Long-term rate	Surface finish	Reference
SRL 202U	200	0.3 μm/day	0.9 μm/$\sqrt{day}$	0.9 μm/day	600 grit	7
SRL 202U	200	1.25 μm/day	---		600 grit	7
SRL 202U	200	0.3 μm/day		5 μm/day	240 grit	7
SRL 202U	90	---	---	0.4 μm/day	---	extrapolated
SRL 165U	200	2.5 μm/day	8 μm/$\sqrt{day}$	7.5 μm/day	240 grit	7
SRL 165U	175	3.75 μm/day	10 μm/$\sqrt{day}$	7.5 - 15 μm/day	240 grit	7
SRL 165U	200	0.25 μm/day	0.9 μm/$\sqrt{day}$	0.4 - 1.6 μm/day	600 grit	7
SRL 165	187	---	---	5.8 μm/$\sqrt{day}$	600 grit	10
SRL 165U	175	0.6 μm/day	1.9 μm/$\sqrt{day}$	0.6 - 1.2 μm/day	600 grit	7
SRL 165U	125	0.2 μm/day	0.8 μm/$\sqrt{day}$	0.2 - 0.5 μm/day	600 grit	7
SRL 165U	90	---	---	0.2 μm/day	---	extrapolated
SRL 131	240	---	11.2 μm/$\sqrt{day}$	21 μm/day	600 grit	11
SRL 131	202	---	5.8 μm/$\sqrt{day}$	7.5 μm/day	600 grit	11
SRL 131	202	---	6.1 μm/$\sqrt{day}$	8 μm/day	600 grit	12
SRL 131	120	---	0.8 μm/$\sqrt{day}$		600 grit	11
SRL 131	75	---	---	0.009 μm/day	600 grit	11
SRL 131	90	---	0.32 μm/$\sqrt{day}$	0.03 μm/day	---	extrapolated

7. W. L. Ebert, Argonne National Laboratory, personal communication (1991).

10. J. J. Mazer, Argonne National Laboratory, personal communication (1991).

11. J. K. Bates, L. J. Jardine, and M. J. Steindler, "The Hydration of Nuclear Waste Glass: An Interim Report," Argonne National Laboratory report ANL-82-11 (1982).

12. T. A. Abrajano, Jr., J. K. Bates, and J. J. Mazer, "Aqueous Corrosion of Natural and Nuclear Waste Glasses. II. Mechanisms of Vapor Hydration of Nuclear Waste Glasses," J. Non-Cryst. solids 108, 269-288 (1989).

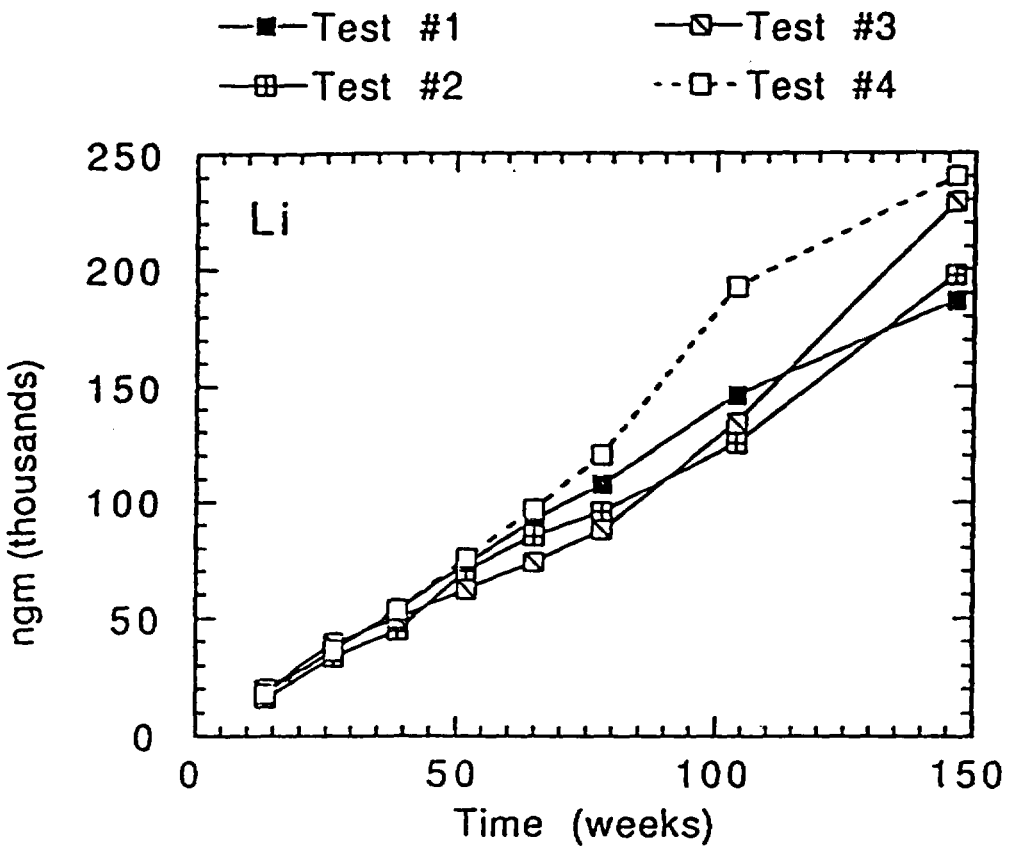

Figure 1. Cumulative Lithium Release from the PVII Tests

J.K. Bates, Argonne National Laboratory, private communication.

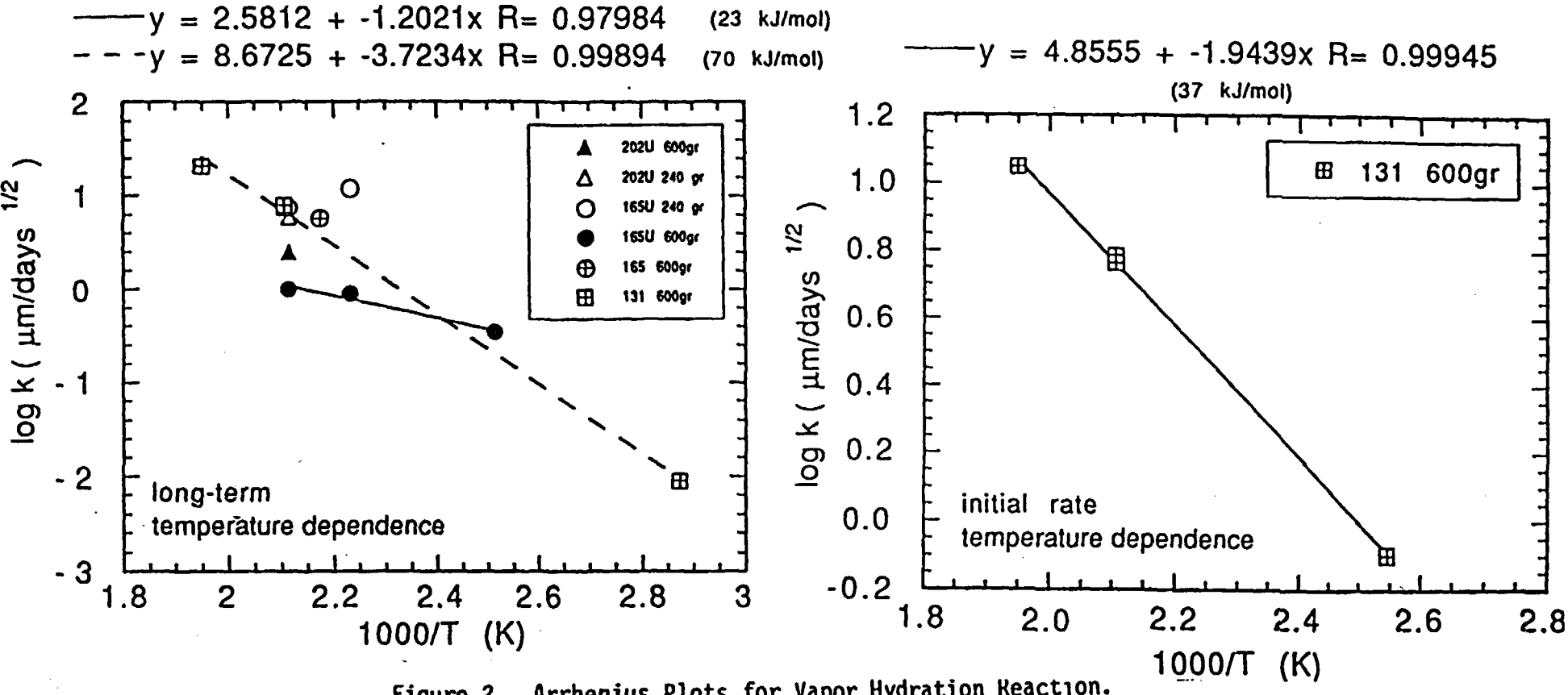

Figure 2. Arrhenius Plots for Vapor Hydration Reaction.
(a) Final Rate. (b) Initial Rate.

7. W. L. Ebert, Argonne National Laboratory, personal communication (1991).

10. J. J. Mazer, Argonne National Laboratory, personal communication (1991).

11. J. K. Bates, L. J. Jardine, and M. J. Steindler, "The Hydration of Nuclear Waste Glass: An Interim Report," Argonne National Laboratory report ANL-82-11 (1982).

12. T. A. Abrajano, Jr., J. K. Bates, and J. J. Mazer, "Aqueous Corrosion of Natural and Nuclear Waste Glasses. II. Mechanisms of Vapor Hydration of Nuclear Waste Glasses," J. Non-Cryst. solids 108, 269-288 (1989).

Table 2. Statistical Analysis of Triplicate Leach Results for Gamma Irradiated SRP 165 Glass[a]. Taken from Bibler[15]

Dose, gray	Average Concentration (ppm), Standard Deviation and Student T Value											
	B			Si			Na			Li		
	Aver.	Dev.	T[b]	Aver.	Dev.	T[b]	Aver.	Dev.	T[b]	Aver.	Dev.	T[b]
Unirrad.	15.3	0.15		109.8	0.52		56.4	0.71		17.8	0.23	
4.0×10^6	14.6	0.34	-3.1	104.7	3.1	-2.8	55.2	1.2	-1.6	17.4	0.36	-1.9
4.7×10^7	15.2	0.06	-1.1	108.1	0.42	-4.4	56.9	0.11	1.1	18.4	0.03	4.0
3.1×10^8	15.5	0.37	0.8	110.1	4.0	0.14	57.9	1.5	1.9	18.4	0.19	3.0

[a]Product Consistent Test: 1.3 grams 100-200 mesh glass leached for 7 days in 13 mL of deionized water at 90°C.

[b]T value for one-sided Student's T test. If $T > +2.1$, then the data are precise enough to establish to the 95% confidence level that the irradiated glass is leaching greater than the unirradiated glass.

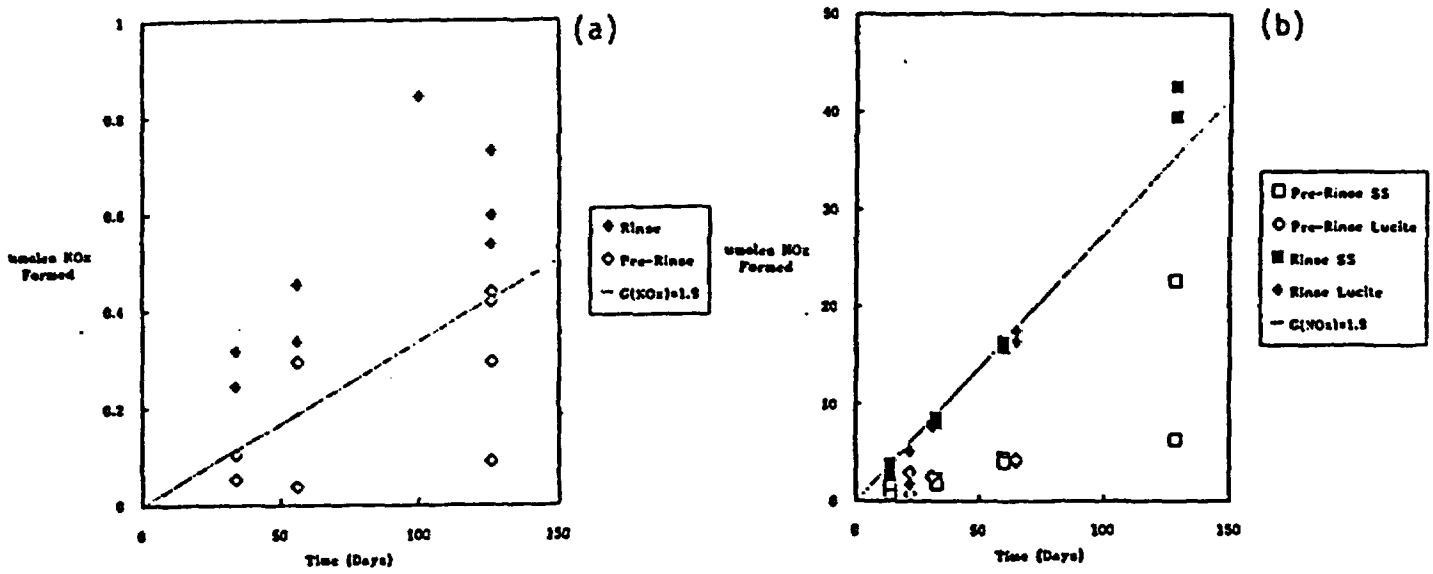

Figure 5. Generation of Nitric Acid in Thin Water Films Due to (a) Gamma Radiation and (b) Alpha Radiation

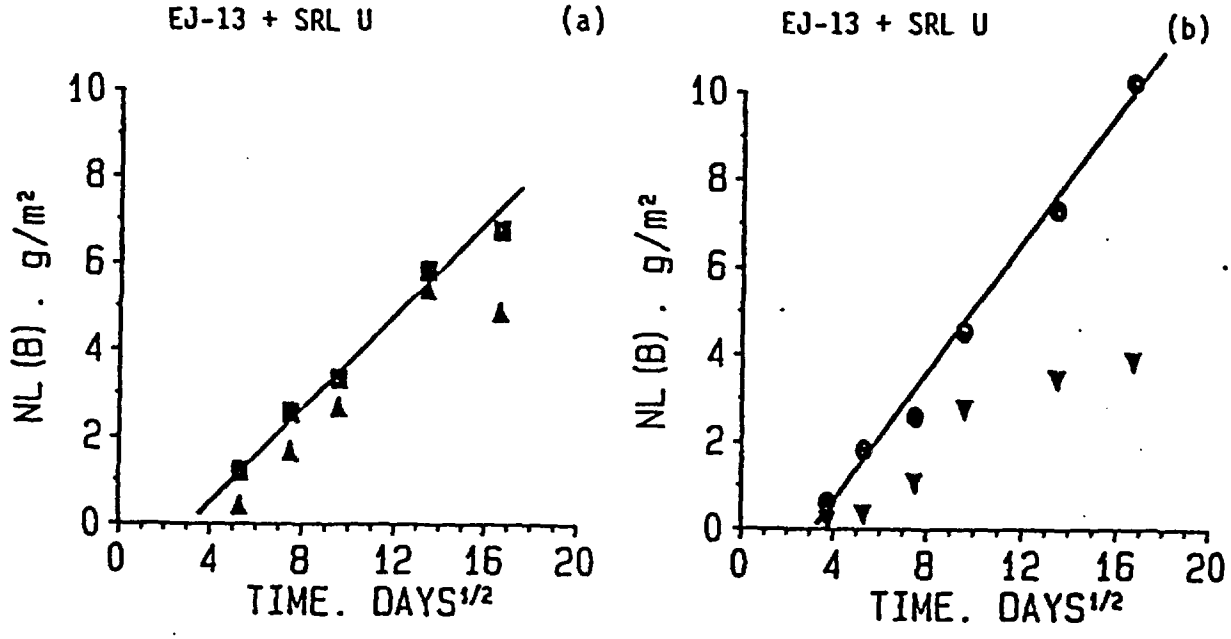

Figure 6. Normalized Boron Mass Loss from SRL U Glass vs. the Square Root of the Reaction Time for EJ-13 Plus SRL U Glass: (a) irradiated, with tuff (▲) or with tuff (■); (b) nonirradiated, without tuff (▼) or with tuff (●). Taken from Ebert.[26]

N.E. Bibler, D.G. Howitt and G.W. Arnold, *Rad. Eff.* 98, 63 (1986).

2.3 Special Cases Waste Forms

2.3.1 Damaged Spent Fuel

2.3.2 Non-LWR Spent Fuel

2.3 Special Cases Waste Forms

Waste Forms that may require special handling or may require special processing or containerizing.

2.3 Special Cases Waste Forms

2.3.1 Damaged Spent Fuel

2.3.2 Non-LWR Spent Fuel

TABLE J-11.1

TYPICAL FUEL ASSEMBLY PARAMETERS*

VENDOR	B&W	B&W	C-E	C-E	W	W	W	ENC	ENC	GE	GE	GE
Fuel Rod Array	15x15	17x17	14x14	16x16	14x14	15x15	17x17	15x15	8x8	7x7	8x8	8x8 R
Reactor Type	PWR	PWR	PWR	PWR	PWR	PWR	PWR	PWR	BWR	BWR	BWR	BWR
Assemblies per Core	177	205	217	177	121	193	193	193	560	764	560	560
Fuel Rod Locations Per Assembly	225	289	196	256	196	225	289	225	64	49	64	64
Fuel Rods Per Assembly	208	264	176	236	179	204	264	204	60	49	63	62
Empty Locations Per Assembly	17	25	5	5	17	21	25	21	4	NONE	1	2
Rod Pitch, mm (in.)	14.4 (0.568)	12.7 (0.501)	14.7 (0.580)	12.9 (0.5063)	14.1 (0.556)	14.3 (0.563)	12.6 (0.496)	14.3 (0.563)	16.3 (0.842)	18.7 (0.738)	16.3 (0.640)	16.3 (0.640)
System Pressure, MPa (psia)	15.2 (2200)	15.5 (2250)	15.5 (2250)	15.5 (2250)	15.5 (2250)	15.5 (2250)	15.5 (2250)	15.5 (2250)	7.14 (1035)	7.14 (1035)	7.14 (1035)	7.14 (1035)
Core Average Power Density, kW/liter	91.4	107.3	78.5	96.4	95.6	98.1	104.7	98.1	40.57	50.732	50.51	49.15
Average LHGR, kW/M (kW/ft)	20.3 (6.20)	18.8 (5.73)	20.0 (6.09)	17.5 (5.34)	20.3 (6.20)	22.0 (6.70)	17.8 (5.44)	22.0 (6.70)	15.2 (4.63)	23.1 (7.049)	17.9 (5.45)	17.7 (5.38)
Axial Peak LHGR, in an Average Rod, W/M (kW/ft)	24.41 (7.44)	22.57 (6.88)	24.00 (7.31)	21.00 (6.41)	24.36 (7.44)	26.40 (8.04)	21.36 (6.53)	26.40 (8.04)	18.24 (6.02)	27.72 (9.16)	21.48 (7.09)	21.24 (6.99)
Max. Peak LHGR, kW/M (kW/ft)	53.0 (16.16)	49.9 (15.20)	53.5 (16.3)	42.7 (13.0)	56.8 (17.3)	61.7 (18.8)	44.6 (13.6)	51.9 (15.83)	47.6 (14.5)	60.2 (18.35)	44.0 (13.4)	44.0 (13.4)
Max. Fuel Temp., °C (°F)	2340 (4245)	2090 (4155)	2140 (3890)	1880 (3420)	2260 (4100)	2340 (4250)	1870 (3400)	2200 (3997)	2040 (3700)	2440 (4430)	1830 (3325)	1890 (3435)
Core Average Enrichment, wt% ^{235}U	3.00	2.67	2.35	2.36	2.90	2.80	2.60	3.02	2.65	2.19	1.80	1.99
Max. Local Exposure, MWd/MTU GJ/kgU	55,000 4752	55,000 4752	50,000 4320	55,000 4752	50,000 4320	50,000 4320	50,000 4320	47,500 4104	35,000 3024	40,000 3456	40,000 3456	45,000 3888
Cladding Material	Zry-4	Zry-4	Zry-4	Zry-4	Zry-4	Zry-4	Zry-4	Zry-4	Zry-2	Zry-2	Zry-2	Zry-2

TABLE J-11.1 (Continued)

VENDOR	B&W	B&W	C-E	C-E	W	W	W	ENC	ENC	GE	GE	GE
Fuel Rod Length, m (in.)	3.904 (153.688)	3.864 (152.125)	3.71 (145.9)	4.09 (161.02)	3.87 (152.36)	3.80 (149.7)	3.85 (151.6)	3.86 (152.0)	3.99 (156.92)	4.09 (161.1)	4.09 (161.1)	4.20 (165.4)
Active Fuel Height, m (in.)	3.602 (141.8)	3.632 (143)	3.47 (136.7)	3.81 (150)	3.66 (144)	3.66 (144)	3.65 (143.7)	3.66 (144)	3.66 (144)	3.66 (144)	3.71 (146)	3.81 (150)
Plenum Length, m (in.)	0.298 (11.27)	0.242 (9.52)	0.22 (8.6)	0.25 (10.00)	0.18 (6.99)	0.21 (8.2)	0.16 (6.3)	0.17 (6.8)	0.27 (10.63)	0.41 (16.0)	0.36 (14.0)	0.25 (10.0)
Fuel Rod OD, mm (in.)	10.922 (0.430)	9.627 (0.379)	11.18 (0.440)	9.70 (0.382)	10.72 (0.422)	10.72 (0.422)	9.50 (0.374)	10.77 (0.424)	12.74 (0.5015)	14.30 (0.563)	12.52 (0.493)	12.27 (0.483)
Cladding ID, mm (in.)	9.576 (0.377)	8.407 (0.331)	9.86 (0.388)	8.43 (0.332)	9.48 (0.3734)	9.48 (0.3734)	8.36 (0.329)	9.25 (0.364)	10.91 (0.4295)	12.68 (0.499)	10.80 (0.425)	10.64 (0.419)
Cladding Thickness, mm (in.)	0.673 (0.0265)	0.610 (0.0240)	0.660 (0.026)	0.635 (0.025)	0.617 (0.0243)	0.617 (0.0243)	0.572 (0.0225)	0.762 (0.030)	0.914 (0.036)	0.813 (0.032)	0.864 (0.034)	0.813 (0.032)
Diametral Gap, micron (mil)	213.4 (8.4)	198.1 (7.8)	216 (8.5)	178 (7.0)	190 (7.5)	190 (7.5)	166 (6.5)	190 (7.5)	254 (10.0)	305 (12.0)	229 (9.0)	228 (9.0)
Fuel Pellet Diameter, mm (in.)	9.362 (0.3686)	8.209 (0.3232)	9.64 (0.3795)	8.26 (0.325)	9.29 (0.3659)	9.29 (0.3659)	8.19 (0.3225)	9.06 (0.3565)	10.66 (0.4195)	12.37 (0.487)	10.57 (0.416)	10.41 (0.410)
Fuel Pellet Length, mm (in.)	15.240 (0.600)	9.525 (0.375)	16.51 (0.650)	9.91 (0.390)	15.24 (0.600)	15.24 (0.600)	13.46 (0.530)	6.93 (0.273)	8.13 (0.320)	12.70 (0.500)	10.67 (0.420)	10.41 (0.410)
Fuel Pellet Density, STD	95	95	94.75	95	94	95	95	94	95	95	95	95

Partial List of Fuel Assemblies considered for Rod Consolidation from RFP No. DE-RP07-86ID12618.

2.3 Special Cases Waste Forms

2.3.1 Damaged Spent Fuel

2.3.2 Non-LWR Spent Fuel

Table 7-1. Number of research and test reactors in each fuel type category

Fuel type	University/ educational	Private research and test	Government-owned (DOE)	Government-owned (non-DOE)
MTR-plate type, U-Al alloy, high enrichment	15	2	14	1
TRIGA (U-Zr hydride fuel)	16	4	2	3
UO_2-polyethylene disks or blocks	4	0	0	0
PULSTAR and other low-enriched pin type	3	2	0	0
Liquid fuels (aqueous solutions)	0	0	1	0
U-Mo alloy, high-enriched (93.2%)	0	0	4	2
FFTF (UO_2- PuO_2)	0	0	1	0
Miscellaneous	0	0	26	0
Totals	38	6	48	6

K.J. Notz, T.D. Welch, R.S. Moore, and W.J. Reich, *Preliminary Waste Form Characteristics*, ORNL-TM-11681 (draft) September, 1990.

Table 7-2. Summary of non-LWR spent fuels

Reactor or site	Estimated quantities		
	End of 1989	Annual rate	End of 2020
HTGR Reactors			
Fort St. Vrain (elements)	732	0[a]	2214[b]
Peach Bottom I			
Core I (elements)	819	0	819
Core II (elements)	820	0	820
Research and Test Reactors[c]			
MTR Plate	--	-	20,000[d]
TRIGA	--	-	4,500
UO_2/Polyethylene	--	-	87
PULSTAR	--	-	170
FFTF (assemblies)	170	30-45	677[e]
Miscellaneous (kg HM)[g]			
ANL West	311		
Babcock & Wilcox	88		
Battelle-PNL	2,348		
HEDL	263[h]		
INEL	39,508[i]		
LANL	38		
ORNL	1,254		
SRS	19,110		

[a]Reactor was shut down in 1989. No further refueling is expected.

[b]Includes final discharge of full core.

[c]Total through 2020, including fuels in reactors at that time. Quantities shown are numbers of individual fuel elements, except for the FFTF.

[d]This is expected to be reprocessed and disposed of as defense HLW.

[e]Through year 2003; does not include final core discharge.

[g]Reported as kg of heavy metal (U plus Pu plus Th). Data are from Integrated Data Base for 1990.

[h]Includes some FFTF and TRIGA fuels.

[i]Not including Shippingport LWBR fuel (982 kg U, mostly U-233, and 56,167 kg Th), 17 Turkey Point 3 assemblies and 69 VEPCO assemblies being used for dry consolidation testing, HTGR fuel, Pulstar and TRIGA fuel, and TMI-2 spent fuel and core debris.

K.J. Notz, T.D. Welch, R.S. Moore, and W.J. Reich, *Preliminary Waste Form Characteristics*, ORNL-TM-11681 (draft) September, 1990.

Table 7-5. Estimated number of canisters required for repository disposal of various non-LWR and special LWR spent fuels[a]

	Number of fuel assemblies			
	In storage, 1988	Total as of year 2020[b]	Estimated fuel assemblies per canister	Estimated number of canisters required
24-in. diam x 12 ft canisters				
Fort St. Vrain	732	2214	4	554
Peach Bottom-1	1639	1639	12	138
TRIGA	800	4500	112	40
PULSTAR	24	170	48	4
CEUSP material	401[c]	401[c]	24	17
Fermi-1 blanket	510	510	12	43
Elk River	188	188	12	16
EBWR	300	300	24	13
Canned fuel at B&W	58[d]	58[d]	24	3
Saxton	14[e]	14[e]		4
Other	-	-	-	60[f]
Total	4,666	9,994		892
28-in. diam x 15 ft canisters				
VEPCO	69	69	4[g]	15
Turkey Point	20	20	4	5
Dresden 1	20	20	8	3
Shippingport LWBR	65	65	1	65
TMI-2 (estimated)	-	-		350
Other	-	-	-	40[f]
Total	174	174		478
Total number of canisters				1,370

[a]Only the major non-LWR and special LWR fuels are listed. An allowance is included for minor fuels not specifically listed.

[b]Reloads and in-core fuel are included in totals.

[c]CEUSP material is stored in 3.5-in. diameter x 24 in. cans; numbers shown are numbers of cans.

[d]There are 58 cans of LWR fuel at B&W, Lynchburg. Cans are 4.25-in. diameter x 33 in. long.

[e]Quantities shown are numbers of cans.

[f]An allowance is included here for fuels not specifically listed.

[g]Some of these assemblies have been compacted.

K.J. Notz, T.D. Welch, R.S. Moore, and W.J. Reich, *Preliminary Waste Form Characteristics*, ORNL-TM-11681 (draft) September, 1990.

Table 7-6. Radioactivity and decay heat of Fort St. Vrain spent fuel per MTIHM

Time after discharge, years	Radioactivity (Ci/MTIHM)	Decay heat (W/MTIHM)
1	3.36E06	1.0E04
10	9.82E05	2.5E03
100	1.17E05	4.0E02
1,000	4.42E02	1.5E01
10,000	1.22E03	3.0E01
100,000	1.40E03	3.0E01
1,000,000	6.17E01	2.0E00

Table 7-7. Estimated radioactivity and decay heat per canister of Fort. St. Vrain fuel

Time after discharge, years	Radioactivity (Ci/canister)	Decay heat W/canister
1	75,600	225
10	22,000	56
100	2,600	9
1,000	10	0.3
10,000	27	0.7
100,000	32	0.7
1,000,000	1.4	0.05

K.J. Notz, T.D. Welch, R.S. Moore, and W.J. Reich, *Preliminary Waste Form Characteristics*, ORNL-TM-11681 (draft) September, 1990.

Table 7-8. Estimated radioactivity and decay heat per canister of FLIP TRIGA fuel

Time after discharge (years)	Radioactivity (Ci/canister)	Decay heat (W/canister)
1	9.0E04	380
5	2.0E04	100
10	1.5E04	80
100	1.6E03	40
1,000	68	2
10,000	9	0.5
100,000	1	0.04
1,000,000	0.16	0.02

Table 7-9. Estimated radioactivity and decay heat per canister of PULSTAR fuel

Time after discharge (years)	Radioactivity (Ci/canister)	Decay heat (W/canister)
1	1.7E05	750
10	3.0E04	82
100	3.0E03	21
1,000	140	4
10,000	35	1
100,000	4	0.08
1,000,000	0.4	0.04

K.J. Notz, T.D. Welch, R.S. Moore, and W.J. Reich, *Preliminary Waste Form Characteristics*, ORNL-TM-11681 (draft) September, 1990.

Table 7-10. Projected volumes of miscellaneous wastes[a]

	Estimated total in 2020 (m^3)	Est. annual rate in 2020 (m^3)
OCRWM-generated TRU waste	600[b]	60-260[c]
Commercial TRU waste		
West Valley decommissioning	300	0
Other decommissioning	680	TBD
Abnormal reactor operations	70[d]	10-30
Industrial/institutional	TBD	10-40
Reactor decommissioning	15060[e]	46[f]
Radioisotope capsules	500[g]	0
Routine reactor operations[h]	8,000	15[b]
Totals	11,710	282-532

[a]Data are given in m^3. One 2-ft by 12-ft canister holds about 1 m^3. "TBD" means to be determined.

[b]Depends on startup date for these facilities; 2010 was assumed.

[c]From dry rod consolidation. The upper limit is a conservative (high) estimate of HEPA filter usage.

[d]Quantity estimated based on two abnormal reactor operations (at Oyster Creek and TMI-2).

[e]Assumes 65 have been decommissioned.

[f]Assumes 2 per year.

[g]Assumes that 90% of existing capsules are packages in canisters by 1995; later packaging would result in fewer canisters because of the decreased thermal output per capsule.

[h]Based on estimated quantity of 3 m^3 per GW(e)-yr being GTCC, and an EIA projection of 52 GW(e) installed capacity in 2020 (no new orders case).

K.J. Notz, T.D. Welch, R.S. Moore, and W.J. Reich, *Preliminary Waste Form Characteristics*, ORNL-TM-11681 (draft) September, 1990.

Table 7-11. Volumes and Activities of Decommissioned LWR Activated Metals[a]

Component	Constr.[b] Material	Disposal Volume[c] (m^3)	Activity (Ci)	Disposal Concentration (Ci/m^3)
Reference BWR:				
Steam separator assembly	S	10	9,600	960
Fuel support pieces	S	5	700	140
Control rods and in-core instruments	S	15	189,000	12,600
Control rod guide tubes	S	4	100	25
Jet pump assemblies	S	14	20,000	1,429
Top fuel guide	S	24	30,000	1,254
Core support plate	S	11	650	59
Core shroud	S	47	6,300,000	134,043
Reactor vessel wall	C	8	2,160	270
Total		138	6,552,310	
Reference PWR:				
Pressure vessel cylindrical wall	C	108	19,170	178
Vessel head	C	57	<10	0.18
Vessel bottom	C	57	<10	0.18
Upper core support assembly	S	11	<10	0.91
Upper support columns	S	11	<100	9.1
Upper core barrel	S	6	<1,000	167
Upper core grid plate	S	14	24,310	1,736
Guide tubes	S	17	<100	6
Lower core barrel	S	91	651,000	7,154
Thermal shields	S	17	146,000	8,594
Core shroud	S	11	3,431,100	311,909
Lower grid plate	S	14	553,400	39,529
Lower support columns	S	3	10,000	333
Lower core forging	S	31	2,500	81
Miscellaneous internals	S	23	2,000	87
Reactor cavity liner	S	14	<10	0.7
Total		485	4,840,820	

a Source: Oztunali 1986.

b Construction material symbols: S = stainless steel, C = carbon steel.

c Disposal volumes include the disposal container after the activated metal components have been cut into manageable pieces.

K.J. Notz, T.D. Welch, R.S. Moore, and W.J. Reich, *Preliminary Waste Form Characteristics*, ORNL-TM-11681 (draft) September, 1990.

Table 7-12. Radioactivity and thermal power of canisters within strontium and cesium capsules[a]

Decay time (years)	Strontium canister (4 capsules)		Cesium canister (4 capsules)	
	Curies	Watts	Curies	Watts
0	412,400	1,380	371,000	918
5	366,300	1,230	330,000	817
10	325,200	1,090	294,000	727
20	256,300	860	233,000	577
50	125,500	420	117,000	290
100	38,200	128	36,800	91
200	3,530	12	3,650	9
300	327	1.1	360	0.9
1,000	1.9E-05	6.4E-08	3.4E-05	8.4E-08

[a]Based on ORIGEN2 calculations. Radioactivity and thermal power include the contributions of the daughter isotopes Y-90 and Ba-137M. Starting point for decay time is December 1985. The assumed thermal limits at a decay time of 10 years are 1,170 W/canister for Sr capsules and 800 W/canister for Cs capsules (Coony 1987).

K.J. Notz, T.D. Welch, R.S. Moore, and W.J. Reich, *Preliminary Waste Form Characteristics*, ORNL-TM-11681 (draft) September, 1990.

Table 8-1 Average Properties of LWR Spent Fuel

BWR Spent Fuel Average Properties:	Historical	Projected	Total
Burnup (GWd/MTU)	21	33	30
Enrichment (%)	2.3	3.2	3.0
Discharged (year)	1981	2007	2001
Thermal Power (W/MT)			
in 2010 (over 5 years old)	–	–	
in 2020 (over 5 years old)	–	–	
in 2050 (all fuel)	–	–	
PWR Spent Fuel Average Properties:	**Historical**	**Projected**	**Total**
Burnup (GWd/MTU)	29	42	39
Enrichment (%)	2.9	3.9	3.7
Discharged (year)	1982	2007	2002
Thermal Power (W/MT)			
in 2010 (over 5 years old)	–	–	
in 2020 (over 5 years old)	–	–	
in 2050 (all fuel)	–	–	

K.J. Notz, T.D. Welch, R.S. Moore, and W.J. Reich, *Preliminary Waste Form Characteristics*, ORNL-TM-11681 (draft) September, 1990.

Major Contributors	Est. Canisters
HTGRs	
Fort St. Vrain	554
Peach Bottom-1	138
Degraded LWR Fuel	
TMI-2	350
Other Contributors	
Shippingport LWBR	65
Fermi-1 Blanket	43
TRIGA	40
All Others	245

R.E. Woodley, *The Characteristics of Spent LWR Fuel Relevant to its Storage in Geologic Repositories*, HEDL-TME 83-28, October, 1983.

3. SCIENTIFIC BASIS FOR PREDICTIVE MODEL DEVELOPMENT

3. SCIENTIFIC BASIS FOR PREDICTIVE MODEL DEVELOPMENT

3.1 SPENT FUEL CLADDING FAILURE

3.1.1 EXPERIMENTAL PARAMETERS FOR FAILURE MODELS

3.1.2 FAILURE MODELS

3.2 SPENT FUEL OXIDATION

3.2.1 EXPERIMENTAL PARAMETERS FOR OXIDATION MODELS

3.2.2 OXIDATION MODELS

3.3 SPENT FUEL FISSION GAS RELEASE

3.3.1 EXPERIMENTAL PARAMETERS FOR FISSION GAS RELEASE

3.3.2 FISSION GAS RELEASE MODELS

3.4 SPENT FUEL DISSOLUTION

3.4.1 EXPERIMENTAL PARAMETERS FOR DISSOLUTION

3.4.1.1 DISSOLUTION RATES

3.4.1.2 SOLUBILITY LIMITS

3.4.1.3 SOLUBILITY LIMITING PHASES

3.4.2 DISSOLUTION MODELS

3.5 GLASS DISSOLUTION

3.5.1 EXPERIMENTAL PARAMETERS FOR GLASS DISSOLUTION

3.5.2 GLASS DISSOLUTION MODELS

3.6 OTHER RELEASE SOURCES OF RADIONUCLIDES

3.6.1 CRUD

3.6.2 HARDWARE

3.6.3 CLADDING

3.1 Spent Fuel Cladding Failure

The Zircaloy cladding that already exists on the fuel rod may be an important barrier that contributes in a performance evaluation of waste forms to their ability to meet the radionuclide release requirement. Several potential mechanisms of Zircaloy cladding degradation during dry storage have been identified, such as hydride reorientation, stress corrosion cracking, creep, and creep fracture.

At the present time three distinct time periods can be identified during repository storage:

1. A high-temperature period (above 250°C) during which the container is probably unbreached, the fuel rods are surrounded by inert gas or air, and no liquid water is present.

2. An intermediate-temperature period (250° to 100°C) when the container is probably unbreached and liquid water (from breached fuel rods containing water) may be present in contact with the fuel rods (90 to 1000 years).

3. A lower-temperature period (below 100°C) when the container may be breached and air, water vapor, and liquid water may be in contact with the spent fuel rods.

Cladding Failure Model

Model equations. LLNL is currently formulating quasi-static rate of displacement and rate of stress equations for a Zircaloy tube with an adjacent thin zirconium oxide film. The equations include contributions from elastic, creep, thermal, and hydride precipitation dependent strains. Given initial conditions and expected repository environmental histories to derive boundary conditions, we will integrate the set of rate equations to assess cladding failure. Our simplest and most conservative modeling assumption, with respect to cladding failure, is a stress or strain limit at which the zirconium oxide film fractures. This failure modeling concept is motivated because of the known large volume change that occurs when zirconium in the Zircaloy is oxidized to zirconium oxide. Hence, the oxide film is expected to remain in a compressive state of hoop stress for the expected large number of fuel rods that initially have low fission gas releases (<1%). This compressive hoop stress will prevent stress corrosion cracking from being initiated. In addition to the strain contribution of hydride precipitate, another potential mechanism of cladding failure is fluoride-Zircaloy corrosion, which is not stress dependent. The available data for fluoride-Zircaloy corrosion are preliminary, but suggest a pin-hole pitting uniformly distributed on the surface.

There have been no activities to evaluate stainless steel cladding failure response. The amount of stainless steel cladding is very small compared to the amount of Zircaloy cladding.

Measured quantities. Initial conditions are required for a rate displacement-stress formulation; thus, measurements for the initial dimensions and state of stress of the Zircaloy and zirconium oxide film are necessary to characterize the cladding. The boundary condition for a rate displacement-stress formulation of the cladding are the inside and outside pressure histories. This means that the fission gas content (released from UO_2 spent fuel matrix) inside the cladding is required for the fuel rods. This data will also have a statistical character because the different UO_2 fuels and burnup cycles may result in different amounts of fission gas content in the fuel rods. We would like to see this expressed as a probabilistic density function f(g,b,t), where the density function, f, is the number of fuel rods per unit fission gas content per unit burnup with fission gas content, g, and burnup, b, at time, t. At t=0, this density function would characterize the initial distribution of fission gas content in fuel rods emplaced in the repository. At later times, the fission gas content may increase because of helium produced due to decaying actinides. Thus, to predict the expected stress state in the Zircaloy and in the oxide film, the expected fission gas released from the UO_2 matrix is a required initial condition that must be measured.

Considerable information on material properties for the elastic strain, creep strain, thermal strain, and fracture responses of Zircaloy cladding is available from reports and analysis for the Dry Storage Spent Fuel Program, reactor design documents, and the open literature. Some of this data may require additional confirmation tests for purposes of QA Level I input to models and analysis. Much of the data is not particularly useful because of the relatively low temperatures expected in a repository compared to in-reactor temperatures and the tensile hoop stress state expected in a repository compared to in-reactor compressive hoop stress state. Also, some testing to establish material properties of zirconium oxide failure is anticipated; again, this may be confirmation tests. The problem of hydride precipitation strains will require measurement of the initial concentrations of hydrogen as well as low temperature hydride platelet orientation statistics in each class of Zircaloy cladding. Additional testing and model development for hydride precipitation and re-orientation and its associated dependence on the state of stress are currently being planned. The initial hydrogen content data may have a statistical character similar to the fission gas content data. Hence, we are interested in it being expressed as a probabilistic density function, $h(H, a_r, a_\theta, b)$, where the density function, h, is the number of fuel rods per unit hydrogen content per unit size in the radial direction per unit size in the theta direction per unit burnup with hydrogen content H, a_r length of hydride platelets in the radial direction, a_θ length of hydride platelets oriented in the theta (hoop) direction, and burnup, b. Note that time is not a variable here as we do not anticipate additional hydrogen pickup by the cladding in the low temperature environment of the repository.

With this statistical information on initial hydrogen content and low temperature orientation, a time-dependent model is being planned to predict the precipitation kinetics of hydride platelets and the effect of stress on the hydride

platelet orientation as the repository temperature decreases. The strain contribution from hydride platelet precipitation is a required part of the model development for assessing probable cladding failure rate.

Finally, the proposed quasi-static displacement-stress rate model assumes that the Zircaloy cladding and its adjacent zirconium oxide film are initially pristine. This assumption must be supported as part of the MCC characterization of spent fuel rods. Certainly there will be a statistical character to the initial qualities of the fuel rods with respect to defects and surface flaws. We will need to have data on flaw size, flaw surface density, etc. We plan to support tests that will subject flawed and defected cladding to temperature and stress states that will provide failure data for additional failure rate models for the number of fuel rods that are not initially pristine.

The following list of references address the progress that has been accomplished in testing, modeling, and understanding the complexities of spent fuel cladding failure response and a range of environmental conditions that may need to be addressed in the design of a geological repository.

Ardell, A.J. "On the Calculation of Melting Temperatures for Low-Temperature Phases of Polymorphic Metals," Acta Metall., 11, 591-594 (June, 1963).

Blackburn, L.D., et al. "Maximum Allowable Temperature for Storage of Spent Nuclear Fuel: An Interim Report," HEDL-TME 78-37, UC-70 (1978).

Chen, I.-W. "Implications of Transformation Plasticity in ZrO_2-Containing Ceramics: II, Elastic-Plastic Indentation," J. Am. Ceram. Soc. 69(3), 192 (1986).

Christian, J.W. "Phase Transformations," in Physical Metallurgy, R.W. Chan, ed., North-Holland Pub. Co., Ch. 10, pp. 443 (1965).

deGroot, S.R. "Thermodynamics of Irreversible Processes," North-Holland Pub. Co. Amsterdam (1957).

Dieter, G.E. Mechanical Metallurgy, second edition, McGraw Hill (1976).

Einziger, E.R., D.M. Bozi, and A.K. Miller. "Transactions," Waste Form Development and Processing, American Nuclear Soc. p. 131 (1980).

Einziger, R.E. and R. Kohli. "Low-Temperature Rupture Behavior of Zircaloy-Clad Pressurized Water Reactor Spent Fuel Rods Under Dry Storage Conditions," Nuc. Tech., 67, 107 (1984).

Ells, C.E. "Hydride Precipitates in Zirconium Alloys," N. Nuc. Mat., 28, 129 (1968).

Ells, C.E. "The Stress Orientation of Hydride in Zirconium Alloys," J. Nuc. Mat., 34, 306 (1970).

Eringen, A.C. "Mechanics of Continua," John Wiley Pub. New York (1967).

Farwick, D.G. and R.A. Moen. "Properties of Light Water Reactor Spent Fuel Cladding," Westinghouse Hanford Report HEDL-TME 78-70 (Aug. 1979).

Gibbs, J. "The Scientific Papers of J. Willard Gibbs," Vol. 1, Dover Pub. Inc., New York (1961).

Hardy, H.K. and T.J. Heal. "Report on Precipitation," in Progress in Metal Physics, 5, 143, 2nd printing, Pergamon Press (1961).

Khan, M.A., N.H. Madsen, and B.A. Chin. "Fracture Predictions in Zircaloy Fuel Cladding: Effects of Radiation on Materials," Twelfth International Symposium, ASTM Stp 870, Philadelphia, pp. 642-655 (1985).

Leger, M. and A. Donner. "The Effect of Stress on Orientation of Hydrides in Zirconium Alloy Pressure Tube Materials," Canadian Meta. Qu., 24, 235 (1984).

Lupis, C.H.P. "Chemical Thermodynamics of Materials," Elsevier Science Pub., New York (1983).

Lustman, B. and F. Kerze, Jr., eds. "The Metallurgy of Zirconium," McGraw Hill, first edition, p. 354 (1955).

Miller, A.K. "Application of the SCCIG Model to Dry Storage of Spent Fuel," Workshop on Spent Fuel Integrity in Dry Storage, Seattle, WA, (Jan 20, 1982).

Onsager, L. "Reciprocal Relations in Irreversible Processes; I and II," Phys. Rev. 37 405, and 38 2265 (1931).

Ostberg, G. "Crack Propagation in Hydrided Zircaloy-2," Int. J. Fract. Mech., 4 95 (1968).

Parfenov, B.G., V.V. Gerasimov, and G.I. Venddiktova. "Corrosion of Zirconium and Zirconium Alloys," (translated from Russian), Israel Program for Scientific Translations, Jerusalem, p. 87 (1969).

Pearson, W.B. "Handbook of Lattice Spacings and Structures of Metals and Alloys," 1, 130.

Pescatore, C., M.G. Cowgill, and T.M. Sullivan. "Zircaloy Cladding Performance Under Spent Fuel Disposal Conditions," Brookhaven National Laboratory Report BNL-52235 (Progress Report May 1 - October 31, 1989).

Rothman, A.J. "Potential Corrosion and Degradation Mechanisms of Zircaloy Cladding on Spent Nuclear Fuel in a Tuff Repository," UCID-20172 (Sept. 1984).

Sawatzky, A. J. Nucl. Mat, 2,321 (1960).

Smith, C.F. and W.B. Crandall, J. Amer. Ceramic Soc., 47(12), 624-627 (Dec., 1964).

Smith, H.D. "Initial Report on Stress Corrosion Cracking Experiments Using Zircaloy-4 Spent Fuel Cladding Rings," Westinghouse Hanford Company, Richland, WA.

Smith, H.D. "Zircaloy Cladding Corrosion Degradation in a Tuff Repository," HEDL-7455, Rev. 1, p. 12 (July, 1985).

Stehle, H., F. Garzarolli, A.M. Garde, and P.G. Smerde. "Zirconium in the Nuclear Industry," Sixth International Symposium, ASTM STP 824, pp. 483-506 (1984).

Stout, R.B. "A Deformation and Thermodynamic Model for Hydride Precipitation Kinetics in Spent Fuel Cladding," Lawrence Livermore National Laboratory, UCRL-100860, (submitted to Symp. on Scientific Basis for Nuclear Waste Management XII, Boston MA, Nov. 27-30, 1989).

Stout, R.B. "Deformation and Thermodynamic Response for a Crack Dislocation Model of Brittle Fracture," Eng. Fract. Mech., 19, 545 (1984).

Stout, R.B. "Modeling the Deformations and Thermodynamics for Materials Involving a Dislocation Kinetics," Cryst. Latt. Def. 9, 65 (1981).

Yaggee, F.L., R.F. Mattas, and L.A. Neimark. "Characterization of Irradiated Zircaloys" Susceptibility to Stress Corrosion Cracking," NP-1557, Research Project 1027, prepared by Argonne National Laboratory for EPRI, pp. 4-27, Fig. 4-7 (Oct., 1980).

3. SCIENTIFIC BASIS FOR PREDICTIVE MODEL DEVELOPMENT

3.1 SPENT FUEL CLADDING FAILURE

3.1.1 EXPERIMENTAL PARAMETERS FOR FAILURE MODELS

3.1.2 FAILURE MODELS

3.2 SPENT FUEL OXIDATION

3.2.1 EXPERIMENTAL PARAMETERS FOR OXIDATION MODELS

3.2.2 OXIDATION MODELS

3.3 SPENT FUEL FISSION GAS RELEASE

3.3.1 EXPERIMENTAL PARAMETERS FOR FISSION GAS RELEASE

3.3.2 FISSION GAS RELEASE MODELS

3.4 SPENT FUEL DISSOLUTION

3.4.1 EXPERIMENTAL PARAMETERS FOR DISSOLUTION

3.4.1.1 DISSOLUTION RATES

3.4.1.2 SOLUBILITY LIMITS

3.4.1.3 SOLUBILITY LIMITING PHASES

3.4.2 DISSOLUTION MODELS

3.5 GLASS DISSOLUTION

3.5.1 EXPERIMENTAL PARAMETERS FOR GLASS DISSOLUTION

3.5.2 GLASS DISSOLUTION MODELS

3.6 OTHER RELEASE SOURCES OF RADIONUCLIDES

3.6.1 CRUD

3.6.2 HARDWARE

3.6.3 CLADDING

OBSERVED RELATIONSHIP: log t_f (TIME TO FAILURE) vs. STRESS (% OF YIELD STRESS)

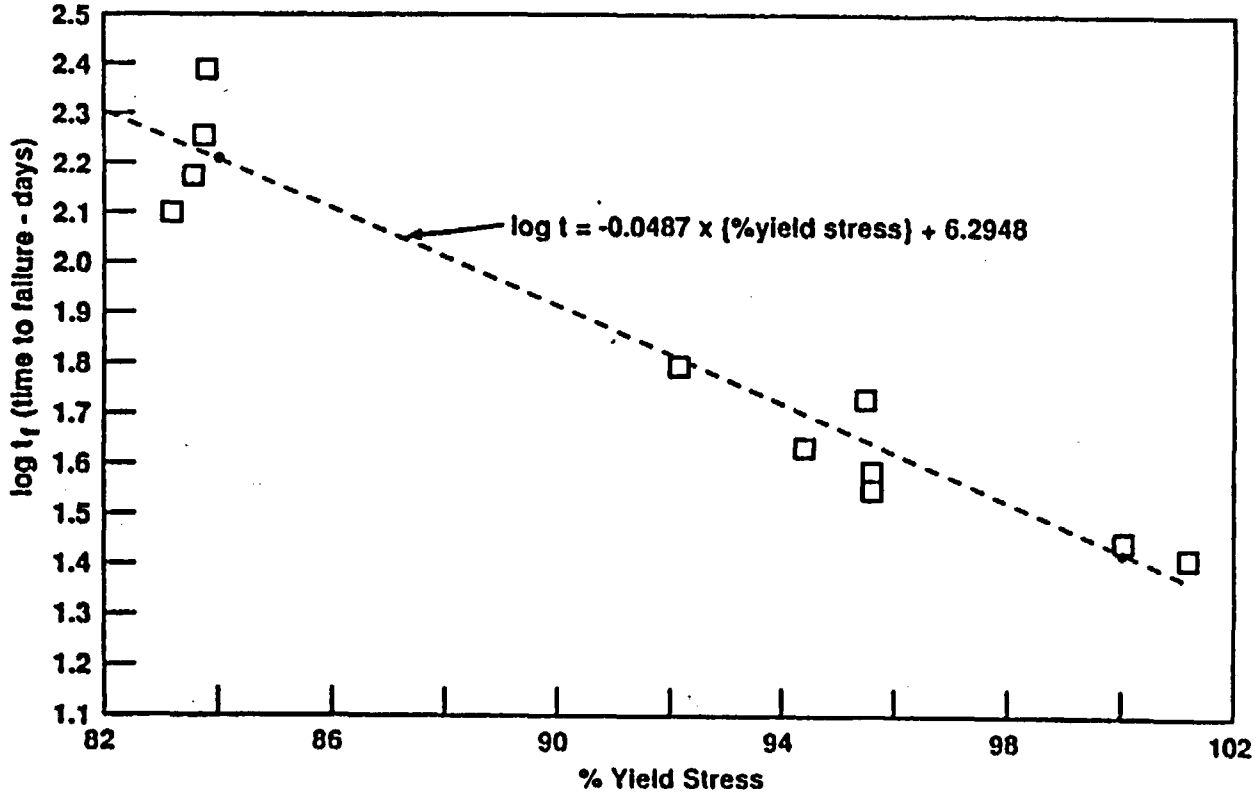

H.D. Smith, *Spent Fuel Cladding Degradation*, presented to the Nuclear Waste Technical Review Board, August, 1990.

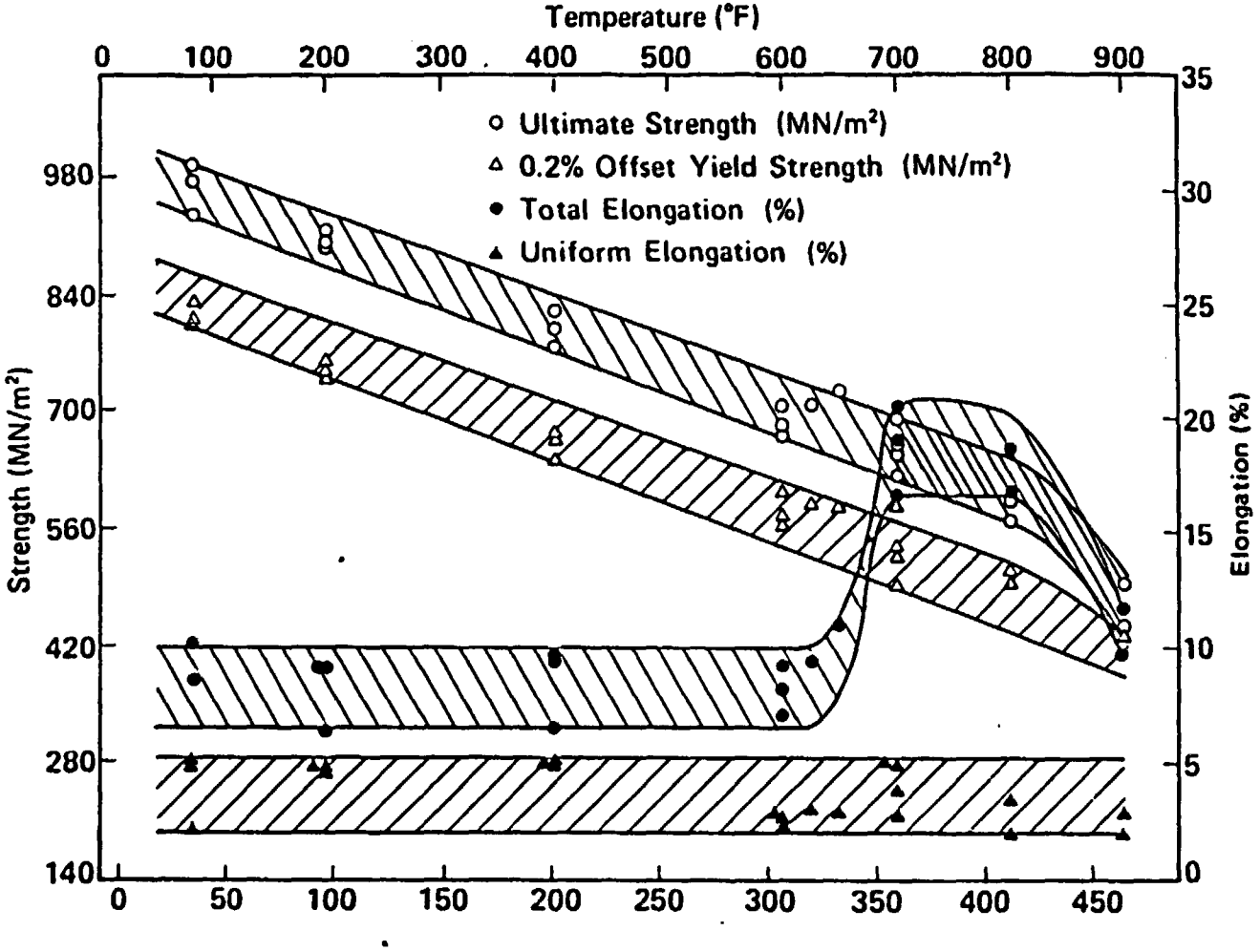

Fig. 2. Effect of temperature on the tensile properties of H.B. Robinson spent fuel cladding. Strain rate = 0.025 / min. A.A. Bauer, L.M. Lowry, "Tensile Properties and Annealing Characteristics of H.B. Robinson Spent Fuel Cladding," Nuclear Technology, Vol. 41, Dec. 1978, pp. 359-372.

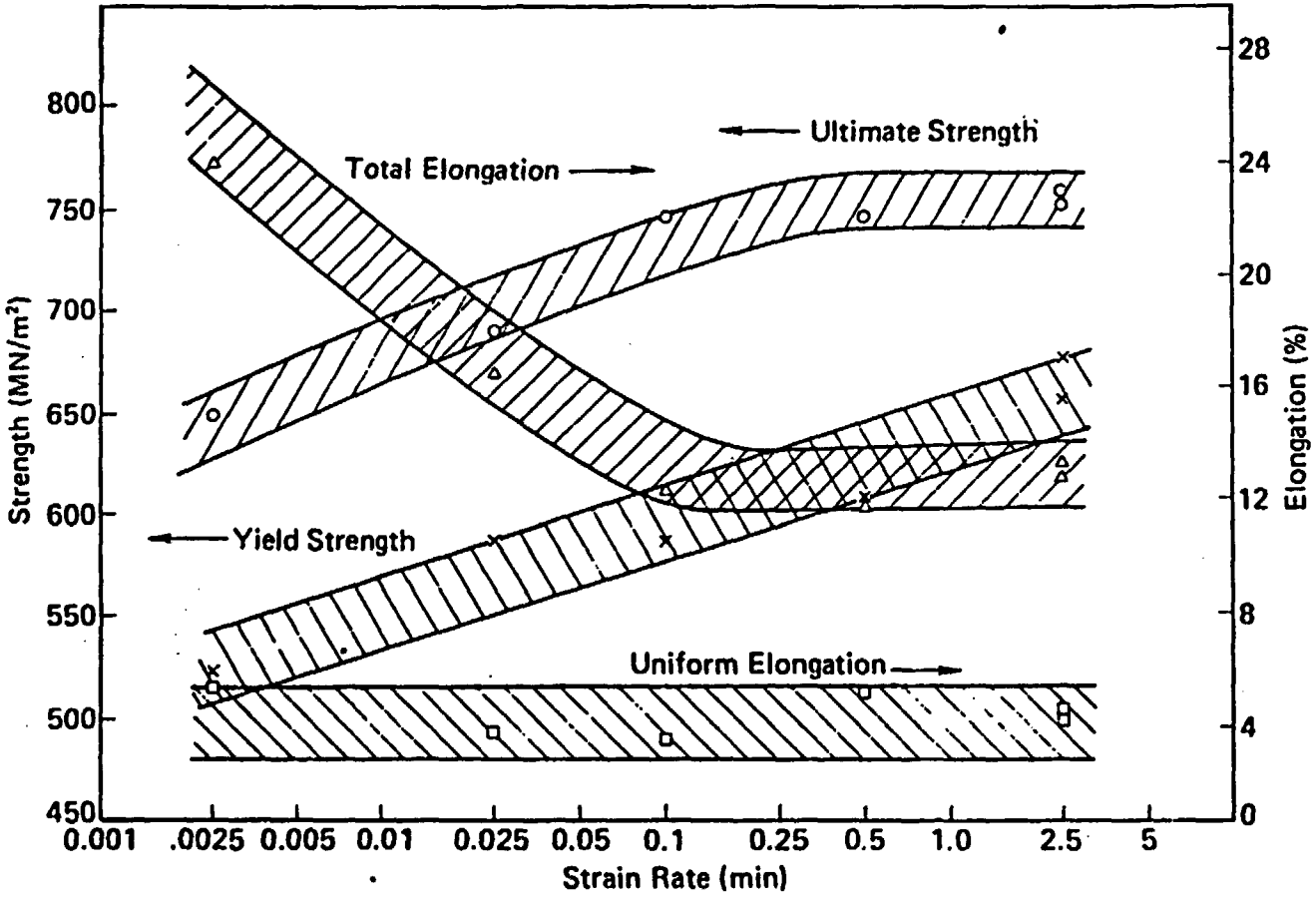

Fig. 3. Effect of strain rate on the tensile properties of H.B. Robinson spent fuel cladding. Test temperature was 371°C. A.A. Bauer, L.M. Lowry, "Tensile Properties and Annealing Characteristics of H.B. Robinson Spent Fuel Cladding," Nuclear Technology, Vol. 41, Dec. 1978, pp. 359-372.

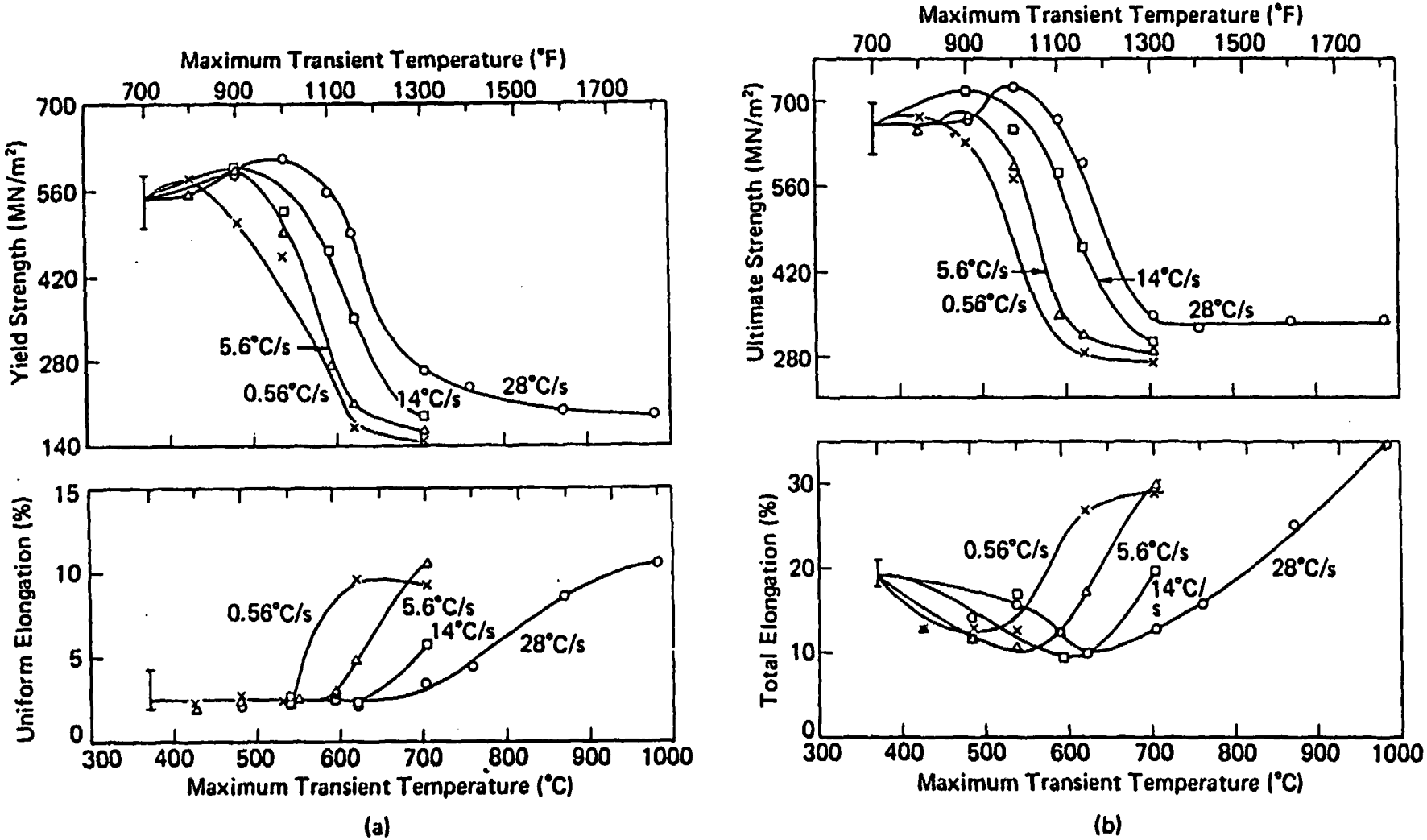

Fig. 4. Response of spent fuel cladding to transient annealing. Test temperature was 371°C. (a) Yield strength and uniform elongation, and (b) ultimate strength and total elongation.
A.A. Bauer, L.M. Lowry, "Tensile Properties and Annealing Characteristics of H.B. Robinson Spent Fuel Cladding," Nuclear Technology, Vol. 41, Dec. 1978, pp. 359-372.

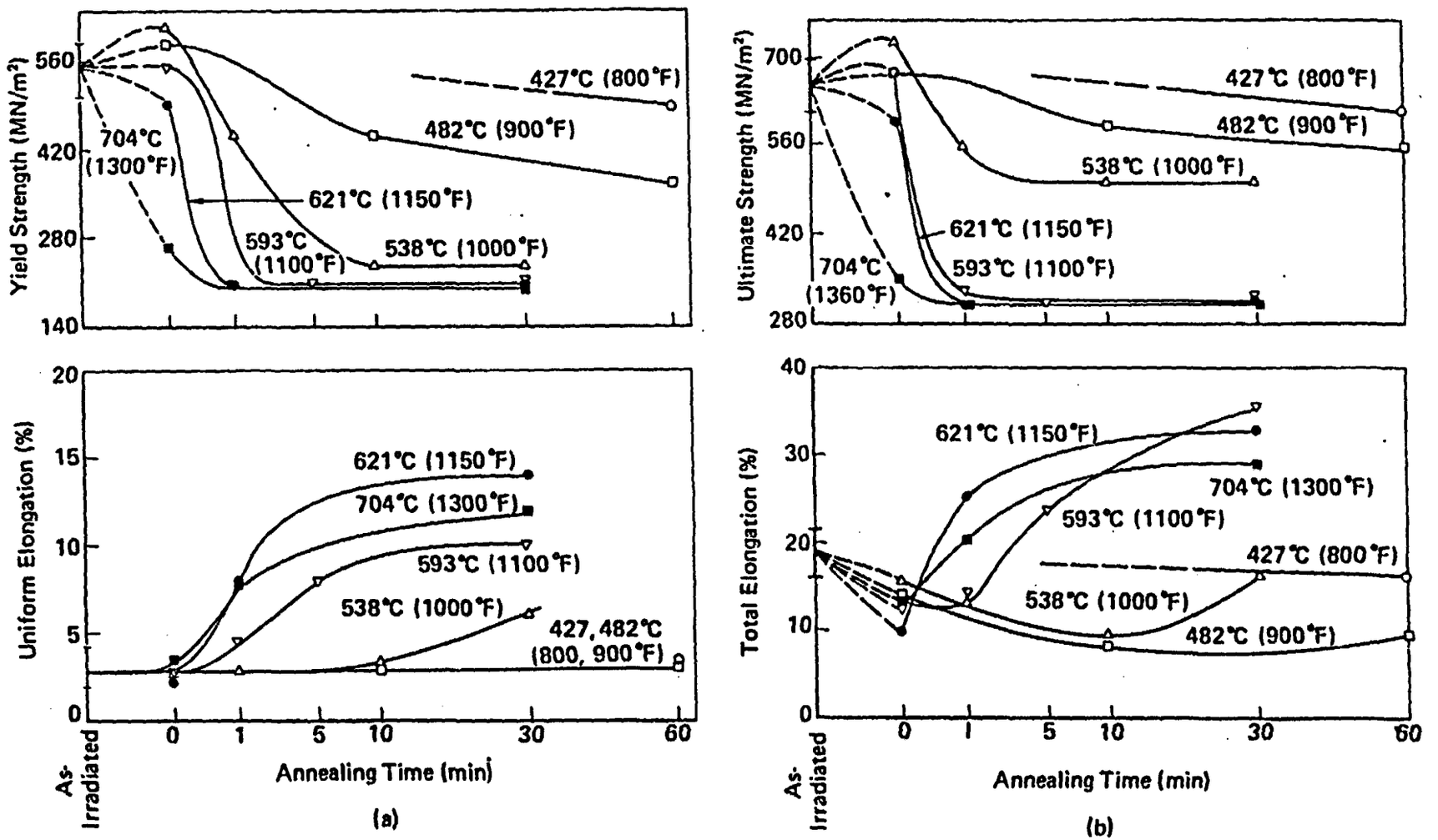

Fig. 5. Response of spent fuel cladding to isothermal annealing. Test temperature was 371°C. (a) Yield strength and uniform elongation, and (b) ultimate strength and total elongation.
A.A. Bauer, L.M. Lowry, "Tensile Properties and Annealing Characteristics of H.B. Robinson Spent Fuel Cladding," Nuclear Technology, Vol. 41, Dec. 1978, pp. 359-372.

TABLE A1

RATES AND OXIDATION DEPTHS OCCURRING IN THE LOW-TEMPERATURE CORROSION OF ZIRCALOY CLADDING

Temperature (°C)	Corrosion Rate ($mg/dm^2 \cdot day$) Eq. 1	Eq. 2	Oxidation Depth (μm)* Eq. 1	Eq. 2
250	4.45×10^{-3}	1.75×10^{-3}	0.071	0.028
300	3.60×10^{-2}	2.35×10^{-2}	0.577	0.377
350	2.08×10^{-1}	2.09×10^{-1}	3.33	3.35
400	9.25×10^{-1}	1.34	14.8	21.5

*Under isothermal conditions for one year.

References

A1. E. Hillner, "Corrosion of Zirconium-Base Alloys - An Overview," Zirconium in the Nuclear Industry, ASTM STP 633, American Society for Testing and Materials, Philadelphia, PA, 1977.

A2. A. B. Johnson Jr, E. R. Gilbert and R. J. Guenther, Behavior of Spent Nuclear Fuel and Storage System Components in Dry Interim Storage, PNL-4189, Pacific Northwest Laboratory, Richland, WA, August 1982.

A3. D. G. Boase and T. T. Vandergraaf, "The Canadian Spent Fuel Storage Canister: Some Material Aspects," Nucl. Tech. 32, p. 60, 1977.

METHOD FOR CORRELATING MAXIMUM OXIDE THICKNESS WITH BURNUP

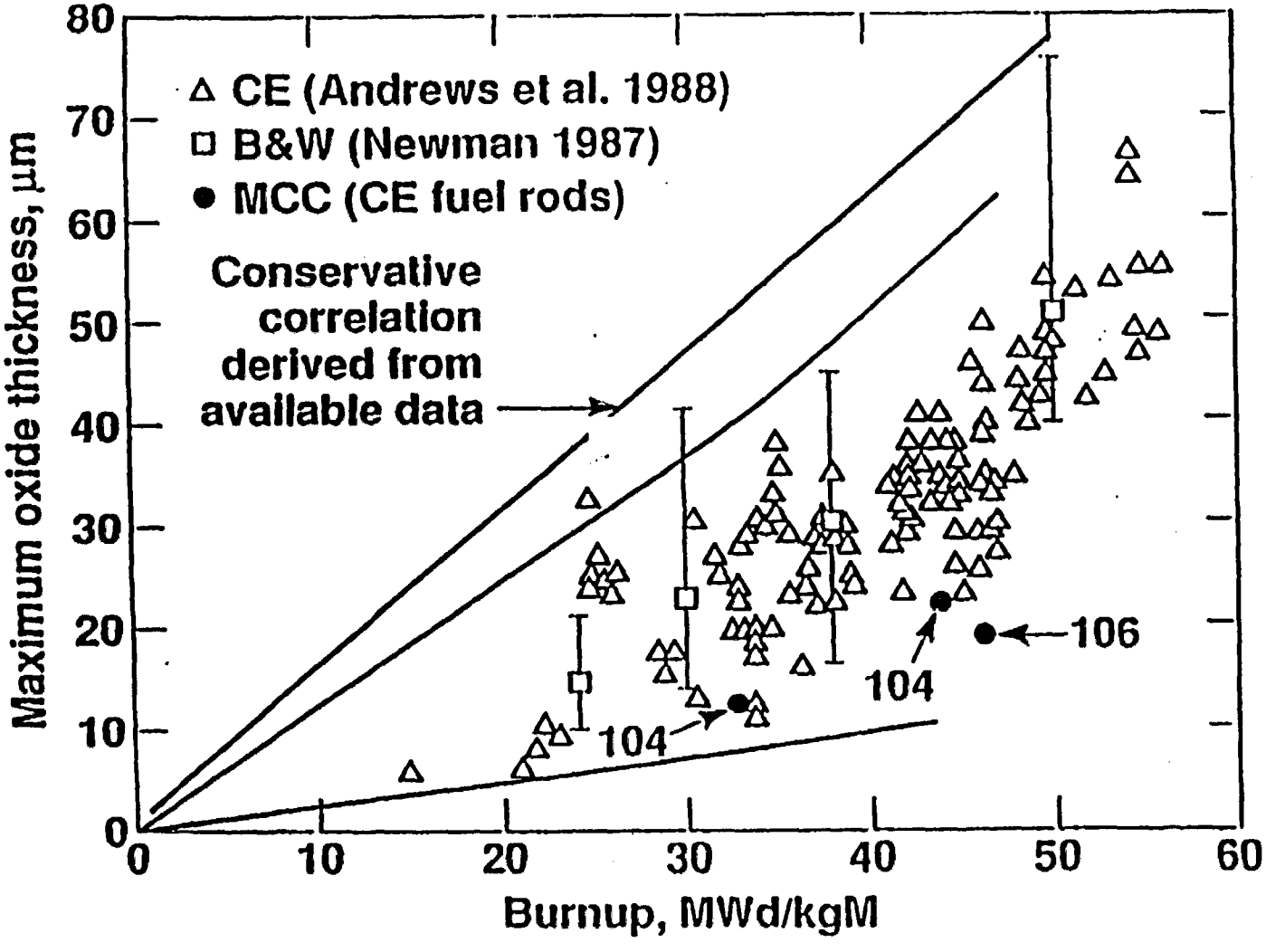

R.B. Stout, *Spent Fuel Characteristics Overview*, presented to the Nuclear Waste Technical Review Board, August, 1990.

3. SCIENTIFIC BASIS FOR PREDICTIVE MODEL DEVELOPMENT

3.1 SPENT FUEL CLADDING FAILURE

3.1.1 EXPERIMENTAL PARAMETERS FOR FAILURE MODELS

3.1.2 FAILURE MODELS

3.2 SPENT FUEL OXIDATION

3.2.1 EXPERIMENTAL PARAMETERS FOR OXIDATION MODELS

3.2.2 OXIDATION MODELS

3.3 SPENT FUEL FISSION GAS RELEASE

3.3.1 EXPERIMENTAL PARAMETERS FOR FISSION GAS RELEASE

3.3.2 FISSION GAS RELEASE MODELS

3.4 SPENT FUEL DISSOLUTION

3.4.1 EXPERIMENTAL PARAMETERS FOR DISSOLUTION

3.4.1.1 DISSOLUTION RATES

3.4.1.2 SOLUBILITY LIMITS

3.4.1.3 SOLUBILITY LIMITING PHASES

3.4.2 DISSOLUTION MODELS

3.5 GLASS DISSOLUTION

3.5.1 EXPERIMENTAL PARAMETERS FOR GLASS DISSOLUTION

3.5.2 GLASS DISSOLUTION MODELS

3.6 OTHER RELEASE SOURCES OF RADIONUCLIDES

3.6.1 CRUD

3.6.2 HARDWARE

3.6.3 CLADDING

3.1.2 Failure Models

Both the experimental testing and the model development activities for cladding failure response are incomplete. At this time only the report by L. Santanam, H. Shaw, and B.A. Chin (Modeling of Zircaloy Cladding Degradation Under Repository Conditions, Lawrence Livermore National Laboratory Report UCRL-100211, July, 1989) contains a preliminary analysis for Zircaloy cladding failure during the high temperature time period. The analysis used a deformation and fracture map methodology that is an extension of the methods applied to analyze Zircaloy cladding deformation and fracture for the dry storage of spent fuel waste form program established by the nuclear utility industry. Substantial testing and model development activities remain to be completed to support creditable repository design that would include the cladding as a long term barrier to the UO_2 spent fuel waste form. It is believed, however, that the Zircaloy-clad fuel rods that have low internal pressures will have low failure rate through both the high temperature and intermediate temperature periods.

3. SCIENTIFIC BASIS FOR PREDICTIVE MODEL DEVELOPMENT

3.1 SPENT FUEL CLADDING FAILURE

3.1.1 EXPERIMENTAL PARAMETERS FOR FAILURE MODELS

3.1.2 FAILURE MODELS

3.2 SPENT FUEL OXIDATION

3.2.1 EXPERIMENTAL PARAMETERS FOR OXIDATION MODELS

3.2.2 OXIDATION MODELS

3.3 SPENT FUEL FISSION GAS RELEASE

3.3.1 EXPERIMENTAL PARAMETERS FOR FISSION GAS RELEASE

3.3.2 FISSION GAS RELEASE MODELS

3.4 SPENT FUEL DISSOLUTION

3.4.1 EXPERIMENTAL PARAMETERS FOR DISSOLUTION

3.4.1.1 DISSOLUTION RATES

3.4.1.2 SOLUBILITY LIMITS

3.4.1.3 SOLUBILITY LIMITING PHASES

3.4.2 DISSOLUTION MODELS

3.5 GLASS DISSOLUTION

3.5.1 EXPERIMENTAL PARAMETERS FOR GLASS DISSOLUTION

3.5.2 GLASS DISSOLUTION MODELS

3.6 OTHER RELEASE SOURCES OF RADIONUCLIDES

3.6.1 CRUD

3.6.2 HARDWARE

3.6.3 CLADDING

3.2 Spent Fuel Oxidation

In any proposed nuclear waste repository for spent fuel from nuclear power reactors, the potential release rates of many radionuclides over a 10,000 year design lifetime depends on the oxidation rate and the oxidation state of any irradiated UO_2 fuel pellets that may be exposed to the atmosphere. This is because UO_2 spent fuel can oxidize into $U_4O_9 \rightarrow U_3O_8 \rightarrow UO_3$, and possibly other oxides, which could influence the surface area and the dissolution rates of any spent fuel that may be exposed to water in a repository. Therefore, experiments to provide both data and a physical basis for rational model development for UO_2 oxidation kinetics are necessary in order to eventually predict potential radionuclide release rates from spent fuel in a repository.

Results from tests at this time imply that the grain boundaries of irradiated UO_2 oxidized more rapidly than the grain volumes at low temperatures (less than 200°C). This two-rate oxidation process of UO_2 spent fuel is difficult to represent mathematically because classical diffusion models with their associated classical initial conditions and external boundary conditions do not physically describe certain geometrical aspects of the experimental observations.

Furthermore, the vast majority of the spent fuel rods placed in the repository will have intact Zircaloy cladding, but approximately 0.01% of the rods will contain cladding defects, usually in the form of small splits or pin holes. Some of the breached rods may contain water. If cladding with small breaches is to provide a barrier function, then it will be necessary to determine if fuel oxidation occurs rapidly enough under repository conditions to split the cladding and expose additional fuel with an oxidation state higher than UO_2 before significant credit can be taken for pin-hole-defected cladding as a barrier to radionuclide release. Thus,

spent fuel oxidation time response is also an input function for modeling the extent and amount of exposed UO_2 spent fuel in failed cladding.

Spent LWR fuel consists primarily of UO_2 pellets, whose density is 92-95% of the theoretical density, enclosed in a Zircaloy sheath. When UO_2 oxidizes in excess oxygen, it passes through certain possibly metastable states, such as U_4O_9 and U_3O_8, before it totally oxidizes to UO_3. The rate at which the fuel oxidizes through the various phases depends on the temperature. The rate may also depend on the moisture content of the atmosphere, previous radiation history of the fuel, and radiation level during storage. The densities of the phases range from a high of 10.3 g/cm^3 for 93% dense UO_2 to 7.3 g/cm^3 for UO_3. Until U_3O_8 , with a density of 8.3 g/cm^3, is formed, intermediate phases have densities approximately equal to that of UO_2. Therefore, as the UO_2 oxidizes through U_3O_8 , the fuel pellets will swell and put a tensile hoop stress on the cladding. Several studies have shown that cladding placed under a hoop stress, caused by the formation of U_3O_8 , will enlarge existing breaches and, in some cases, will fracture where there had been on previous pin hole (small) breaches.

In the following Section 3.2.1, information and data are provided from TGA (Thermogravimetric Apparatus) Tests and ODB (Oven Dry Bath) tests. The temperature-time response with spent fuel oxidation testing below 260°C remains to be completed. Above 260°C, it appears that the oxidation time response is sufficiently rapid to be instantaneous relative to repository time duration. Thus, atmospherically exposed UO_2 spent fuel in failed waste packages as a model for kinetics, transforms instantly to U_3O_8 (or UO_3) above 260°C.

The temperature-time response of oxidizing UO_2 below 260°C will be described with a preliminary model in Section 3.2.2. This model represents two time sub-

domains. The first sub-domain is the time interval for oxidizing spent fuel to a U_4O_9 lattice structure and to attain the O to U of ~2.4 plateau that has been observed. The time interval will be evaluated based on the time for the U_4O_9 front to propagate to the center of a spent fuel grain. This is a conservative model as it assumes that all grain boundaries oxidized and crack open instantaneously when the UO_2 spent fuel is initially exposed to atmospheric oxygen. The model can also describe the weight gain time response during partial oxidation of UO_2 grains to U_4O_9 grains.

The second sub-domain is the time interval on the ~2.4 O/U plateau before a transition away from the plateau level appears. This transition in oxygen weight gain is conjectured to be the result of the initial formation of the U_3O_8 phase, which would occur most likely on the outer boundary of the existing U_4O_9 grains. At the present time, no data are available on the subsequent time response or geometrical character of the U_3O_8 oxidation response. Thus, it is conservative to assume that the total time interval for UO_2 spent fuel to transform to U_3O_8 is the sum of the two sub-domain time intervals. However, it is conservative to assume that the total time interval for UO_2 spent fuel to transform to U_3O_8 is the sum of the two sub-domain time intervals (time to reach U_4O_9 plus time to initiate the U_3O_8 phase). Note that a critical part of the assumption is that an individual grain must all be at an O/U of ~2.4 before the phase transition to U_3O_8 can be initiated. Once the relatively low (compared to UO_2) density state of U_3O_8 has been attained, the dissolution/release performance of spent fuel has been significantly decreased because of the large (~potentially three orders of magnitude) increase in exposed spent fuel surface area, relative to the initial surface area of fragmented spent fuel pellets. Thus, the time-temperature-phase transformation responses for the different spent fuel oxidation processes can significantly impact the potential release rate of radionuclides from spent fuel waste forms.

3. SCIENTIFIC BASIS FOR PREDICTIVE MODEL DEVELOPMENT

3.1 SPENT FUEL CLADDING FAILURE

3.1.1 EXPERIMENTAL PARAMETERS FOR FAILURE MODELS

3.1.2 FAILURE MODELS

3.2 SPENT FUEL OXIDATION

3.2.1 EXPERIMENTAL PARAMETERS FOR OXIDATION MODELS

3.2.2 OXIDATION MODELS

3.3 SPENT FUEL FISSION GAS RELEASE

3.3.1 EXPERIMENTAL PARAMETERS FOR FISSION GAS RELEASE

3.3.2 FISSION GAS RELEASE MODELS

3.4 SPENT FUEL DISSOLUTION

3.4.1 EXPERIMENTAL PARAMETERS FOR DISSOLUTION

3.4.1.1 DISSOLUTION RATES

3.4.1.2 SOLUBILITY LIMITS

3.4.1.3 SOLUBILITY LIMITING PHASES

3.4.2 DISSOLUTION MODELS

3.5 GLASS DISSOLUTION

3.5.1 EXPERIMENTAL PARAMETERS FOR GLASS DISSOLUTION

3.5.2 GLASS DISSOLUTION MODELS

3.6 OTHER RELEASE SOURCES OF RADIONUCLIDES

3.6.1 CRUD

3.6.2 HARDWARE

3.6.3 CLADDING

3.2.1 Experimental Parameters for Oxidation Models

The testing activities to determine oxidation response are thermogravimetric analysis (TGA) method and oven dry bath (ODB) method. Both methods provide measurements of weight gain due to oxidation of the sample during the time interval of the testing and under controlled temperature and some controlled atmospheric gas variations. In the case of TGA testing, the sample size is small, around 200 mg, and this initial weight is typical of an average fragment from a spent fuel pellet. In the case of ODB testing, the sample size is considerably larger, around 10 grams of spent fuel. (The larger initial sample weights of ODB testing provides a well-controlled procedure to obtain oxidized spent fuel samples for future oxidized spent fuel dissolution testing.) In each testing method, the weight gain time response is measured, and samples can be obtained for microscopic examinations at various oxidation stages (times) during the weight gain time response. The weight gain time response is usually reported as the oxygen to heavy metal atomic ratio, with an O to U or O to M ratio notation (the first is oxygen to uranium and the second is oxygen to heavy metal, which ideally would include all actinide atoms but is dominated by the uranium atomic number density). For example, an O/U of 2.0 is UO_2. The microscopic analyses are performed on samples to identify the sequence of crystallographic lattice structures that occur during the oxidation of spent fuel. From the weight gain measurements and the phase identification analysis, the oxidation response for the existing test matrix of spent fuel samples has shown that UO_2 spent fuel transforms first to a non-stoichiometric U_4O_9 lattice structure phase with an O/U of ~2.4 at temperatures below 200 C. Transitions to higher oxidation phases (U_3O_8 and UO_3) have not yet been observed in ODB tests below 200 C. Higher temperature TGA and ODB testing are being initiated to determine the phases and the kinetics of oxidation plus phase transformation mechanisms. The critical temperature range to establish oxidation response and phase change kinetics (stable versus metastable transformations) is between 200 C and 260 C. Both TGA

and ODB testing activities are in progress to provide additional data in the 200 C to 260 C temperature interval. Above 260 C, the rate of spent fuel oxidation and the phase transformations proceed rapidly to U_3O_8 and UO_3 lattice structures in short periods of time (weeks/years) relative to repository disposal time periods (100 to 1000 years).

The following set of figures present a visual and brief statement format that provides information and data obtained with the existing spent fuel oxidation testing methods. The oxidation response of spent fuel is not believed to be a radionuclide release process (there is a possible gaseous release mechanism which remains to be characterized). Rather, the oxidation response of spent fuel is considered primarily a degradation process which transforms the physical and chemical state of the waste form. As a result, the oxidation phases UO_2, U_4O_9, U_3O_8, or UO_3 have potentially different intrinsic dissolution rates that determine the aqueous release rate response. In addition to the dissolution rates, the potential magnitude of surface area exposed greatly increases as UO_2 oxidizes to the higher phases. In going from UO_2 to U_4O_9, grain boundaries between grain volumes crack open because of the slight volume decrease during this phase transformation. Furthermore, the phase transformations from the U_4O_9 lattice structure to U_3O_8 and UO_3 have significant volume increases which can microcrack and flake grain volumes to smaller particles and/or powdered forms. Thus, the aqueous radionuclide release rate is potentially increased for higher oxidized phases if groundwater access occurs to wet the increased exposed surfaces of oxidized spent fuel.

SPENT FUEL OXIDATION RESPONSE

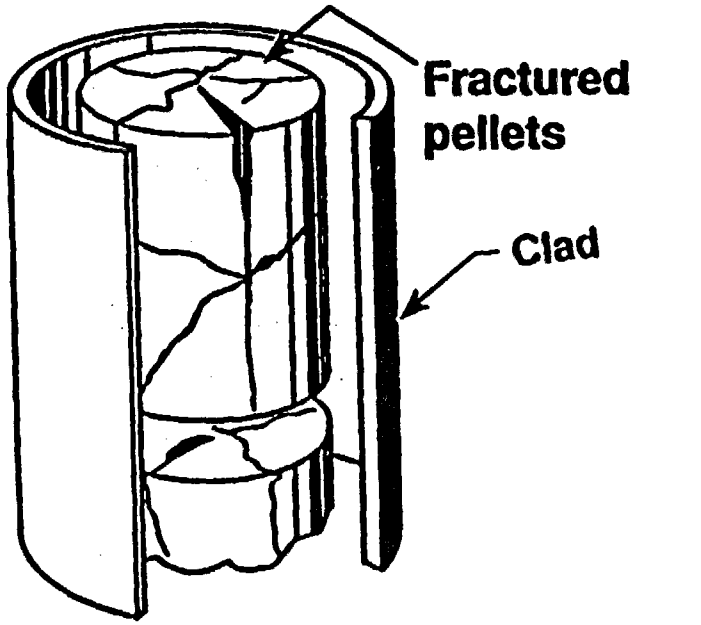

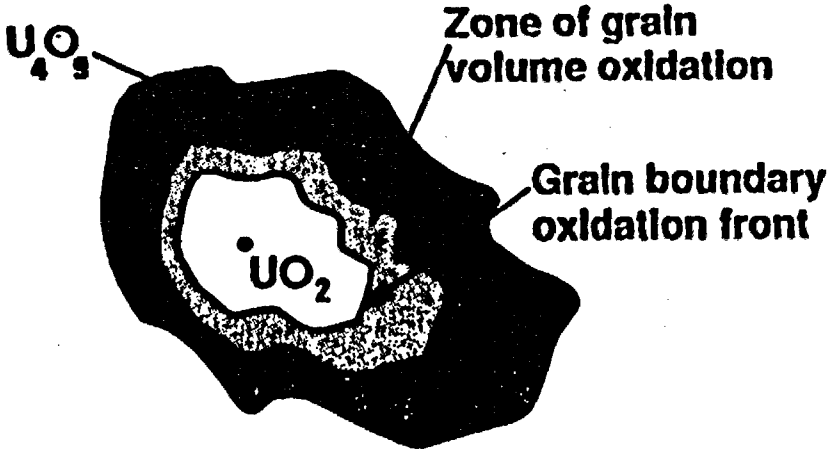

Fragment cross-section

FUEL PELLETS, NOMINALLY 0.5cm TO 0.6cm RADIUS AND ~2cm LENGTH, FRACTURE INTO FRAGMENTS DUE TO THERMAL STRAINS DURING FIRST FULL POWER CYCLE.

FUEL FRAGMENTS OXIDIZE AFTER CLADDING BREACH.

MODEL - OXIDATION KINETICS DEPEND STATISTICALLY ON FRAGMENT SIZES AND SHAPES IN A TEST SAMPLE; ANY FRAGMENT CAN BE SUBDIVIDED INTO DIFFERENT SIZED PYRAMIDAL VOLUME SUBSETS TO OBTAIN A STATISTICAL DISTRIBUTION FUNCTION.

3.2.1-3

Figure 3.2.1-1

Spent fuel waste form characteristics observations

- UO_2 fuel pellets (initially ~0.5 cm radius and ~1–3 cm length) break into fragments during reactor operation. This fragmentation increases the surface area of spent fuel for oxidation and dissoution responses.

- A fragment of UO_2 spent fuel will oxidize to higher oxidation weight gains (UO_{2+x}) and at low temperatures other oxidation state phases (U_4O_9, U_3O_7, U_3O_8, UO_3 plus possible hydrates).

- A fragment of spent fuel (oxidized or not) will dissolve in aqueous solutions.

3.2.1-4

Figure 3.2.1-2

Why Study Spent Fuel Oxidation?

- Small fraction (< 0.1%) of rods will enter repository breached and be available for oxidation when container is compromised
- Cladding corrosion may lead to additional breaches
- High temperature data indicate that low-density U_3O_8 can form, destroying fuel and cladding
- Four oxidation effects:
  - Change phase of fuel
  - Open additional internal fuel surfaces to leachant
  - Release trapped fission gas
  - Split cladding; change path for radioisotope release

Question?
Δ(O/M) as a function of time, temperature, and atmosphere

3.2.1-5

Figure 3.2.1-3

Basis for YMP Spent Fuel Oxidation Testing from Early Work

- Temperature was an important variable
- Effect of atmospheric moisture and burnup is uncertain
- Low-temperature oxidation data were not available
- Assumed UO_2 and spent fuel had similar oxidation behavior

Figure 3.2.1-4

TGA Apparatus

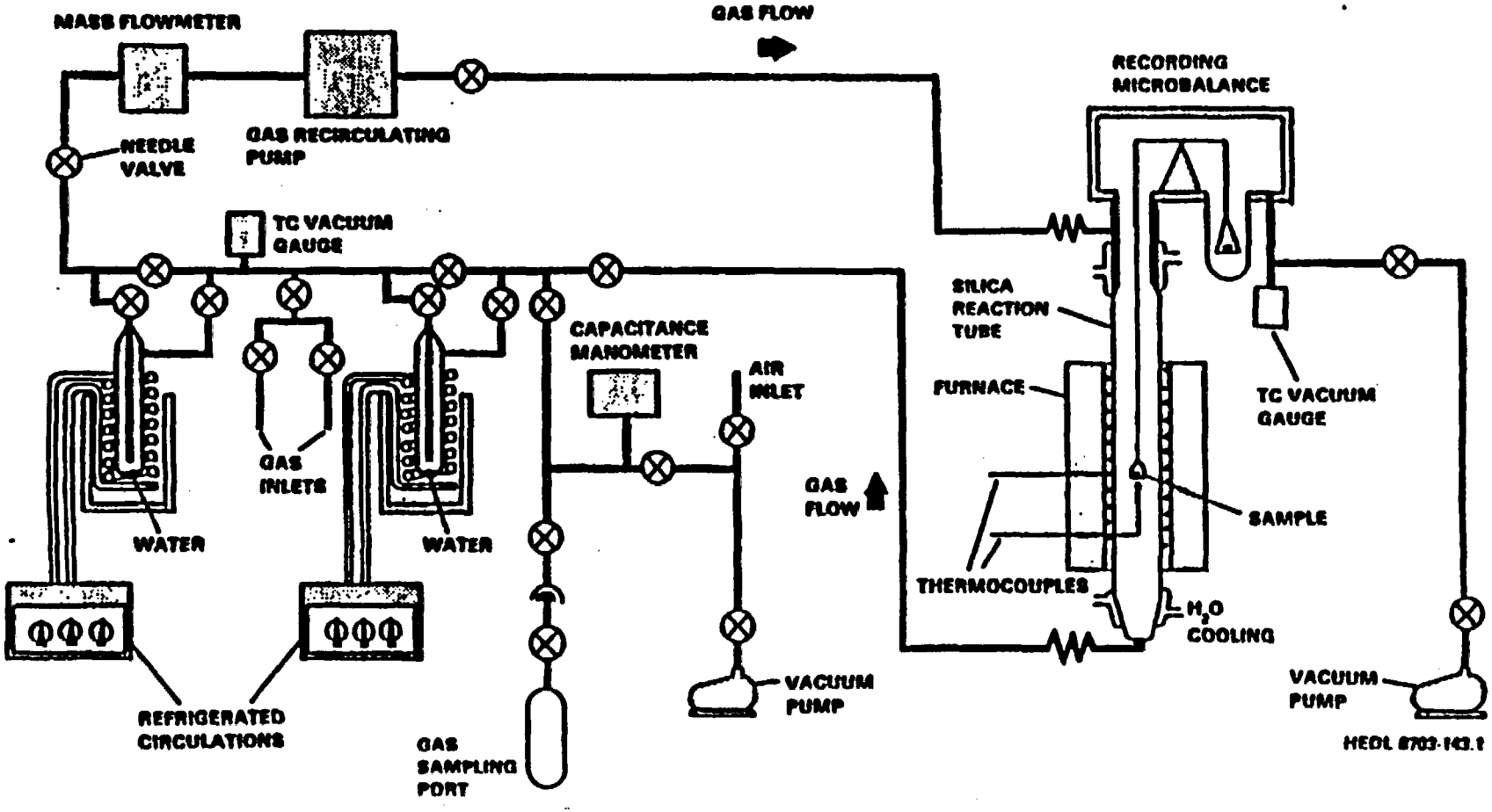

Figure 3.2.1-5

TGA DATA ANALYSIS

ASSUMPTIONS

1. UNIFORM SPHERICAL GRAINS
2. GRAINS OXIDIZE INDEPENDENTLY
3. PLANAR OXIDATION FRONT

DESCRIPTION

$$1 - [1 - 3\,\Delta(O/M)]^{1/3} = (k't)^{1/2}$$

WHERE

$\Delta(O/M)$	=	CHANGE IN OXYGEN TO METAL RATIO
k'	=	OXIDATION RATE CONSTANT
t	=	OXIDATION TIME

3.2.1-8

Figure 3.2.1-6

FITTING TGA DATA TO OBTAIN RATE CONSTANT

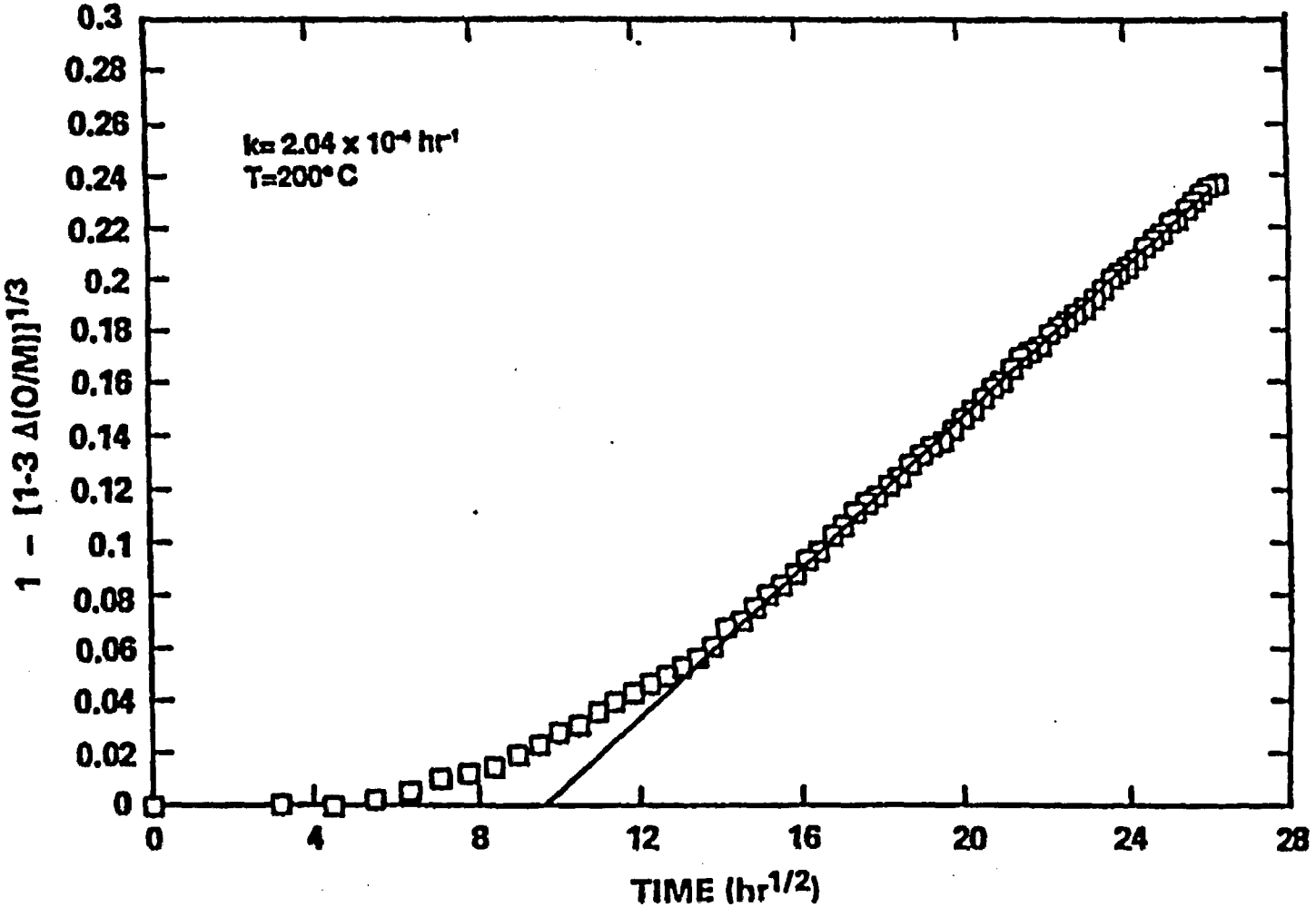

Figure 3.2.1-7

TGA Oxidation Summary

- Different oxidation behavior in unirradiated UO_2
- Spent fuel oxidation is a two-step process: oxygen penetration of the grain boundaries followed by oxidation of the bulk grains
- Arrhenius dependence on temperature. The activation energy is consistent with O_2 diffusion into UO_2.
- Moisture level has little effect
- Oxidation more rapid at the pellet surface
- The majority of the mechanistic data comes from the microstructural examination of the oxidized fuel

Figure 3.2.1-8

Dry-Bath Oxidation Program

- To provide rate data for oxidation model
- Determine long-term oxidation behavior
- Source of fuel for leach testing

Figure 3.2.1-9

Test Variables

Temperature: 195°, 175°, 130°, 110°C

Dew Points: -55, +80°C

Sample Configuration: As-irradiated fragments
pulverized fuel

Fuels: HB Robinson PWR (ATM-101)
Turkey Point PWR
Cooper BWR (ATM-105)
Calvert Cliffs PWR (ATM-103, -104, -106)

Grain Size Range: 5 to 30 μm

Burnup Range: 25 to 48 GWd/MTU

FGR Range: 0.1% to 18%

Current Test Times: Up to 40 kh (5.0 yr)

3.2.1-12

Figure 3.2.1-10

Oxidation of LWR Spent Fuel

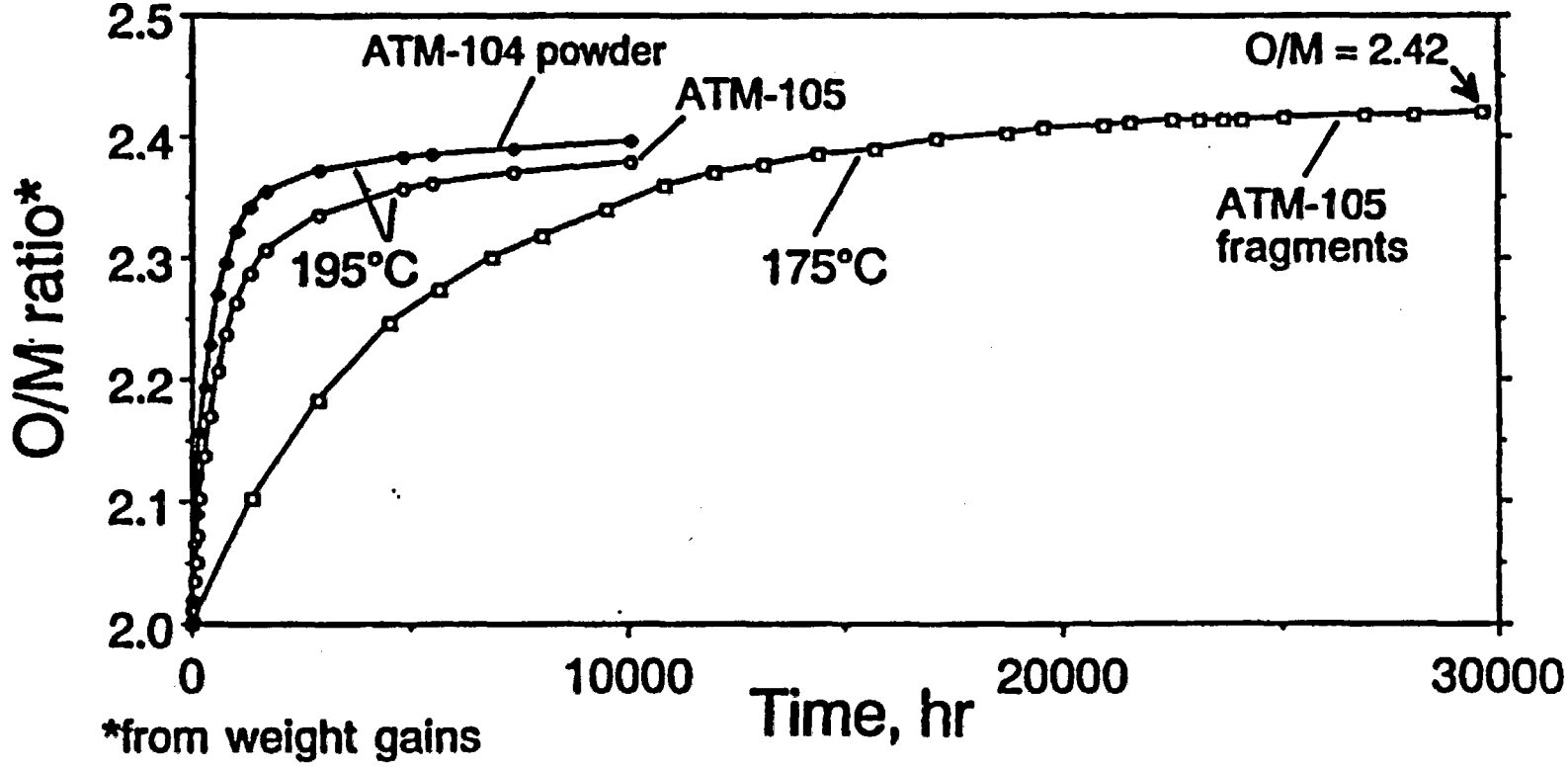

Figure 3.2.1-11

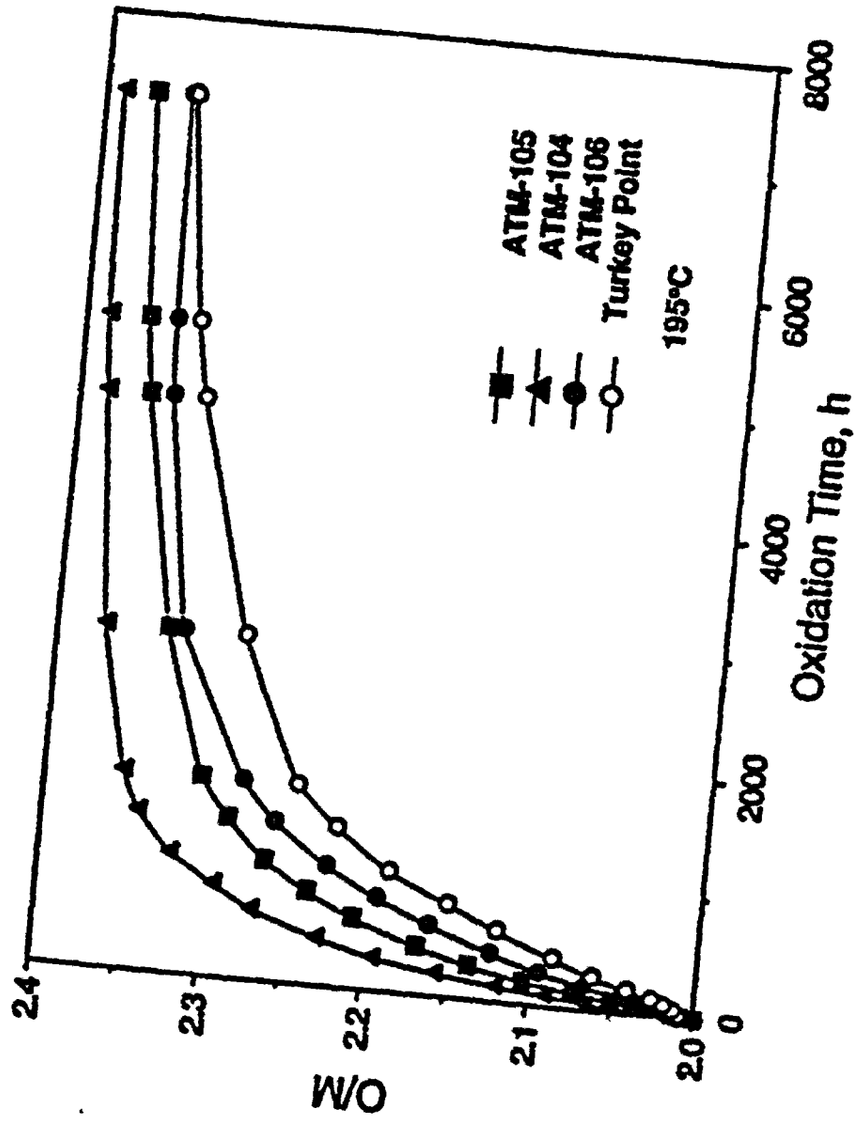

Figure 3.2.1-12

Change in O/M with Time, 175°C

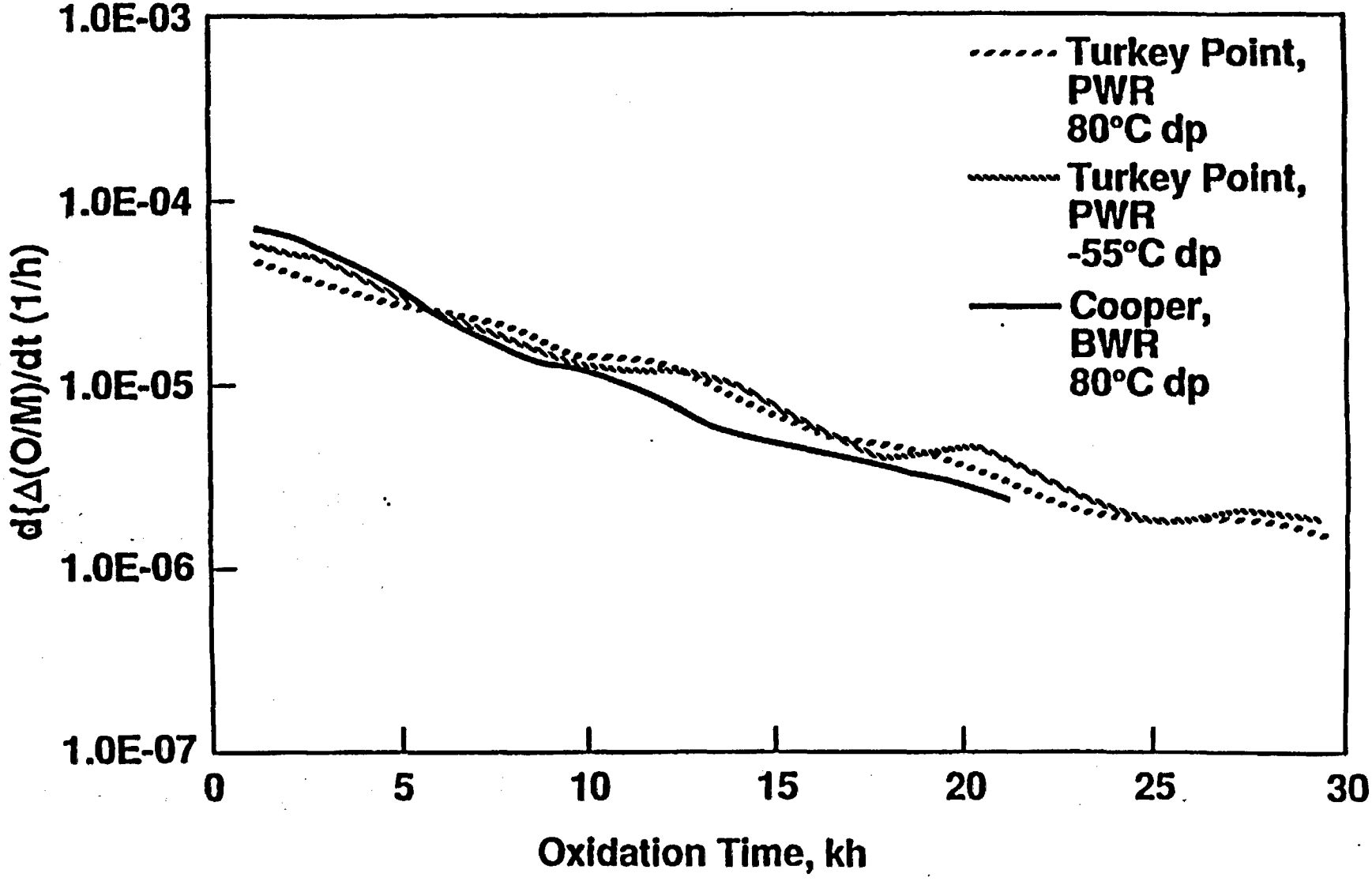

Figure 3.2.1-13

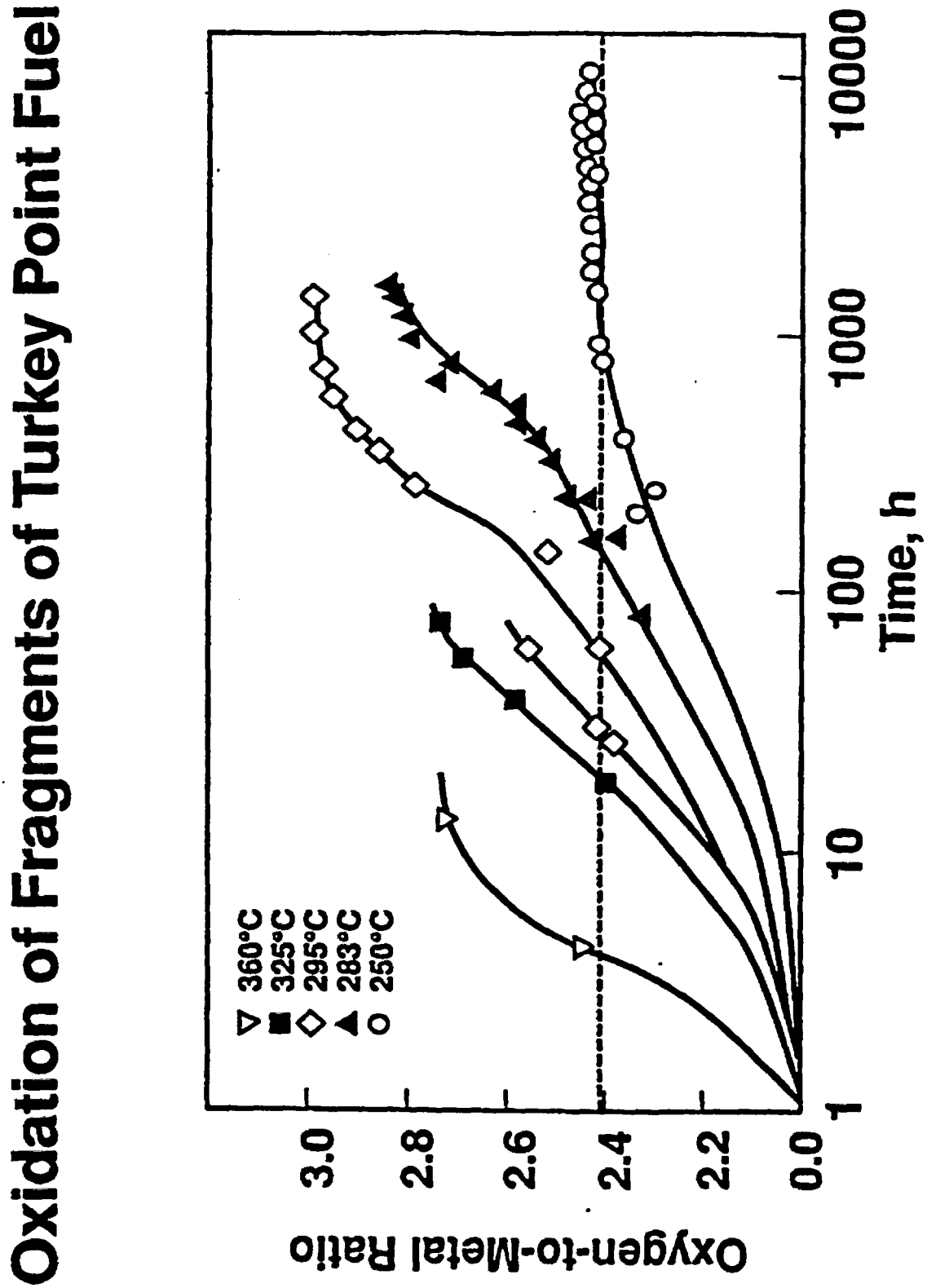

Data are from Reference: R. E. Einziger and R. V. Strain, *Nuc. Technol.*, 75:82 (1986).

Figure 3.2.1-14

Generalized Spent Fuel Oxidation Curve

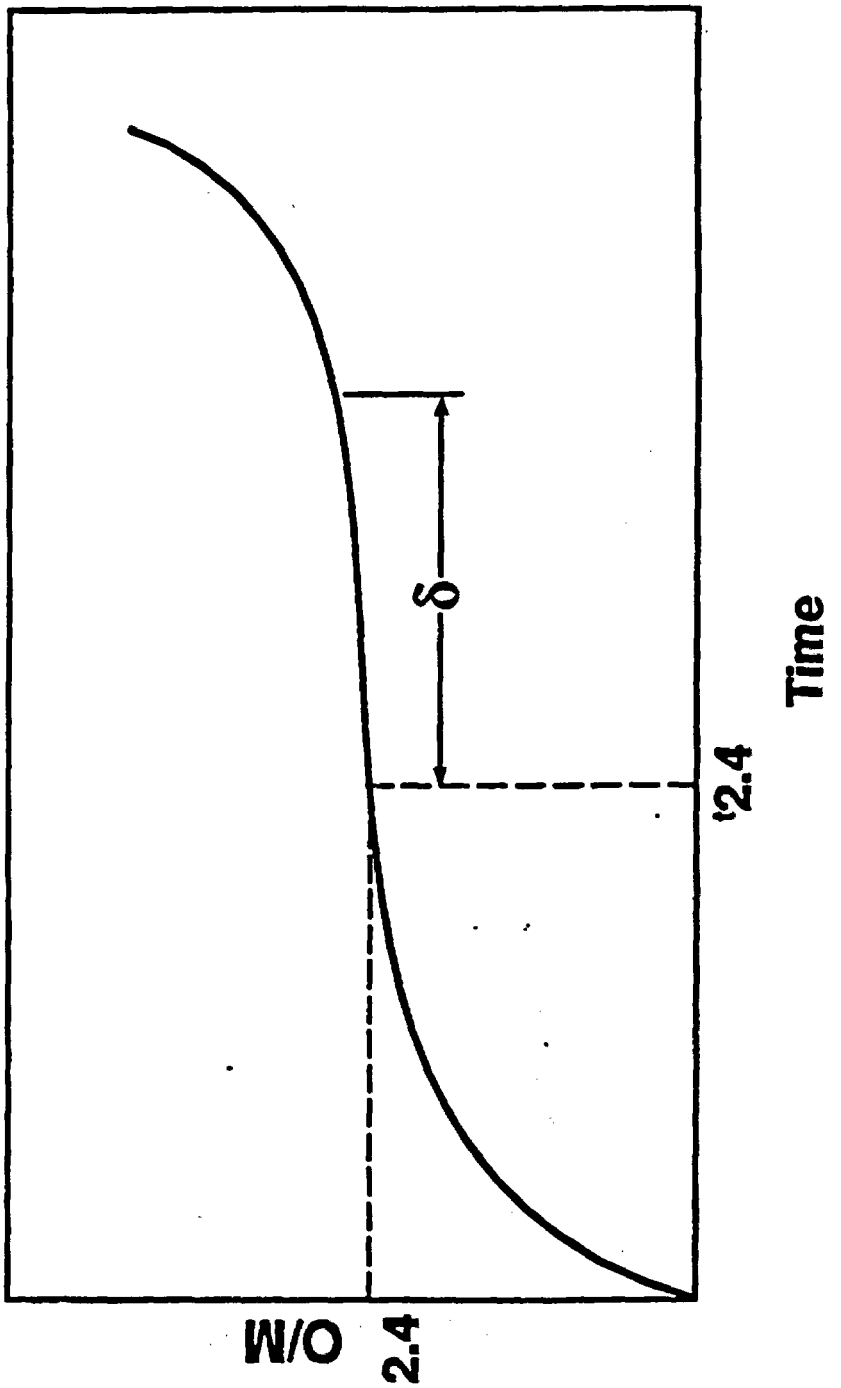

δ = time on O/M 2.4 plateau until new phase transition

Figure 3.2.1-15

Figure 3.2.1-16

Time Required to Propagate Existing Cladding Defects

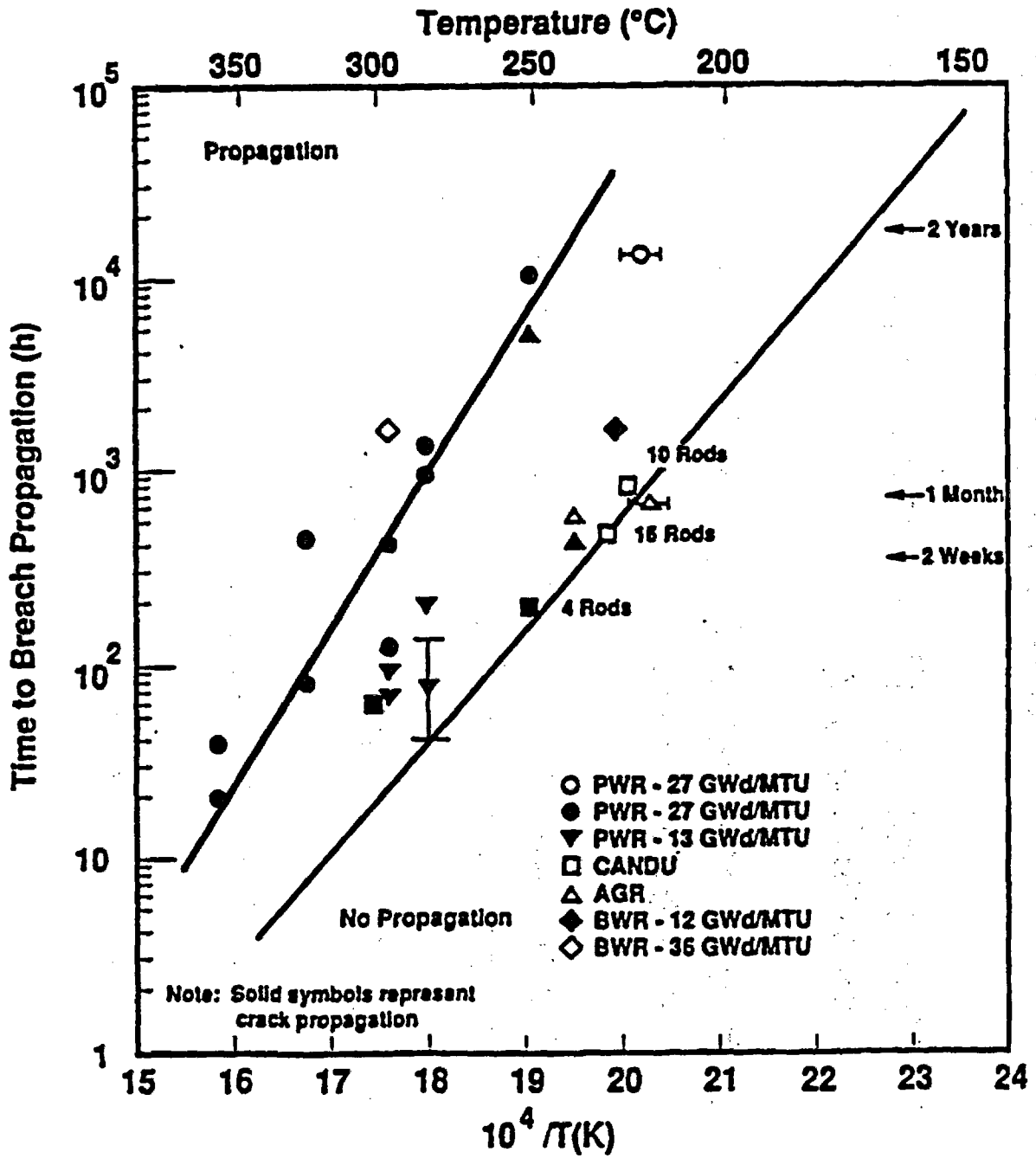

Figure 3.2.1-17

Preliminary Conclusions

1. Spent fuel has different oxidation behavior than unirradiated UO_2
2. Fuel variability affects oxidation rate in a transitory manner
3. After transient, all tested fuels show similar oxidation behavior
4. No effect of atmospheric moisture
5. Test temperatures too low for oxidation beyond $UO_{2.4}$
6. Only UO_2 and U_4O_9 phases found at O/M <2.4
7. At 95°C, >2000 years to reach plateau

Figure 3.2.1-18

Information Needs:

1. No tests of high-burnup or Gd-containing fuels
2. Long-term stability of $UO_{2.4}$.
   Thermodynamics to aid modeling?
3. Oxidation kinetics beyond $UO_{2.4}$ (to U_3O_8)
4. Tests on low burnup fuel (12 GWd/MTU) ?
5. Leaching studies from oxidized and
   non-oxidized fuel

Figure 3.2.1-19

3. SCIENTIFIC BASIS FOR PREDICTIVE MODEL DEVELOPMENT

3.1 SPENT FUEL CLADDING FAILURE

3.1.1 EXPERIMENTAL PARAMETERS FOR FAILURE MODELS

3.1.2 FAILURE MODELS

3.2 SPENT FUEL OXIDATION

3.2.1 EXPERIMENTAL PARAMETERS FOR OXIDATION MODELS

3.2.2 OXIDATION MODELS

3.3 SPENT FUEL FISSION GAS RELEASE

3.3.1 EXPERIMENTAL PARAMETERS FOR FISSION GAS RELEASE

3.3.2 FISSION GAS RELEASE MODELS

3.4 SPENT FUEL DISSOLUTION

3.4.1 EXPERIMENTAL PARAMETERS FOR DISSOLUTION

3.4.1.1 DISSOLUTION RATES

3.4.1.2 SOLUBILITY LIMITS

3.4.1.3 SOLUBILITY LIMITING PHASES

3.4.2 DISSOLUTION MODELS

3.5 GLASS DISSOLUTION

3.5.1 EXPERIMENTAL PARAMETERS FOR GLASS DISSOLUTION

3.5.2 GLASS DISSOLUTION MODELS

3.6 OTHER RELEASE SOURCES OF RADIONUCLIDES

3.6.1 CRUD

3.6.2 HARDWARE

3.6.3 CLADDING

3.2.2 Oxidation Models
Below 260°C Repository UO_2 Spent Fuel Oxidation Response

For UO_2 spent fuel exposed to atmospheric oxygen at temperatures less than 260°C, the elapsed time to oxidize to a new U_4O_9 phase and a weight gain "oxide" of $UO_{2.4}$ depends exponentially on temperature and on the grain size of the UO_2. For simplified model development purposes, it is assumed that this oxidation process for UO_2 spent fuel is such that all grain boundaries oxidize and crack open instantaneously. Following the opening of grain boundaries, each grain volume surface is exposed to oxygen and an oxidation front propagates into each grain volume. Behind this front, the "oxide phase" has a crystal lattice structure of U_4O_9 but an oxygen weight gain that corresponds to $UO_{2.4}$ "oxide." The following rate of propagation for the oxidation front into a grain volume is based on preliminary data that are currently available. This rate of front propagation is empirically estimated (Einziger et al., 1992) to be represented by

$$\dot{H}(t) = \sqrt{2k}/2\sqrt{t} \qquad \text{3.2.2 (1)}$$

Equation 3.2.2(1) can be integrated over time to obtain the thickness of the U_4O_9 oxidation zone around a grain for a constant temperature history as

$$H(t) = \sqrt{2kt} \qquad \text{3.2.2 (2)}$$

where $k(\mu m/h) = 1.04 \times 10^8 \exp(-24.0\ kcal.mol^{-1}/RT)$

R = 1.986 cal/mol/°K)

T = temperature in °K

t = time (h) in hours

For a grain of nominal dimension $2H_o$, the time interval at constant temperature for a UO_2 grain to change phase to the U_4O_9 phase at an O/M of ~2.4 is

$$t_{2.4} = H_o^2/2k \qquad 3.2.2\ (3)$$

H_O in units of μm (10^{-6} meter)

$t_{2.4}$ in unit of hours

In the more general case, the above equation for $\dot{H}$ can be used in evaluating U_4O_9 weight gain time response expressions provided in the description that follows the elapsed time response modeling. The nominal dimension H_O for this weight gain response model is obtained by subdividing the grain volumes into pyramidal sub-volumes. For time-dependent temperature histories, the closed-form integration of Equation 3.2.2 (1) cannot be performed, and it will be necessary to use a numerical integration method.

After a grain has attained an O/M plateau at ~2.4, there appears to be a transition time interval denoted as δ (see Section 3.2.1) before significant subsequent oxidation weight gains occcur. The dependence of this time interval on temperature has not yet been well established, but has been conjectured to have the function form:

$$\delta = \delta_O \exp\ (Q/RT) \qquad 3.2.2\ (4)$$

where consistent dimensions for the parameters would be

δ_O = units of hours

Q = units of kcal/mol

R = 1.986 cal/mol/°K

At this time, sufficient experimental data are not available to provide estimated values for δ_O and Q at temperatures below 260°C. If such values were available, then it is conjectured that the next oxidation phase, namely U_3O_8, (or $UO_{2.66}$), begins to form and initiates the transition from the plateau. Then the elapsed time until

the appearance of the transition from the O/M ~2.4 plateau can be denoted as $t_{2.66}$ and would be given by

$$t_{2.66} \equiv t_{2.4} + \delta \qquad \text{(hours)} \qquad 3.2.2\ (5)$$

This is the time at which U_3O_8 is conjectured to be initially forming on the boundary of U_4O_9 grains. Although an estimate for the δ elapsed time is not available from existing data, previous experimental work on defected cladding and splitting of the cladding after formation of U_3O_8 at higher temperature will be used to provide a direct estimate for the elapsed time $t_{2.66}$. These data (Einziger and Strain, 1986), which have been augmented with other data, are shown in Figure 3.2.2-1. The top line will be taken as a $t_{2.66}$ elapsed time line for purposes here. Note that it is not a lower bound line to the $t_{2.66}$ elapsed time for temperatures above 260°C, and that extrapolation is necessary for temperatures below 260°C. Nonetheless, for conceptual design and preliminary performance assessments, this will provide an approximation for the initial formation of the U_3O_8 phase of spent fuel. The equation of the line has the form

$$t_{2.66} = t_{2.66(0)} \exp (Q/RT) \qquad 3.2.2\ (6)$$

and estimated values and definitions for parameters in Equation 3.2.2 (6) are

$t_{2.66(0)} = 1.37 \times 10^{-15}$ hour

$Q = 44{,}100$ cal/mole

$R = 1.986$ cal/mole/°K

T = temperature °K

For UO_2 spent fuel first exposed to the atmosphere, and held at a fixed temperature of 150°C, the extrapolated elapsed time for U_3O_8 to initially form is approximately 9.75×10^7 hours or 1.1×10^4 years. The subsequent rate response of the U_4O_9 grains oxidizing to U_3O_8 remains to be experimentally established.

Time Required to Propagate Existing Cladding Defects

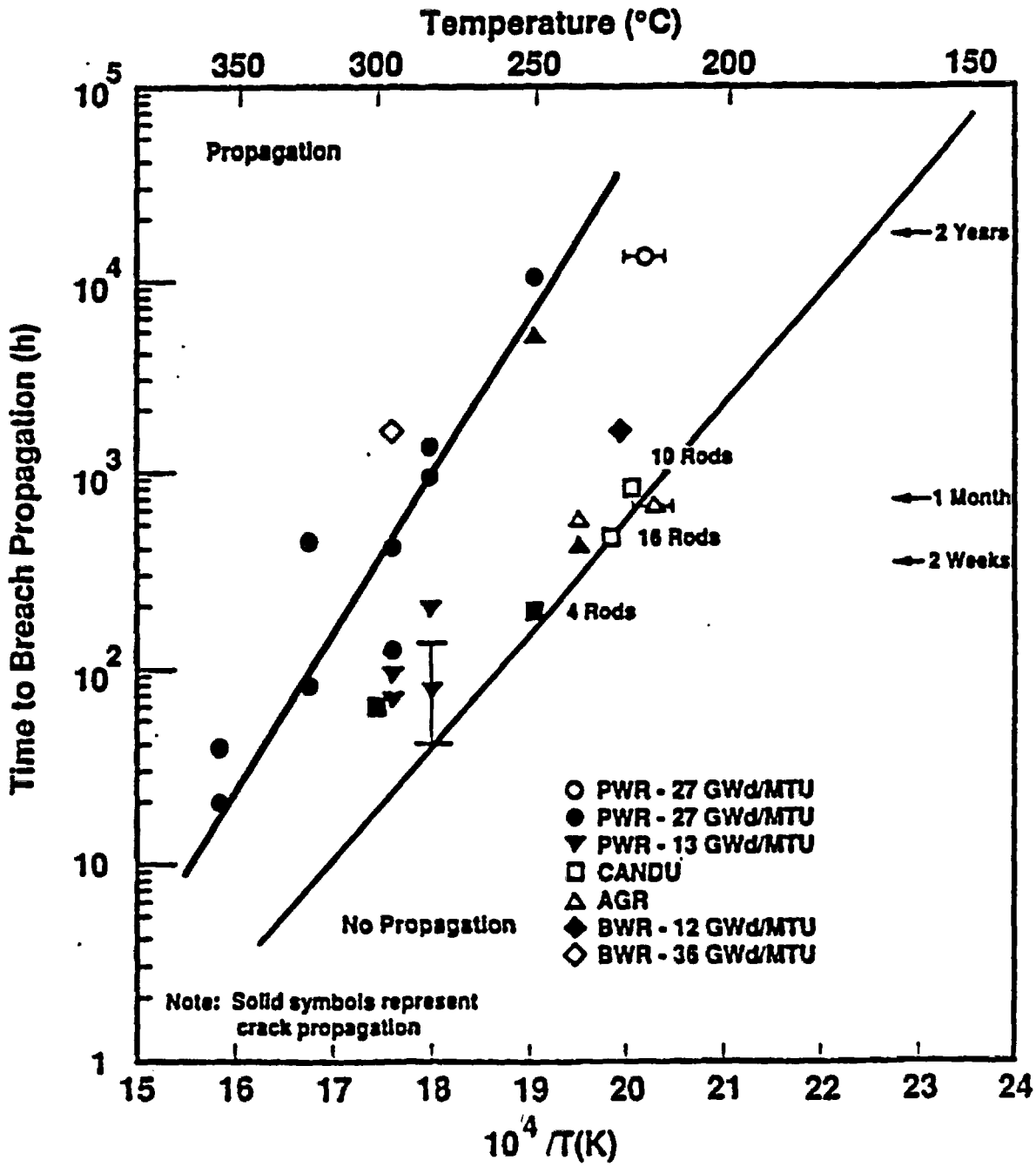

Figure 3.2.2-1

Once the U_3O_8 oxidation rate response has been established, and if a U_3O_8 front also propagates as an oxidation front into the U_4O_9 grains, then the following model of oxidation weight gain time response can be applied (Stout, et al. 1990). This model, as noted above, subdivides a grain into pyramidal subvolumes, and assumes that an oxidation front (either the U_4O_9 or the U_3O_8) propagates into the interior of the grain such that the front remains geometrically similar to the original grain boundary. This rate response model can be used to predict the extent of partial oxidation at low temperatures; for example, some U_4O_9 and UO_2 (or U_3O_8 and U_4O_9) may exist simultaneously at temperatures below 100°C when water would be first potentially available. The application of the oxidation weight gain response would predict the amount of spent fuel inventory which exists in each known oxidation phase. This information, along with intrinsic dissolution rate data for each phase, would be used to provide estimates of the radionuclide release rate over the long time periods (thousands of years) of interest in performance assessment and waste package design analysis.

Oxidation weight gain response depends on oxidation phase, oxidation front motion and surface area

Oxidation phase ~ amount (mass) of O_2 added per unit volume of UO_2 in a fragment.

Oxidation front motion ~ velocity of front (cm/unit time).

Surface area ~ area at oxidation front; decreases in time as front propagates into a fragment.

$$\text{Weight gain} \sim \left[\begin{array}{c}\text{Mass of } O_2 \\ \text{added at front}\end{array}\right] \cdot \left[\begin{array}{c}\text{Front} \\ \text{velocity}\end{array}\right] \cdot \left[\begin{array}{c}\text{Surface area} \\ \text{at front}\end{array}\right]$$

Figure 3.2.2-2

Grain set decomposed to pyramidal volume subsets

A set of grain volumes (in cross section)

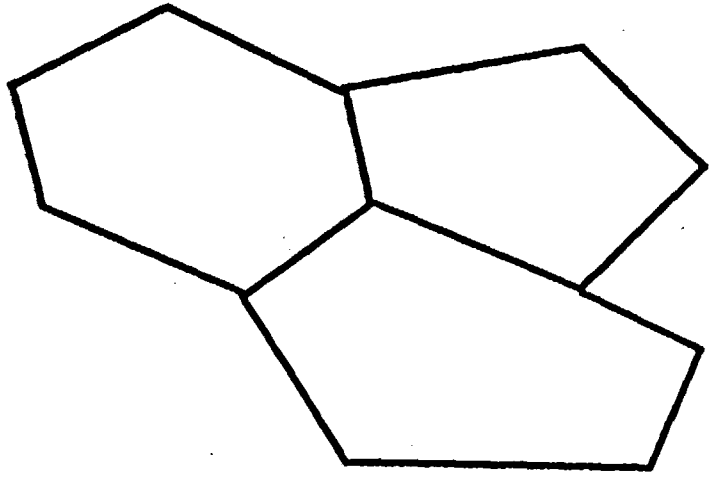

Put a point at the center of each grain, and decompose into a set of pyramids (triangles in cross section).

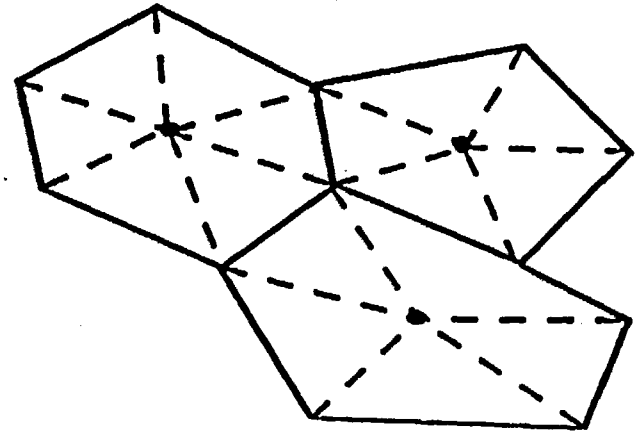

Figure 3.2.2-3

Density function: probable number of grain pyramids

- Exists a large number of grain pyramids, many of which will be of the same "size" (compact domain set).

  A "size" can be identified by attributes (a, b, c), as illustrated below.

  Let G(x, t, a, b, c) denote the probably number of pyramids of size (a, b, c) in a unit spatial volume of grains about point x at time t.

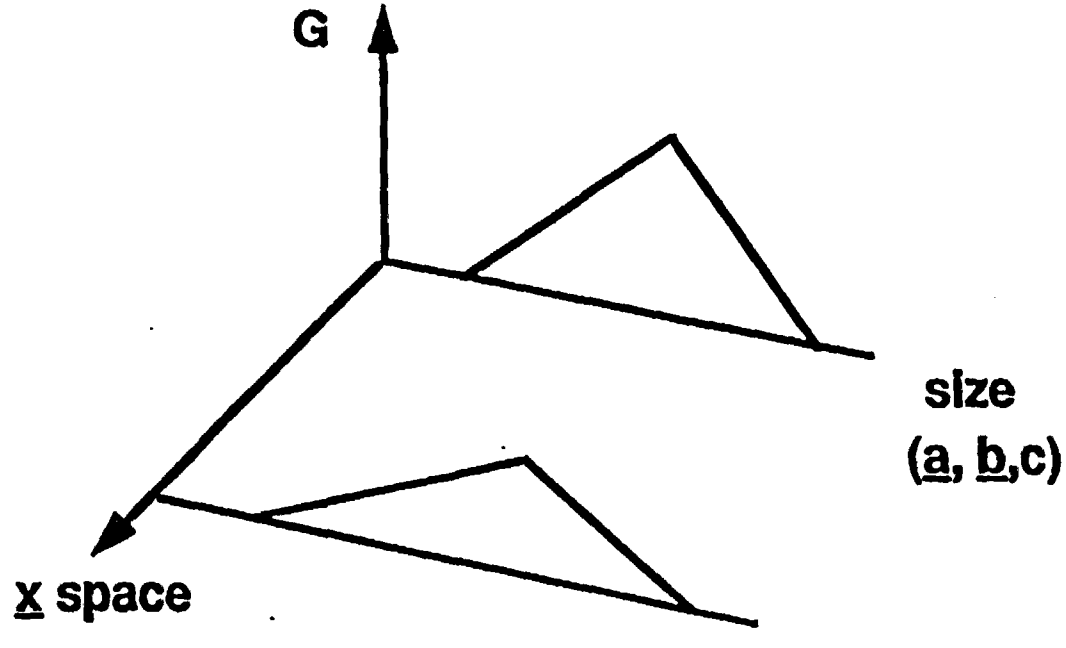

Grain volume oxidation front

Pyramidal volume in an oxidizing grain and its associated physical attributes.

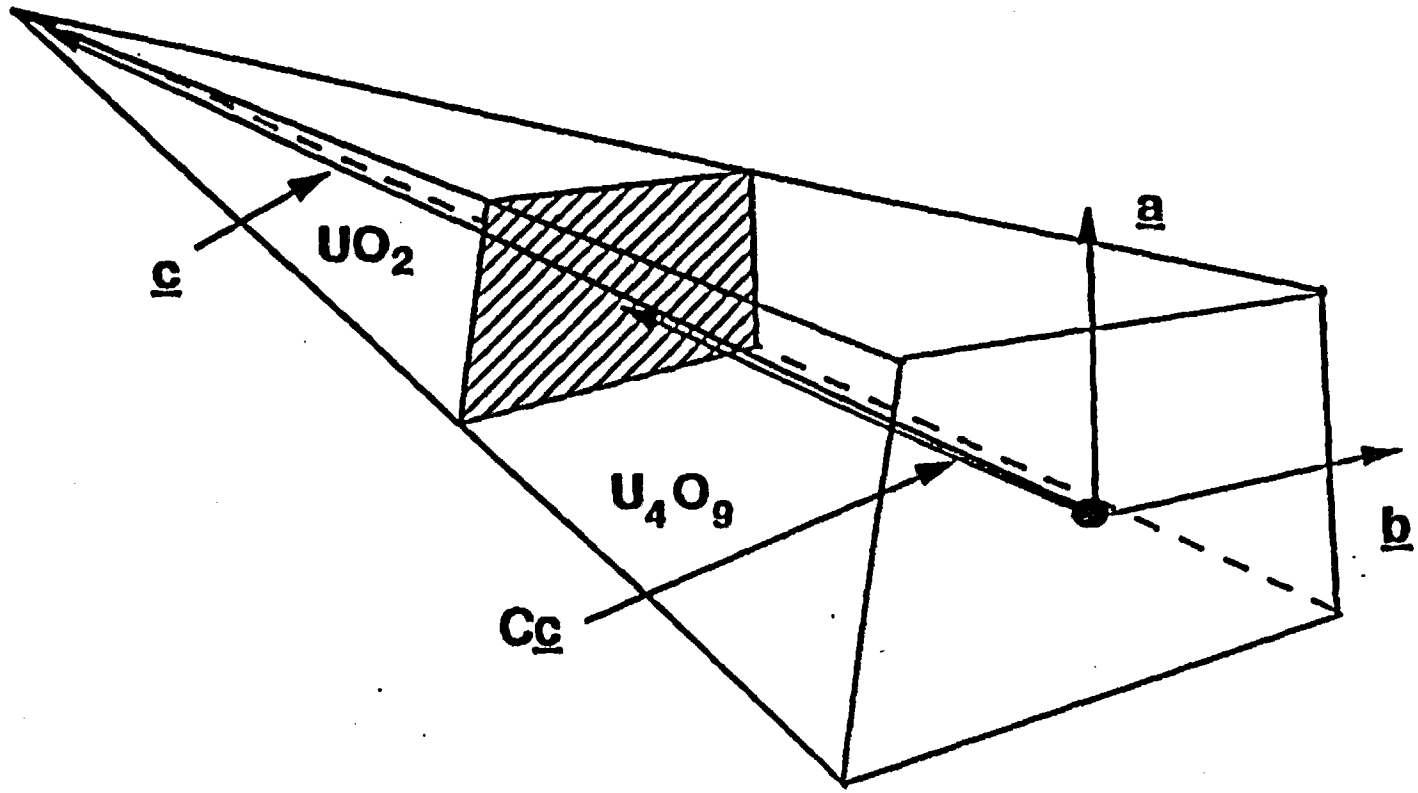

Figure 3.2.2-5

Density function: probable number of grain pyramids

- Exists a large number of grain pyramids, many of which will be of the same "size" (compact domain set).

  A "size" can be identified by attributes (a, b, c), as illustrated below.

  Let G(x, t, a, b, c) denote the probably number of pyramids of size (a, b, c) in a unit spatial volume of grains about point x at time t.

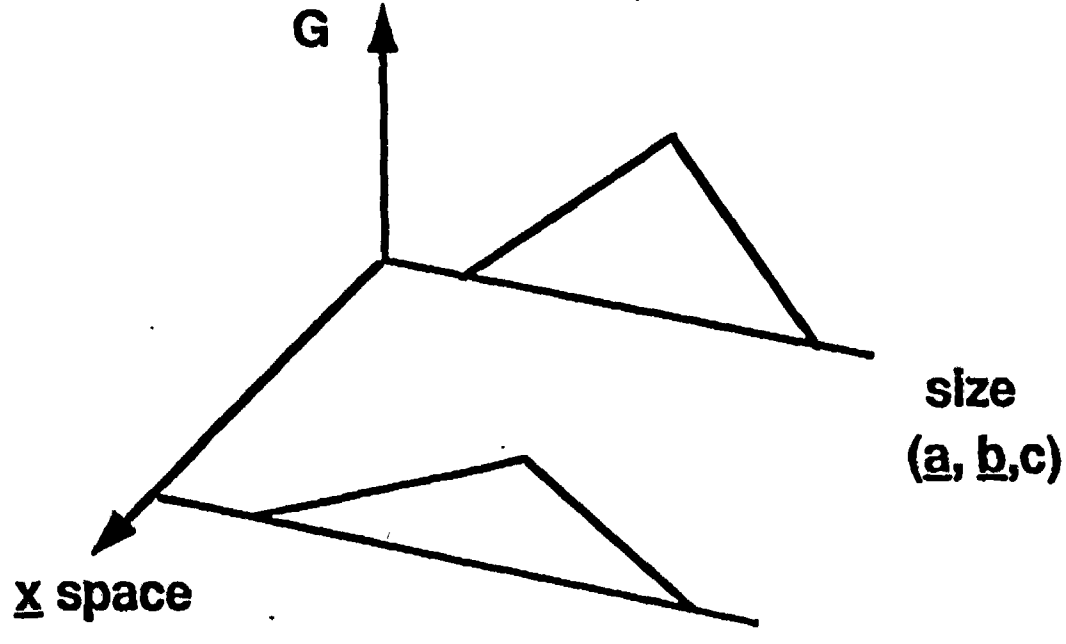

Figure 3.2.2-6

Fragment set decomposed to pyramidal volume subsets

A set of fragments (in cross section)

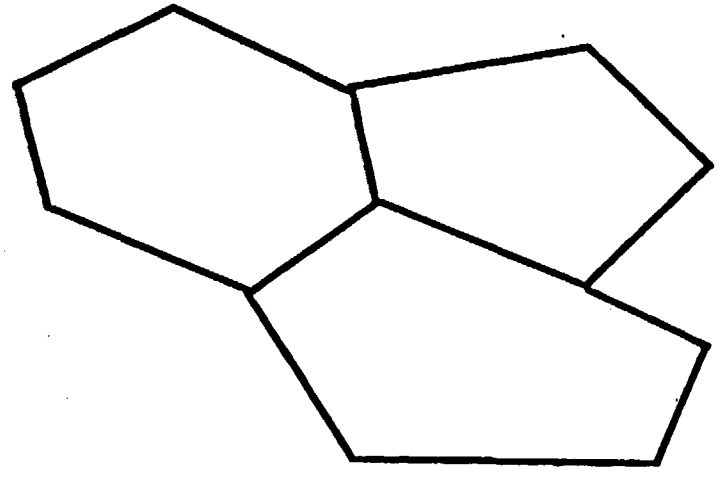

Put a point at the center of each fragment, and decompose into a set of pyramids (triangles in cross section).

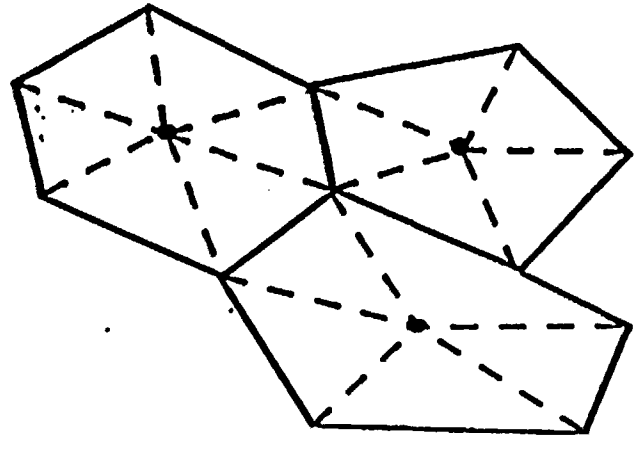

Figure 3.2.2-7

Physical attributes of pyramidal volumes for fragments

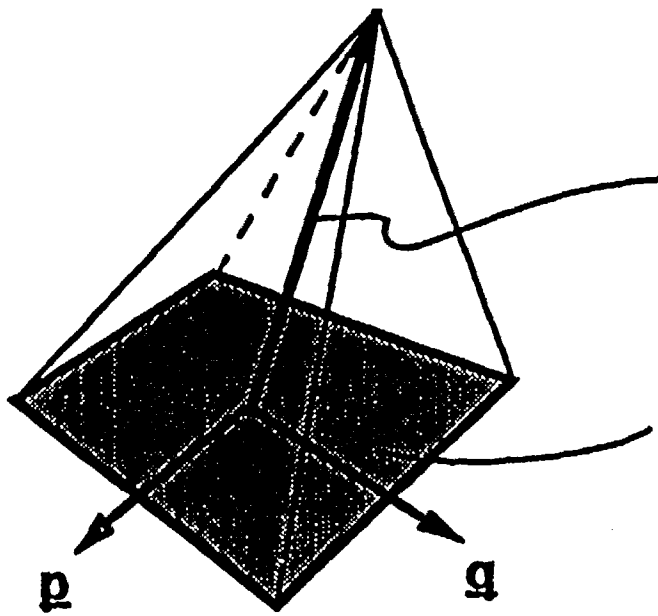

Height vector $\underline{h}$ perpendicular to the base

Base vectors $\underline{p}$ and $\underline{q}$ on fragment boundary such that $\underline{p}$ cross $\underline{q}$ measures both area and orientation of the pyramid's base

Each fragment pyramid characterized by a set of vector attributes ($\underline{p}$, $\underline{q}$, $\underline{h}$)

Figure 3.2.2-8

Fragment pyramidal volume oxidation front

Pyramidal volume in an oxidizing fragment and its associated physical attributes.

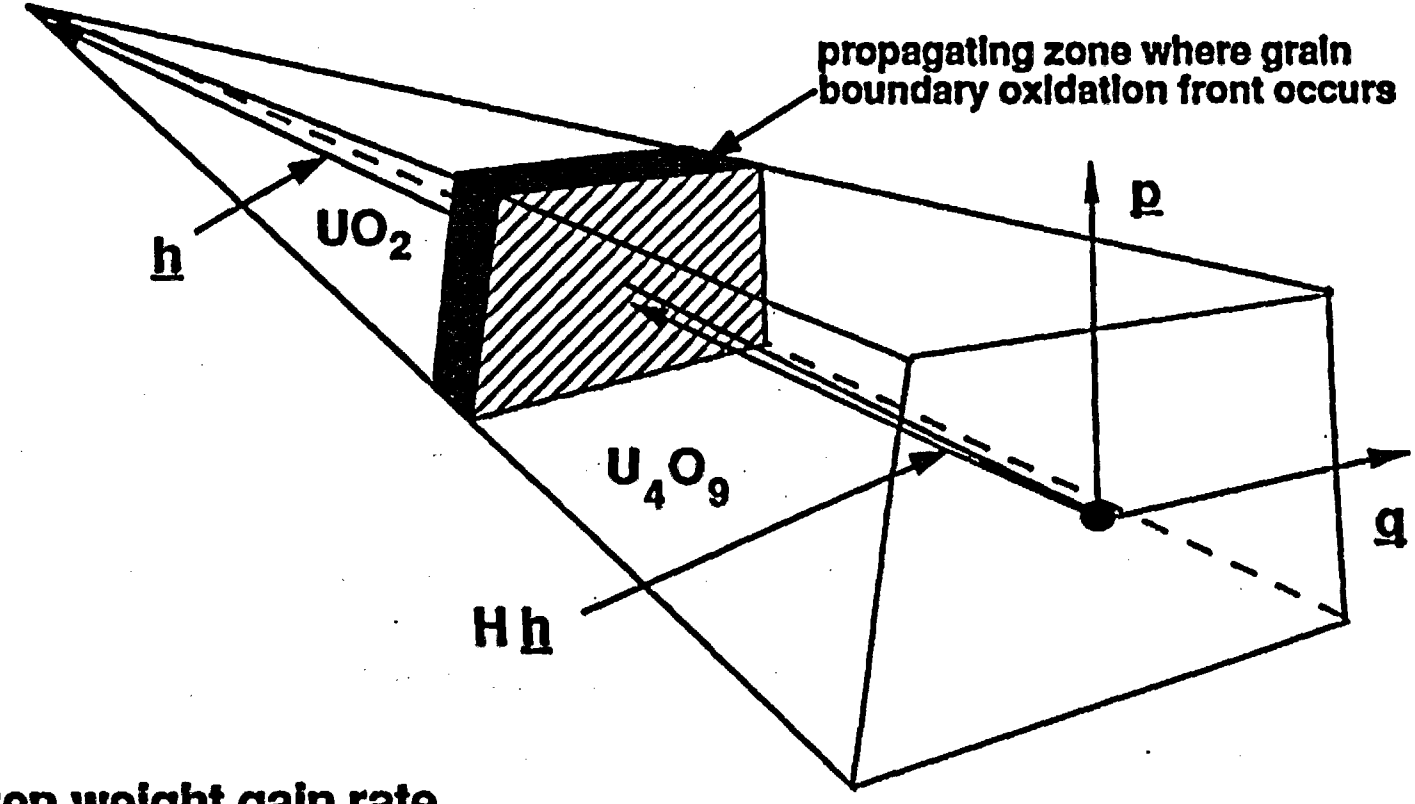

oxygen weight gain rate

$$\dot{O}(t) = Ne_{ijk}\, p_j\, q_k h_l\, (1-H)^2\, \dot{H}$$

Figure 3.2.2-9

Density function: probable number of fragment pyramids

- Exists a large number of fragment pyramids, many of which will be of the same "size" (compact domain set).

  A "size" can be identified by attributes (p, q, h), as illustrated below.

  Let F(x, t, p, q, h) denote the probably number of pyramids of size (p, q, h) in a unit spatial volume of fragments about point x at time t.

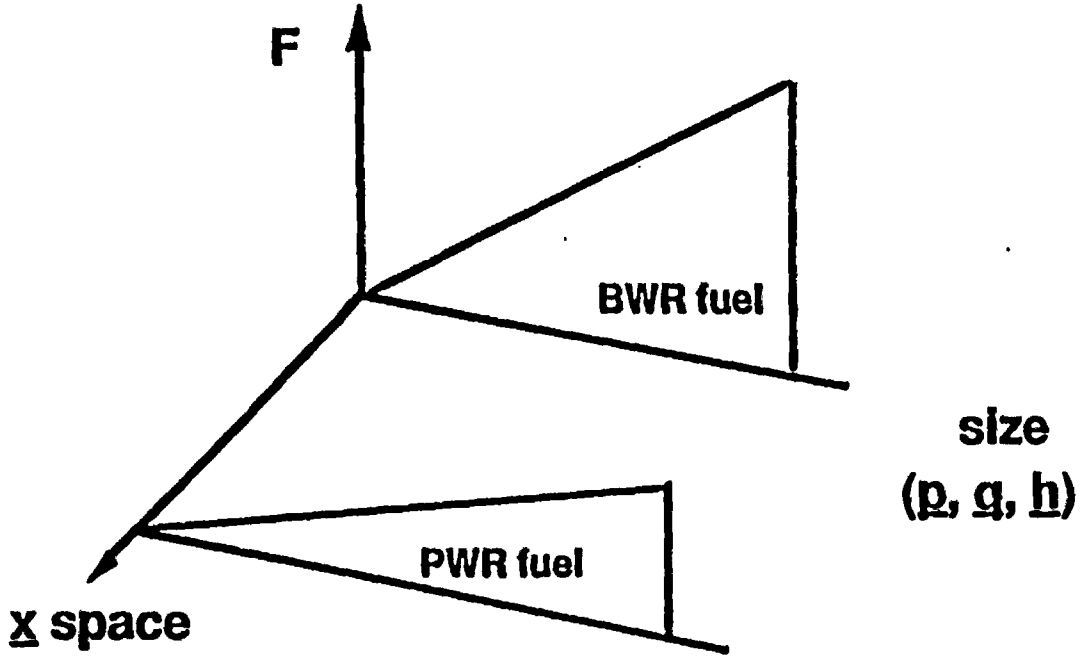

Figure 3.2.2-10

Oxygen weight gain for a density of fragments

The probable number of pyramidal volume of species $\underline{f} \sim (\underline{p}, \underline{q}, \underline{h}, H, \dot{H})$ in

a $d\underline{x}$ volume at time t is $F(x, t, \underline{f})\, d\underline{f} d\underline{x}$;

Then the oxygen weight gain for this number is

$$\dot{O}(\underline{x}, t, f) = Ne_{ijk}\, p_j\, q_k\, h_l\, (1-H)^2\, \dot{H} F(\underline{x}, t, f)\, df d\underline{x}$$

Integrate over the domain of fragment species {f} and the spatial volume

volume of B of fragments

$$\dot{O}(t) = \int_{B\{f\}} \int Ne_{ijk}\, p_j\, q_k\, h_l\, (1-H)^2\, \dot{H} F(\underline{x}, t, f)\, df d\underline{x}$$

The above formula for the case of a distribution of grain volume oxidizing would replace the fragment density function F with a grain density $G(\underline{x}, t, \underline{a}, b, c, h, \dot{h})$ to become

$$\dot{O}(t) = \int_{B\{g\}} \int Ne_{ijk}\, a_j\, b_k\, c_i\, (1-h)^2\, \dot{h} G(\underline{x}, t, g)\, dg d\underline{x}$$

$$\dot{h} = 2.12 \times 10^{13}\ (m/hr)\ \exp(-27000/RT)$$

where $\dot{h}$ is from Section 3.2.2

Figure 3.2.2-11

Figure 3.2.2-12

R.B. Stout, et al., "Spent Fuel Waste Form Characterization: Grain and Fragment Size Statistical Dependence for Oxidation Response, LLNL Report UC RL-107910, May, 1991.

Adachi, T., M. Ohnuki, et al., "Dissolution Study of Spent PWR Fuel: Dissolution Behavior and Chemical Properties on Insoluble Residues," *J. Nucl. Mater.*, **174**, 60-71 (1990). (Readily available.)

Aronson, S., R.B. Roof, and J. Belle. "Kinetic Study of the Oxidation of Uranium Oxide," *J. Chem. Phys.* **27**, 137 (1957). (Readily available)

Boltzmann, L. "Lectures on Gas Theory," translated by S.G. Brush, Univ. of California Press, Berkeley, CA (1964). NNA.920401.0117

Carslaw, H.S. and J.C. Jaeger. "Conduction of Heat in Solids," second edition, Oxford University Press, New York (1959). NNA.900522.0259

Einziger, R.E. and H.C. Buchanan. "Long-Term, Low Temperature Oxidation of PWR Spent Fuel," Westinghouse Hanford Co. Report, WHC-EP-0070 (June,1987). NNA.900620.0297

Einziger, R.E. and R.E. Woodley. "Predicting Spent Fuel Oxidation States in a Tuff Repository," Westinghouse Hanford Co. Report HEDL-SA-3627, (April, 1985). NNA.870915.0073

Einziger, R.E. "Technical Test Description of Activities to Determine the Potential for Spent Fuel Oxidation in a Tuff Repository," Westinghouse Hanford Co. Report HEDL-7540 (June, 1985). NNA.920302.0060

Einziger, R.E. "Test Plan for Series 2 Thermogravimetric Analyses of Spent Fuel Oxidation," Westinghouse Hanford Co. Report HEDL-7556 (February, 1986). NNA.920302.0061

Einziger, R.E., "Test Plan for Long-Term, Low-Temperature Oxidation of Spent Fuel, Series 1," Westinghouse Hanford Co. Report HEDL-7560 (June, 1986). NNA.920302.0062

Einziger, R.E. and R.V. Strain, *Nucl. Technol.*, **75**, 82 (1986). (Readily available)

Einziger, R.E., L.E. Thomas, H.C. Buchanan and R.B. Stout, *J. Nucl. Mater.*, **190**, 53 (1992) (Readily available)

Finch, R., and R. Ewing, "Alteration of Natural UO_2 Under Oxidizing Conditions from Shinkolobwe, Katanga, Zaire: A Natural Analogue for the Corrosion of Spent Fuel," *Radiochim. Acta*, **52/53**, 395-401 (1991). NNA.900507.0149

Gleiter, H. and B. Chalmers. "High-Angle Grain Boundaries," in *Prog. in Mat. Sci.*, Vol. 16, Pergamon Press, New York (1972). (Readily available)

Grambow, B. "Spent Fuel Dissolution and Oxidation: An Evaluation of the Literature," SKB Tech. Rept. 89-13, Svensk Kärnbränslehantering AB, Stockholm, 42 pgs. (1989). NNA.891013.0094

Grambow, B., R. Forsyth, et al. "Fission Product Release from Spent UO_2 Fuel Under Uranium-Saturated Oxic Conditions," *Nucl. Tech.*, 92, 204-213 (November, 1990). (Readily available)

Olander, D.R. "Combined Grain-Boundary and Lattice Diffusion in Fine-Grained Ceramics," *Advances in Ceramics*, 17, 271 (1986). (Readily available)

Slattery, J.C. *Momentum, Energy and Mass Transfer in Continua*, R.E. Krieger Pub. Co., New York (1978). NNA.920401.0115

Stout, R.B., H.F. Shaw, and R.E. Einziger, LLNL Report UCRL-100859, September, 1989. (Readily available)

Stout, R.B., E. Kansa, R.E. Einziger, H.C. Buchanan, and L.E. Thomas, LLNL Report UCRL-104932. (Readily available)

Stout, R.B. "Statistical Model for Particle-Void Deformation Kinetics in Granular Materials During Shock Wave Propagation," Lawrence Livermore National Laboratory Report UCRL-101623 (July, 1989). NNA.900517.0267

Thomas, L., O. Slagle, and R. Einziger, "Nonuniform Oxidation of LWR Spent Fuel in Air," *J. Nucl. Mat.*, 184 117-126 (1991). NNA.910509.0071

Thomas, L., R. Einziger, and R. Woodley, "Microstructural Examination of Oxidized Spent PWR Fuel by Transmission Electron Microscopy," *J. Nucl. Mat.*, 166, 243-251 (1989). NNA.900709.0482

Thomas, L.E., R.E. Einziger, and R.E. Woodley. "Microstructural Examinations of Oxidized Spent Fuel by Transmission Electron Microscopy," *J. Nucl. Mat.*, in press. YMPO Accession NML 880707.0043.

Wood, P. and G.H. Bannister. "Investigation of the Mechanism of UO_2 Oxidation in Air: The Role of Grain Size," Proc. Workshop on Chemical Reactivity of Oxide Fuel and Fission Product Release, K.A. Simpson and P. Wood, eds., Berkeley Nuclear Lab., U.K., p. 19 (1987). NNA.920401.0116

Woodley, R.E., R.E. Einziger, and H.C. Buchanan. "Measurement of the Oxidation of Spent Fuel Between 140 and 225 C by Thermogravimetric Analysis," Westinghouse Hanford Co. Report WHC-EP-0107 (Sept., 1988). NNA.880927.0069

3. SCIENTIFIC BASIS FOR PREDICTIVE MODEL DEVELOPMENT

3.1 SPENT FUEL CLADDING FAILURE

3.1.1 EXPERIMENTAL PARAMETERS FOR FAILURE MODELS

3.1.2 FAILURE MODELS

3.2 SPENT FUEL OXIDATION

3.2.1 EXPERIMENTAL PARAMETERS FOR OXIDATION MODELS

3.2.2 OXIDATION MODELS

3.3 SPENT FUEL FISSION GAS RELEASE

3.3.1 EXPERIMENTAL PARAMETERS FOR FISSION GAS RELEASE

3.3.2 FISSION GAS RELEASE MODELS

3.4 SPENT FUEL DISSOLUTION

3.4.1 EXPERIMENTAL PARAMETERS FOR DISSOLUTION

3.4.1.1 DISSOLUTION RATES

3.4.1.2 SOLUBILITY LIMITS

3.4.1.3 SOLUBILITY LIMITING PHASES

3.4.2 DISSOLUTION MODELS

3.5 GLASS DISSOLUTION

3.5.1 EXPERIMENTAL PARAMETERS FOR GLASS DISSOLUTION

3.5.2 GLASS DISSOLUTION MODELS

3.6 OTHER RELEASE SOURCES OF RADIONUCLIDES

3.6.1 CRUD

3.6.2 HARDWARE

3.6.3 CLADDING

3. SCIENTIFIC BASIS FOR PREDICTIVE MODEL DEVELOPMENT

3.1 SPENT FUEL CLADDING FAILURE

3.1.1 EXPERIMENTAL PARAMETERS FOR FAILURE MODELS

3.1.2 FAILURE MODELS

3.2 SPENT FUEL OXIDATION

3.2.1 EXPERIMENTAL PARAMETERS FOR OXIDATION MODELS

3.2.2 OXIDATION MODELS

3.3 SPENT FUEL FISSION GAS RELEASE

3.3.1 EXPERIMENTAL PARAMETERS FOR FISSION GAS RELEASE

3.3.2 FISSION GAS RELEASE MODELS

3.4 SPENT FUEL DISSOLUTION

3.4.1 EXPERIMENTAL PARAMETERS FOR DISSOLUTION

3.4.1.1 DISSOLUTION RATES

3.4.1.2 SOLUBILITY LIMITS

3.4.1.3 SOLUBILITY LIMITING PHASES

3.4.2 DISSOLUTION MODELS

3.5 GLASS DISSOLUTION

3.5.1 EXPERIMENTAL PARAMETERS FOR GLASS DISSOLUTION

3.5.2 GLASS DISSOLUTION MODELS

3.6 OTHER RELEASE SOURCES OF RADIONUCLIDES

3.6.1 CRUD

3.6.2 HARDWARE

3.6.3 CLADDING

3.3.1 Experimental Parameters for Fission Gas Release

The Materials Characterization Center has estimated distributions of burnup and fission gas release for the current and projected spent fuel inventories through 2020.[1] This was done both to help assure that the current suite of Approved Testing Materials is representative of the spent fuel inventory and to help define additional spent fuel ATM needs.

From the developed distributions it was concluded that the current ATM's may be considered representative, in terms of fission gas release and burnup, of nearly 100% of the spent fuel inventory discharged through 1988. However, those ATM's may be considered representative of only 61% of the total projected inventory discharged through 2020. That is because 39% of the inventory is projected to have burnup levels in excess of 45 MWd/kgM while none of the ATM's have burnups in excess of 45 MWd/kgM.

Noting that there are no ATM's representative of high burnup spent fuel, it is recommended that the next ATM to be acquired be representative of a modern fuel design (e.g., BWR 8x8 barrier or PWR 17x17) and have the highest possible burnup. It should also have low fission gas release so as to be representative of the large volume of fuel in the low fission gas release/high burnup category of spent fuel. A second ATM to be acquired should have the characteristics of high fission gas release/high burnup to be both representative of the other currently unrepresented category of spent fuel and provide an ATM that would be bounding of the expected spent fuel characteristics.

---

[1] M. E. Cunningham, et al., "The Impact of Burnup and Fission Gas Release Distributions of the U.S. Spent Fuel Inventory on the Selection of Spent Fuel Test Materials for the U.S. Geological Repository Project," PNL report in preparation, September, 1990.

The current and above-proposed ATM's will be representative of standard design, non-failed LWR spent fuel. Fuel that will still not be represented by ATM's will include stainless steel-clad fuel, fuel that failed either in-reactor or during interim storage, and miscellaneous test and experimental fuel. It is estimated that these two fuel types will account for 2-5% of the total emplacement inventory.

One significant spent fuel classification that is not included in a burnup-fission gas release distribution is fuel that contains a burnable neutron poison. However, the MCC does have an early vintage Gd_2O_3 burnable poison fuel in its inventory and if a modern high burnup BWR fuel assembly is acquired, modern burnable poison fuel would be part of such an assembly.

Example of Justification for Grouping Varying Rod Designs

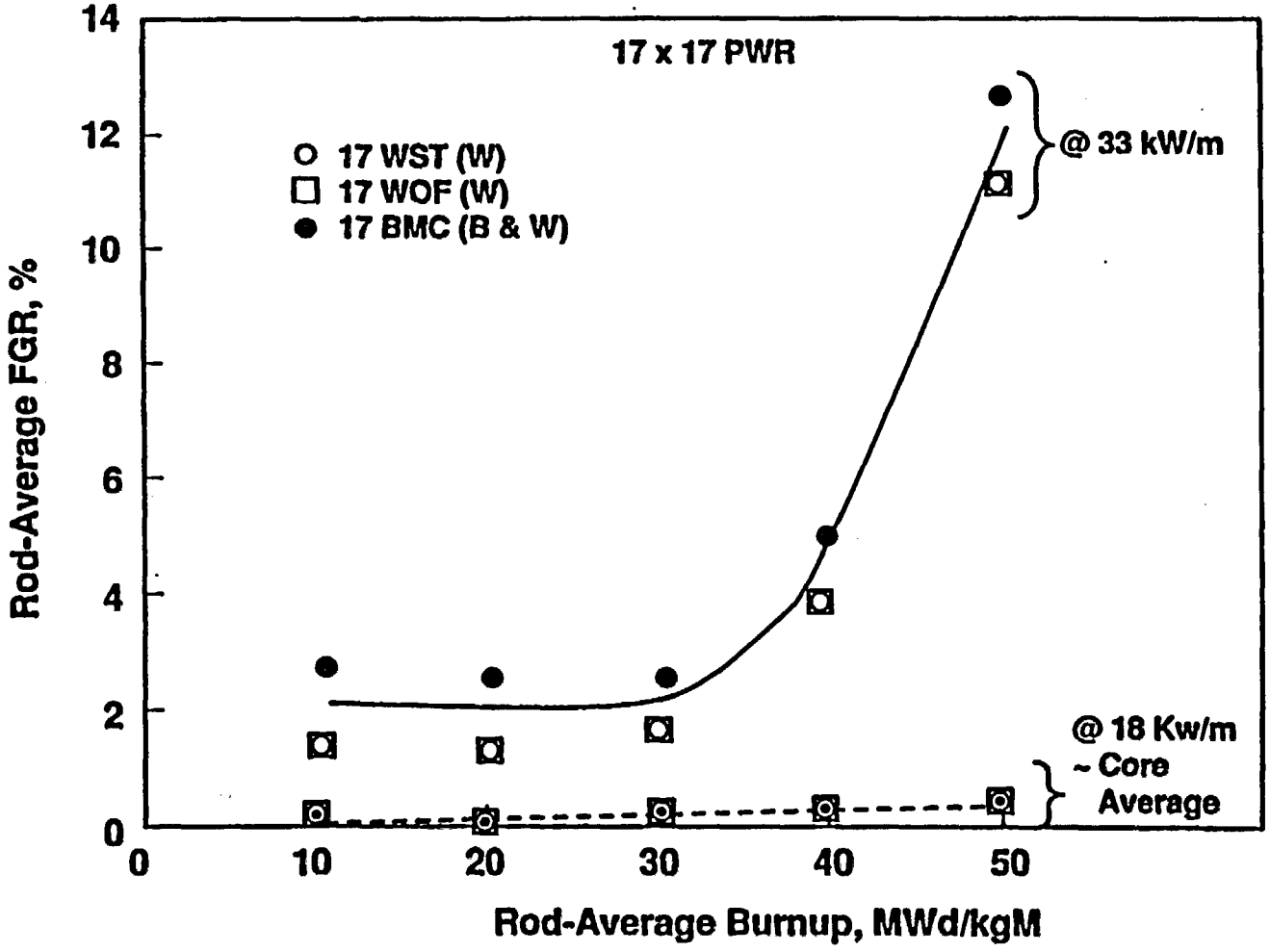

LHGR, Burnup, and FGR Correlation for BWR Rod-Types

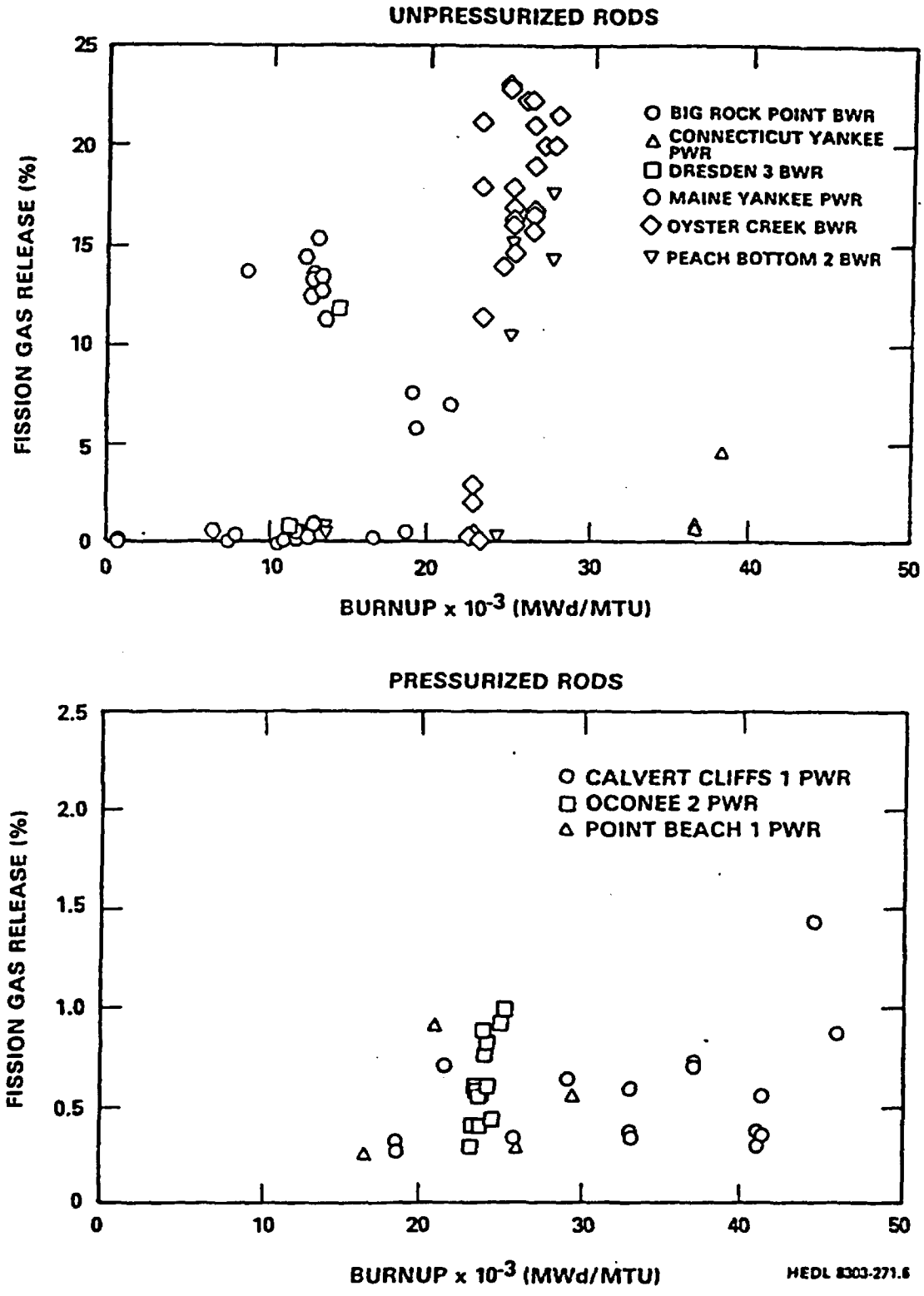

FIGURE 14. Comparison of Fission Gas Release from Unpressurized and Pressurized LWR Fuel Rods.(8)

R.E. Woodley, *The Characteristics of Spent LWR Fuel Relevant to its Storage in Geologic Repositories*, HEDL-TME 83-28, October, 1983.

LHGR, Burnup,and FGR Correlation for PWR Rod-Types

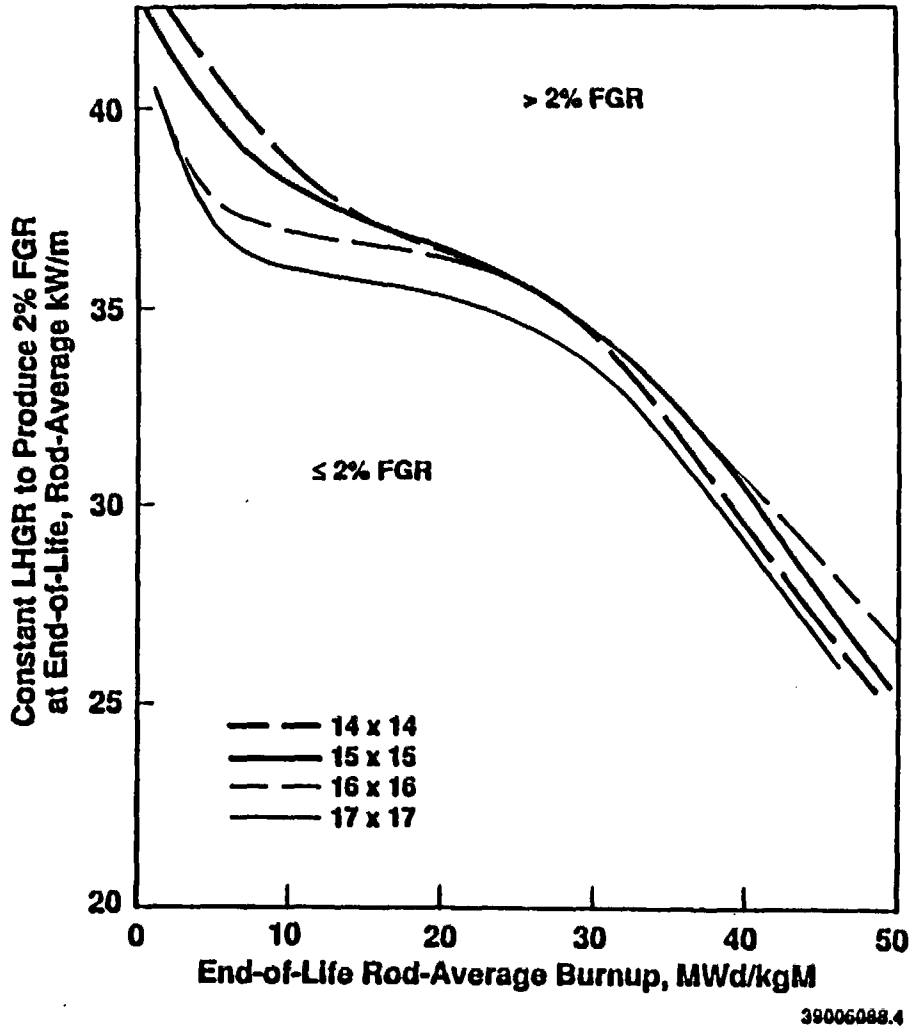

3. SCIENTIFIC BASIS FOR PREDICTIVE MODEL DEVELOPMENT

3.1 SPENT FUEL CLADDING FAILURE

3.1.1 EXPERIMENTAL PARAMETERS FOR FAILURE MODELS

3.1.2 FAILURE MODELS

3.2 SPENT FUEL OXIDATION

3.2.1 EXPERIMENTAL PARAMETERS FOR OXIDATION MODELS

3.2.2 OXIDATION MODELS

3.3 SPENT FUEL FISSION GAS RELEASE

3.3.1 EXPERIMENTAL PARAMETERS FOR FISSION GAS RELEASE

3.3.2 FISSION GAS RELEASE MODELS

3.4 SPENT FUEL DISSOLUTION

3.4.1 EXPERIMENTAL PARAMETERS FOR DISSOLUTION

3.4.1.1 DISSOLUTION RATES

3.4.1.2 SOLUBILITY LIMITS

3.4.1.3 SOLUBILITY LIMITING PHASES

3.4.2 DISSOLUTION MODELS

3.5 GLASS DISSOLUTION

3.5.1 EXPERIMENTAL PARAMETERS FOR GLASS DISSOLUTION

3.5.2 GLASS DISSOLUTION MODELS

3.6 OTHER RELEASE SOURCES OF RADIONUCLIDES

3.6.1 CRUD

3.6.2 HARDWARE

3.6.3 CLADDING

3.3.2 Gaseous Radionuclide Release

Fission gas release has been predicted using a "standard" model, the so-called ANS-5.4 model,[1] as revised by C.E. Beyer of PNL.[2]

Similar fission gas release curves were presented at the "Status and Future Directions of Spent Fuel ATM Acquisition and Characterization" meeting at PNL March 28-29, 1989, by C.E. Beyer of the MCC. These curves were generated using the revised ANS 5.4 Gas Release Model and we have fit these curves to a very simple and easily used equation for burnup ≥ 20 MWd/kgM and for gas release ≤ 60%. This equation is

$$\log_{10}(\textit{fractional}\ \text{release}) = \frac{13}{8}\log_{10}\ (\text{burn - up [MWd/kgM]})\ \frac{-4420}{T(K)}$$

We have calculated points at 30 and 40 MWd/kgM and superimposed them on Beyer's curves to show the agreement. Additional curves for 30,50, and 60 MWd/kgM calculated using our simple expression are also plotted.

---

[1] Method for Calculating Fractional Release of Volatile Fission Products from Oxide Fuel," ANSI/ANS-5.4-1982.

[2] Memo from C.E. Beyer (PNL) to J.C. Voglewede (USNRC), May 24, 1982.

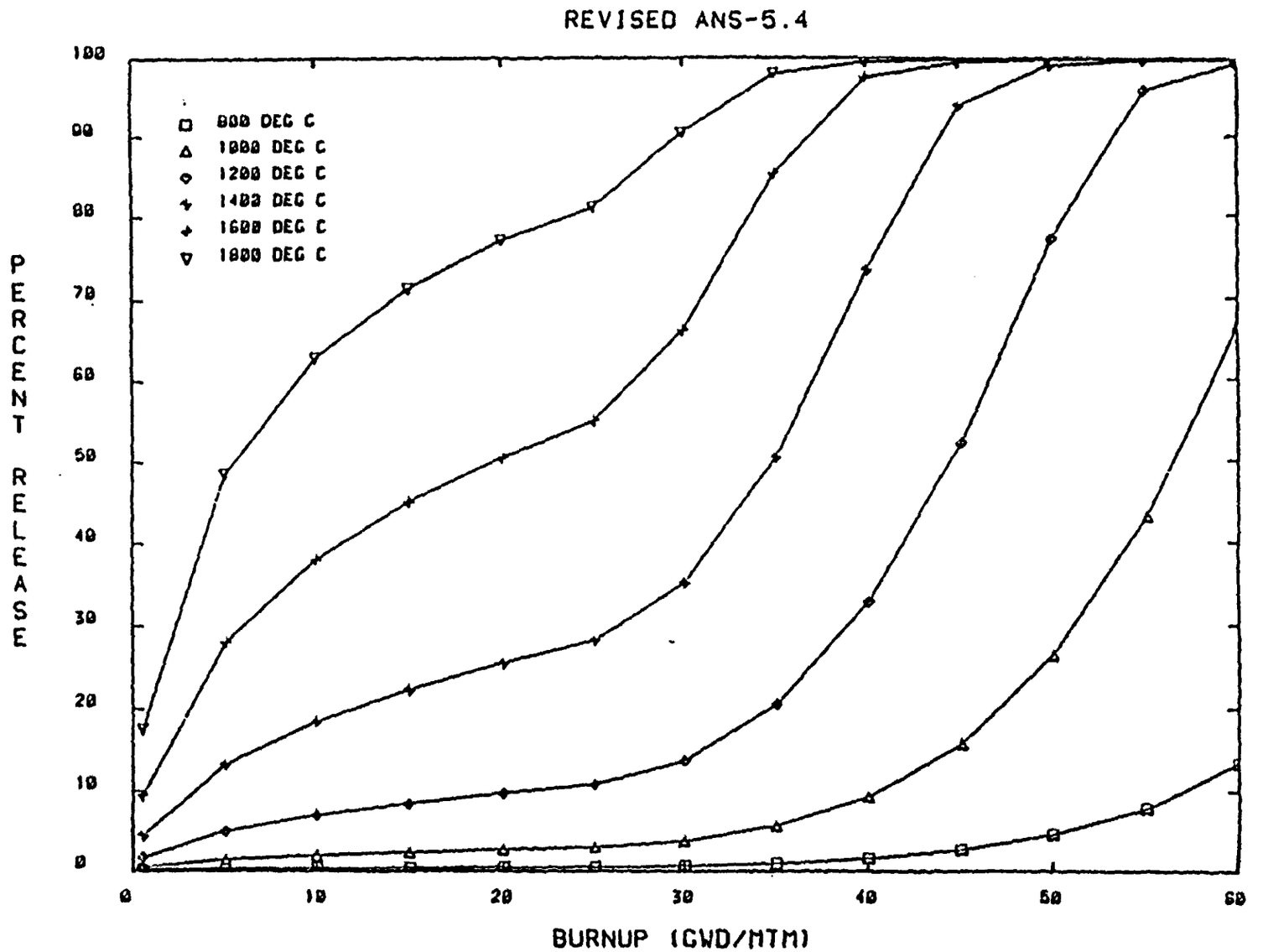

Figure 1. Revised ANS 5.4 Model Predictions at Isothermal Temperatures as a Function of Burnup.

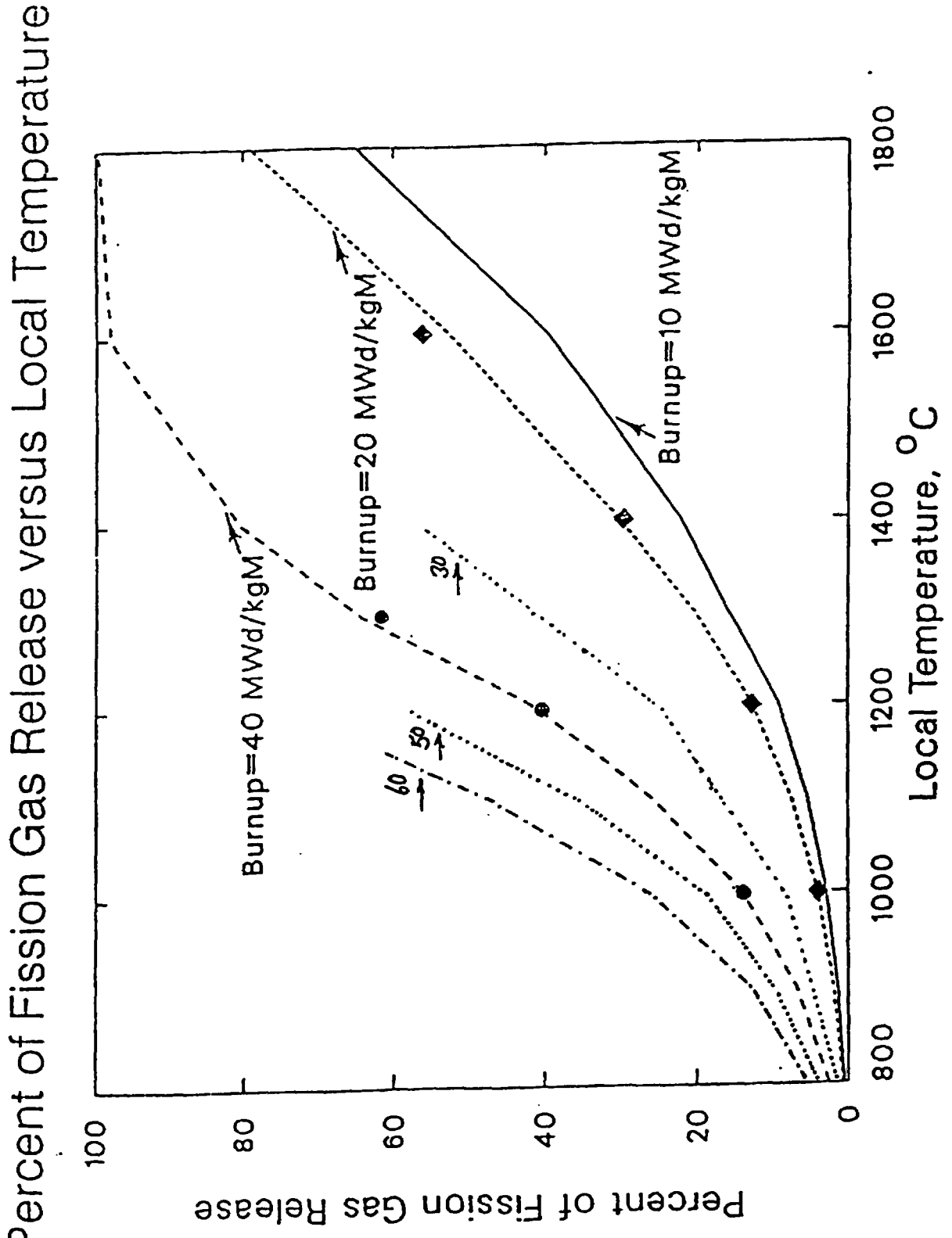

C.E. Beyer, in *Status and Future Direction of Spent Fuel ATM Acquisition and Characterization,* meeting in Richland, Washington, March, 1989.

3. SCIENTIFIC BASIS FOR PREDICTIVE MODEL DEVELOPMENT

3.1 SPENT FUEL CLADDING FAILURE

3.1.1 EXPERIMENTAL PARAMETERS FOR FAILURE MODELS

3.1.2 FAILURE MODELS

3.2 SPENT FUEL OXIDATION

3.2.1 EXPERIMENTAL PARAMETERS FOR OXIDATION MODELS

3.2.2 OXIDATION MODELS

3.3 SPENT FUEL FISSION GAS RELEASE

3.3.1 EXPERIMENTAL PARAMETERS FOR FISSION GAS RELEASE

3.3.2 FISSION GAS RELEASE MODELS

3.4 SPENT FUEL DISSOLUTION

3.4.1 EXPERIMENTAL PARAMETERS FOR DISSOLUTION

3.4.1.1 DISSOLUTION RATES

3.4.1.2 SOLUBILITY LIMITS

3.4.1.3 SOLUBILITY LIMITING PHASES

3.4.2 DISSOLUTION MODELS

3.5 GLASS DISSOLUTION

3.5.1 EXPERIMENTAL PARAMETERS FOR GLASS DISSOLUTION

3.5.2 GLASS DISSOLUTION MODELS

3.6 OTHER RELEASE SOURCES OF RADIONUCLIDES

3.6.1 CRUD

3.6.2 HARDWARE

3.6.3 CLADDING

3.4 Spent Fuel Dissolution

The dissolution of a waste form and the associated release of the included radionuclides will be limited by two boundary conditions in a geologic repository: (1) in the case of contact with fast moving water, the dissolution rate of the waste form will determine the rate at which radionuclides are released, (2) in the case of contact with slowly moving water (slow relative to the dissolution rate), the rate of release of radionuclides will be determined by their solubility under the prevailing conditions. Thus, in order to assess performance of a repository, both rates of dissolution and solubility limits should be available.

Many researchers have investigated the dissolution of UO_2, spent fuel and uraninite (a naturally occurring UO_2 mineral) in aqueous solutions, under either reducing or oxidizing conditions, and as a function of various other environmental variables. Experimental data on the dissolution rates of UO_2, spent fuel and uraninite have been reviewed by Amell and Langmuir,[1] Parks and Pohl,[2] Bruno, et al.,[3] and most recently by Grambow.[4]

Important variables considered in the many investigations were pH, temperature, oxygen fugacity, carbonate/bicarbonate concentrations and other reacting media. The dissolution data are very scattered, and vary as much as six orders of magnitude.[4] The dependence of the dissolution of rates of UO_2, spent fuel and uraninite on these variables is not clear because of uncertainties regarding redox chemistry of uranium in solutions and in solid phases, secondary-phase formation, and surface area measurement. In addition, the previous studies were conducted under experimental conditions which were either unconstrained or which simulated complex repositorial conditions. The results of such studies are difficult

The results are equivocal due to the difference in experimental designs, the diverse history of the fuel samples, the formation of secondary phases during the tests, and the complexity of the solution and surface chemistry of UO_2. Data indicate that UO_2 is easily oxidized to U_4O_9 and U_3O_7 in air[9,10] and can be further oxidized to either U_3O_8[9,10,11] or schoepite, $UO_3{\cdot}2H_2O$.[12] The UO_2 surface oxidation leads to higher leach rates because of higher dissolution rates of U_3O_7, U_3O_8, or schoepite relative to that of UO_2 and because of the increase of surface area of the fuels due to surface cracking.

[1] A.R. Amell, and D. Langmuir, "Factors Influencing the Solution Rate of Uranium Dioxide Under Conditions Applicable to In-Situ Leaching," Bureau of Mines Open File Report 84-79, U.S. Dept. of Interior, Bureau of Mines (1978).

[2] G.A. Parks, and D.C. Pohl, "Hydrothermal Solubility of Uraninite," Geochim. Cosmochim. Acta, 52, 863 (1988).

[3] J. Bruno, I. Casas, and I. Puigdomenech, "The Kinetics of Dissolution of UO_2(s) Under Reducing Conditions," Radiochim. Acta, 44/45, 11 (1988).

[4] B. Grambow, "Spent Fuel Dissolution and Oxidation. An Evaluation of Literature Data," SKB Technical Report 89-13 (1989).

[5] D.E. Grandstaff, "A Kinetic Study of the Dissolution of Uraninite," Econ. Geo., 71, 1493 (1976).

[6] W.E. Schortmann, and M.A. DeSesa, "The Kinetics of the Dissolution of Uranium Dioxide in Carbonate-Bicarbonate Solutions," Proc. 2nd Intern. United National Conf. Peaceful Uses of Atomic Energy, United Nations, Geneva, 3, 333 (1958).

[7] R.L. Pearson and M.E. Wadsworth, "A Kinetic Study of the Dissolution of UO_2 in Carbonate Solution," Trans. Metal. Soc. AIME, 212, 294 (1958).

[8] F. Habashi and G.A. Thurston, "Kinetics and Mechanisms of the Dissolution of Uranium Dioxide," Energ. Nucl. 14, 238 (1967).

[9] S. Aronson, "Oxidation and Corrosion of Uranium Dioxide in Uranium Dioxide: Properties and Nuclear Applications," J. Belle, ed., U.S. Atomic Energy Comm., 377 (1961).

[10] R.E. Einziger, "Test Plan for Long-Term, Low-Temperature Oxidation of BWR Spent Fuel," PNL-6427, Pacific Northwest Laboratory (1988).

[11] S. Aronson, "Oxidation of UO2 in Water Containing Oxygen," Bettis Tech. Rev., Westinghouse Atomic Power Div., Report WAPD-BT-10, 93 (1958).

[12] T. Wadsten, "The Oxidation of Polycrystalline Uranium Dioxide in Air at Room Temperature," T. Nucl. Mat., 64, 315 (1977).

3. SCIENTIFIC BASIS FOR PREDICTIVE MODEL DEVELOPMENT

3.1 SPENT FUEL CLADDING FAILURE

3.1.1 EXPERIMENTAL PARAMETERS FOR FAILURE MODELS

3.1.2 FAILURE MODELS

3.2 SPENT FUEL OXIDATION

3.2.1 EXPERIMENTAL PARAMETERS FOR OXIDATION MODELS

3.2.2 OXIDATION MODELS

3.3 SPENT FUEL FISSION GAS RELEASE

3.3.1 EXPERIMENTAL PARAMETERS FOR FISSION GAS RELEASE

3.3.2 FISSION GAS RELEASE MODELS

3.4 SPENT FUEL DISSOLUTION

3.4.1 EXPERIMENTAL PARAMETERS FOR DISSOLUTION

3.4.1.1 DISSOLUTION RATES

3.4.1.2 SOLUBILITY LIMITS

3.4.1.3 SOLUBILITY LIMITING PHASES

3.4.2 DISSOLUTION MODELS

3.5 GLASS DISSOLUTION

3.5.1 EXPERIMENTAL PARAMETERS FOR GLASS DISSOLUTION

3.5.2 GLASS DISSOLUTION MODELS

3.6 OTHER RELEASE SOURCES OF RADIONUCLIDES

3.6.1 CRUD

3.6.2 HARDWARE

3.6.3 CLADDING

Spent Fuel Dissolution Release Rate

Cladding gap, fragment surface, (grain boundary and areas), grain inventory releases illustrated

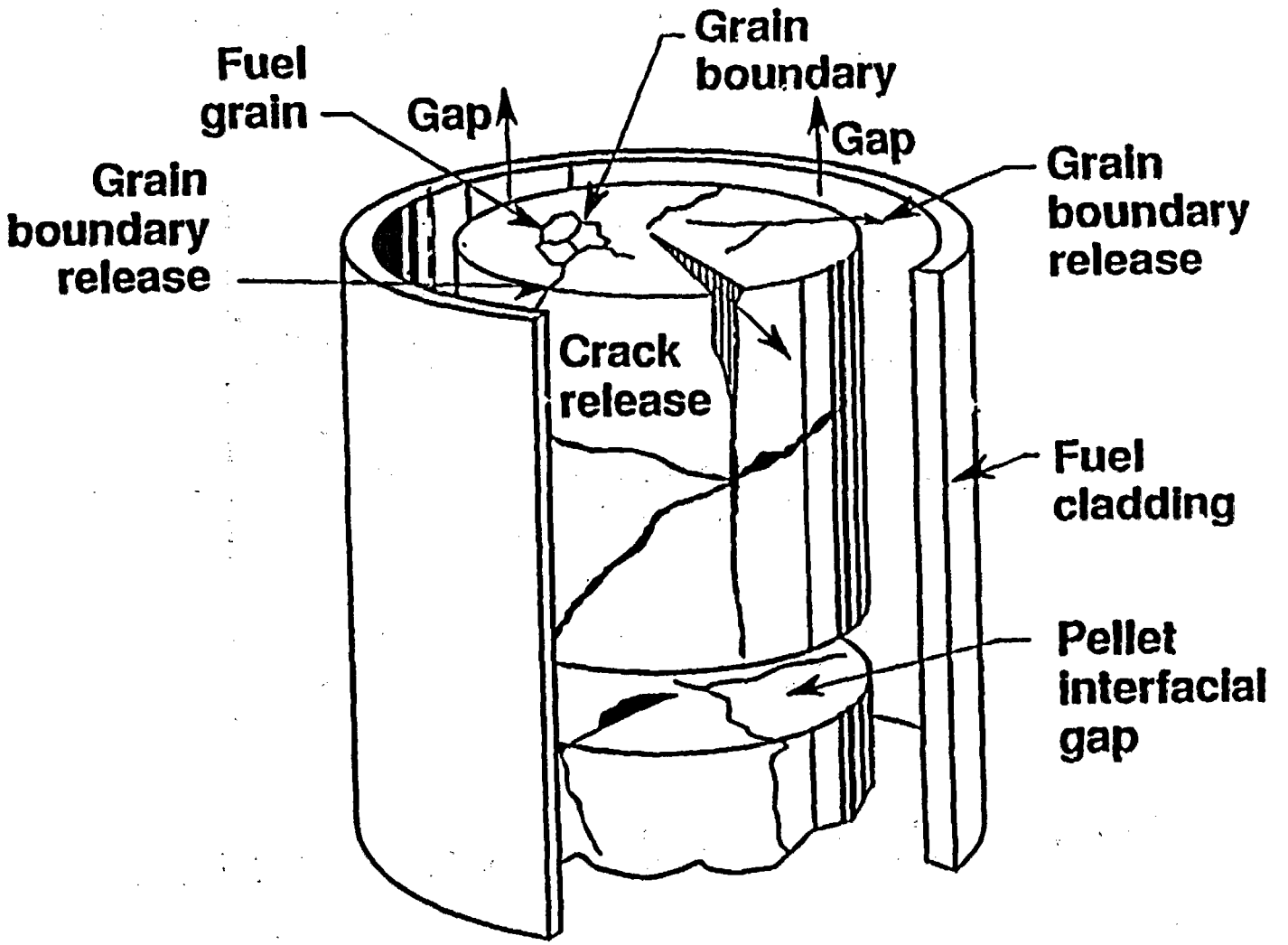

SOLUBLE RADIONUCLIDE RELEASE

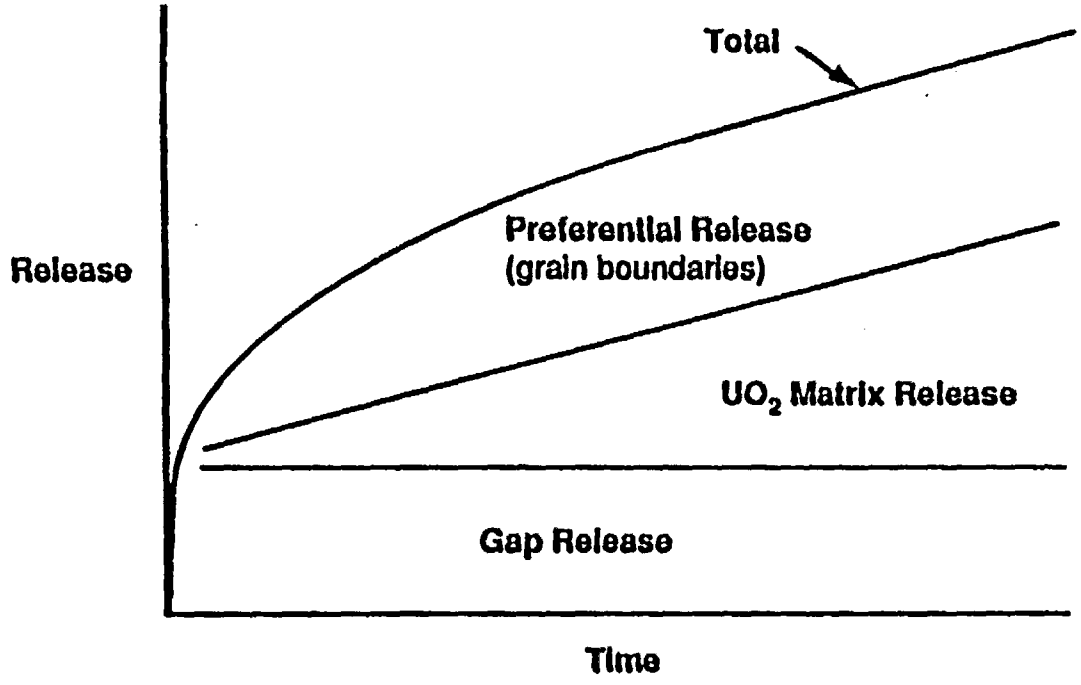

- **Rapid release of "gap inventories" with initial water contact (days)**
- **Preferential release from grain boundaries and other sources of radionuclide concentration (years)**
- **Releases are controlled by matrix dissolution after exposed grain boundaries and other sources of radionuclide concentration become depleted** (assuming fuel is not substantially degraded by oxidation)

A SCHEMATIC VIEW OF SF DISSOLUTION*

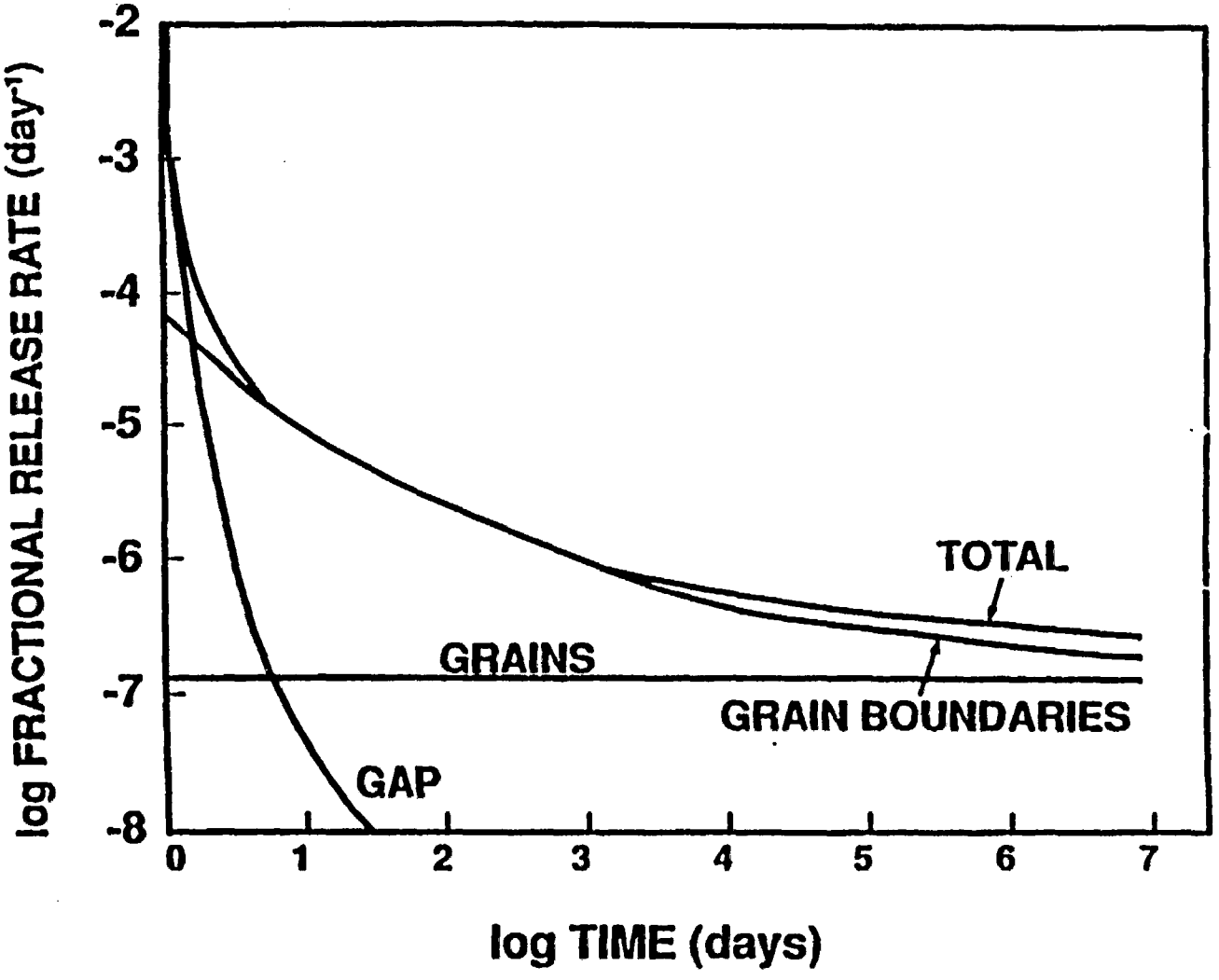

*L.H. JOHNSON AND D.W. SHOESMITH, "RADIOACTIVE WASTE FORMS FOR THE FUTURE," W. LUTZE AND R.C. EWING, EDS., ELSEVIER (1988) P. 686

3. SCIENTIFIC BASIS FOR PREDICTIVE MODEL DEVELOPMENT

3.1 SPENT FUEL CLADDING FAILURE

3.1.1 EXPERIMENTAL PARAMETERS FOR FAILURE MODELS

3.1.2 FAILURE MODELS

3.2 SPENT FUEL OXIDATION

3.2.1 EXPERIMENTAL PARAMETERS FOR OXIDATION MODELS

3.2.2 OXIDATION MODELS

3.3 SPENT FUEL FISSION GAS RELEASE

3.3.1 EXPERIMENTAL PARAMETERS FOR FISSION GAS RELEASE

3.3.2 FISSION GAS RELEASE MODELS

3.4 SPENT FUEL DISSOLUTION

3.4.1 EXPERIMENTAL PARAMETERS FOR DISSOLUTION

3.4.1.1 DISSOLUTION RATES

3.4.1.2 SOLUBILITY LIMITS

3.4.1.3 SOLUBILITY LIMITING PHASES

3.4.2 DISSOLUTION MODELS

3.5 GLASS DISSOLUTION

3.5.1 EXPERIMENTAL PARAMETERS FOR GLASS DISSOLUTION

3.5.2 GLASS DISSOLUTION MODELS

3.6 OTHER RELEASE SOURCES OF RADIONUCLIDES

3.6.1 CRUD

3.6.2 HARDWARE

3.6.3 CLADDING

3.4.1.1 Dissolution Rates

Recent measurements on both UO_2 and spent fuel (SF) under comparable conditions have provided dissolution rates for UO_2 between 25°C and 85°C in waters of various composition and for SF on deionized water (DIW) at 25°C. These experiments were done in equilibrium with air. The results are shown in figures 1 and 2. The rate of dissolution of SF in DIW at 25°C is 1.2-1.7 x 10^{-12} g cm^{-2} sec^{-1} as compared to UO_2 in DIW at 25°C at ~5 x 10^{-12} g cm^{-2} sec^{-1}. Given the great variability in other reported values this is reasonable agreement. In fact, the observed dissolution rate for SF in 25°C is about the same as of UO_2 in (DIW + Ca + Si), a simulation of ground water.

The measured dissolution rates for UO_2 and spent fuel allow us to calculate actual times for dissolution. As is evident from figure 3, the overall dissolution rate is greatest at early time and approaches zero as t_∞ is approached; therefore, we have also calculated the total dissolution time extrapolated from the initial rate, t_∞*. These times calculated for the size distribution in Table I are given in Table II. The actual dissolution rates used are derived from the bottom curve in figure 1. The rate equation used is

$$G(t)\ (g\ cm^{-2}\ sec^{-1}) = 6.43 \times 10^{-9} \exp-\left(\frac{4740}{RT(K)}\right) \qquad (5)$$

A model for the dissolution is used in which the dissolution front propagates linearally in time, much like a recently published model for the advance of the oxidation front during oxidation of UO_2 and spent fuel. This implies that the particle geometry is retained.

Leider, H.R., et al. "Estimating the Time for Dissolution of Spent Fuel Exposed to Unlimited Water," LLNL Report UCRL-ID-107289, December, 1991. (See Section 2.1.3.5 for more complete discussion.)

We can describe the change in characteristic dimension of a SF particle (a sort of "radius"), X as follows:

$$X(t) = X_o - \left(\frac{G}{\rho}\right)t$$

where X(t) = the characteristic dimension as a function of time

X_0 = the original dimension (half of the actual size)

t = time

G = dissolution rate per unit area

ρ = density

The time for complete dissolution of a particle, of original size X_0, is then $t_\infty = \frac{X_o \rho}{G}$.

Table 1

Approximate Size (cm) $2X_0$)	Weight (Volume Fraction)
0.15	.02
0.25	.14
0.35	.29
0.50	.38
0.70	.17

Table II

Temperature (°C)	Dissolution Time (years)	
	t_∞*	t_∞
25	8.0×10^3	5.5×10^4
85	2.2×10^3	1.5×10^4

3. SCIENTIFIC BASIS FOR PREDICTIVE MODEL DEVELOPMENT

3.1 SPENT FUEL CLADDING FAILURE

3.1.1 EXPERIMENTAL PARAMETERS FOR FAILURE MODELS

3.1.2 FAILURE MODELS

3.2 SPENT FUEL OXIDATION

3.2.1 EXPERIMENTAL PARAMETERS FOR OXIDATION MODELS

3.2.2 OXIDATION MODELS

3.3 SPENT FUEL FISSION GAS RELEASE

3.3.1 EXPERIMENTAL PARAMETERS FOR FISSION GAS RELEASE

3.3.2 FISSION GAS RELEASE MODELS

3.4 SPENT FUEL DISSOLUTION

3.4.1 EXPERIMENTAL PARAMETERS FOR DISSOLUTION

3.4.1.1 DISSOLUTION RATES

3.4.1.2 SOLUBILITY LIMITS

3.4.1.3 SOLUBILITY LIMITING PHASES

3.4.2 DISSOLUTION MODELS

3.5 GLASS DISSOLUTION

3.5.1 EXPERIMENTAL PARAMETERS FOR GLASS DISSOLUTION

3.5.2 GLASS DISSOLUTION MODELS

3.6 OTHER RELEASE SOURCES OF RADIONUCLIDES

3.6.1 CRUD

3.6.2 HARDWARE

3.6.3 CLADDING

3.4.1.1 Dissolution Rates

Recent measurements on both UO_2 and spent fuel (SF) under comparable conditions have provided dissolution rates for UO_2 between 25°C and 85°C in waters of various composition and for SF on deionized water (DIW) at 25°C. These experiments were done in equilibrium with air. The results are shown in figures 1 and 2. The rate of dissolution of SF in DIW at 25°C is 1.2-1.7 x 10^{-12} g cm^{-2} sec^{-1} as compared to UO_2 in DIW at 25°C at ~5 x 10^{-12} g cm^{-2} sec^{-1}. Given the great variability in other reported values this is reasonable agreement. In fact, the observed dissolution rate for SF in 25°C is about the same as of UO_2 in (DIW + Ca + Si), a simulation of ground water.

The measured dissolution rates for UO_2 and spent fuel allow us to calculate actual times for dissolution. As is evident from figure 3, the overall dissolution rate is greatest at early time and approaches zero as t_∞ is approached; therefore, we have also calculated the total dissolution time extrapolated from the initial rate, t_∞^*. These times calculated for the size distribution in Table I are given in Table II. The actual dissolution rates used are derived from the bottom curve in figure 1. The rate equation used is

$$G(t)\ (g\ cm^{-2}\ sec^{-1}) = 6.43 \times 10^{-9} \exp-\left(\frac{4740}{RT(K)}\right) \qquad (5)$$

A model for the dissolution is used in which the dissolution front propagates linearally in time, much like a recently published model for the advance of the oxidation front during oxidation of UO_2 and spent fuel. This implies that the particle geometry is retained.

Leider, H.R., et al. "Estimating the Time for Dissolution of Spent Fuel Exposed to Unlimited Water," LLNL Report UCRL-ID-107289, December, 1991. (See Section 2.1.3.5 for more complete discussion.)

We can describe the change in characteristic dimension of a SF particle (a sort of "radius"), X as follows:

$$X(t) = X_o - \left(\frac{G}{\rho}\right)t$$

where X(t) = the characteristic dimension as a function of time

X_0 = the original dimension (half of the actual size)

t = time

G = dissolution rate per unit area

ρ = density

The time for complete dissolution of a particle, of original size X_0, is then $t_\infty = \frac{X_o \rho}{G}$.

Table 1

Approximate Size (cm) $2X_0$)	Weight (Volume Fraction)
0.15	.02
0.25	.14
0.35	.29
0.50	.38
0.70	.17

Table II

Temperature (°C)	Dissolution Time (years)	
	t_∞*	t_∞
25	8.0×10^3	5.5×10^4
85	2.2×10^3	1.5×10^4

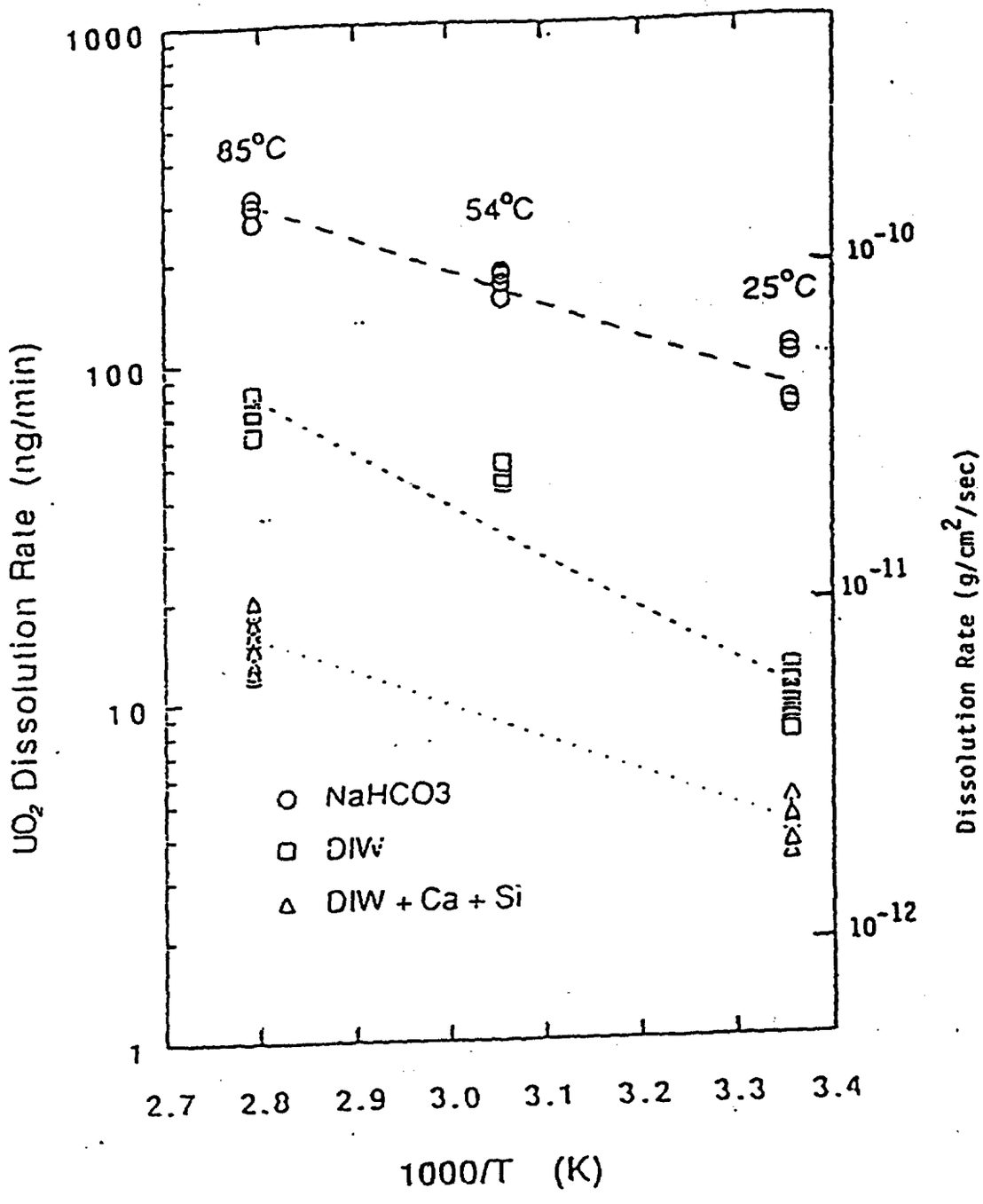

Figure 1

Gray, W. and Wilson, C., "Effects of Water Composition and Temperature on the Dissolution Rate of UO_2," presented at 1990 Spent Fuel Workshop, Gull Harbor, Manitoba, Canada (1990) NNA.910821.0008.

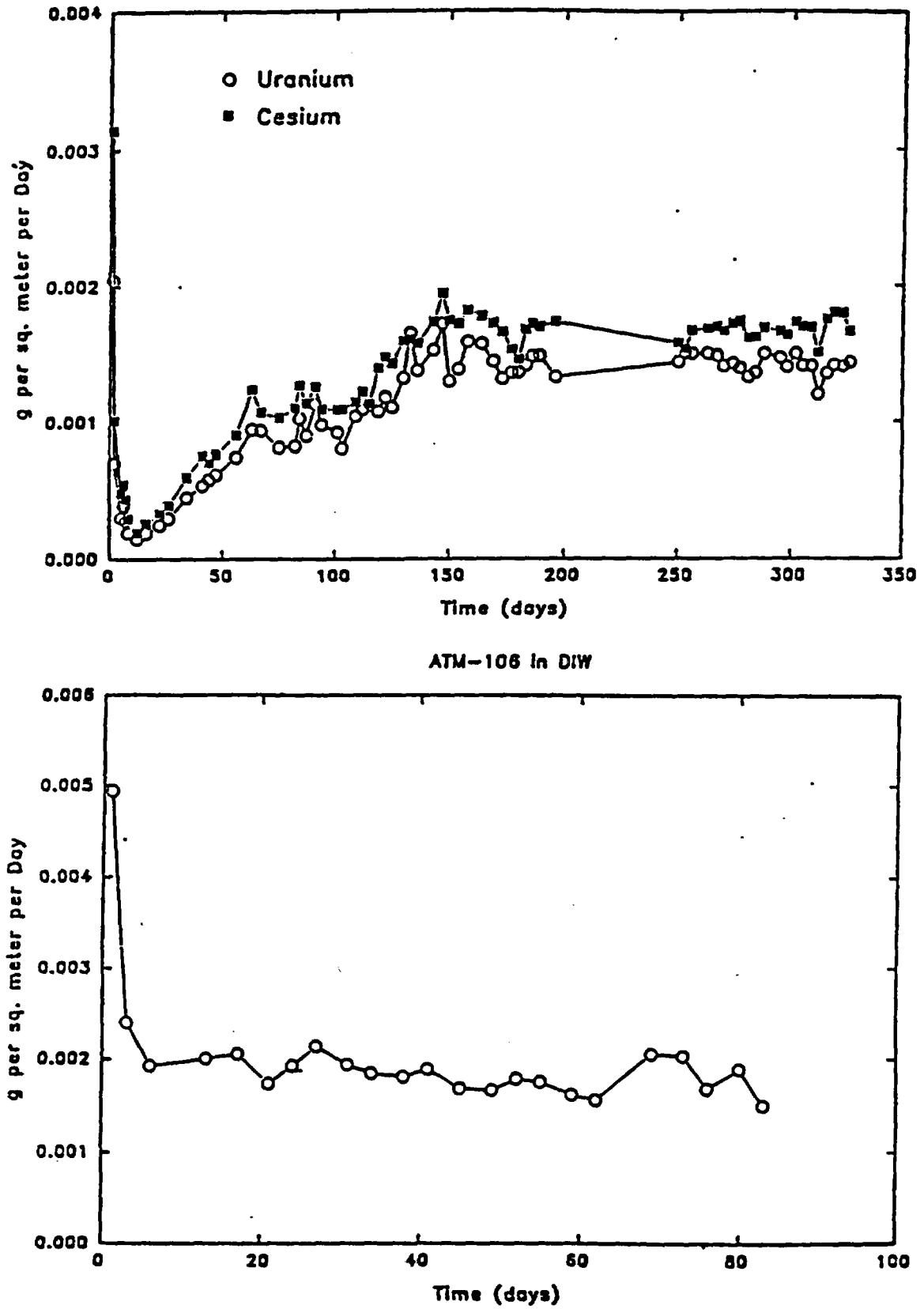

Figure 2

Gray, W. and Wilson, C., "Spent Fuel Grain Boundary Inventory and Testing the Congruency of UO_2 Matrix Dissolution of Spent Fuel," presented at 1990 Spent Fuel Workshop, Gull Harbor, Manitoba, Canada (1990) NNA.910821.0009.

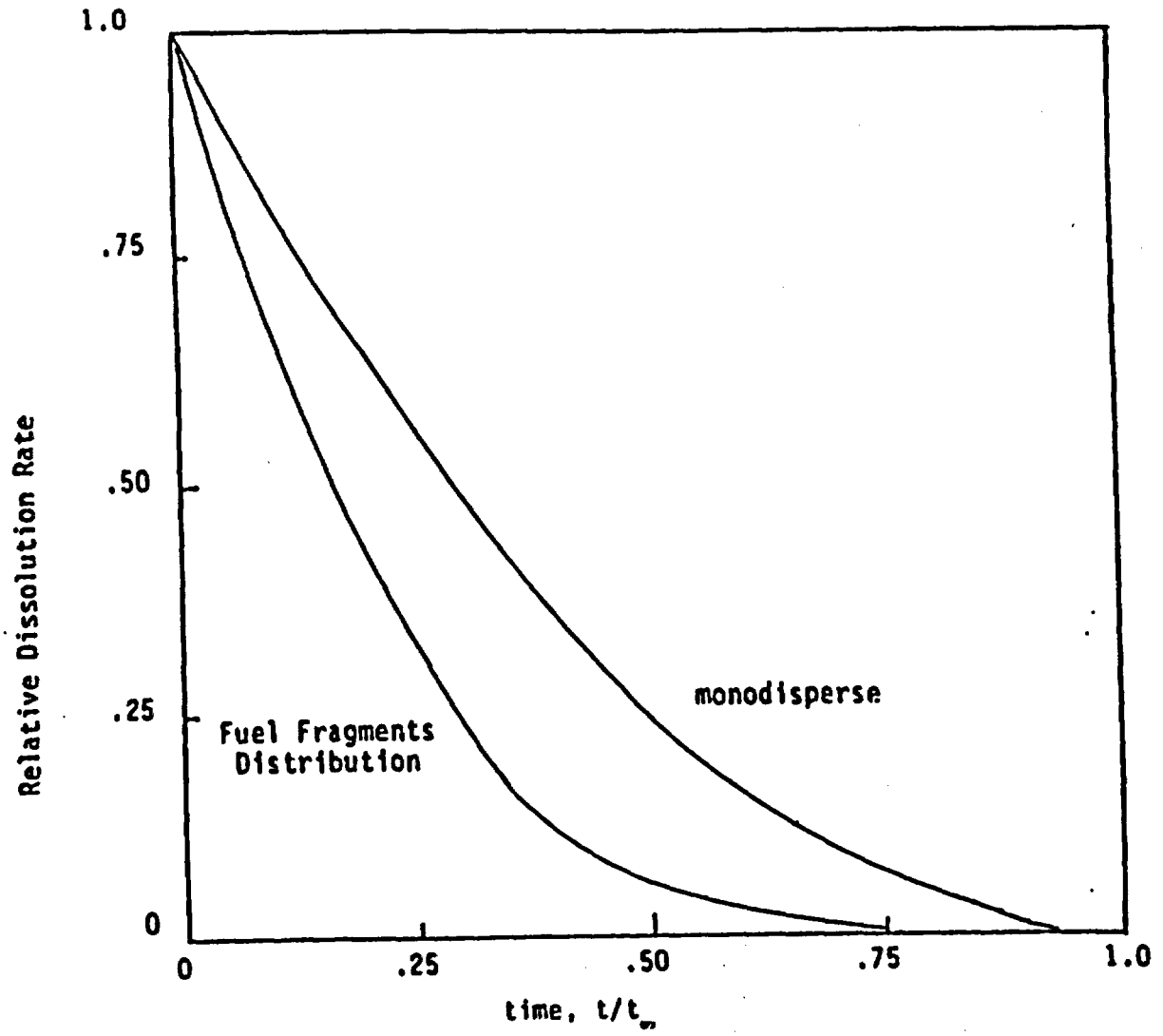

Figure 4

Figure 3. Dissolution Rate for Set of Fragments

Leider, H.R., S.N. Nguyen, R.B. Stout, H.C. Weed, "Estimating the Time for Dissolution of Spent Fuel Exposed to Unlimited Water," LLNL Report UCRL-ID-107289, Dec. 1991.

TABLE 3.6. Particle-Size Distribution of Fuel Rods from NRU LOCA Test MT-3 (Rausch 1984)

Rod Section	Total Weight of Fuel, g	% of Total Sample Weight Retained on Each Sieve Size: No. 3-1/2 (5.6 mm or 0.233 in.)	No. 5 (4.00 mm or 0.157 in.)	No. 7 (2.80 mm or 0.111 in.)	No. 10 (2.00 mm or 0.0787 in.)	No. 18 (1.00 mm or 0.0394 in.)	No. 50 (300 μm or 0.0117 in.)	Receiver (<300 μm or <0.0117 in.)
2DS (1)[a]	243.753	15.98	69.84	12.69	0.71	0.23	0.25	0.31
3BS (1)	225.212	19.88	65.57	13.35	0.71	0.08	0.19	0.22
3DS (2)	253.991	18.66	61.03	15.83	2.20	1.13	0.73	0.42
3ES (3)	254.497	18.88	58.28	20.2	1.53	0.44	0.27	0.31
5CS (3)	270.867	28.49	54.95	14.92	0.74	0.38	0.24	0.30
5DS (3)	246.704	20.13	64.58	13.61	0.64	0.31	0.32	0.42
3BSA (3)	136.598	8.43	70.17	18.97	1.22	0.37	0.33	0.52
3BSB (11)	146.223	49.83	45.00	4.52	0	0.07	0.26	0.33

(a) Number in parentheses indicates the number of whole pellets before size analysis.

TABLE 3.7. Particle-Size Distribution of Fuel Fragments from H. B. Robinson Spent Fuel with a Burnup of 28 MWd/kgM (Katayama, Bradley and Harvey 1980)

Sieve Number	Sieve Opening, mm	Weight, g	Fraction Retained
3	6.73	0	0
4	4.73	192.883	0.1007
5	4.00	634.765	0.3331
10	2.00	1031.170	0.5384
20	0.841	35.205	0.01838
40	0.420	11.242	0.005869
60	0.250	4.979	0.002599
80	0.177	1.424	0.0007434
100	0.149	1.042	0.0005440
140	0.105	1.204	0.0006286
200	0.074	0.769	0.0004015
200	0.074	0.737	0.0003848

3. SCIENTIFIC BASIS FOR PREDICTIVE MODEL DEVELOPMENT

3.1 SPENT FUEL CLADDING FAILURE

3.1.1 EXPERIMENTAL PARAMETERS FOR FAILURE MODELS

3.1.2 FAILURE MODELS

3.2 SPENT FUEL OXIDATION

3.2.1 EXPERIMENTAL PARAMETERS FOR OXIDATION MODELS

3.2.2 OXIDATION MODELS

3.3 SPENT FUEL FISSION GAS RELEASE

3.3.1 EXPERIMENTAL PARAMETERS FOR FISSION GAS RELEASE

3.3.2 FISSION GAS RELEASE MODELS

3.4 SPENT FUEL DISSOLUTION

3.4.1 EXPERIMENTAL PARAMETERS FOR DISSOLUTION

3.4.1.1 DISSOLUTION RATES

3.4.1.2 SOLUBILITY LIMITS

3.4.1.3 SOLUBILITY LIMITING PHASES

3.4.2 DISSOLUTION MODELS

3.5 GLASS DISSOLUTION

3.5.1 EXPERIMENTAL PARAMETERS FOR GLASS DISSOLUTION

3.5.2 GLASS DISSOLUTION MODELS

3.6 OTHER RELEASE SOURCES OF RADIONUCLIDES

3.6.1 CRUD

3.6.2 HARDWARE

3.6.3 CLADDING

3.4.1.2. Solubility Limits

Attached are solubility data developed from two reports:

1) C.N. Wilson, "Results from Cycles 1 and 2 of NNWSI Series 2 Dissolution Tests,": HEDL-TME85-22, May, 1987.

2) C. N. Wilson, "Results from the NNWSI Series 3 Spent Fuel Dissolution Tests," PNL-7170, June, 1990.

The pertinent solubility data taken after "steady-state" was reached are given in Table 1. (See also Section 2.1.3.5 for additional explanation. In cases where several values from different samples with different geometrics and different burnup histories were shown, the most conservative upper value is indicated. Since we don't know the cause of the scatter, it is prudent to assume the worst case, pending a better understanding of the spread in the steady-state solubilities. Where filtered and unfiltered values were available, the filtered data were used because solubility is the information desired.

For slow flow of water over the spent fuel, the solubility can be used to determine the mass of each radionuclide dissolved as a function of time. Given solubilities, C, a flow rate of water contacting the spent fuel, Φ, and a time, t, over which dissolution occurs, the total amount of any nuclide, i, dissolved and transported, M_i, is given by $M_i = C_i \Phi t$.

Table 1. Solubility Data, C_i

Species	Upper Limit Steady-State Concentration (µg/ml)	
	25°C	85°C
U	≤ 5	≤ 0.5
$^{239+240}Pu$	$\leq 5 \times 10^{-3}$	$\leq 6 \times 10^{-5}$
^{241}Am	$\leq 3 \times 10^{-4}$	$\leq 1.5 \times 10^{-7}$
^{244}Cm	$\leq 1.2 \times 10^{-5}$	$\leq 2.4 \times 10^{-9}$
^{237}Np	$\leq 4 \times 10^{-4}$	$\leq 1.4 \times 10^{-3}$

3. SCIENTIFIC BASIS FOR PREDICTIVE MODEL DEVELOPMENT

3.1 SPENT FUEL CLADDING FAILURE

3.1.1 EXPERIMENTAL PARAMETERS FOR FAILURE MODELS

3.1.2 FAILURE MODELS

3.2 SPENT FUEL OXIDATION

3.2.1 EXPERIMENTAL PARAMETERS FOR OXIDATION MODELS

3.2.2 OXIDATION MODELS

3.3 SPENT FUEL FISSION GAS RELEASE

3.3.1 EXPERIMENTAL PARAMETERS FOR FISSION GAS RELEASE

3.3.2 FISSION GAS RELEASE MODELS

3.4 SPENT FUEL DISSOLUTION

3.4.1 EXPERIMENTAL PARAMETERS FOR DISSOLUTION

3.4.1.1 DISSOLUTION RATES

3.4.1.2 SOLUBILITY LIMITS

3.4.1.3 SOLUBILITY LIMITING PHASES

3.4.2 DISSOLUTION MODELS

3.5 GLASS DISSOLUTION

3.5.1 EXPERIMENTAL PARAMETERS FOR GLASS DISSOLUTION

3.5.2 GLASS DISSOLUTION MODELS

3.6 OTHER RELEASE SOURCES OF RADIONUCLIDES

3.6.1 CRUD

3.6.2 HARDWARE

3.6.3 CLADDING

3.4.1.3 Solubility Controls on Radionuclide Concentrations in Solution: Preliminary Results for U, Np, Pu, and Am

Radionuclide concentrations in solution are limited by the precipitation of solids. This is a presentation of calculations of the dissolved concentrations of the radionuclides U, Np, Pu, and Am in equilibrium with potential radionuclide-bearing solids in J-13 water at 25 C. Elemental concentrations vary as a function of solution composition, Eh and pH, among other parameters. To illustrate the potential impact of such variations, the dependance of radionuclide concentrations is solution as well as the identity of the radionuclide-bearing precipitate are calculated as a function of pH. These calculations can be used as a first approximation to estimate potential ranges in radionuclide concentrations in solution.

The chemical composition of J-13 water used in the calculations is given in Table 1. The redox potential of J-13 water was determined by assuming equilibrium with the atmosphere at an oxygen partial pressure of 0.2 bars. At a pH of 7.6, this corresponds to an Eh of 0.77 volts.

Geochemical modeling codes EQ3NR ver. 3245R123, and EQ6 ver. 3245R118, supported by EQLIB version 3245R152 and the thermodynamic data base DATA0.com.R6, were used to make the calculations. All calculations were carried out at 25°C.

Table 1.

J-13 Water		
Element	Concentration	
	mg/l	molality (moles/kg)
Li	0.042	6.053E-6
Na	43.9	1.909E-3
K	5.11	1.307E-4
Ca	12.5	3.119E-4
Mg	1.92	7.897E-5
Sr	0.035	3.995E-7
Al	0.012	4.447E-7
Fe	0.006	1.074E-7
Si	27.0	9.613E-4
NO_3	9.6	1.548E-4
F	2.2	1.158E-4
Cl	6.9	1.946E-4
HCO_3	125.3	2.054E-3
SO_4	18.7	1.947E-4
pH	7.6	
* average J-13 water analysis of LLNL laboratory supply (Table 1, Delany, 1985)		

Table 2.

U		
Solid	Concentration	
	mg/l	molality (moles/kg)
Haiweeite $Ca(UO_2)_2Si_6O_{15}\cdot 5H_2O$	0.1641E-3	0.6893E-9
Soddyite $(UO_2)_2SiO_4\cdot 2H_2O$	0.015	0.6096E-7
Sklodowskite $Mg(H_3O)_2(UO_2)_2-(SiO_4)_2\cdot 4H_2O$	11.05	0.4642E-4
$CaUO_4$	12.59	0.5289E-4
Schoepite $UO_3\cdot 2H_2O$	38.90	0.1634E-3
$UO_2(OH)_2$(beta)	56.73	0.2383E-3
Uranophane $Ca(UO_2)_2(SiO_3)_2(OH)_2$	142.48	0.5986E-03

Table 3.

Np		
Solid	Concentration	
	mg/l	molality (moles/kg)
NpO_2	0.59	0.2468E-5
$NpO_2(OH)$(am)	129.39	0.5459E-3
$NaNpO_2CO_3\cdot 3.5H_2O$	139.99	0.5906E-3
am = amorphous		

Table 4.

Pu		
Solid	Concentration	
	mg/l	molality (moles/kg)
PuO_2	0.39E-6	0.1612E-11
$PuO_2(OH)_2$	0.015	0.6204E-7
$Pu(OH)_4$	27.97	0.1146E-3

Table 5.

Am		
Solid	Concentration	
	mg/l	molality (moles/kg)
$AmOHCO_3$	0.0041	0.1696E-7
$Am(OH)_3$	8.42	0.3464E-4
$Am(OH)_3$(am)	158.66	0.6529E-3

C.J. Bruton, *Solubility Controls on Radionuclide Concentrations in Solution: Preliminary Results for U, Np, Pu, and Am*, LLNL draft report, November, 1990.

TABLE II
Phases Identified on Reacted UO_2 Surface

Phase	Formula	Appearance
Schoepite	$UO_3 \cdot 2H_2O$	Dark yellow crystals
Dehydrated Schoepite	$UO_3 \cdot 0.8H_2O$	Yellow crystals with reflective face
Compreignacite	$K_2U_6O_{19} \cdot 11H_2O$	Yellow crystals
Uranophane	$Ca(UO_2)_2(SiO_3)_2(OH)_2 \cdot 5H_2O$	Fine white needles
Boltwoodite	$K(H_3O)UO_2(SiO_4) \cdot nH_2O$	Yellow crystals
Sklodowskite	$Mg(UO_2)_2(SiO_3OH)_2 \cdot 5H_2O$	Fine needles
Becquerelite	$CaU_6O_{19} \cdot 10H_2O$	Dark yellow crystals
Fluoropolymer	Not determined	White feathers

J.K. Bates, *Identification of Secondary Phases Formed During Unsaturated Reaction of UO_2 with EJ-13 Water*, Materials Research Society Symposium proceedings 176, 499 (1990).

3. SCIENTIFIC BASIS FOR PREDICTIVE MODEL DEVELOPMENT

3.1 SPENT FUEL CLADDING FAILURE

3.1.1 EXPERIMENTAL PARAMETERS FOR FAILURE MODELS

3.1.2 FAILURE MODELS

3.2 SPENT FUEL OXIDATION

3.2.1 EXPERIMENTAL PARAMETERS FOR OXIDATION MODELS

3.2.2 OXIDATION MODELS

3.3 SPENT FUEL FISSION GAS RELEASE

3.3.1 EXPERIMENTAL PARAMETERS FOR FISSION GAS RELEASE

3.3.2 FISSION GAS RELEASE MODELS

3.4 SPENT FUEL DISSOLUTION

3.4.1 EXPERIMENTAL PARAMETERS FOR DISSOLUTION

3.4.1.1 DISSOLUTION RATES

3.4.1.2 SOLUBILITY LIMITS

3.4.1.3 SOLUBILITY LIMITING PHASES

3.4.2 DISSOLUTION MODELS

3.5 GLASS DISSOLUTION

3.5.1 EXPERIMENTAL PARAMETERS FOR GLASS DISSOLUTION

3.5.2 GLASS DISSOLUTION MODELS

3.6 OTHER RELEASE SOURCES OF RADIONUCLIDES

3.6.1 CRUD

3.6.2 HARDWARE

3.6.3 CLADDING

Release rate response—depends on inventory, dissolution front motion, surface area, and solubility

For the case of highly soluble species (CS, I, Sr, Tc, etc.):

Inventory ~ amount of a radionuclide species per unit mass

Dissolution response ~ material removal (mass) per unit area per unit time

Surface area ~ area of fragments size distribution decreases as fragments dissolve over time.

Release rate ~ [inventory] • [dissolution] • [area]

Release rate spent fuel ~ [gap inventory] • [gap dissolution] • [gap area]

$$+\left[\begin{matrix}\text{grain boundary}\\ \text{inventory}\end{matrix}\right]\cdot\left[\begin{matrix}\text{grain boundary}\\ \text{dissolution}\end{matrix}\right]\cdot\left[\begin{matrix}\text{grain boundary}\\ \text{area}\end{matrix}\right]$$

$$+\left[\begin{matrix}\text{grain volume}\\ \text{inventory}\end{matrix}\right]\cdot\left[\begin{matrix}\text{grain volume}\\ \text{dissolution}\end{matrix}\right]\cdot\left[\begin{matrix}\text{grain volume}\\ \text{area}\end{matrix}\right]$$

Oxidation front and dissolution front analog

Grain boundary/volume oxidation front motion through a pellet fragment has geometrical and model development similarities to an idealized dissolution surface motion progressing into a fragment.

This means that model development concepts for oxidation kinetics can be also applied to dissolution response for a distribution of fragments.

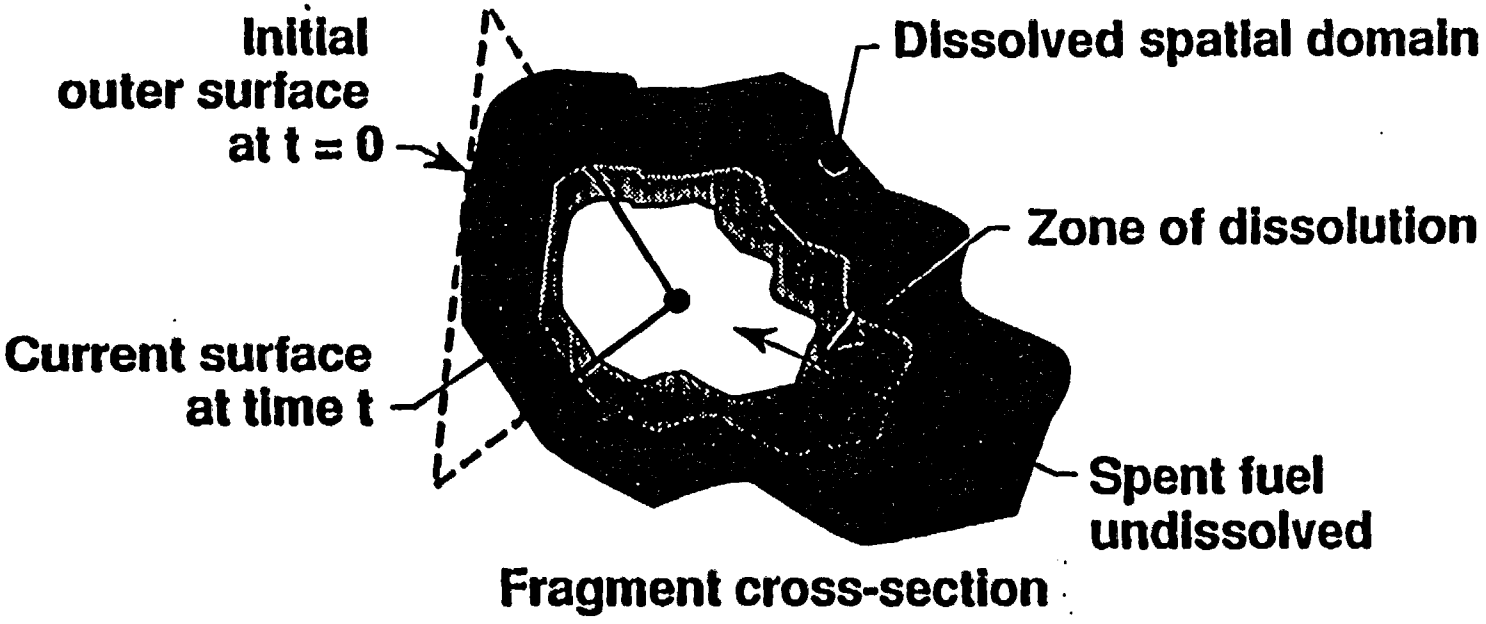

Fragment pyramidal volume dissolution front

Pyramidal volume in a dissolving fragment and its associated physical attributes.

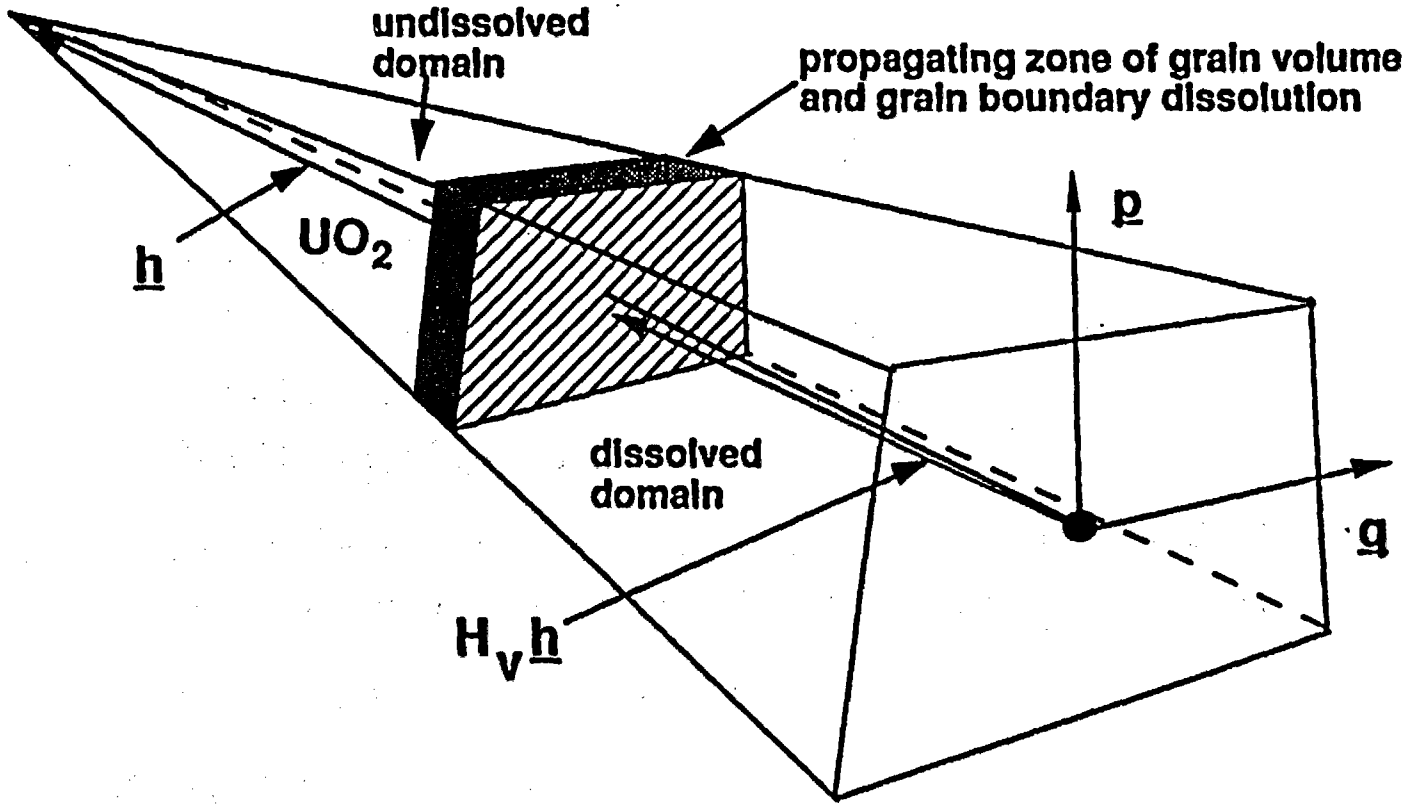

Dissolution rate on a grain volume and grain boundary surface

Fragment surface p x q with grain statistical density G(g).

- I_{VK} – Grain volume inventory species K^{th} radionuclide.
- $\dot{H}_V h$ – Dissolution rate of grain volumes exposed on surface p x q of fragment.
- I_{BK} – Grain boundary inventory species K^{th} radionuclide.
- $\dot{H}_B h$ – Dissolution rate of grain boundary exposed on surface p x q of fragment.

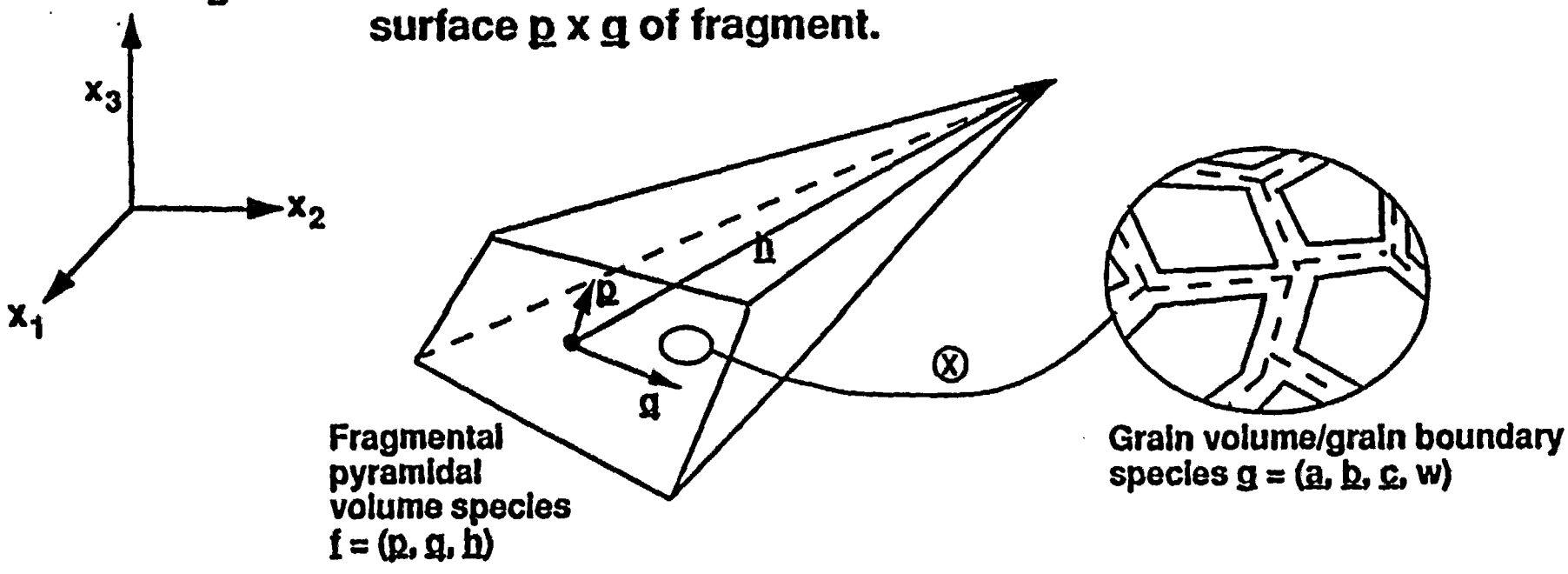

Statistical representation of grain and fragment geometrical influences on dissolution rate

$$\dot{D}_K(\underline{x}, t, f)\, df\, d\underline{x} = I_{VK}\dot{H}_V [h_\ell e_{\ell jk} p_j q_k - \int_{\{g\}} (h_\ell e_{\ell mn} wc_m e_{ijk} a_j b_k p_i q_n$$

$$+ h_\ell e_{\ell mn} wc_n e_{ijk} a_j b_k q_i p_m)\, G(\underline{x}, t, g)\, dg]\, (1-H_V)^2\, F(\underline{x}, t, f)\, df\, d\underline{x} +$$

$$I_{BK}\dot{H}_B \int_{\{g\}} (e_{\ell mn} wc_m e_{ijk} a_j b_k p_i q_n h_\ell + e_{\ell mn} wc_n e_{ijk} a_j b_k q_i p_m h_\ell$$

$$+ e_{jin} wc_j e_{\ell km} a_k b_m p_i q_n h_\ell)\, G(\underline{x}, t, g)\, dg\, df\, (1-H_B)^2\, F(\underline{x}, t, f)\, df\, d\underline{x}$$

3. SCIENTIFIC BASIS FOR PREDICTIVE MODEL DEVELOPMENT

3.1 SPENT FUEL CLADDING FAILURE

3.1.1 EXPERIMENTAL PARAMETERS FOR FAILURE MODELS

3.1.2 FAILURE MODELS

3.2 SPENT FUEL OXIDATION

3.2.1 EXPERIMENTAL PARAMETERS FOR OXIDATION MODELS

3.2.2 OXIDATION MODELS

3.3 SPENT FUEL FISSION GAS RELEASE

3.3.1 EXPERIMENTAL PARAMETERS FOR FISSION GAS RELEASE

3.3.2 FISSION GAS RELEASE MODELS

3.4 SPENT FUEL DISSOLUTION

3.4.1 EXPERIMENTAL PARAMETERS FOR DISSOLUTION

3.4.1.1 DISSOLUTION RATES

3.4.1.2 SOLUBILITY LIMITS

3.4.1.3 SOLUBILITY LIMITING PHASES

3.4.2 DISSOLUTION MODELS

3.5 GLASS DISSOLUTION

3.5.1 EXPERIMENTAL PARAMETERS FOR GLASS DISSOLUTION

3.5.2 GLASS DISSOLUTION MODELS

3.6 OTHER RELEASE SOURCES OF RADIONUCLIDES

3.6.1 CRUD

3.6.2 HARDWARE

3.6.3 CLADDING

3.5 Glass Dissolution

Hydrolysis of Si-O bonds by water initiates glass dissolution and causes the formation of a hydrous reacted layer. Elements released during hydrolysis diffuse outwards into solution while the hydrous altered layer re-polymerizes. The overall rate of reaction appears to be controlled by the rate of dissolution of the re-polymerized hydrous surface layer. Secondary phases consisted of elements present in the leachate and elements released from the glass precipitate from solution or segregate from amorphous material on the glass surface. These alteration layers do not appear to provide a transport barrier.

Current models for glass dissolution combine a rate equation derived from irreversible thermodynamics with reaction path computer codes that account for solution speciation and precipitation of solids. Although these models account for the major features observed in short-term dissolution tests of waste glasses, there remain uncertainties when extrapolating these models to long time periods. The most critical of these uncertainties is that of the nature of the chemical process which determines the long-term dissolution rate of the glass.

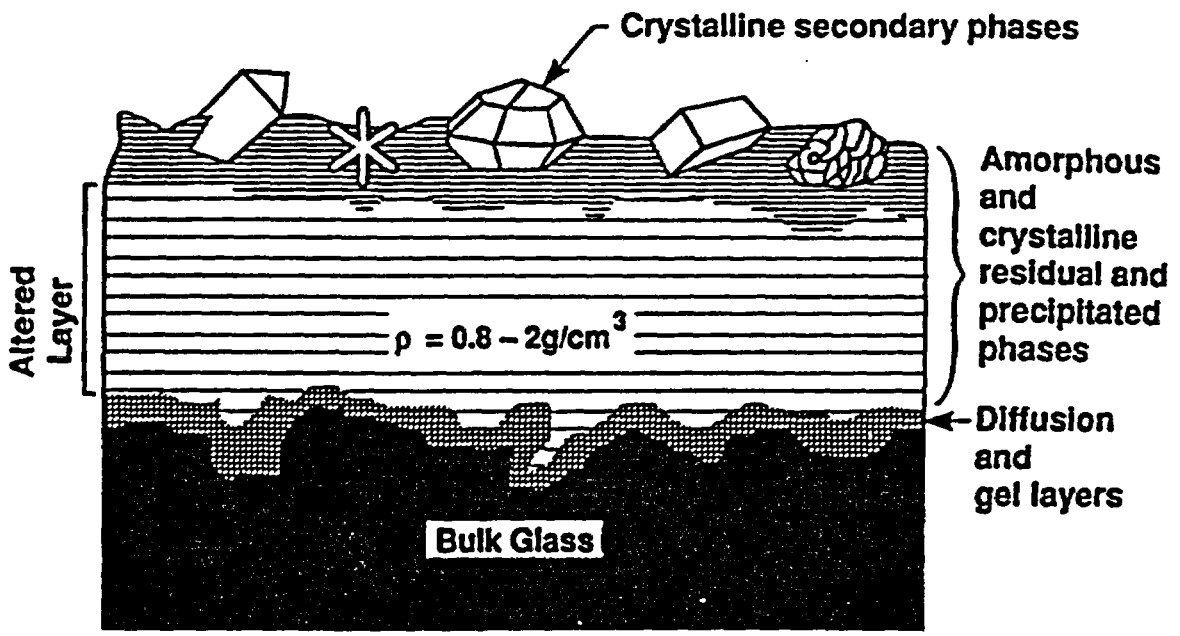

Features observed on reacted glass surfaces.

3. SCIENTIFIC BASIS FOR PREDICTIVE MODEL DEVELOPMENT

3.1 SPENT FUEL CLADDING FAILURE

3.1.1 EXPERIMENTAL PARAMETERS FOR FAILURE MODELS

3.1.2 FAILURE MODELS

3.2 SPENT FUEL OXIDATION

3.2.1 EXPERIMENTAL PARAMETERS FOR OXIDATION MODELS

3.2.2 OXIDATION MODELS

3.3 SPENT FUEL FISSION GAS RELEASE

3.3.1 EXPERIMENTAL PARAMETERS FOR FISSION GAS RELEASE

3.3.2 FISSION GAS RELEASE MODELS

3.4 SPENT FUEL DISSOLUTION

3.4.1 EXPERIMENTAL PARAMETERS FOR DISSOLUTION

3.4.1.1 DISSOLUTION RATES

3.4.1.2 SOLUBILITY LIMITS

3.4.1.3 SOLUBILITY LIMITING PHASES

3.4.2 DISSOLUTION MODELS

3.5 GLASS DISSOLUTION

3.5.1 EXPERIMENTAL PARAMETERS FOR GLASS DISSOLUTION

3.5.2 GLASS DISSOLUTION MODELS

3.6 OTHER RELEASE SOURCES OF RADIONUCLIDES

3.6.1 CRUD

3.6.2 HARDWARE

3.6.3 CLADDING

Table I. Compositions in weight percent of several nuclear waste glasses and basalt glass. SRL-165, JSS-A, PNL 76-68, SRL-131, basaltic glass.

	SRL-165-U	JSS-A	PNL 76-68	SRL-131	basaltic glass
Al_2O_3	4.08	4.9	0.7	3.1	14
B_2O_3	6.76	14.4	9.3	9.9	–
BaO	0.06	–	0.5	0.1	–
CaO	1.62	4.0	2.4	1.0	11
CeO_2	–	0.9	0.9	0.2	–
Cs_2O	0.07	1.4	0.9	0.3	–
Fe_2O_3	11.3	2.9	9.3	14.3	4
FeO	0.35	–	–	–	8
K_2O	–	–	–	0.1	0.2
La_2O_3	–	0.9	4.1	0.3	–
Li_2O	4.18	2.0	–	3.9	–
MgO	0.70	–	–	1.2	7
MnO	2.27	–	.04	4.2	.2
MoO_3	–	1.7	1.9	–	–
Na_2O	10.8	9.8	13.9	14.8	2.5
NiO	0.85	–	–	1.5	–
SiO_2	52.8	45.2	41.5	38.6	51
SrO	.11	–	0.4	0.1	–
TiO_2	0.14	–	3.0	0.8	2
ZnO	0.04	2.5	4.6	–	–
ZrO_2	0.66	2.6	1.8	0.3	–
U_3O_8	0.96	0.5	–	1.6	–
P_2O_5	0.29	–	0.7	0.1	0.1

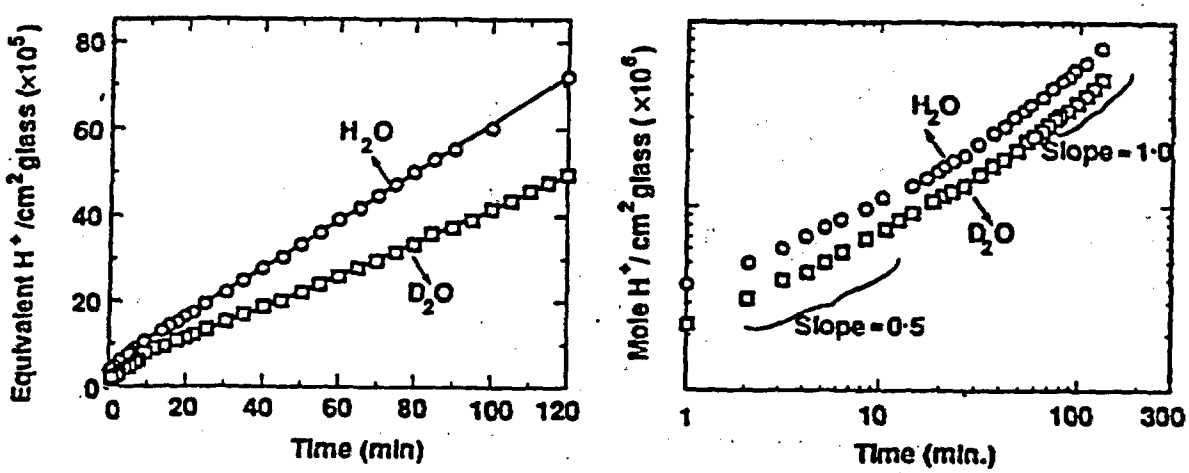

(a) Log plot of extent of reaction (measured as cumulative hydrogen consumption) for leaching of sodium silicate glass in water and D_2O. The separation in the leaching curves remained constant through both stages of reaction, the curved and linear parts of the release curves shown in (b), indicating no change in rate-controlling mechanism throughout the reaction

W.L. Bourcier, "Overview of Chemical Modeling of Nuclear Waste Glass Dissolution," UCRL-JC-104531 preprint, Nov. 1990. Prepared for presentation at the Materials Research Society 1990 Fall Meeting, Boston, MA.

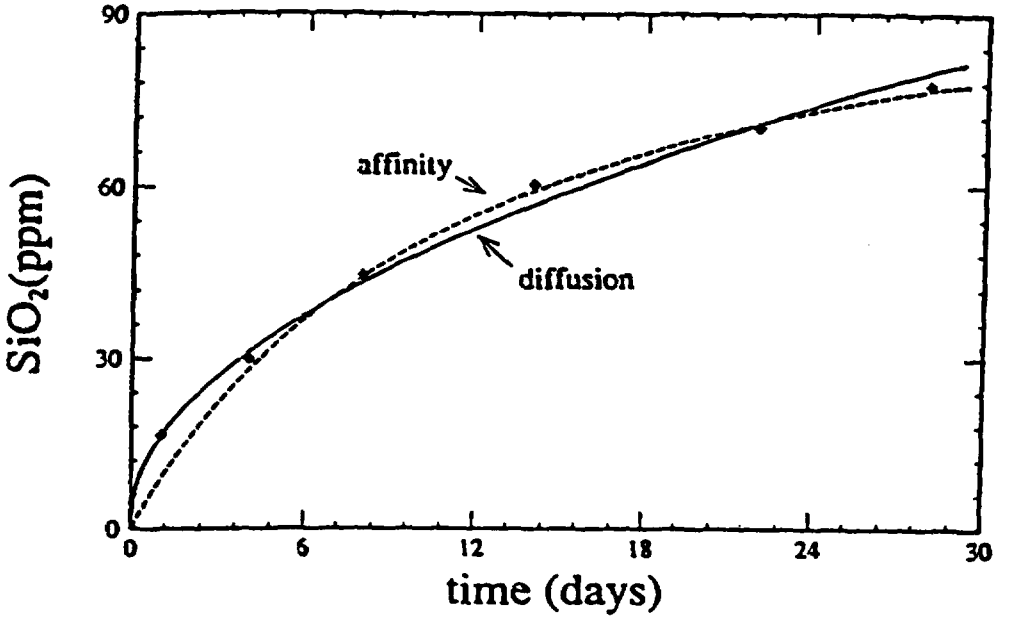

Cumulative release of silica from SRL-165 glass leached in 0.003 molal sodium bicarbonate (solid diamonds). Curves are regressed on data using equations for diffusion (rate = $A + Bt^{1/2}$ and surface affinity control (rate = $Ak_f(1-Q/K)$), where A and B are fitting parameters.

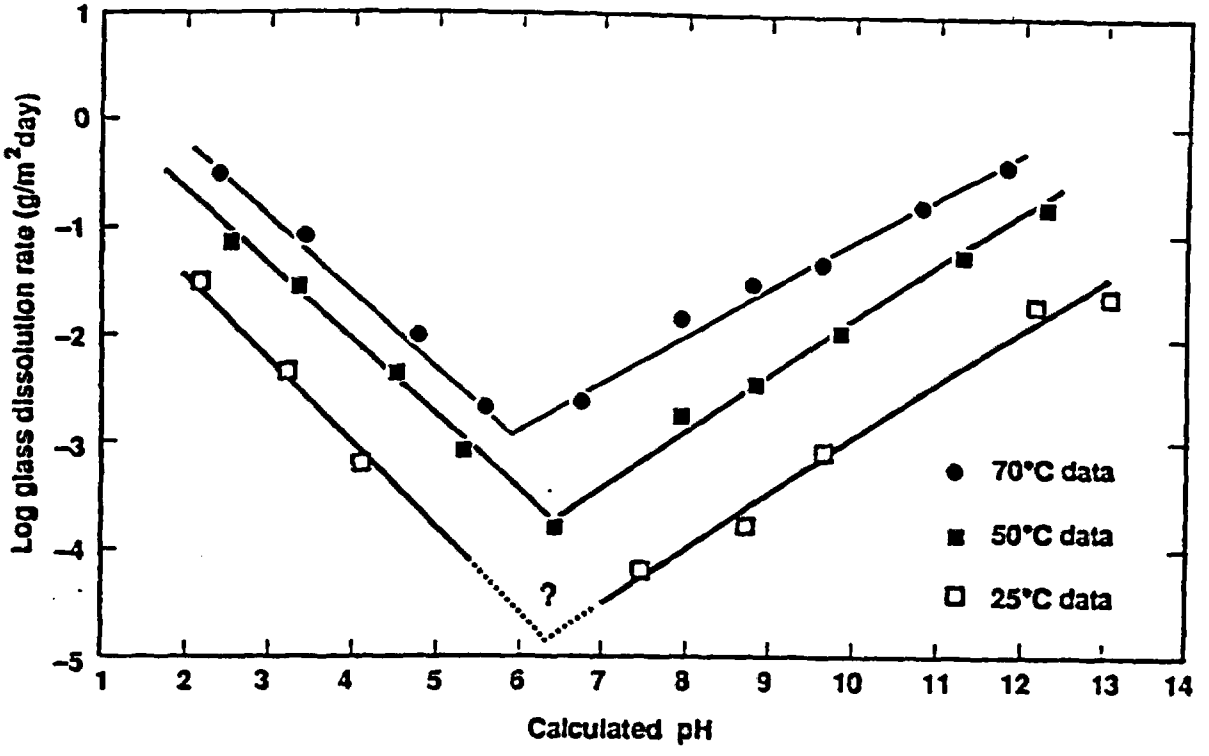

*p*H dependence of dissolution rate of Na-Ca-Al-B-Si glass determined from flow-through constant *p*H dissolution tests

W.L. Bourcier, "Overview of Chemical Modeling of Nuclear Waste Glass Dissolution," UCRL-JC-104531 preprint, Nov. 1990. Prepared for presentation at the Materials Research Society 1990 Fall Meeting, Boston, MA.

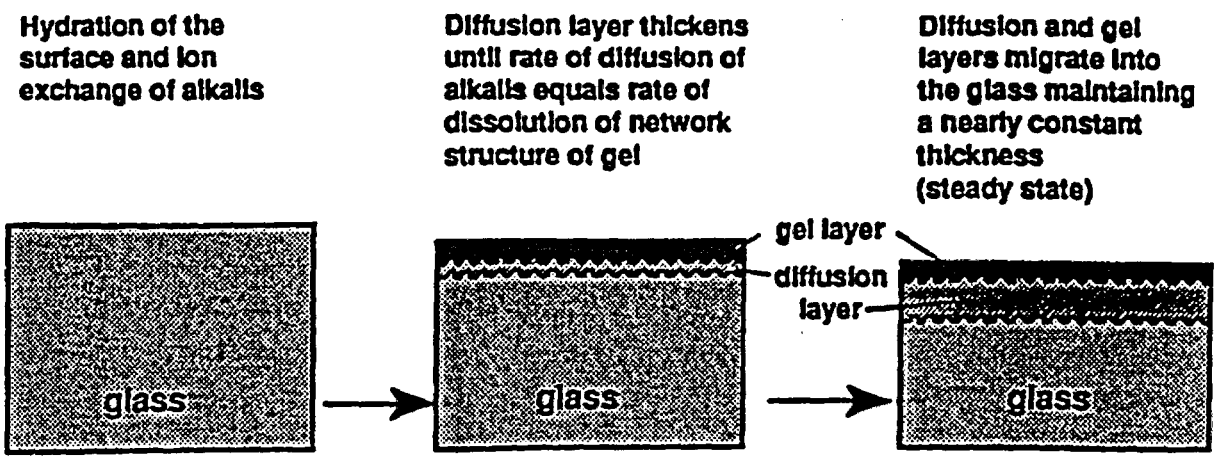

Schematic diagram showing evolution of glass alteration layers terminating with a steady state condition where the thickness of the diffusion layer remains constant.

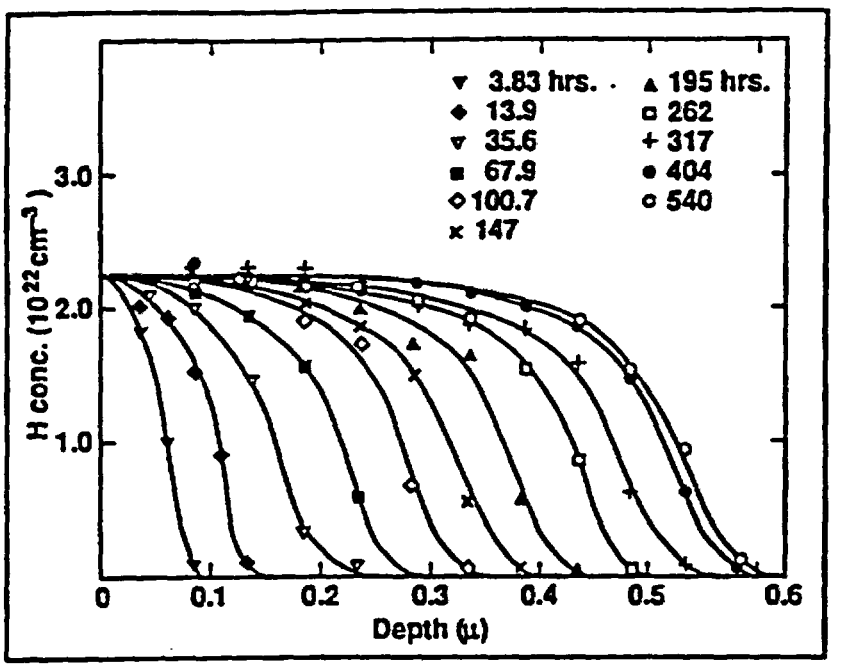

Hydrogen depth profiles in soda-lime glass hydrated in water at 90°C for times up to 540 hours. Steady state is indicated by unchanging profile over last 100 hours.

W.L. Bourcier, "Overview of Chemical Modeling of Nuclear Waste Glass Dissolution," UCRL-JC-104531 preprint, Nov. 1990. Prepared for presentation at the Materials Research Society 1990 Fall Meeting, Boston, MA.

3. SCIENTIFIC BASIS FOR PREDICTIVE MODEL DEVELOPMENT

3.1 SPENT FUEL CLADDING FAILURE

3.1.1 EXPERIMENTAL PARAMETERS FOR FAILURE MODELS

3.1.2 FAILURE MODELS

3.2 SPENT FUEL OXIDATION

3.2.1 EXPERIMENTAL PARAMETERS FOR OXIDATION MODELS

3.2.2 OXIDATION MODELS

3.3 SPENT FUEL FISSION GAS RELEASE

3.3.1 EXPERIMENTAL PARAMETERS FOR FISSION GAS RELEASE

3.3.2 FISSION GAS RELEASE MODELS

3.4 SPENT FUEL DISSOLUTION

3.4.1 EXPERIMENTAL PARAMETERS FOR DISSOLUTION

3.4.1.1 DISSOLUTION RATES

3.4.1.2 SOLUBILITY LIMITS

3.4.1.3 SOLUBILITY LIMITING PHASES

3.4.2 DISSOLUTION MODELS

3.5 GLASS DISSOLUTION

3.5.1 EXPERIMENTAL PARAMETERS FOR GLASS DISSOLUTION

3.5.2 GLASS DISSOLUTION MODELS

3.6 OTHER RELEASE SOURCES OF RADIONUCLIDES

3.6.1 CRUD

3.6.2 HARDWARE

3.6.3 CLADDING

3.5.2 Glass Dissolution Model

The rate equation used in the general model (W. L. Bourcier, Overview of Chemical Modeling of Nuclear Waste Glass Dissolution, *Mat. Res. Soc. Symp. Proc.*, 212, 3-18, 1991) of glass dissolution analysis is

$$\frac{dc_i}{dt} = \frac{A}{V} \nu k_+ (a_{H^+})^n \left(1 - e^{Aff/RT}\right) \quad (1)$$

where

c_i = concentration of species i in solution

A/V = surface area over solution volume (cm^{-1})

ν = stoichiometric factor for species e' in glass waste form

k_+ = forward rate constant (moles/cm^2/sec)

n = exponent for pH dependence of rate

Aff = affinity to dissolve (kcals/mole)

R = gas constant

T = temperature, Kelvins

to calculate the dissolution rate of the glass. Equation 1 is derived by starting with the general rate equation

$$\frac{dc_i}{dt} = \frac{A}{V} \nu k_+ (a_{H^+})^n + \frac{A}{V} \nu k_- (a_{H^+})^n \quad (2)$$

where k_+ is the forward rate constant (dissolution) and k- is the backward rate constant (dissolution). The principle of detailed balancing states that the net rate of a reaction is the difference between the rates of the forward and reverse reactions. At equilibrium, therefore, the rates are equal and $K_{eq} = \frac{k_+}{k_-}$

Equation 1, is derived assuming the principle of detailed balancing applies and that the driving force for a reaction is proportional to the extent of disequilibrium, or affinity of the reaction. The further from equilibrium, the stronger is the driving force. The origin of this rate equation is important because implicit in its use is the assumption that a *precipitation rate for glass* is not only possible, but must occur as the glass approaches "saturation."

Fortunately, application of this model to glass dissolution can be justified because the model is applied to the dissolution reaction of the gel layer and not the glass. A reverse reaction to precipitate the gel layer from solution is possible and highly likely. The affinity effect on glass dissolution corresponds to the effect of increasing the concentrations of species in solution, in particular silica, on the rate of precipitation of the hydrated silica-rich gel layer at the gel-water interface.

The models incorporate rate equation 1 into a general reaction path program that provides for speciation of the aqueous phases, and precipitation of secondary phases as they become saturated, and the effects of surface layer formation on solution chemistry.

A simplified method of calculating glass release rates is described in the following:

March 17, 1993.

TO: Ray Stout

FROM: William Bourcier

SUBJECT: Draft input for LLNL PA calculation, Glass Wasteform

Experimental and modeling work on borosilicate glass to date shows that the important parameters which need to be considered in order to predict radionuclide release rates from glass are temperature, exposed surface area, solution pH, and dissolved silica concentration in solution. Below we have supplied the equations and parameters needed to calculate conservative release rates of radionuclides from glass. We also include suggestions as to how to further simplify the model to make it appropriate for input into a first-cut comprehensive performance assessment model of a repository.

The rate equation commonly used to describe glass dissolution is:

$$R = sk_{T,pH}(1-Q/K) \qquad (1)$$

where R is the dissolution rate of glass in grams/day, s is the surface area of glass exposed to solution in m^2, k is the rate constant for glass which is primarily a function of temperature and pH, Q is the concentration of dissolved silica, and K a thermodynamic parameter for borosilicate glass that is approximated here as the solubility product for amorphous silica. Each of these parameters must be known or estimated in order to calculate radionuclide release rates from glass. Suggested values for each of these parameters are as follows:

Surface Area, *s*

The surface area of uncracked glass in a DWPF canister is about $5m^2$. However, after being poured and cooled, the glass undergoes fracturing. Estimates for the increase in glass surface area due to fracturing range from 2 to 100 times the geometric surface area. A reasonable and conservative value to use is 25 (Baxter, 1983). A surface area of $125m^2$/canister is therefore recommended.

Rate Constant, *k*

The rate constant has been measured over a range of pH and temperature conditions. The following data and regression equation describe the rate constant as a function of pH and temperature and is valid from 10 to 100°C and pH values from 1-12:

Table 1. Log_{10} glass dissolution rate in $g/m^2/day$.

pH	T = 25	50	70
1	-1.25	0.02	0.51
2	-1.73	-0.68	-0.18
3	-2.21	-1.38	-0.87
4	-2.69	-2.08	-1.56
5	-3.17	-2.78	-2.25
6			-2.94
7	-4.53	-3.43	-2.3
8	-4.02	-2.92	-1.9
9	-3.51	-2.41	-1.5
10	-3	-1.9	-1.1
12	-1.98	-0.88	-0.3

$$\log_{10}\text{Rate}(g\ \text{glass}/m^2/\text{day}) = -0.00172029 - 0.0231246T + 0.00148569T^2 - 1.13605\times10^{-5}T^3 - 1.1558pH + 0.0812918pH^2 + 0.000137686pH^3$$ (T in degrees C).

Solution Chemistry, *Q* and *K*

The major effect of groundwater chemistry on the glass dissolution rate (other than pH) is the concentration of dissolved silica. In this simple model, *Q* equals the concentration of dissolved silica in the water contacting the glass. The local groundwater chemistry in the vicinity of the repository will likely be dominated by the host rocks (Wilder, 1992) and the silica concentration is therefore expected to be close to cristobalite saturation at the ambient temperature. Cristobalite is a common constituent of the host rocks at Yucca Mountain. Table 2 lists concentrations of silica in equilibrium with cristobalite at temperatures from 0 to 150°C from the thermodynamic database SUPCRT92 (Johnson, Oelkers, and Helgeson, 1992).

"*K*" in equation (1) for the waste glass is assumed equal to the equilibrium constant for amorphous silica in this simple model. *K* actually varies as a function of glass composition, but for most waste glass compositions, the experimentally determined value of K is of the same general magnitude but less than the value of *K* for amorphous silica. Our simplification therefore gives conservative estimates. Table 2 lists values of $\log_{10}K$ (in molality) for temperatures from 0 to 150°C. As an example, at 60°C, $Q/K = 10^{-3.02}/10^{-2.43} = 0.26$. The term (1-Q/K)= (1-0.26) or 0.74. The glass reaction rate therefore is about 74% of the rate under silica-free conditions.

Table 2. Cristobalite and Amorphous Silica Solubilities

T°C =	0	25	60	90	100	150
Cristobalite	-3.89	-3.45	-3.02	-2.75	-2.68	-2.36
Amorphous Silica	-2.99	-2.71	-2.43	-2.26	-2.20	-1.98

Solution pH

Experimental studies of tuff-water interactions have shown that the pH of reacted J-13 water maintains a pH slightly higher than neutral (Knauss, Beiriger and Peifer, 1987). Therefore, for anticipated repository conditions, a slightly alkaline pH of about 8 is recommended as a substitute for the lack of any more rigorous calculation of groundwater chemistry. This pH value should be used to estimate rate constants for glass dissolution from Table 1 (it should also be consistent with any data for solubility limited radionuclide concentrations which are also highly dependent on pH). Note however that glass dissolution rates and radionuclide release rates are very sensitive to pH and nothing more than a qualitative estimate of release rates is possible without a more rigorous treatment of solution chemistry in the repository performance assessment model.

Temperature Dependence of Glass Dissolution Rate

Experiments have shown that glass dissolution rates follow an Arrhenius relation where rate$\propto e^{-E/RT}$ where R is the gas constant, T is temperature (Kelvins) and the activation energy (E) is about 20 kcal/mole. This corresponds roughly to dissolution rate increasing by a factor of 3 for a ten degree rise in temperature. This simple rule can be used to describe the effect of temperature on glass dissolution rate if the data in Table 1 cannot be explicitly used.

Radionuclide Content of Glass

Table 3 lists anticipated radionuclide contents for SRL glasses. More information on glass compositions is provided in the Wasteform Characteristics Report. Conservative estimates for release rates for radionuclides from the glass wasteform are given by multiplying the glass dissolution rate (R) by the weight fraction of radionuclide in the glass from Table 3.

Example Calculation

What is the rate of release of ^{235}U from one canister of glass at 70°C in cristobalite-saturated groundwater of pH=8? The rate constant for glass dissolution at 70°C and pH = 8 is $10^{-1.9}$ g/m^2/day. The affinity term (1-Q/K) has a value of $(1-10^{-2.93}/10^{-2.37})$ or 0.72. The bulk dissolution rate of glass is therefore 0.0091 g/m^2/day. Surface area for one canister is 125 m^2, so that the total rate of glass dissolution is 1.13 g/day/canister. Predicted ^{235}U content of SRL waste glass is 72.78 g/canister. Total weight of glass in a canister is 1682 kg so that the weight fraction of ^{235}U is 4.3×10^{-5}. Release rate of ^{235}U is therefore $1.13 \times 4.3 \times 10^{-5} = 4.89 \times 10^{-5}$g/day or .018 g/year.

Recommended Simplifications

Assume a constant pH of 8 and cristobalite saturation of the groundwater. Use Table 1 to provide the rate constant as a function of temperature at pH = 8. Use Table 2 to provide the factor that accounts for the lowering of glass dissolution rate due to dissolved silica. This provides a simple function of glass dissolution rate with temperature and no other variables need to be considered.

Limitations

This simplified treatment of estimating glass dissolution rates provides conservative estimates for release rates of radionuclides. It ignores solubility limits of some radioactive species (such as the actinides) and instead uses the conservative assumption that the radionuclides will be released as fast as the glass structure breaks down. Experiments have shown that the actinides more commonly are included in alteration phases at the surface of the glass either as minor components of other phases or as phases made up predominantly of actinides. We do not take any credit for this process in this simple treatment. In order to perform accurate

estimates of solubility-limited release rates, we need to know detailed information on water chemistry (pH, Eh, etc.) which demands a much more complex PA model that explicitly accounts for coupled chemical interactions between all of the repository materials (spent fuel, glass, metals, etc.).

This simple model ignores all solution chemistry other than pH and silica concentration. We know from a variety of experiments that species such as dissolved Mg and Fe can change glass dissolution rates by up to several orders of magnitude. Mg decreases the rate, Fe increases the rate. We do not account for effects such as these in this model.

We also ignore vapor phase alteration of the glass. If a canister containing glass is breached and humid air reaches the glass, the glass will react and form a thick alteration rind composed of hydrated glass and secondary phases. The durability of this material with respect to later contact with liquid water may be much greater or much less than the unaltered glass. We do not account for this effect here.

Table 3. Radioisotope content per HLW container for borosilicate glass from the Savannah River Site (from Wasteform Characteristics Report, Table 6.14). Contents in grams of each isotope. Mass of glass in each canister is 1682 kilograms. Only elements with more than 1 gram per canister are reported here.

Isotope	g/canister	Isotope	g/canister
U-234	.549e1	Tc-99	.182e3
U-235	.727e2	Pd-107	.286e2
U-236	.174e2	Sn-126	.156e2
U-238	.312e5	Cs-135	.863e2
Np-237	.126e2	Cs-137	.499e3
Pu-238	.867e2	Ce-143	.401e3
Pu-239	.208e3	Ce-144	.309e1
Pu-240	.381e2	Nd-144	.411e3
Pu-241	.162e2	Pm-147	.261e2
Pu-242	.321e1	Sm-147	.877e2
Am-241	.321e1	Sm-148	.192e2
Cm-244	.132e1	Sm-149	.742e1
Se-79	.243e1	Sm-151	.941e1
Rb-87	.996e1	Eu-154	.229e1
Sr-90	.343e3	Eu-155	.102e1
Zr-93	.444e3		

References

Baxter, R. G. (1983). Description of defense waste processing facility reference waste form and canister. (Report No. DP-1606). Savannah River Plant.

Johnson, J. W., E. H. Oelkers, and H. C. Helgeson, (1992) SUPCRT92: A software package for calculating the standard molal thermodynamic properties of minerals, gases, aqueous species, and reactions from 1 to 5000 bar and 0 to 1000°C. *Computers and Geosciences*, 18, 899-947.

Knauss, K. G., W.J. Beiriger, and D. W. Peifer (1987). Hydrothermal interaction of solid wafers of Topopah Spring Tuff with J-13 water at 90° and 150°C using Dickson-type, gold-bag rocking autoclaves: Long-term experiments. (UCRL 53722). Lawrence Livermore National Laboratory.

Wilder, D. G. E. (1992). Near-field environment report volume I: Technical basis for BES design (UCRL-LR No. 107476), Lawrence Livermore National Laboratory.

3. SCIENTIFIC BASIS FOR PREDICTIVE MODEL DEVELOPMENT

3.1 SPENT FUEL CLADDING FAILURE

3.1.1 EXPERIMENTAL PARAMETERS FOR FAILURE MODELS

3.1.2 FAILURE MODELS

3.2 SPENT FUEL OXIDATION

3.2.1 EXPERIMENTAL PARAMETERS FOR OXIDATION MODELS

3.2.2 OXIDATION MODELS

3.3 SPENT FUEL FISSION GAS RELEASE

3.3.1 EXPERIMENTAL PARAMETERS FOR FISSION GAS RELEASE

3.3.2 FISSION GAS RELEASE MODELS

3.4 SPENT FUEL DISSOLUTION

3.4.1 EXPERIMENTAL PARAMETERS FOR DISSOLUTION

3.4.1.1 DISSOLUTION RATES

3.4.1.2 SOLUBILITY LIMITS

3.4.1.3 SOLUBILITY LIMITING PHASES

3.4.2 DISSOLUTION MODELS

3.5 GLASS DISSOLUTION

3.5.1 EXPERIMENTAL PARAMETERS FOR GLASS DISSOLUTION

3.5.2 GLASS DISSOLUTION MODELS

3.6 OTHER RELEASE SOURCES OF RADIONUCLIDES

3.6.1 CRUD

3.6.2 HARDWARE

3.6.3 CLADDING

3. SCIENTIFIC BASIS FOR PREDICTIVE MODEL DEVELOPMENT

3.1 SPENT FUEL CLADDING FAILURE

3.1.1 EXPERIMENTAL PARAMETERS FOR FAILURE MODELS

3.1.2 FAILURE MODELS

3.2 SPENT FUEL OXIDATION

3.2.1 EXPERIMENTAL PARAMETERS FOR OXIDATION MODELS

3.2.2 OXIDATION MODELS

3.3 SPENT FUEL FISSION GAS RELEASE

3.3.1 EXPERIMENTAL PARAMETERS FOR FISSION GAS RELEASE

3.3.2 FISSION GAS RELEASE MODELS

3.4 SPENT FUEL DISSOLUTION

3.4.1 EXPERIMENTAL PARAMETERS FOR DISSOLUTION

3.4.1.1 DISSOLUTION RATES

3.4.1.2 SOLUBILITY LIMITS

3.4.1.3 SOLUBILITY LIMITING PHASES

3.4.2 DISSOLUTION MODELS

3.5 GLASS DISSOLUTION

3.5.1 EXPERIMENTAL PARAMETERS FOR GLASS DISSOLUTION

3.5.2 GLASS DISSOLUTION MODELS

3.6 OTHER RELEASE SOURCES OF RADIONUCLIDES

3.6.1 CRUD

3.6.2 HARDWARE

3.6.3 CLADDING

3.6.1 Crud

The corrosion products in the coolant of a power reactor form an activated radionuclide subset which, when deposited on the surfaces of a spent fuel assembly, are termed "crud." In reference (1), the crud subset of radionuclides with their specific surface activity was provided as "worst case" estimates for PWR and BWR assemblies; these were estimated irrespective of fuel manufacturer, handling of assemblies, reactor zone, axial location, and burnup. Table I below combines crud data from reference (1) and their half-life data from reference (2). Crud composition and structure are described extensively in reference (2) and summarized in reference (1) as being of two types:

(a) a fluffy, easily removed crud found usually on BWR rods and is composed mainly of hematite (Fe_2O_3)

(b) A tenacious, tightly bound crud found usually on PWR and is composed mainly of a nickel-substituted spinel ($Ni_xFe_{3-x}O_4$ with $x \cong 1$).

Table I

Nuclide	Half-life (days)	Crud Activity Density $\mu Ci/cm^2$ (reactor shutdown)	
		PWR Fuel	BWR Fuel
^{51}Cr	28	391	35
^{54}Mn	312	380	635
^{58}Co	71	1400	63
^{59}Fe	45	300	87
^{60}Co	1924	140	1250
^{65}Zn	244	N/A	56
^{95}Zr	65	36	30

Because of the relatively short half-lifes of the crud radionuclides, the release of crud appears as a potential problem primarily during transportation (Ref. 1 and 2) and preclosure radiological design of repository facilities (Ref. 3). From Table I, the longest half-life is ~5.3 yr for the crud radionuclide ^{60}Co, which at the end of 1,000 years would have an activity decay multiplier of 1.6×10^{-57}. Thus , the total activity of crud inventory would be small at 1,000 years, even though there exist several square miles of assembly surface (1 sq. mile ~2.6×10^{10} cm^2).

References

1. R.P. Sandoval, R.E. Einziger, H. Jordan, A.P. Malinauskas, and W.J. Mings, "Estimate of the CRUD Contribution to Shipping Cask Containment Requirements," *Nucl. Tech.*, 98, 196 (1992).

2. R.P. Sandoval, R.E. Einziger, H. Jordan, A.P. Malinauskas, and W.J. Mings, "Estimate of the CRUD Contribution to Shipping Cask Containment Requirements," SAND88-1358, TCC-0811, Sandia National Laboratories (Jan. 1991).

3. L.J. Jardine, "Preclosure Radiological Safety Analysis for Normal Conditions of the Yucca Mountain Repository," SLTR87-7013, Sandia National Laboratories (April, 1988).

3. SCIENTIFIC BASIS FOR PREDICTIVE MODEL DEVELOPMENT

3.1 SPENT FUEL CLADDING FAILURE

3.1.1 EXPERIMENTAL PARAMETERS FOR FAILURE MODELS

3.1.2 FAILURE MODELS

3.2 SPENT FUEL OXIDATION

3.2.1 EXPERIMENTAL PARAMETERS FOR OXIDATION MODELS

3.2.2 OXIDATION MODELS

3.3 SPENT FUEL FISSION GAS RELEASE

3.3.1 EXPERIMENTAL PARAMETERS FOR FISSION GAS RELEASE

3.3.2 FISSION GAS RELEASE MODELS

3.4 SPENT FUEL DISSOLUTION

3.4.1 EXPERIMENTAL PARAMETERS FOR DISSOLUTION

3.4.1.1 DISSOLUTION RATES

3.4.1.2 SOLUBILITY LIMITS

3.4.1.3 SOLUBILITY LIMITING PHASES

3.4.2 DISSOLUTION MODELS

3.5 GLASS DISSOLUTION

3.5.1 EXPERIMENTAL PARAMETERS FOR GLASS DISSOLUTION

3.5.2 GLASS DISSOLUTION MODELS

3.6 OTHER RELEASE SOURCES OF RADIONUCLIDES

3.6.1 CRUD

3.6.2 HARDWARE

3.6.3 CLADDING

3.6.2 Hardware

See Section 2.2.2.5

3. SCIENTIFIC BASIS FOR PREDICTIVE MODEL DEVELOPMENT

3.1 SPENT FUEL CLADDING FAILURE

3.1.1 EXPERIMENTAL PARAMETERS FOR FAILURE MODELS

3.1.2 FAILURE MODELS

3.2 SPENT FUEL OXIDATION

3.2.1 EXPERIMENTAL PARAMETERS FOR OXIDATION MODELS

3.2.2 OXIDATION MODELS

3.3 SPENT FUEL FISSION GAS RELEASE

3.3.1 EXPERIMENTAL PARAMETERS FOR FISSION GAS RELEASE

3.3.2 FISSION GAS RELEASE MODELS

3.4 SPENT FUEL DISSOLUTION

3.4.1 EXPERIMENTAL PARAMETERS FOR DISSOLUTION

3.4.1.1 DISSOLUTION RATES

3.4.1.2 SOLUBILITY LIMITS

3.4.1.3 SOLUBILITY LIMITING PHASES

3.4.2 DISSOLUTION MODELS

3.5 GLASS DISSOLUTION

3.5.1 EXPERIMENTAL PARAMETERS FOR GLASS DISSOLUTION

3.5.2 GLASS DISSOLUTION MODELS

3.6 OTHER RELEASE SOURCES OF RADIONUCLIDES

3.6.1 CRUD

3.6.2 HARDWARE

3.6.3 CLADDING

Interdepartmental letterhead

Mail Station L-352 **CHEMISTRY & MATERIALS SCIENCE DEPARTMENT**

Ext: 2-0456 Corrosion & Electrochemical Processes Section
Materials Division

MEMORANDUM - January 23, 1991
91-02RVKm

TO: Ray Stout, L-201
FROM: Rich Van Konynenburg
SUBJECT: ***Carbon-14 Information for Preliminary Waste Form Characteristics Document***

In response to your request, here is some information about carbon-14 associated with spent fuel:

According to my current best estimates, the inventory of carbon-14 in spent fuel is as follows:

BWR

Total: $3.71 \times 10^{-5} \frac{\text{curies per MTIHM}}{\text{MWd/MTIHM}}$

Zircaloy only: $1.38 \times 10^{-5} \frac{\text{curies per MTIHM}}{\text{MWd/MTIHM}}$

(Nearly half of the BWR zircaloy inventory is in the fuel channel.)

PWR

Total: $3.03 \times 10^{-5} \frac{\text{curies per MTIHM}}{\text{MWd/MTIHM}}$

Zircaloy only: $5.45 \times 10^{-6} \frac{\text{curies per MTIHM}}{\text{MWd/MTIHM}}$

Based on the work of Smith and Baldwin, as much as 2% of the total spent fuel ^{14}C inventory can be released at 350°C in air in 8 hours.

According to recent work in Germany (D. Kopp and H. Münzel, "Release of Volatile Carbon-14 Containing Products from Zircaloy," *J. Nucl. Mater.* 173, 1-6 (1990), oxygen is necessary for volatile ^{14}C release to occur.

To be conservative, one could assume that sufficient oxygen would be present in the argon fill gas in a waste container to bring about release of the entire 2% of the inventory into the fill gas prior to breach of the container.

RVK:mlm

Distribution
Author File
Ballou, L. L-206
Clarke, W. L-352

CONSTANT TEMPERATURE TESTS, THICK OXIDE

Harry D. Smith, "Spent Fuel Cladding Degradation," presented to the Nuclear Waste Technical Review Board, August, 1990.

OBSERVED ^{14}C RELEASE FROM ZIRCALOY-4 SPENT FUEL CLADDING

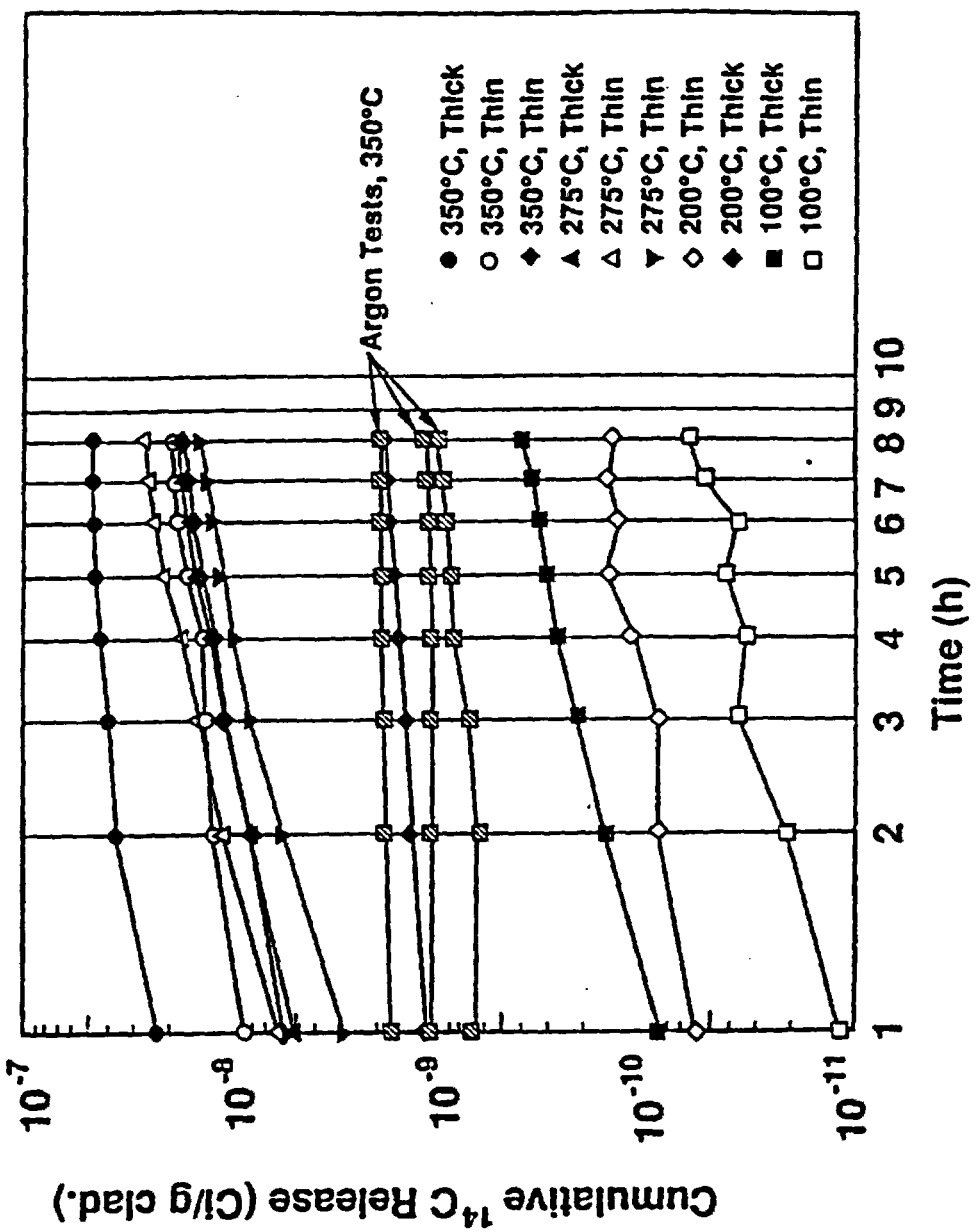

Harry D. Smith, "Spent Fuel Cladding Degradation," presented to the Nuclear Waste Technical Review Board, August, 1990.

Adachi, T., M. Ohnuki, et al. "Dissolution Study of Spent PWR Fuel: Dissolution Behavior and Chemical Properties on Insoluble Residues," *J. Nucl. Mat.*, 174, 60-71 (1990).

Aronson, S., R.B. Roof, and J. Belle. "Kinetic Study of the Oxidation of Uranium Oxide," *J. Chem. Phys.* 27, 137 (1957).

Bates, J.K., "Identification of Secondary Phases Formed During Unsaturated Reaction of UO_2 with EJ-13 Water," Materials Research Society Symposium proceedings 176, 499 (1990). NAA.910128.0029

Bates, J.K., "Integrated Glass Alteration Tests," presented to the Nuclear Waste Technical Review Board, (August, 1990). NAA.920302.0059

Bates, J.K., et al., "NNWSI Waste Form Testing at Argonne National Laboratory Semi-Annual Report, January – June, 1988," UCRL-21000-88-1, (January, 1991). NAA.910128.0062

Beyer, C.E., in "Status and Future Direction of Spent Fuel ATM Acquisition and Characterization meeting" in Richland, Washington, (March, 1989). NAA.920401.0114

Boltzmann, L. "Lectures on Gas Theory," translated by S.G. Brush, Univ. of California Press, Berkeley, CA (1964). NAA.920401.0117

Bourcier, W.L., "Modeling of Glass Dissolution," presented to the Nuclear Waste Technical Review Board, (August, 1990). NAA.920302.0057

Bruton, C.J., "Solubility Controls on Radionuclide Concentrations in Solution: Preliminary Results for U, Np, Pu, and Am," LLNL draft report, (November, 1990).

Carslaw, H.S. and J.C. Jaeger. "Conduction of Heat in Solids," second edition, Oxford University Press, New York (1959). NAA.900522.0259

E.R. Johnson Associates, Inc. (compilers), "Acceptance of Non-Fuel Assembly Hardware by the Federal Waste Management System," ORNL/SUB./86-SA094/8, JAI-328, (March, 1990). NAA.900427.0017

Einziger, R.E. and H.C. Buchanan. "Long-Term, Low Temperature Oxidation of PWR Spent Fuel," Westinghouse Hanford Co. Report, WHC-EP-0070 (June, 1987). NAA.900620.0297

Einziger, R.E. and R.E. Woodley. "Predicting Spent Fuel Oxidation States in a Tuff Repository," Westinghouse Hanford Co. Report HEDL-SA-3627, (April, 1985). NAA.870915.0073

Einziger, R.E. "Technical Test Description of Activities to Determine the Potential for Spent Fuel Oxidation in a Tuff Repository," Westinghouse Hanford Co. Report HEDL-7540 (June, 1985). NAA.920302.0060

Einziger, R.E. "Test Plan for Series 2 Thermogravimetric Analyses of Spent Fuel Oxidation," Westinghouse Hanford Co. Report HEDL-7556 (February, 1986). NAA.920302.0061

Einziger, R.E., "Spent Fuel Oxidation," presented to Nuclear Waste Technical Review Board, (August, 1990). NAA.920302.0054

Einziger, R.E., "Test Plan for Long-Term, Low-Temperature Oxidation of Spent Fuel, Series 1," Westinghouse Hanford Co. Report HEDL-7560 (June, 1986). NAA.920302.0062

Finch, R. and R. Ewing, "Alteration of Natural UO_2 Under Oxidizing Conditions from Shinkolobwe, Katanga, Zaire: A Natural Analogue for the Corrosion of Spent Fuel," *Radiochim. Acta*, 52/53, 395-401 (1991). NAA.900507.0149

Gleiter, H. and B. Chalmers. "High-Angle Grain Boundaries," in *Prog. in Mat. Sci.*, Vol. 16, Pergamon Press, New York (1972).

Grambow, B. "Spent Fuel Dissolution and Oxidation: An Evaluation of the Literature," SKB Tech. Rept. 89-13, Svensk Kärnbränslehantering AB, Stockholm, 42 p. (1989). NAA.891013.0094

Grambow, B., R. Forsyth, et al. "Fission Product Release from Spent UO_2 Fuel Under Uranium-Saturated Oxic Conditions," *Nucl. Tech.*, 92, 204-213 (November, 1990).

Gray, W. and Wilson, C., "Effects of Water Composition and Temperature on the Dissolution Rate of UO_2," presented at 1990 Spent Fuel Workshop, Gull Harbor, Manitoba, Canada, (1990). NNA.910821.0008

Gray, W. and Wilson, C., "Spent Fuel Grain Boundary Inventory and Testing the Congruency of UO_2 Matrix Dissolution of Spent Fuel," presented at 1990 Spent Fuel Workshop, Gull Harbor, Manitoba, Canada, (1990). NNA.910821.0009

Knauss, K.G., "Experimental Basis for Glass Dissolution," presented to the Nuclear Waste Technical Review Board, (August, 1990).

Leider, H.R., S.N. Nguyen, R.B. Stout, H.C. Weed, "Estimating the Time for Dissolution of Spent Fuel Exposed to Unlimited Water," LLNL Report #UCRL-ID-107289, (Dec., 1991). NNA.911211.0002

Notz, K.J., "Characteristics of Potential Repository Waste," DOE/RW-0184-R1, V.1 (draft), (July, 1990). NNA.900427.0056

Notz, K.J., T.D. Welch, R.S. Moore, and W.J. Reich, "Preliminary Waste Form Characteristics," ORNL-TM-11681 (draft) (September, 1990). NNA.901113.0010

Olander, D.R. "Combined Grain-Boundary and Lattice Diffusion in Fine-Grained Ceramics," *Advances in Ceramics*, 17, 271 (1986).

Palmer, R.A., "West Valley Demonstration Project High Level Waste Qualification Activities," presented to the Nuclear Waste Technical Review Board, (August, 1990). NNA.920302.0056

Plodinec, M.J., "Defense Waste Processing Facility High Level Waste Qualification Activities," presented to the Nuclear Waste Technical Review Board, (August, 1990). NNA.920302.0055

Puigdomenech, I., and J. Bruno, "Modeling Uranium Solubilities in Aqueous Solutions: Validation of a Thermodynamic Data Base for the EQ3/6 Geochemical Codes," SKB technical report 88-21, (October, 1988). NNA.890425.0186

Roddy, W.J., H.C. Claiborne, R.C. Ashline, P.T. Johnson, and B.T. Rhyne, "Physical and Decay Characteristics of Commercial LWR Spent Fuels," ORNL/TM-9591/V.1, (October, 1985). NNA.891016.0145

Site Characterization Plan, Yucca Mountain Site, Nevada, Research and Development Area, DOE/RW-0199, Vol. III, Part A, (December, 1988).

Slattery, J.C. "Momentum, Energy and Mass Transfer in Continua," R.E. Krieger Pub. Co., New York (1978). NNA.920401.0115

Smith, H.D., "Spent Fuel Cladding Degradation," presented to the Nuclear Waste Technical Review Board, (August, 1990). NNA.920302.0052

Stout, R.B. and L. Thigpen. "A Model for the Deformations and Thermodynamics of Materials Involving a Microcrack Kinetics," *Cryst. Latt. Defects and Amorph. Mat.*, 10, 129 (1984).

Stout, R.B. "Modeling the Deformations and Thermodynamics for Materials Involving a Dislocation Kinetics," *Cryst. Latt. Defects*, 9, 65 (1981).

Stout, R.B. "Statistical Model for Particle-Void Deformation Kinetics in Granular Materials During Shock Wave Propagation," Lawrence Livermore National Laboratory Report UCRL-101623 (July, 1989). NNA.900517.0267

Stout, R.B., "Spent Fuel Characteristics Overview," presented to the Nuclear Waste Technical Review Board, (August, 1990).

Thomas, L., O. Slagle, and R. Einziger, "Nonuniform Oxidation of LWR Spent Fuel in Air," *J. Nucl. Mat.*, 184 117-126 (1991). NNA.910509.0071

Thomas, L., R. Einziger, and R. Woodley, "Microstructural Examination of Oxidized Spent PWR Fuel by Transmission Electron Microscopy," *J. Nucl. Mat.*, 166, 243-251 (1989). NNA.900709.0482

Thomas, L.E., R.E. Einziger, and R.E. Woodley. "Microstructural Examinations of Oxidized Spent Fuel by Transmission Electron Microscopy," *J. Nucl. Mat.*, in press. NML 880707.0043.

Wilson, C.N., "Indications for the Formation of Pu, Am, and Cm Colloids in Semi-Static Spent Fuel Dissolution Tests," presented at the 1990 Spent Fuel Workshop, (September, 1990). NNA.920302.0064

Wilson, C.N., "Results from Cycles 1 and 2 on NNWSI Series 2 Dissolution Tests," HEDL-TME 85-22, (May, 1987). NNA.900716.0358

Wilson, C.N., "Results from the NNWSI Series 3 Spent Fuel Dissolution Tests," PNL 7170, (June, 1990). NNA.900329.0142

Wood, P. and G.H. Bannister. "Investigation of the Mechanism of UO2 Oxidation in Air: The Role of Grain Size," Proc. Workshop on Chemical Reactivity of Oxide Fuel and Fission Product Release, K.A. Simpson and P. Wood, eds., Berkeley Nuclear Lab., U.K., p. 19 (1987). NNA.920401.0116

Woodley, R.E., "The Characteristics of Spent LWR Fuel Relevant to its Storage in Geologic Repositories," HEDL-TME 83-28, (October, 1983). NNA.870406.0337

Woodley, R.E., R.E. Einziger, and H.C. Buchanan. "Measurement of the Oxidation of Spent Fuel Between 140° and 225°C by Thermogravimetric Analysis," Westinghouse Hanford Co. Report WHC-EP-0107 (September, 1988). NNA.880927.0069

The following number is for Office of Civilian Radioactive Waste Management Records Management purposes only and should not be used when ordering this document:

Accession Number: NNA.920501.0001

Technical Information Department · Lawrence Livermore National Laboratory
University of California · Livermore, California 94551